Title
IN SITU STRESS MEASUREMENTS AT THE STRIPA MINE, SWEDEN

Author
Doe, T.W.

Publication Date
1983-03-01

LBL-15009
SAC-44
UC-70

SWEDISH-AMERICAN COOPERATIVE PROGRAM ON RADIOACTIVE WASTE STORAGE IN MINED CAVERNS IN CRYSTALLINE ROCK

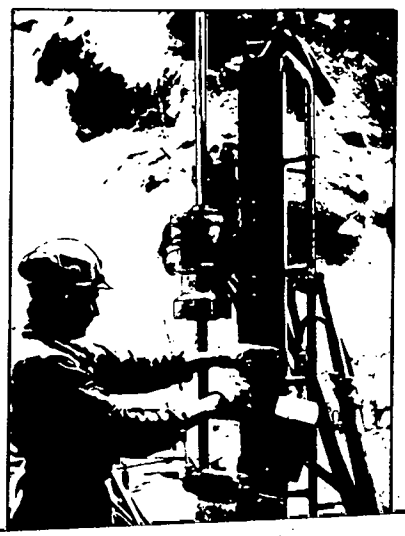

Technical Information Report No. 44

IN SITU STRESS MEASUREMENTS AT THE STRIPA MINE, SWEDEN

T.W. Doe, K. Ingevald, L. Strindell, B. Leijon,
W. Hustrulid, E. Majer, and H. Carlsson
Lawrence Berkeley Laboratory
University of California
Berkeley, California 94720

March 1983

A Joint Project of

Swedish Nuclear Fuel Supply Co.
Fack 10240 Stockholm, Sweden

Operated for the Swedish
Nuclear Power Utility Industry

Lawrence Berkeley Laboratory
Earth Sciences Division
University of California
Berkeley, California 94720, USA

Operated for the U.S. Department of
Energy under Contract DE-AC03-76SF00098

DISCLAIMER

LBL-15009
SAC-44
UC-70

IN SITU STRESS MEASUREMENTS AT THE STRIPA MINE, SWEDEN

T.W. Doe, K. Ingevald, L. Strindell, B. Leijon, W. Hustrulid, E. Majer, and H. Carlsson

March, 1983

This work was supported by the Assistant Secretary for Nuclear Energy, Office of Civilian Waste Management of the U.S. Department of Energy under Contract DE-AC03-76SF00098. Funding for this report is administered by the Office of Crystalline Repository Development at Battelle Memorial Institute.

PREFACE

This report is one of a series documenting the results of the Swedish-American cooperative research program in which the cooperating scientists explore the geological, geophysical, hydrological, geochemical, and structural effects anticipated from the use of a large crystalline rock mass as a geologic repository for nuclear waste. This program has been sponsored by the Swedish Nuclear Power Utilities through the Swedish Nuclear Fuel Supply Company (SKBF), and the U.S. Department of Energy (DOE) through the Lawrence Berkeley Laboratory.

The principal investigators are L.B. Nilsson and O. Degerman for SKBF, and N.G.W. Cook, P.A. Witherspoon, and J.E. Gale for LBL. Other participants will appear as authors of the individual reports.

Previous technical reports in this series are listed below.

1. Swedish-American Cooperative Program on Radioactive Waste Storage in Mined Caverns by P.A. Witherspoon and O. Degerman. (LBL-7049, SAC-01).

2. Large Scale Permeability Test of the Granite in the Stripa Mine and Thermal Conductivity Test by Lars Lundstrom and Haken Stille. (LBL-7052, SAC-02).

3. The Mechanical Properties of the Stripa Granite by Graham Swan. (LBL-7074, SAC-03).

4. Stress Measurements in the Stripa Granite by Hans Carlsson. (LBL-7078, SAC-04).

5. Borehole Drilling and Related Activities at the Stripa Mine by P.J. Kurfurst, T. Hugo-Persson, and G. Rudolph. (LBL-7080, SAC-05).

6. A Pilot Heater Test in the Stripa Granite by Hans Carlsson. (LBL-7086, SAC-06).

7. An Analysis of Measured Values for the State of Stress in the Earth's Crust by Dennis B. Jamison and Neville G.W. Cook. (LBL-7071, SAC-07).

8. Mining Methods Used in the Underground Tunnels and Test Rooms at Stripa by B. Andersson and P.A. Halen. (LBL-7081, SAC-08).

9. Theoretical Temperature Fields for the Stripa Heater Project by T. Chan, Neville G.W. Cook, and C.F. Tsang. (LBL-7082, SAC-09).

10. Mechanical and Thermal Design Considerations for Radioactive Waste Repositories in Hard Rock. Part I: An Appraisal of Hard Rock for Potential Underground Repositories of Radioactive Waste by N.G.W. Cook; Part II: In Situ Heating Experiments in Hard Rock: Their Objectives and Design by N.G.W. Cook and P.A. Witherspoon. (LBL-7073, SAC-10).

11. Full-Scale and Time-Scale Heating Experiments at Stripa: Preliminary Results by N.G.W. Cook and M. Hood. (LBL-7072, SAC-11).

12. Geochemistry and Isotope Hydrology of Groundwaters in the Stripa Granite: Results and Preliminary Interpretation by P. Fritz, J.F. Barker, and J.E. Gale. (LBL-8285, SAC-12).

13. Electrical Heaters for Thermo-Mechanical Tests at the Stripa Mine by R.H. Burleigh, E.P. Binnall, A.O. DuBois, D.O. Norgren, and A.R. Ortiz. (LBL-7063, SAC-13).

14. Data Acquisition, Handling, and Display for the Heater Experiments at Stripa by Maurice B. McEvoy. (LBL-7063, SAC-14).

15. An Approach to the Fracture Hydrology at Stripa: Preliminary Results by J.E. Gale and P.A. Witherspoon. (LBL-7079, SAC-15).

16. Preliminary Report on Geophysical and Mechanical Borehole Measurements at Stripa by P. Nelson, B. Paulsson, R. Rachiele, L. Andersson, T. Schrauf, W. Hustrulid, O. Duran, and K.A. Magnussen. (LBL-8280, SAC-16).

17. Observations of a Potential Size-Effect in Experimental Determination of the Hydraulic Properties of Fractures by P.A. Witherspoon, C.H. Amick, J.E. Gale, and K. Iwai. (LBL-8571, SAC-17).

18. Rock Mass Characterization for Storage in Nucler Waste in Granite by P.A. Witherspoon, P. Nelson, T. Doe, R. Thorpe, B. Paulsson, J.E. Gale, and C. Forster. (LBL-8570, SAC-18).

19. Fracture Detection in Crystalline Rock Using Ultrasonic Shear Waves by K.H. Waters, S.P. Palmer, and W.F. Farrell. (LBL-7051, SAC-19).

20. Characterization of Discontinuities in the Stripa Granite--Time Scale Heater Experiment by R. Thorpe. (LBL-7083, SAC-20).

21. Geology and Fracture System at Stripa by A. Okliewicz, J.E. Gale, R. Thorpe, and B. Paulsson. (LBL-8907, SAC-21).

22. Calculated Thermally Induced Displacements and Stresses for Heater Experiements at Stripa by T. Chan and N.G.W. Cook. (LBL-7061, SAC-22).

23. Validity of Cubic Law for Fluid Flow in a Deformable Rock Fracture by P.A. Witherspoon, J. Wang, K. Iwai, and J.E. Gale. (LBL-9557, SAC-23).

24. Determination of In-Situ Thermal Properties of Stripa Granite from Temperature Measurements in the Full-Scale Heater Experiments: Methods and Primary Results by J. Jeffry, T. Chan, N.G.W. Cook and P.A. Witherspoon. (LBL-8424, SAC-24).

25. Instrumentation Evaluation, Calibration, and Installation for Heater Tests Simulating Nuclear Waste in Crystalline Rock, Sweden by T. Schrauf, H. Pratt, E. Simonson, W. Hustrulid, P. Nelson, A. DuBois, E. Binnall, and R. Haught. (LBL-8313, SAC-25)

26. Part I: Some Results From a Field Investigation of Thermo-Mechanical Loading of a Rock Mass When Heater Canisters are Emplaced in the Rock by M. Hood. Part II: The Application of Field Data from Heater Experiments Conducted at Stripa, Sweden for Repository Design by M. Hood, H. Carlsson, and P.H. Nelson. (LBL-9392, SAC-26).

27. Progress with Field Investigations at Stripa by P.A. Witherspoon, N.G.W. Cook, and J.E. Gale (LBL-10559, SAC-27).

28. A Laboratory Assessment of the Use of Borehole Pressure Transients to Measure the Permeability of Fractured Rock Masses by C.B. Forster and J.E. Gale. (LBL-8674, SAC-28).

29. Thermal and Thermomechanical Data for In Situ Heater Experiments at Stripa, Sweden by T. Chan, E. Binnall, P. Nelson, O. Wan, C. Weaver, K. Ang, J. Braley, and M. McEvoy. (LBL-11477, SAC-29).

30. The Effect of Radon Transport in Groundwater Upon Gamma Ray Borehole Logs by P.H. Nelson, R. Rachiele, and A. Smith. (LBL-11180, SAC-30).

31. Strength and Permeability Tests on Ultra-Large Stripa Granite Core by R. Thorpe, D.J. Watkins, W.E. Ralph, R. Hsu, and S. Flexser. (LBL-11203, SAC-31).

32. Ultrasonic and Acoustic Emission Results from the Stripa Heater Experiments. Part I: A Cross-Hole Investigation of a Rock Mass Subjected to Heating by B.N.P. Paulsson and M.S. King. Part II: Acoustic Emission Monitoring During Cool-Down of the Stripa Heater Experiment by R. Rachiele. (LBL-10975, SAC-32).

33. Numerical Modeling to Assess Possible Influence of the Mine Openings on Far-Field In Situ Stress Measurements at Stripa by T. Chan, V. Guvanasen, and N. Littlestone (LBL-12469, SAC-33).

34. A Field Assessment of the Use of Borehole Pressure Transients to Measure the Permeability of Fractured Rock Masses by C.B. Forster and J.E. Gale. (LBL-11829, SAC-34).

35. Water Inflow into Boreholes During the Stripa Experiments by P.H. Nelson, R. Rachiele, J.S. Remer and H.S. Carlsson (LBL-12547, SAC-35).

36. Petrology and Radiogeology of the Stripa Pluton by H. Wollenberg, S. Flexser, and L. Andersson. (LBL-11654, SAC-36).

37. Geohydrological Data from the Macopermeability Experiment at Stripa, Sweden by C.R. Wilson, J.C.S. Long, R.M. Galbraith, K. Karasaki, H.K. Endo, A.O. DuBois, M.J. McPherson, and G. Ramqvist. (LBL-12520, SAC-37).

38. Characterization of Discontinuities in the Stripa Granite--Full-Scale Heater Experiments by B.N.P. Paulsson, P.H. Nelson, and P.J. Kurfurst. (LBL-9063, SAC-38).

39. Application of Borehole Geophysics at an Experimental Waste Storage Site by P.H. Nelson, K.A. Magnusson, and R. Rachiele. (LBL-11982, SAC-39).

40. Laboratory Investigations of Thermomechanical Properties of Stripa Granite by L. Myer and R. Rachiele. (LBL-13435, SAC-40)

41. Petrologic Changes and Damage in the Stripa Quartz Monzonite in Response to Heater Tests by S. Flexser, H. Wollenberg, and D.E. Wedge. (LBL-14929, SAC-41).

TABLE OF CONTENTS

LIST OF FIGURES

Page

LIST OF TABLES

ABSTRACT

The state of stress at the Stripa test mine in Sweden has been studied through a program of hydraulic fracturing and overcoring stress measurements performed both in a 381 meter deep vertical borehole drilled from the surface and from shorter boreholes drilled around the heater experiment drifts.

Far-field measurements were obtained in the deep vertical hole by using the Swedish State Power Board's Leeman triaxial cell and hydraulic fracturing. The two methods agree well on the orientation of the maximum horizontal stress and on the interpolated stress values for the depth of the test facility. On the basis of a regression analysis of the stress data versus depth, the following conclusions have been reached: (1) determination of stress at a particular depth should be made by interpolation of data from well above and below the depth of interest; (2) extrapolation of values beyond the depth range of the data cannot be done with confidence; and (3) stress determinations should be based on more than just a few measurements.

The hydraulic fracturing experiments were interpreted by using the first breakdown pressure and a tensile-strength term. The tensile-strength term is based on an analysis of laboratory tensile-strength data and compensates for the size effect through methods of statistical fracture mechanics.

Near-field stress measurements were made from one vertical and two horizontal boreholes in the heater test area. The vertical hole was used for both Swedish State Power Board Leeman cell measurements and hydraulic

fracturing. One horizontal hole was used for hydraulic fracturing, the other for overcoring. Overcoring measurements employed the University of Luleå (LuH) triaxial cell, the USBM borehole deformation gauge, and the CSIRO hollow inclusion triaxial cell. All the data are in excellent agreement that the near-field maximum stress roughly parallels the drift and is horizontal. All methods agree on the magnitudes of the stresses. The shut-in pressure values and the overcoring results both indicate that the intermediate and least principal stresses are skewed about 45° from the stress measurement holes in the plane of the boreholes.

Acoustic emissions from the hydraulic fractures were monitored in the heater test area to determine their location and orientation. The emissions were successfully monitored for only one test, which showed that the fracture propagated primarily from one side of the hole in the direction of the heater drift axis.

The maximum stress direction at Stripa rotates from northwest in the far field to northeast in the near field. This rotation appears to be due to the influence of the mine as a whole rather than to the experimental drifts.

Statistical analysis of the stress measurement data may help to design stress measurement programs for other sites. If the variance of the data is assumed to be similar to that at Stripa, stress measurement programs should include at least 20 measurements by both overcoring and hydraulic fracturing. We consider these two methods to be complementary.

Overcoring can indicate where the borehole direction does not coincide with a principal stress (such coincidence is an important assumption in hydrofracture analysis), while hydraulic fracturing provides a measure of the in situ stress on a larger scale than overcoring.

1. INTRODUCTION
(T. W. Doe)

1.1 Purposes

For the past several years, the Stripa Mine in central Sweden has been the site of hydrologic and rock mechanics field testing to evaluate the feasibility of storing radioactive wastes in granitic rocks. Data on the state of stress has been recognized as necessary for the analysis of the field testing data at the site, and over the past two summers (1981-1982) we have been carrying out a program of in situ stress measurements by hydrofracturing and a variety of overcoring techniques.

While determining the state of stress for the analysis of the heater test data was the primary purpose of these experimental measurements, the work also provided an opportunity to compare the results of several techniques at a common site, and to evaluate the effect of a large mine on the state of stress. This work might thus help to resolve some of the controversy surrounding stress measurement techniques. Hydraulic fracturing, which has become very popular for measurements at depth, has been questioned over such issues as the noncollinearity of the hole with principal stress directions, the role of rock tensile strength, and the interpretation of shut-in pressure records. Overcoring measurements have been notorious for a large degree of scatter in the data and have been challenged over questions about the influence of small-scale, local heterogeneities on the results of strain cell measurements. Hydraulic fracturing and overcoring have not been carried out in a common borehole, nor have many measurements by the two methods been made in the immediate vicinity of one another underground.

Another purpose has been to develop a measurement data set sufficiently large to allow statistical treatment of the uncertainties associated with stress determinations. In particular, we wished to determine how accurately the in situ stresses need to be known for repository design, and how many measurements must be made to achieve the desired accuracy.

1.2 Geologic Setting

The geology and fracture system of the Stripa area have been described by Olkiewicz et al. (1979) and is briefly summarized below. The host rock for the heater experiments is the Stripa granite, a small pluton with a monzogranitic composition and a Precambrian age. The granite was post-tectonically intruded into strongly folded leptite (undifferentiated metasedimentary and metavolcanic rocks of Precambrian age). The leptites are predominantly metavolcanic in origin with interbedded carbonates and iron formation. The granite is for the most part concordantly intruded into the leptite sequence, which has been folded about NE-SW axes gently plunging to the northeast.

The Stripa mine was developed to exploit the iron formation, and most of the workings follow the strike and dip of the bedding. The contact between the granite and the leptite strikes NE-SW and dips to the southwest, following the structural trend. As the iron formation often occurs near the granite contact, haulage ways commonly pass through the granite. It was off of such workings that the drifts for the Stripa experiments were excavated. The experimental drifts lie within the footwall of the contact; hence the experimental areas lie beneath the

major stopes and other workings of the mine (Fig. 1.1). Figure 1.2 shows the surface geology of the granite and leptite, along with the location of stress measurement boreholes and the experimental drifts. The granite outcrops north of the mine were chosen as the site of the borehole for far-field measurements, SBH-4.

1.3 Stress Measurement Methods Used

The Stripa stress measurement program employed both hydraulic fracturing and overcoring methods.

The hydraulic fracturing was performed in accordance with methods developed by Haimson (1978) and Zoback et al. (1980) over the last 10 years. A section of borehole is isolated with inflatable packers, and the interval is pressurized until the rock fractures. The magnitude of the stresses is determined from the pressure at which the rock fractures and from characteristics of the subsequent pressure-time record. The orientation of the maximum horizontal stress is determined from the orientations of the fracture. Details are discussed in Chapter 2.

Hydraulic fracturing measures the complete state of stress only when the borehole direction coincides with the orientation of the minimum or intermediate principal stress. This usually requires the borehole to be vertical to allow one stress to be assumed from the overburden weight. If the borehole is skewed with respect to one of these principal stresses, interpretation would at best be limited to the stress normal to the hole and possibly the minimum stress, although this would not include its orientation.

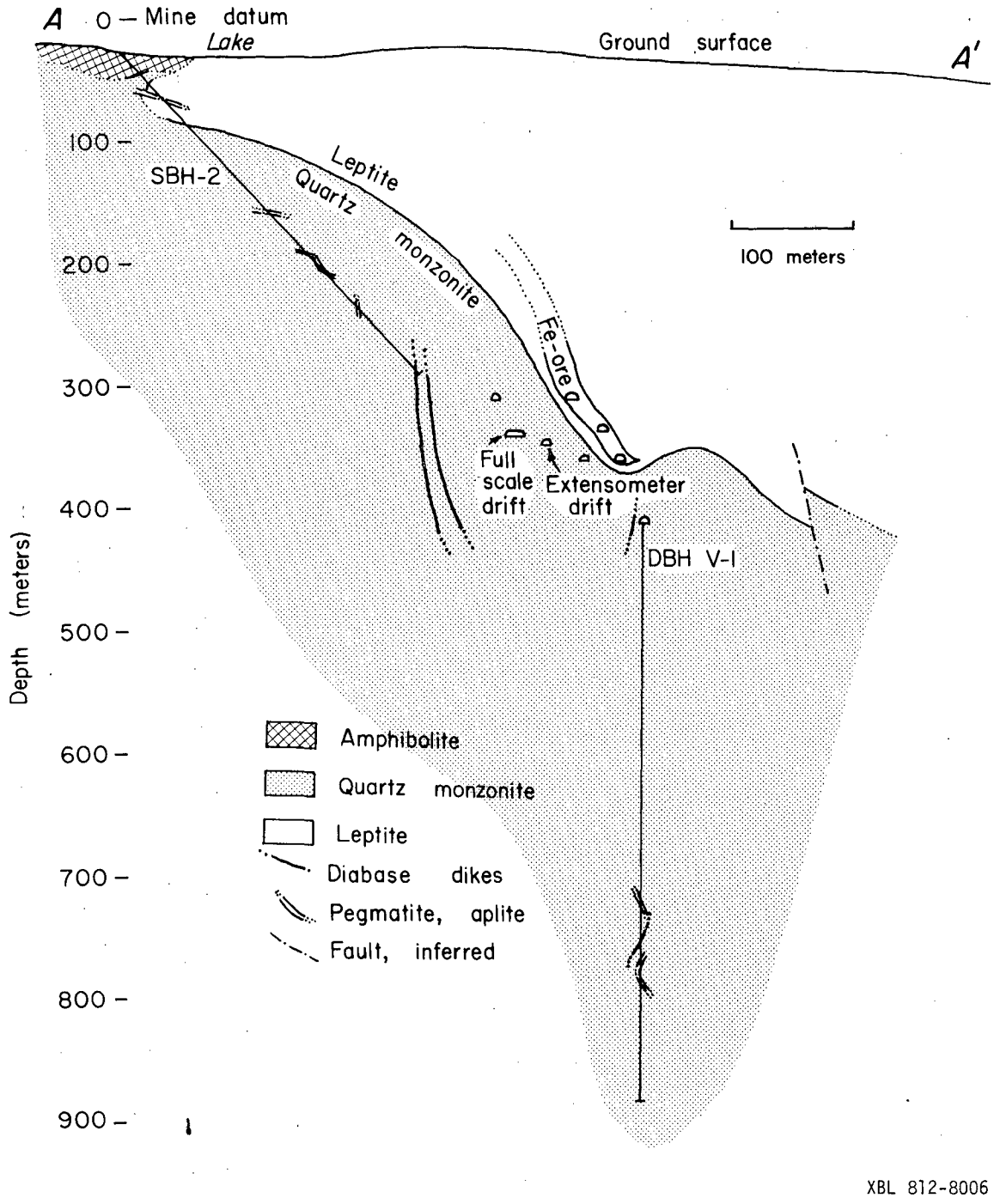

Fig. 1.1 East-west vertical cross-section through the test area (from Wollenberg et al., 1981).

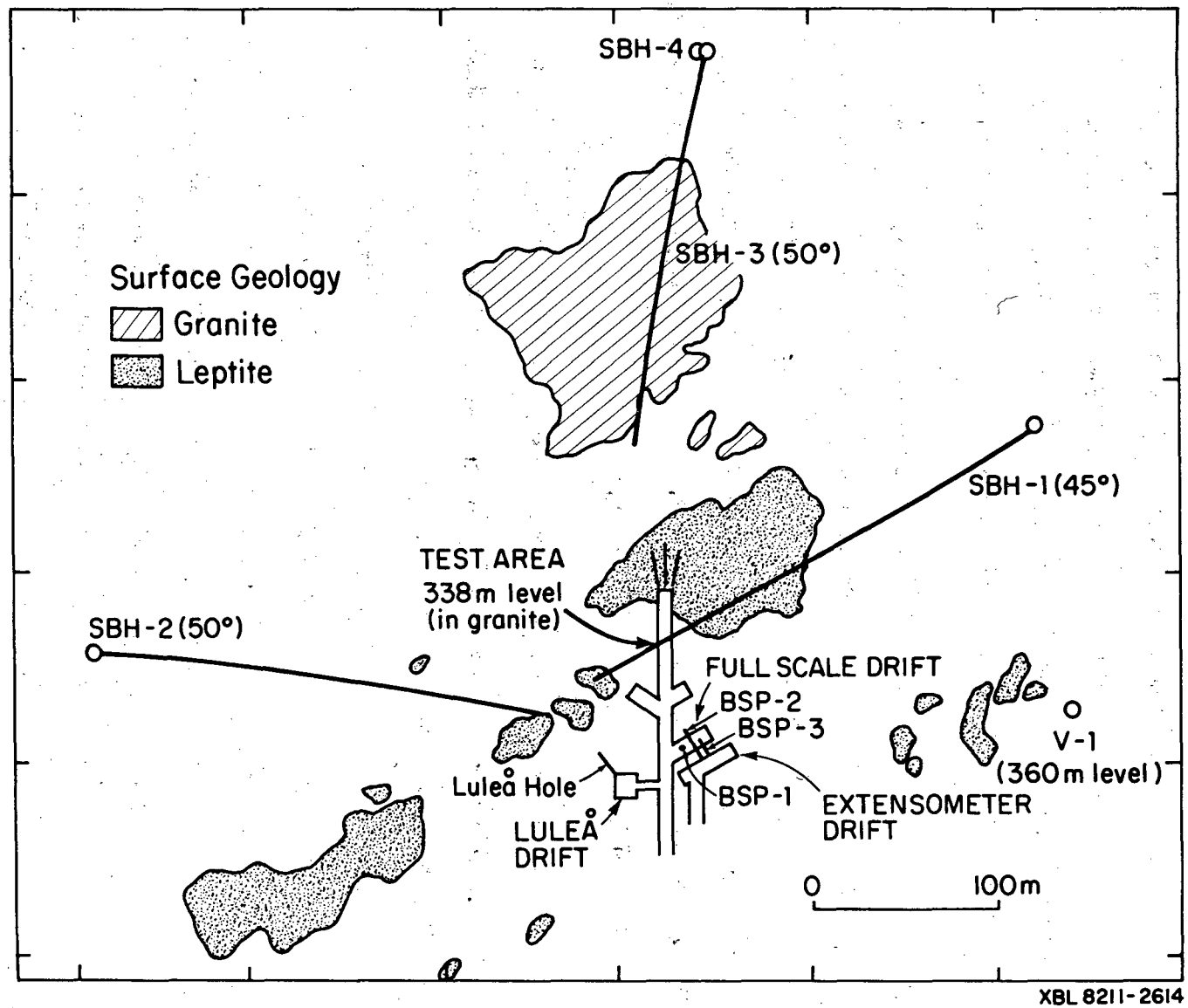

Fig. 1.2 Surface geology at Stripa and location of stress measurement holes.

Interpreting hydraulic fracturing records when the hole is not coincident with a principal stress direction is easier if the orientation of the fracture is known. It is generally thought that fractures will initiate coaxially with the borehole and change orientation away from the hole to be normal to the minimum stress. Chapter 9 describes an attempt to map the fracture acoustically to determine its true orientation.

The overcoring methods included the following: The U.S. Bureau of Mines (USBM) borehole deformation gauge, the University of Luleå (LuH) triaxial cell, the CSIRO (Australian Council of Scientific and Industrial Research Organizations) hollow inclusion gauge, and the Swedish State Power Board deep-hole Leeman triaxial cell. Figure 1.3 illustrates the basic configurations of these methods.

All the overcoring methods determine the stress from the strain or deformation of an overcored pilot borehole. The USBM gauge (Chapter 4) measures the diametral deformation of the borehole, using strain-gauged cantilevers. It cannot measure the complete state of stress from a single borehole, but it is rapid and simple to operate. The other overcoring methods are adaptations of the original Leeman triaxial cell, which measures the strain at nine or more positions on or near the wall of the pilot borehole. The Leeman gauge configuration allows the complete state of stress to be calculated from a single borehole. The LuH cell (Chapter 3) is very similar to the original Leeman cell. The basic procedure consists of bonding three strain-gauge rosettes containing four gauges each to the wall of the pilot bore. The University of Luleå's contribution consists of improving the emplacement of the gauges and

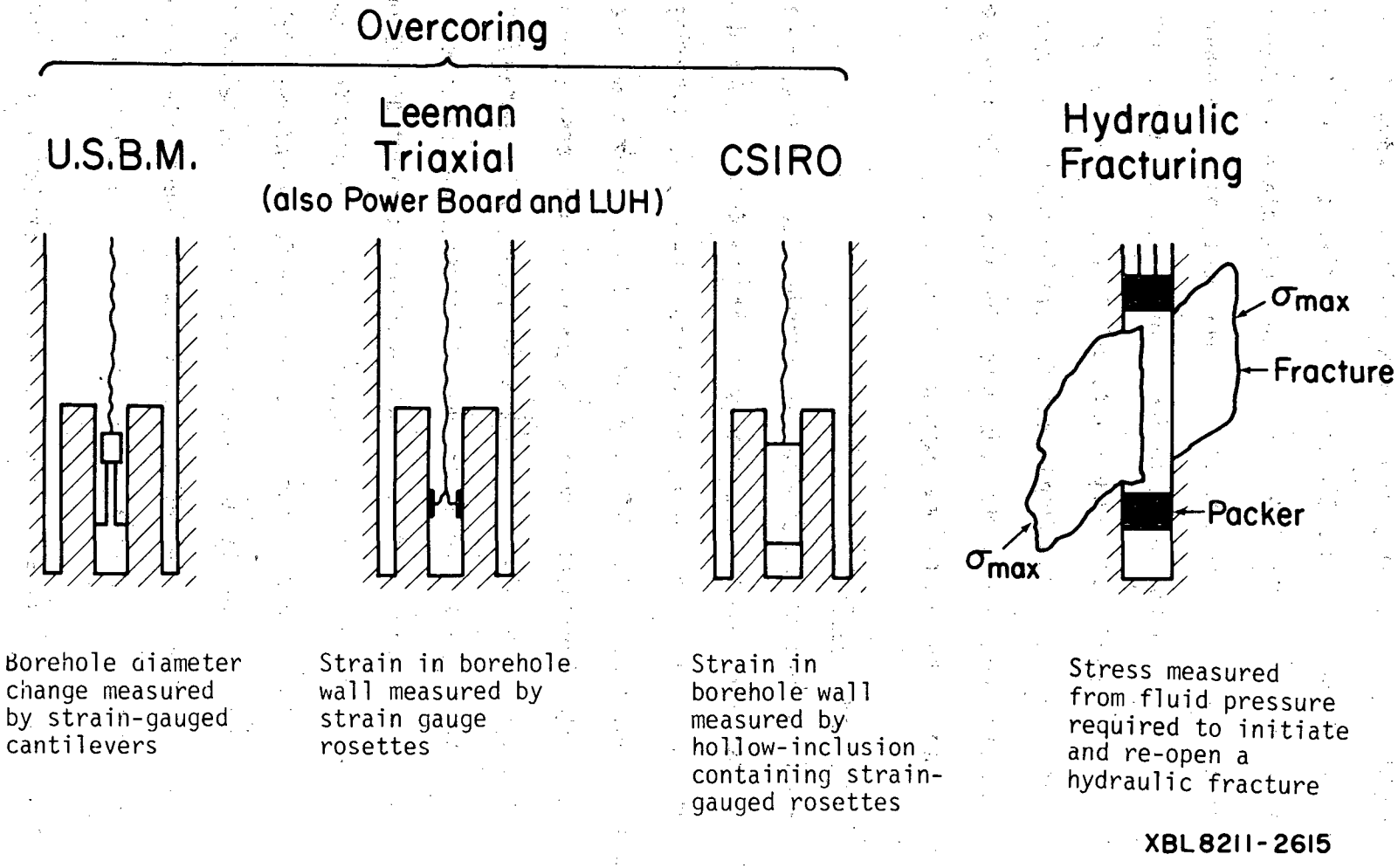

Fig. 1.3 Basic configuration of methods used to measure stress at Stripa.

better cleaning of the pilot bore. The Swedish State Power Board's Leeman cell (Chapters 2 and 5) is a wire-line adaptation of the original cell for use in 76-mm holes (the standard NX hole diameter used in most site exploration). The Power Board's arrangements allow measurements to be made in holes as long as 500 meters. The CSIRO hollow inclusion cell (Chapter 6) puts the strain gauges into a hollow epoxy inclusion that is grouted into the rock. Interpretation is similar to that of other triaxial cell methods except for adding calibration factors to account for the material between the gauges and the rock.

1.4 Experimental Approach

The stress measurement program was carried out in two stages. The first stage was to determine the state of stress at a location where the influence of the mine openings would be small (the far-field stress). A 381 m borehole, SBH-4, was drilled about 300 m north of the mine (Fig. 1.2). The locations of this and other stress measurement boreholes are given in mine coordinates in Table 1.1. During the drilling, the Swedish State Power Board made 17 stress measurements with its deep-hole triaxial cell. These measurements were performed in groups of four or five at four depths: 100, 200, 300, and 380 m. After the hole was completed, 16 hydrofracturing tests were performed between 25 m and 369 m depth, with a majority made around the depth of the test facility (about 320 m). This work was the first to combine deep-hole over coring with hydraulic fracturing at a common site or in a common hole.

The second stage was to measure the in situ stress in the immediate vicinity of the full-scale heater experiment (Figs. 1.2 and 1.4). For

Table 1.1. Collar locations of stress measurement holes. (Stripa mine coordinates, meters)

Borehole	X	Y	Z
BSP-1	315.57	992.48	338.80
BSP-2	309.2	1002.5	344.8
BSP-3	311.92	1007.80	344.80
SBH-4	674.4	1001.2	29.1

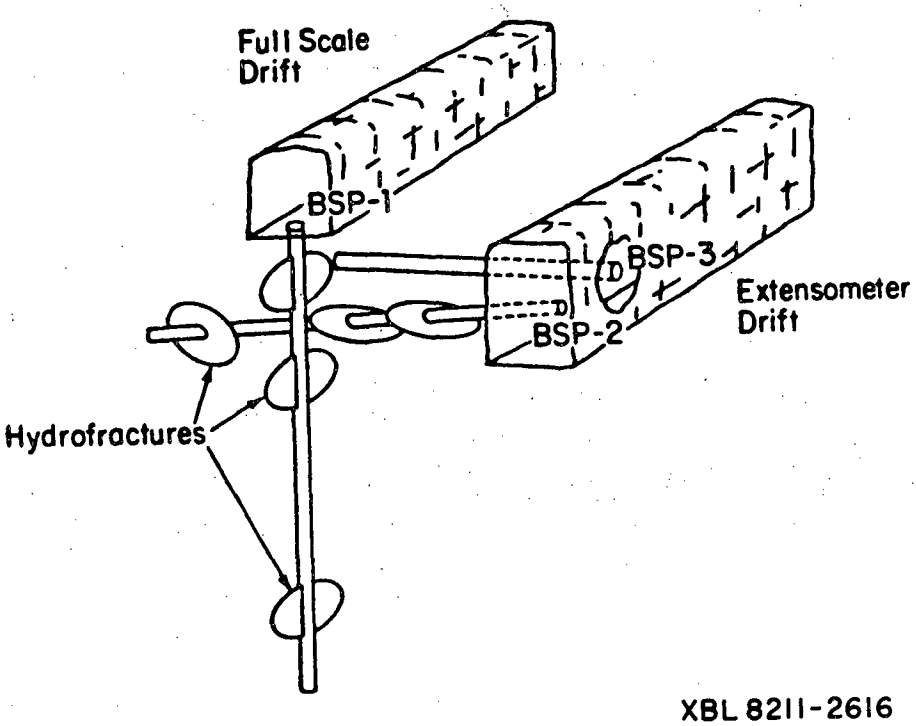

Fig. 1.4 Relative positions of the full-scale drift, the extensometer drift, and the stress measurement boreholes. Orientations of typical hydraulic fractures are shown for the 76 mm holes, BSP-1 and 2. Swedish State Power Board overcores were taken in BSP-3.

this stage, three holes were drilled. A hole for hydrofracturing and Power Board overcore measurements, BSP-1 (BSP stands for bergspänning, "rock stress" in Swedish), was drilled vertically downward from the center line of the full-scale drift to a depth of 25 m. BSP-2, a horizontal hole, was 76 mm in diameter and 20 m long, and was used exclusively for hydrofracturing tests. Hole BSP-3 had a diameter of 150 mm and was drilled to a length of 12 m for USBM, CSIRO, and LuH traxial cell measurements. It was drilled at a small angle upward from the horizontal so that water, which affects the bonding of triaxial strain cells, would drain from the hole.

An acoustic emission experiment was set up to detect the propagation of the hydraulic fracture and map its location; it is discussed in Chapter 9.

Besides making a simple comparison of the stress values from the various overcoring techniques, the underground experiment had the following objectives:

- investigating the effect of the hole orientation on the hydrofracture results;
- measuring the influence of the extensometer and full-scale drifts on the in situ stress orientations and magnitudes; and
- investigating the correspondence of the acoustically mapped hydrofracture plane with the plane normal to the least principal stress, as determined by overcoring.

Plans called for making the shallowest overcoring measurements close to the collar of the holes so as to measure the magnitude of the stress concentration around the tunnel. To predict the possible magnitude of the stress concentration and plan the location of the boreholes,

Chan et al. (1981) performed a series of two-dimensional boundary element calculations of the stress field in the area of the full-scale drift, based on the far-field measurements. The results, shown in Fig. 1.5, allowed some idea of what should be expected from the field measurements. Along BSP-1, the vertical hole drilled downward from the center line of the full-scale drift, the principal stress orientations and magnitudes varied little from the far-field values. Along the horizontal holes, BSP-2 and BSP-3, there was a considerable change in the stresses, owing to the influence of the extensometer drift. The maximum stress was vertical near this drift, but it rotated towards the horizontal as the holes approached the full-scale drift.

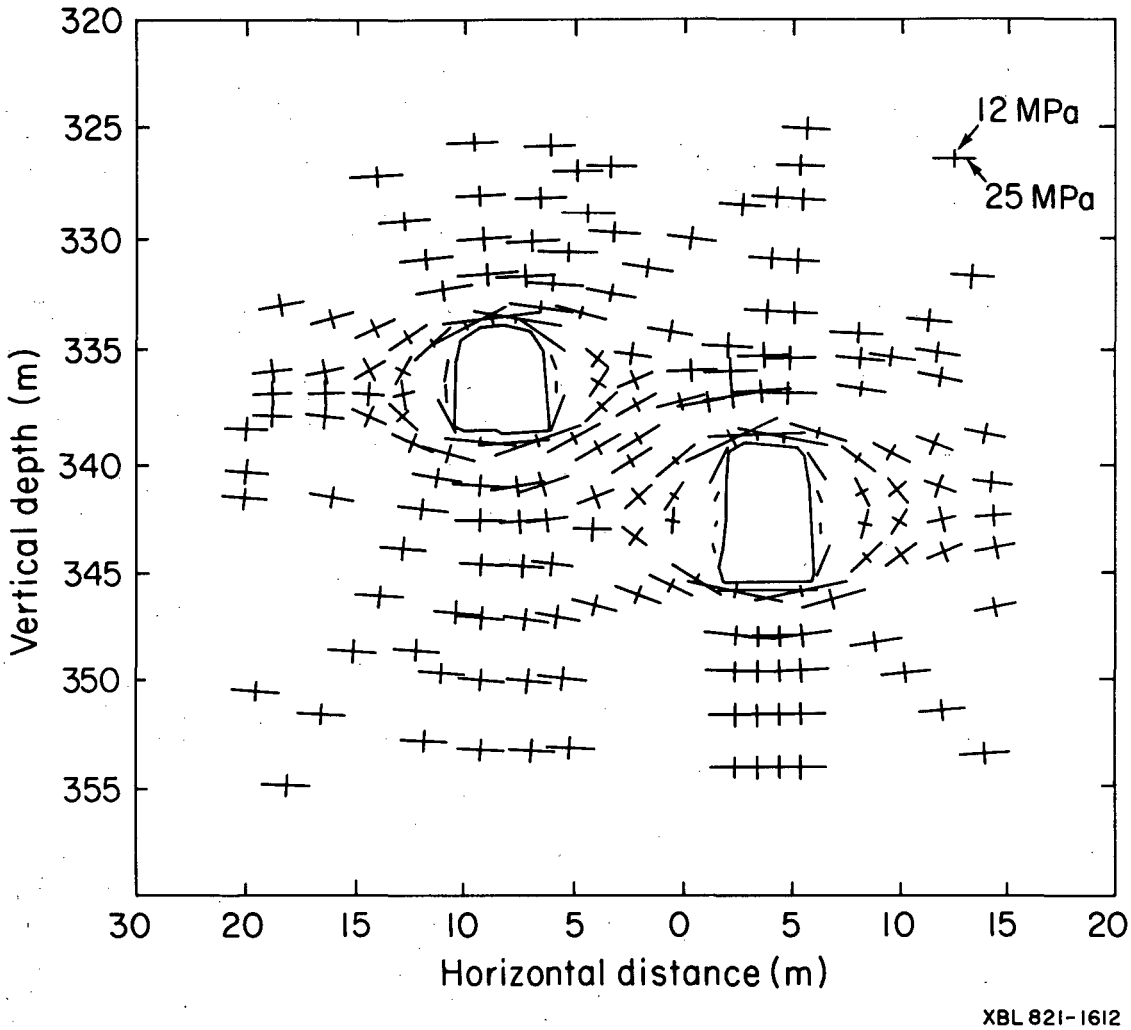

Fig. 1.5 Stress distributions around the full-scale and extensometer drifts, as predicted by boundary element calculation based on far-field results (Chan and Saari, 1981).

2. FAR-FIELD HYDRAULIC FRACTURING AND OVERCORING MEASUREMENTS IN SBH-4 (T.W. Doe, K. Ingevald, and L. Strindell)

2.1 Introduction

The importance of in situ stress measurements for predicting the behavior of underground openings is widely recognized, but the methods have long been the subject of controversy. Besides being generally limited to holes only tens of meters in length, overcoring methods have been surrounded by questions as to the cause of data scatter, roles of residual stresses, and appropriate scale over which to measure strains. The only alternative method for deep measurements, hydraulic fracting, has gained increased acceptance, but questions remain, particularly those concerning noncoincidence of the borehole with one of the principal stresses, the role of tensile strength in data interpretation, and the determination of fracture orientation away from the borehole.

The Swedish State Power Board has recently developed a workable method of performing overcoring measurements in holes hundreds of meters in length. With the need to obtain in situ stress values for the Stripa experiments, we undertook the task of running both the Power Board's Leeman triaxial cell and hydraulic fracturing in the same hole. The objective was therefore twofold--to provide in situ stress data for analysis of the heater test results and to perform basic research on appropriate methods of measuring in situ stress in deep holes. Although overcoring measurements have been made from underground openings at sites where hydraulic fractures had been made from the surface (Haimson, 1981), this work is the first to measure stress in the same deep hole by hydraulic fracturing and overcoring.

2.2 Description of Borehole and Testing

The borehole for the stress measurements, SBH-4, is located approximately 250 m north of the experimental test area at the 348 m level of the mine (Fig. 2.1). The borehole penetrated only medium-grained granite. The collar of SBH-4 at the surface had a vertical mine coordinate of +29.4. The total depth was 381 m or +410.4 in mine coordinates. The borehole showed only slight deviation from the vertical, having a displacement of 4.9 m to the southwest at 372 m depth. The hole was drilled with a 76-mm diameter, double-tube core barrel. The core was continuously logged for fractures to help identify suitably unfractured test zones.

Overcoring measurements were made in groups of four or five every 100 m in the hole. Hydraulic fractures were made roughly every 50 m, with additional measurements below 300 m.

2.3 Overcoring Measurements

2.3.1 Background

Overcoring measurements used the Swedish State Power Board's deep-hole Leeman triaxial cell. The technique measures the complete state of stress from a single hole by overcoring a set of 3 three-component strain-gauge rosettes cemented to the wall of a 38-mm pilot hole. Each rosette has an axial, a tangential, and an oblique (45°) component. Although the tools and theory of the Leeman triaxial cell were developed over 10 years ago (Leeman and Hayes, 1966; Leeman, 1971), earlier versions required dry boreholes and could only be emplaced in holes a few tens of meters long. The Swedish modifications include

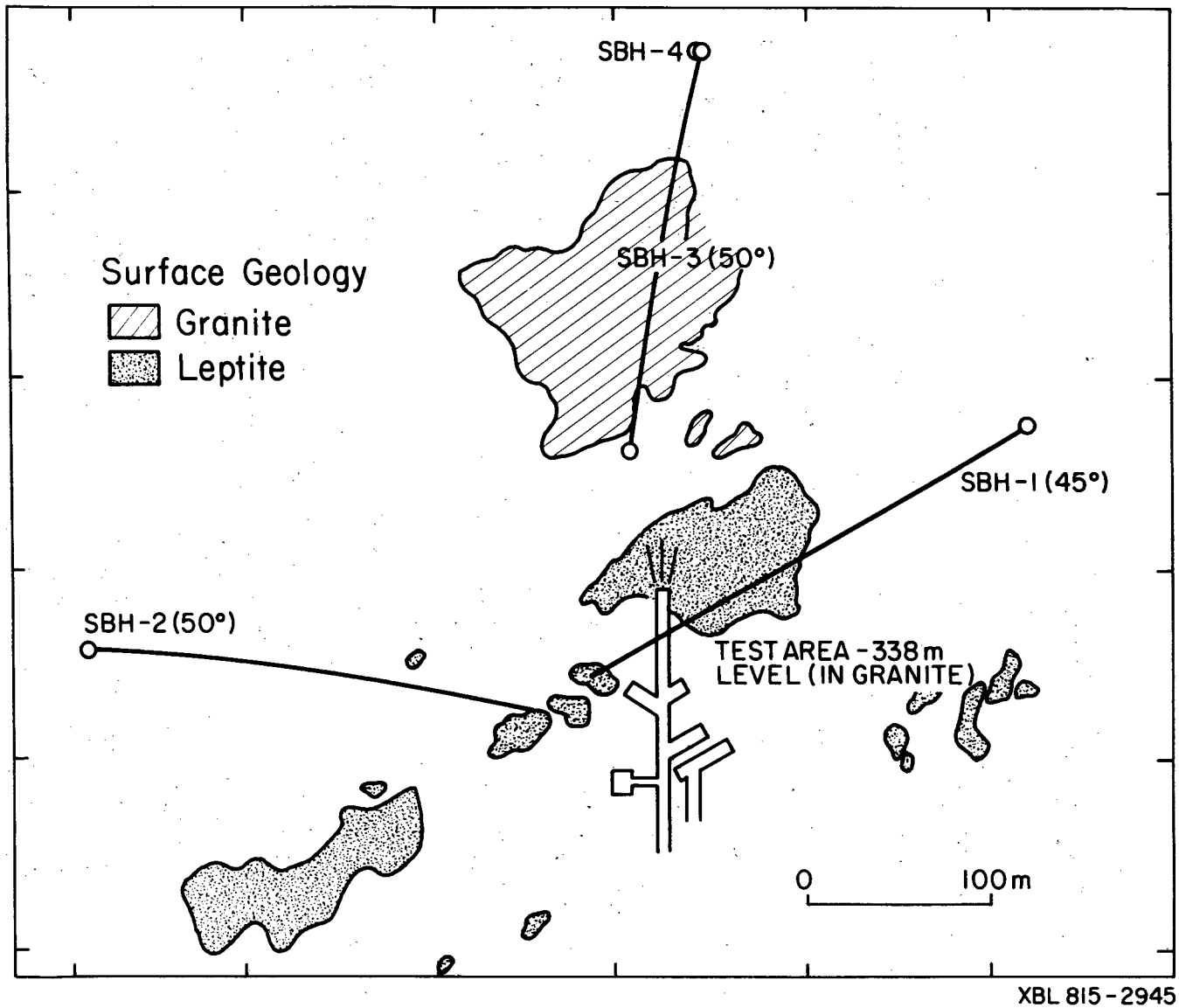

Fig. 2.1 Location of underground experiment areas and surface boreholes at Stripa. Stress measurement hole is collared at SBH-3 and vertical. Scale is in meters.

design of a wire-line emplacement tool for the gauges and development of an underwater cement. Further details may be found in Hiltscher et al. (1979).

2.3.2 Performance of the Measurements

Figure 2.2 shows schematically the course of the measurement procedure.

(1) A borehole with a diameter of 76 mm is drilled to the desired depth. The last core must be broken by pulling and not by twisting. This breaks the core perpendicular to the borehole axis, which greatly facilitates drilling of the smaller bore.

(2) The small bore (36 mm diameter) is centered on the bottom of the larger bore and drilled for about 400 mm.

(3) From the small core, it can be judged whether the rock and the pilot borehole wall are suitable for stress measurement. If the proper conditions are not fulfilled, the 76 mm bore must be continued and the procedure repeated further down. The bore must be thoroughly washed (about 30 minutes at 2 MPa overpressure in a hole 300 m in depth) before the small core is hoisted to remove all drill cuttings. Otherwise, the cuttings will settle, become attached to the bore walls, and disturb the cementing of the gauge. The success of the washing can be checked by inspecting the bottom of the small bore and the glue pot after the overcored gauges have been recovered. The probe, strain-gauge chamber, and glue pot are shown in Fig. 2.3.

(4) While the probe is hanging over the borehole, the acrylic glue is mixed, the glue pot is filled, the strain-gauge rosettes are submerged in the glue, and air bubbles are pressed out of the polyurethane foam layer within the glue pot. Then the probe is lowered into the borehole, rather quickly at first (it is slowed by the water in the hole) and very carefully for the last few meters. Finally, the glue pot and the strain-gauge carrier are inserted into the pilot hole.

(5) When the correct position for cementing is reached (this position is adjustable), two pinpoints touch the bottom of the large bore. The weight of the probe then pushes the glue pot downward, liberating the tongues of the gauge carrier, and the downward-moving, central cone presses the strain gauges against the bore wall. During the hardening of the cement (about 2 hours), the compass is heated electrically, so that the fluid is melted and the compass needle can adjust itself. After the heat is turned off, the fluid solidifies, thus locking the compass (Fig. 2.4) into its downhole orientation. After the cement has hardened, nine strain gauges are measured for the first time.

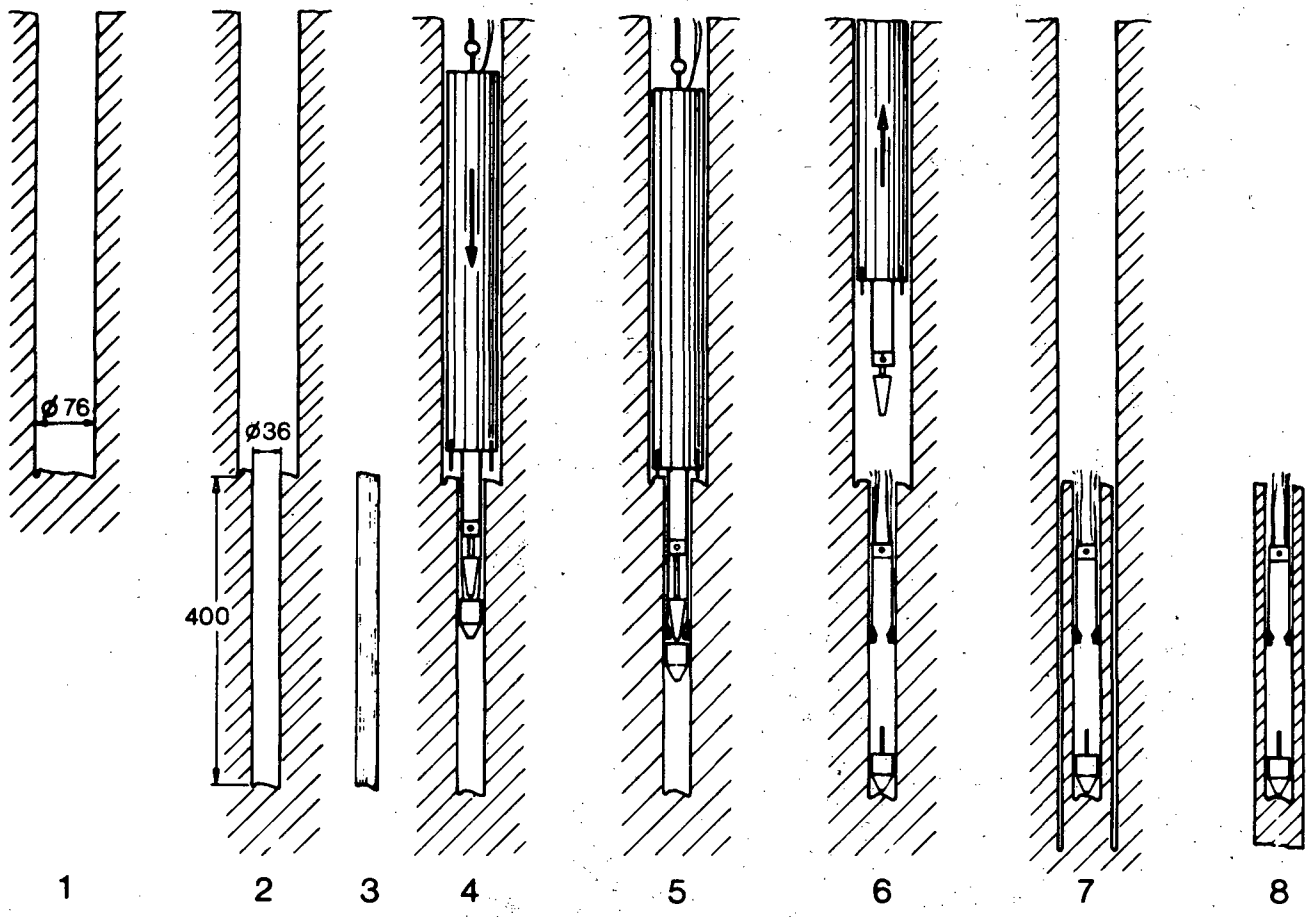

XBL 8011-12797

Fig. 2.2 Procedure for overcoring stress measurements: (1) main 76 mm borehole, (2) drilling of 36 mm pilot hole, (3) appraisal of rock quality, (4) positioning of stress probe before setting gauges, (5) cementing gauges, recording initial strains, (6) release of strain-gauge carrier and removal of probe, (7) overcoring, (8) removal of strain gauges and second strain measurement (from Hiltscher, et al., 1979).

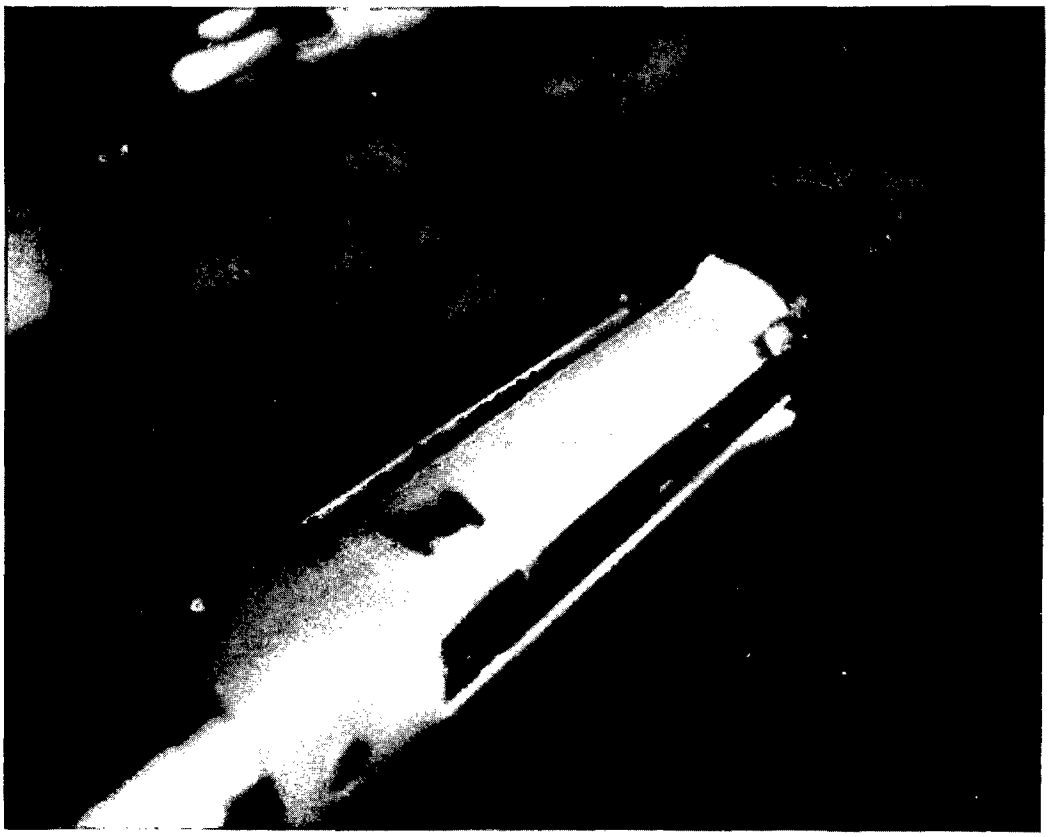

CBB 809-11101

Fig. 2.3 Leeman cell stress gauge.

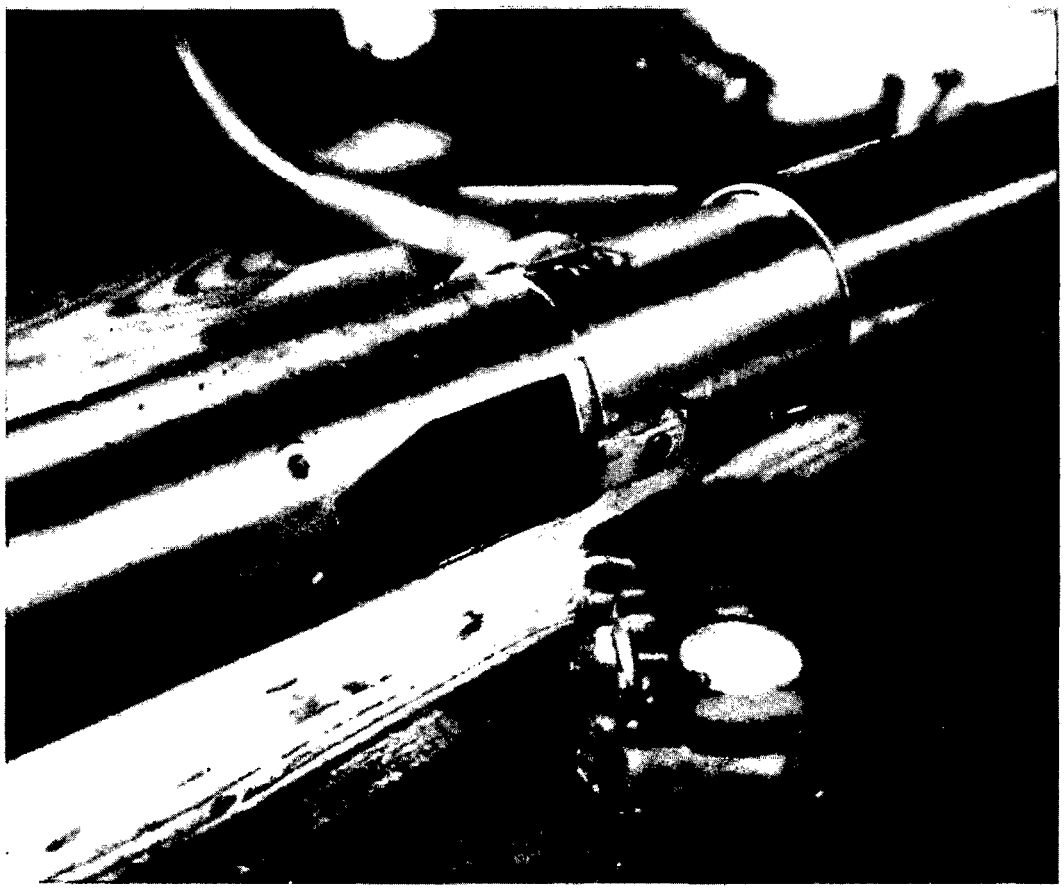

CBB 809-11095

Fig. 2.4 Compass for orienting Leeman stres measurement probe.

(6) The probe is hoisted. At the start of the movement, the gauge carrier is detached and the wires cut off. The carrier is left in the borehole with the gauges, fixed to them by a soft butyl-rubber tape.

(7) By overcoring with the 76 mm bit, a destressed, hollow core containing the gauges is obtained.

(8) As soon as this core has been hoisted, the wires of the gauges are reconnected to those of the probe. The gauges on the relaxed core are measured again, using exactly the same wiring as before. During this second measurement, the core must be carefully kept at the same temperature as in the borehole. In order to observe any creep or the influence of any water trapped in the cement, the measurements are continued for about half an hour. Barring complications, one measurement at a depth of 200 m requires about 5 hours, including all drilling and hardening time.

In all, 17 measurements were made at 110, 200, 300, 325 and 380 m depth. The rock contained relatively numerous joints, but most of these were healed. In two cases, the measurements were complicated by the filling of the pilot hole with debris from zones of severely fractured rock. These zones were found at depths of about 90 and 340 m. The fracture zones were grouted with cement, and the measurements were carried out without difficulty.

2.3.3 Gauge Calibration and Stress Calculation

Before the result of a measurement can be accepted, tests must ascertain that the prerequisites for a correct measurement have been fulfilled. Strain gauges glued in a moist atmosphere or underwater onto a cylindrical borehole wall of possibly unsuitable quality must alway be regarded with suspicion. If the gauges show a large amount of creep after relaxation, that is, after the second measurement, intruding water will usually be found to be the cause, and the measurements must be rejected.

The reliability of the gauges and the stress-strain of the rock are checked by cutting the strain cell-bearing cores to a length of 300 mm. The cores are then loaded both in uniaxial compression and with external hydrostatic pressure. This double calibration checks the linearity of the stress-strain relationship of the rock and gives its Poisson's ratio and modulus of elasticity in both axial and transversal directions. Simultaneously, possible creep of the rock can be observed. Laboratory tests further verify the proper bonding of the gauges to the borehole wall. Such calibrations have been carried out on six cores, and an example of the results is shown in Fig. 2.5.

Finally, the magnitudes and directions of the three principal stresses can be calculated for the core from the measurement data according to the formulae of Leeman and Hayes (1966). In most cases, the rock material is not quite isotropic, but more or less orthotropic as regards its modulus of elasticity and Poisson's ratio. This orthotropy could be considered approximately in the calculation of the stresses. The simplest approximation, however, is to use mean values of the elastic constants in the calculations, as if the material were isotropic. This approximation has been made in the present report. There are, however, differences in the modulus of elasticity and the Poisson's ratio between measuring depths. These values, shown in Table 2.1, were used in calculations for the respective levels.

At greater depths, it is necessary to introduce a correction for the additional stresses caused by the water column above the measuring point, stresses that are unloaded while the core is being hoisted. These values

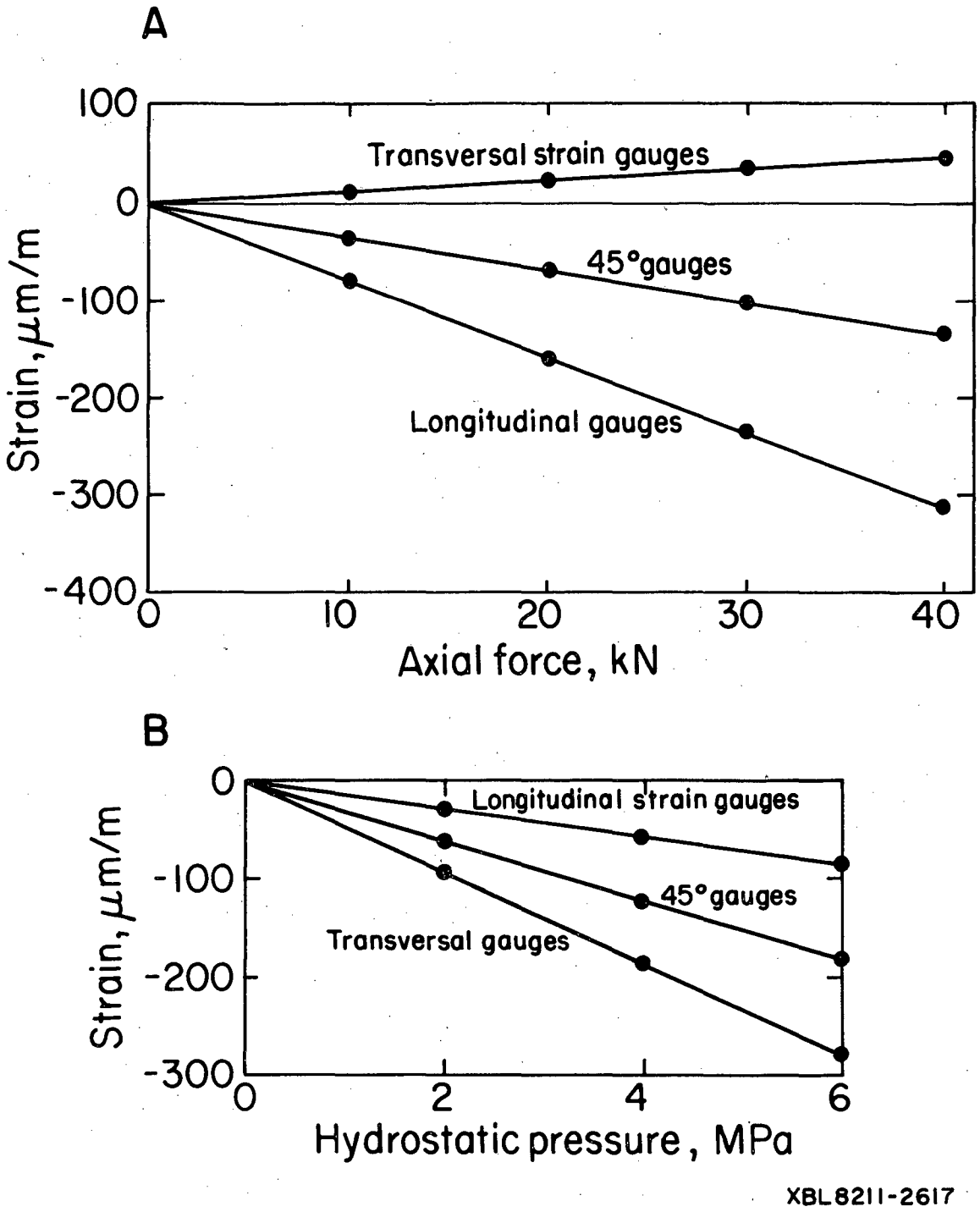

Fig. 2.5 Calibration of strain gauges in core (from overcoring test 109.2): (a) axial loading, (b) hydrostatic loading. Points represent average of three gauges.

Table 2.1. Measured primary strains and calculated corresponding stresses.

Point	Strain (μm/m) Rosette no. 1			Rosette no. 2			Rosette no. 3			Compass Bearing
	$\varepsilon_{long.}$	$\varepsilon_{trans.}$	$\sigma_{45°}$	ε_{long}	$\varepsilon_{trans.}$	$\varepsilon_{45°}$	$\varepsilon_{long.}$	$\varepsilon_{trans.}$	$\varepsilon_{45°}$	
108-1	155	33	36	73	146	15	112	254	232	25°
109-2	42	107	68	-21	-60	-4	10	15	58	158°
110-3	40	54	100	88	444	128	64	117	141	247°
112-4	62	14	-16	31	-2	90	46	134	73	358°
198-5	30	256	143	-14	-60	29	8	441	199	252°
199-6	108	467	338	171	519	770	139	446	387	31°
200-7	63	576	303	-10	343	166	26	223	104	345°
201-8	-21	661	375	-22	750	340	-22	12	-29	330°
300-9	84	459	448	85	581	278	85	209	36	-- a
302-10	89	250	107	92	550	288	90	305	145	313°
303-11	2	590	651	-5	274	250	-1	309	225	-- a
304-12	205	650	334	44	204	103	124	347	104	232°
326-13	92	402	100	10	123	100	50	348	219	79°
374-14	-44	187	199	18	439	162	-13	325	105	325°
379-15	43	772	574	39	249	155	41	374	15	349°
381-16	51	823	591	35	710	357	43	-232	-250	331°
381-17	123	414	452	126	680	364	125	85	-14	314°

Point	Depth (m)	Principal stresses (MPa) σ_1	σ_2	σ_3	Vertical stress (MPa) σ_v	Sec. stresses[a] (MPa) σ_{Hmin}	σ_{Hmax}	Bearing for σ_{Hmax}	E (GPa)	ν
108-1	108.47	15.8	6.8	2.3	12.1	2.7	10.2	36°	66	0.18
109-2	109.72	3.4	1.1	-1.3	1.2	-1.2	3.2	55°		
110-3	110.49	18.3	6.0	4.3	9.0	4.4	15.2	42°		
112-4	112.75	6.8	4.1	-0.7	5.0	-0.7	4.5	31°		
198-5	198.39	14.1	3.2	2.8	3.3	2.8	14.0	121°	58	0.16
199-6	199.65	29.1	18.8	8.3	16.9	18.8	20.5	176°		
200-7	200.28	19.1	11.1	6.9	6.9	11.1	19.1	85°		
201-8	201.79	27.5	9.7	4.0	4.2	9.6	27.4	93°		
300-9	300.72	27.6	20.1	9.3	15.6	15.6	25.8	--b	70	0.19
302-10	302.53	23.0	15.2	14.0	15.3	14.1	22.9	109°		
303-11	303.15	26.2	14.7	4.4	6.9	14.6	23.7	--b		
304-12	304.25	26.8	19.6	13.5	19.2	14.1	26.5	133°		
326-13	326.02	19.7	11.1	8.1	10.1	10.4	18.4	144°	70	0.19
374-14	374.27	19.5	14.0	2.7	4.7	12.1	19.5	132°	73	0.19
379-15	379.10	34.4	18.7	7.0	12.9	15.9	31.4	72°		
380-16	380.10	39.1	16.2	1.3	12.5	5.7	38.4	88°		
381-17	381.20	30.6	22.6	8.3	19.9	12.5	29.2	88°		

[a]The compass was not functioning for the measuring points 300-9 and 303-11.

[b]σ_{Hmax} and σ_{Hmin} are secondary principal stresses in the horizontal plane.

should be subtracted from the measured strain values before the calculation of the stresses is carried out. These corrections are about 5 % of the actual strains at 300 m depth.

2.4 Hydraulic Fracturing Stress Measurement Procedures

2.4.1 Fracturing Equipment

The complete system for hydrofracturing is shown in Figs. 2.6 and 2.7. The system uses a straddle packer assembly consisting of two 67 mm diameter Lynes packer elements separated by perforated tubing sufficient to give a straddle interval of 0.6 m. Mounted above the packer assembly was a watertight housing containing two pressure transducers, one to monitor the pressure in the injection test zone and the other to monitor the packer pressure. Both transducers were of a strain-gauge type with a pressure rating of 34 MPa. A nine-conductor electrical cable manufactured by Advanced Cable Co. transmitted signals from the transducers to the surface.

Water for fracturing was conducted through Hydril 1-inch (25-mm) tubing, which had a threaded joint capable of sealing to 70 MPa. The Hydril tubing also supported hoisting of the packer assembly. The packers were inflated through two 3/16-inch (4.8 mm) Eastman Hytron hydraulic hoses strapped to the Hydril tubing along with the electrical cable. Two hoses were provided as a precaution against problems in deflating the packers, which were water-inflated. In wells where the water level is depressed--as it is at Stripa, because of drainage by the mine--packers may not completely deflate. In that event, the second inflation line would have blown the water out of the first inflation line with compressed air.

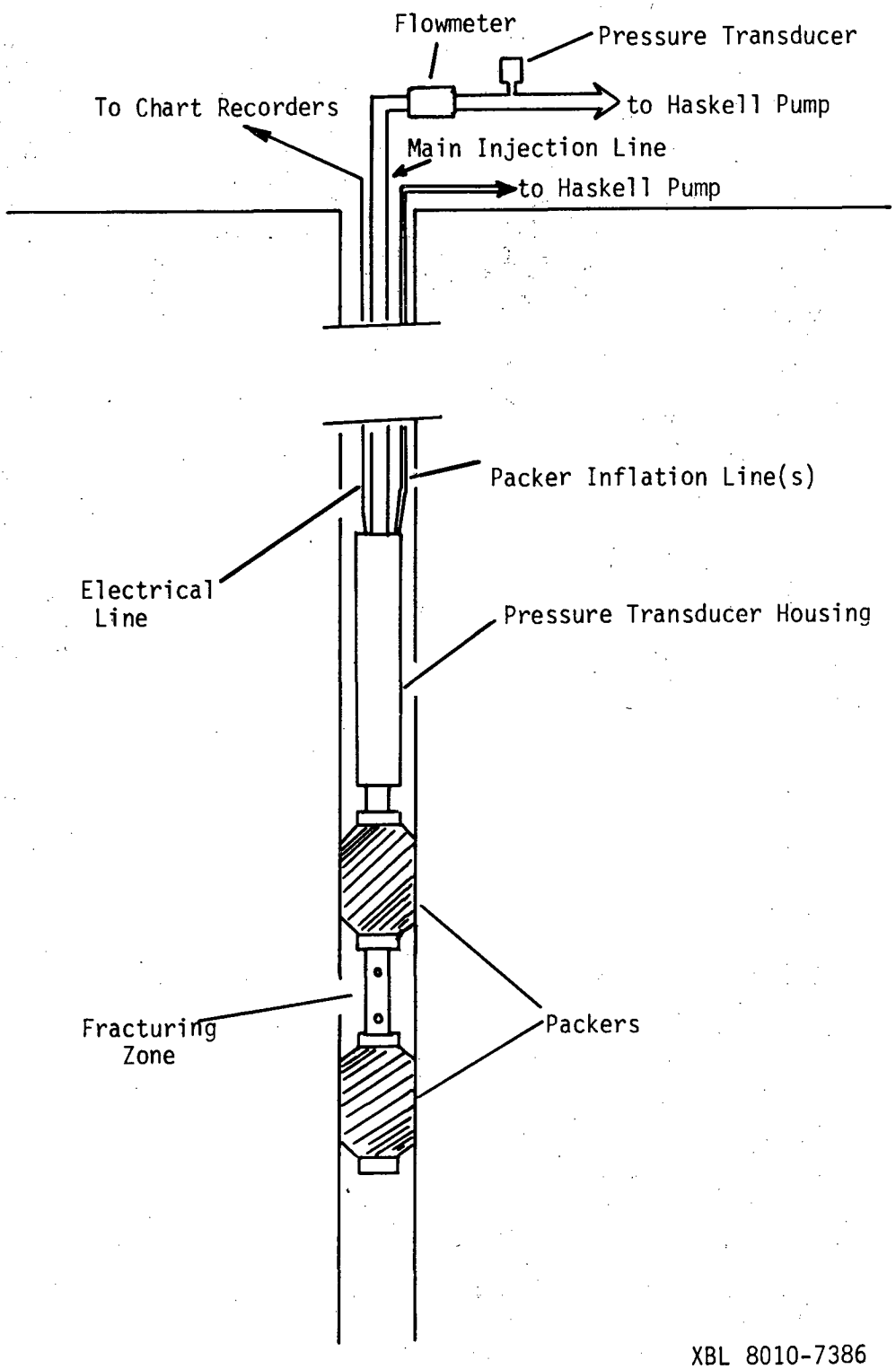

Fig. 2.6 Schematic of packer system for hydraulic fracturing stress measurements.

CBB 809-11091

Fig. 2.7 Photograph of straddle packer system for hydraulic fracturing. Foreground: upper and lower straddle packers; background: pressure transducer housing. Hytron tubing on reels and ends of Hydrill rod can be seen in upper right.

Fracturing was accomplished by a Haskell, air-actuated hydraulic pump capable of developing a flow of about 4 liters per minute at 40 MPa. It was also used to inflate the packers in most tests. The pump was equipped with an air charged accumulator to dampen the pressure surges.

In addition to the pressure transducers downhole, a pressure transducer was mounted in the flow manifold on the surface to serve as a back-up in case of electrical failure of the downhole instruments. A Flow Technologies Omniflow turbine flowmeter was also mounted in the manifold. The flowmeter was rated for 1 to 20 liters/min.

Data from the pressure transducers and flowmeter were recorded on two time-based strip-chart recorders--one recording packer pressure, test zone pressure, and flow rate and the other recording the test zone pressure and manifold pressure.

As the packer assembly was lowered into the hole, the lengths of each pipe placed in the tube string was tallied. These lengths were recorded to the nearest millimeter to assure location of the packers at the desired test zones. The fracture tests were conducted from the top of the hole down so that the time to remove the packers would be minimal had problems arisen. Test zones were selected to be free of pre-existing fractures.

Once the packers had been lowered to the desired zone, they were inflated to a pressure exceeding the expected breakdown pressure. For most tests, this pressure was about 17 MPa. Originally we had expected to set the packers at a lower pressure, relying on the pressure increase

in the zone between the packers to increase the pressure of the seal. Such interaction of packer and injection-zone pressures has been observed by others also engaged in hydraulic fracturing for stress measurement (Kim and Smith, 1980). The correspondence of zone and packer pressure only occurred when we used packers that did not contain bands of carbide grit at the ends of the elements. These bands are welded to some packers to improve their grip on the borehole wall. When we used packers containing the grit bands, the packer pressure would not increase with the zone pressure.

Once the packers were set, pressure in the test zone was raised at a rate of 14 MPa/minute until fracturing was indicated by an increase in the pumping rate. As soon as fracturing was felt to have occurred, the manifold was shut in and the pressure monitored for 2 to 4 minutes. This procedure was repeated two to four times to observe secondary breakdown pressures, and to obtain more shut-in pressure values. One test, in which the test zone was slowly pumped up to the pressure where the fracture would just begin to open, was run at each test level to further set the value of the of the shut-in pressure. A typical record is shown in Fig. 2.8.

When the fracturing experiment was completed, the pressure on the packers was released at the surface, and the hole was filled with water to speed deflation. Since the packer pressure was being monitored downhole, the release of the packers could clearly be seen by the equilibration of the packer and zone pressures; hence, damage to the packers from premature hoisting was easily avoided.

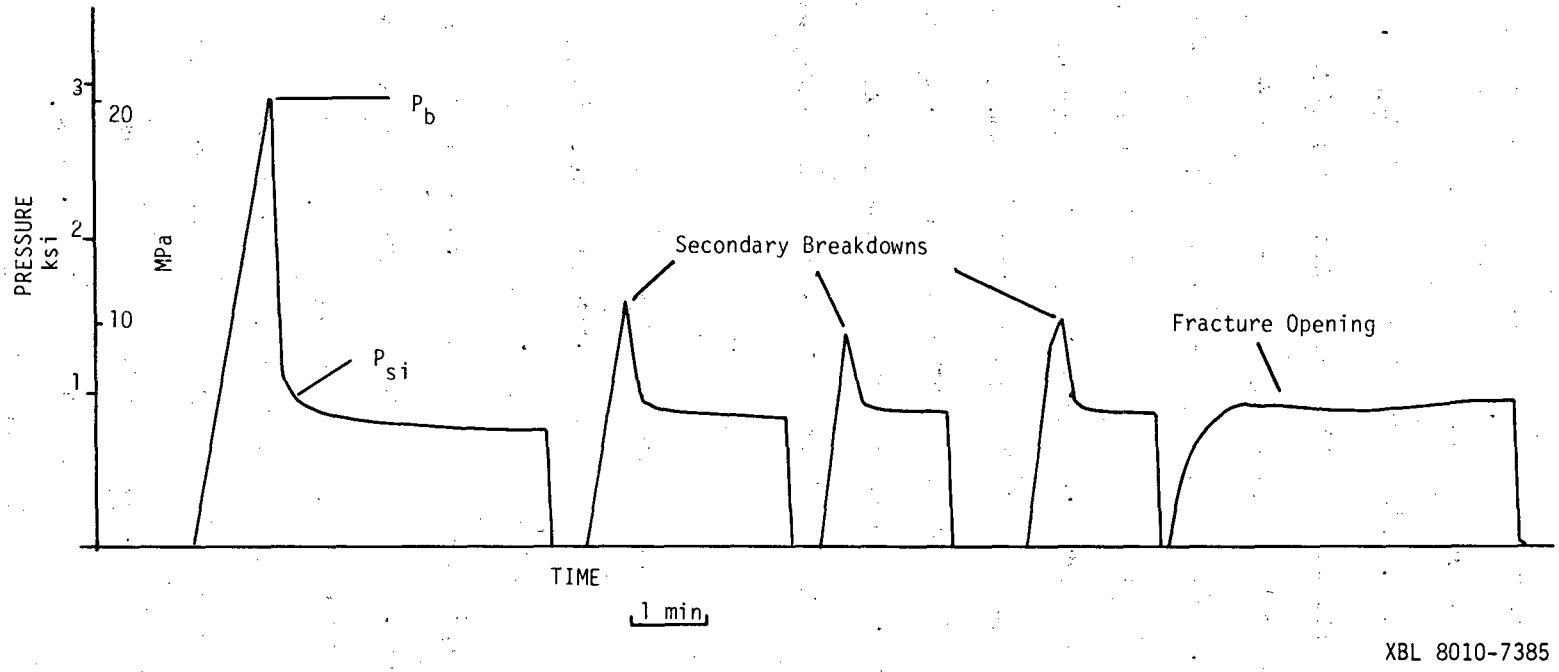

Fig. 2.8 Typical hydraulic fracturing pressure-time record (test 17, 304.9 m).

2.4.2 Impression Packer Equipment and Procedures

Once the fracture experiments were completed, impressions of the test zone were carried out to determine the orientation of the fractures. The equipment consisted of a TAM International Inc., 1-7/8 inch (48 mm) packer element with a removable sleeve coated with a soft rubber. This rubber was capable, under pressure, of extrusion into the fracture. The packer was placed below a Sperry Sun 35 mm, single shot, magnetic borehole survey compass modified to screw directly into the packer end cap. The compass was separated from the packer by 3 feet of nonmagnetic tubing to eliminate any effect the packer might have on the compass. This assembly was attached to a wire line, inflated pneumatically through the hydraulic tubing that was used in the fracturing experiment, and hoisted. The wire-line hoist included a cable counter to assure proper depth of emplacement.

Once the packer sleeve was in place, a film disc was inserted into the camera on the borehole compass. The camera was set by a timer to record compass orientation after lowering and inflation of the packer. For the greatest depths, this delay was only 45 minutes, including 15 minutes for inflation of the packer. Packer pressure was set between the shut-in pressure and the secondary breakdown pressure to assure opening of the fracture and extrusion of the packer rubber into the crack. The packer was left inflated during the exposure of the film disc in the compass (about one half hour). Retrieving the impression packer from the deepest tests took about 25 minutes, a considerable saving of time over conventional emplacement of packers on rigid tubing. Once the impression system was out of the hole, the film disc was immediately

developed and stored. Most of the impression sleeves were used two or three times, and the impressions from each test were painted with different colors as soon as the packer was dry to avoid confusion. Figure 2.9 is a schematic of the system, which hangs from the tower of the drill rig in Fig. 2.10.

2.4.3 Hydrofracturing Data Analysis: Basic Relationships

Three methods of analyzing hydrofracture data have been proposed. The first is the elastic solution based on a hole in an infinite plate (Haimson and Fairhurst, 1970):

$$\sigma_{Hmax} = 3\sigma_{Hmin} - P_{b1} + T - P \qquad (2.1)$$

where σ_{Hmax} = maximum horizontal stress

σ_{Hmin} = minimum horizontal stress = P_{si}, the shut in-pressure

P_{b1} = first breakdown pressure

T = hydrofracture tensile strength

P = pore pressure

The locations of P_{b1} and P_{si} on the pressure-time record are shown in Fig. 2.8, and the values for the SBH-1 data are given in Table 2.2. Determination of P_{si} and T are discussed further in Sections 2.4.4 and 2.4.5.

The second method arises from the difficulties of obtaining reliable tensile strength data. Bredehoeft et al. (1976) suggested that tensile strength should be the difference between the first and subsequent breakdown pressures, so that from Eq. (2.1) the stress formula would be:

$$\sigma_{Hmax} = 3\sigma_{Hmin} - P_{b2} - P \qquad (2.2)$$

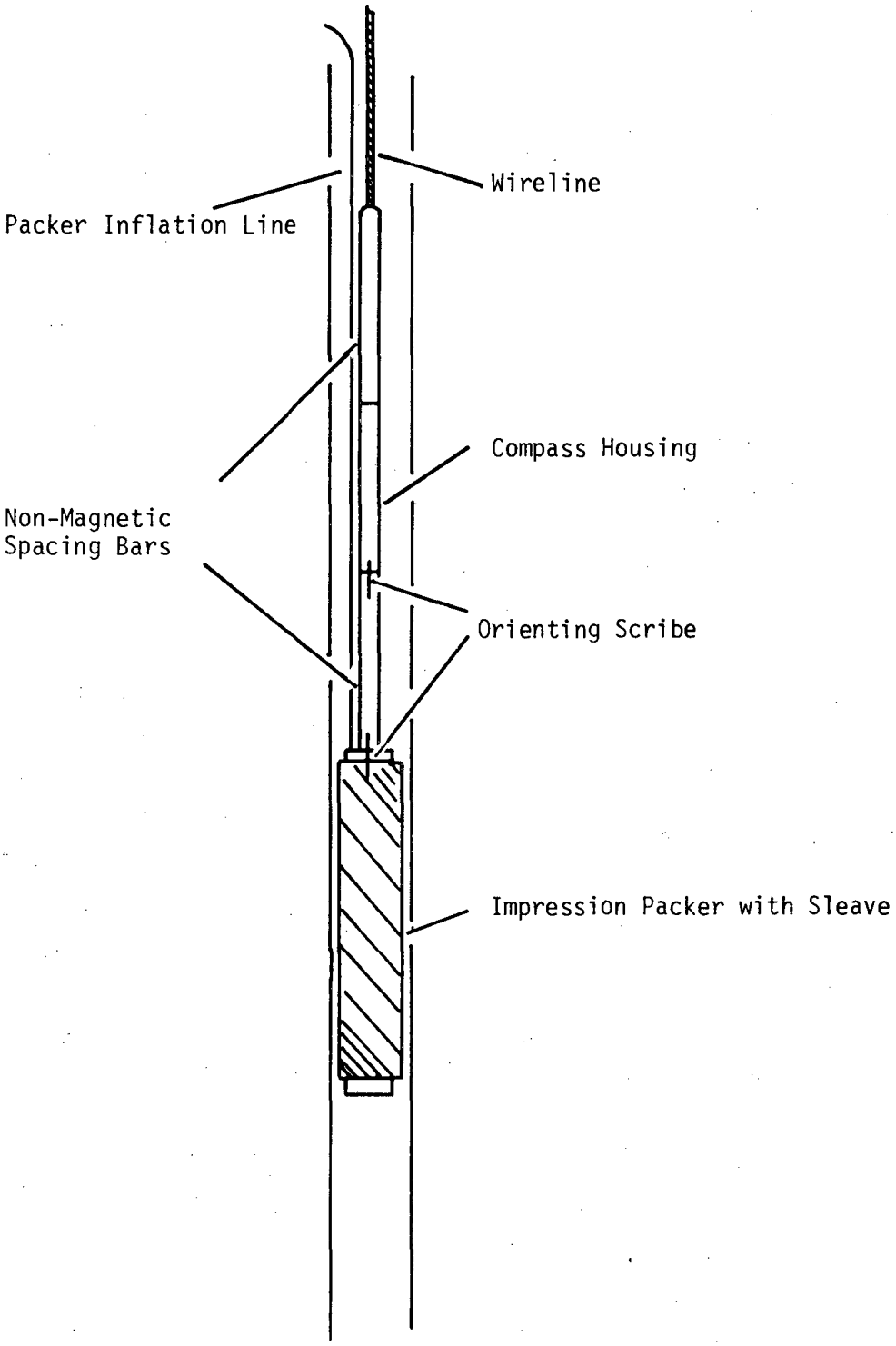

Fig. 2.9 Diagram of impression packer system.

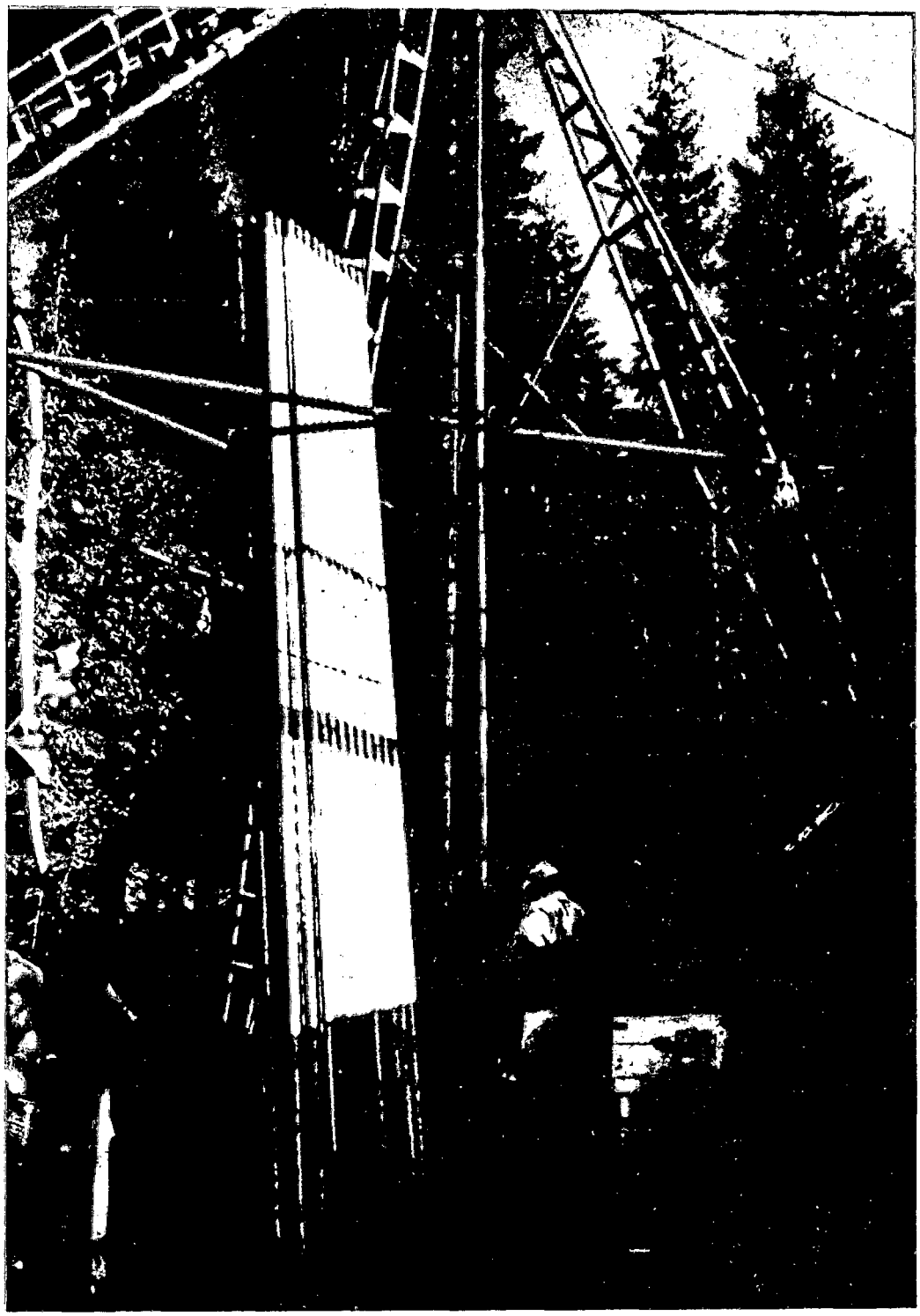

CBB 809-11089

Fig. 2.10 Surface installation of impression packer system.

Table 2.2. Hydrofracture results, SBH-4.

Test	Depth (m)	Pore Pressure P_H (MPa)	First Breakdown P_{b1} (MPa)	Second Breakdown P_{b2} (MPa)	Field Tensile Strength $(P_{b1}-P_{b2})$ (MPa)	Shut-in Pressure P_S (MPa)	Vertical Stress σ_v (MPa)	In Situ Stresses Second Breakdown Method		In Situ Stresses First Breakdown Method	
								σ_{Hmax} (MPa)	σ_{Hmin} (MPa)	σ_{Hmax}[a] (MPa)	σ_{Hmin} (MPa)
1	28.5	0.3	4.1	2.6	1.1	1.4	0.7	1.8	1.7	10.6	1.7
4	52.2	0.5	6.9	4.8	2.1	3.7	1.3	6.6	4.1	14.9	4.1
5	101.2	1.0	9.9	6.2	3.7	5.2	2.6	10.3	6.1	16.9	6.1
6	153.2	1.5	7.7	5.2	2.6	4.1	3.9	8.7	5.6	16.6	5.6
7	203.8	2.0	13.6	6.5	7.1	4.5	5.2	9.0	6.5	12.0	6.5
19	201.4	2.0	9.7	6.6	3.1	5.4	5.2	11.6	7.4	18.8	7.4
8	251.6	2.5	14.4	13.2	4.1	9.9	6.5	18.8	12.3	25.7	12.3
18	279.6	2.7	16.1	9.7	6.5	8.0	7.1	17.1	10.8	20.8	10.8
17	304.9	3.0	20.0	10.1	9.9	6.6	7.8	12.8	9.6	13.2	9.6
9	308.6	3.0	11.7	7.6	4.1	6.1	7.9	13.7	9.1	19.9	9.1
10	318.1	3.1	18.6	13.0	5.6	8.6	8.1	15.9	11.7	20.7	11.7
16	325.8	3.2	16.0	11.6	4.9	10.5	8.4	23.0	13.7	29.0	13.7
11	328.6	3.2	14.4	8.3	5.2	7.9	8.5	18.8	11.2	23.9	11.2
13	356.7	3.5	14.8	12.6	2.3	8.8	9.1	17.4	12.3	26.9	12.3
14	367.1	3.6	14.5	10.3	4.1	7.0	9.4	14.4	10.6	20.6	10.6
15	369.7	3.6	15.0	11.3	3.7	8.6	9.5	18.2	12.3	24.9	12.3

[a] T_0 = 10.3 MPa.

It should be recognized that this formula is applicable only for $\sigma_{Hmax} \leq 2\sigma_{Hmin}$. If $\sigma_{Hmax} = 2\ \sigma_{Hmin} = 2\ P_{si}$, Eq. (2.2) becomes (for zero pore pressure):

$$2\ P_{si} = 3\ P_{si} - P_{b2}$$

or

$$P_{b2} = P_{si} \quad ;$$

hence, the second breakdown would be less than the shut-in pressure. Such ratios of σ_{Hmax} to σ_{Hmin} are common, and errors in analysis could arise if the second breakdown were strongly influenced by such factors as pumping rate.

A third method was proposed by Abou-Sayed et al. (1978) and is based on fracture mechanics. Although it is an elegant treatment of the problem, solution depends on knowing fracture toughness and the size of the critical flaw from which the fracture initiated. Because the latter cannot easily be determined, Abou-Sayed's fracture mechanics approach was not used except as a method for interpreting size effect data for the tensile tests (Sec. 2.4.6).

2.4.4 Shut-in Pressure

The breakdown pressures were readily determined from the pressure-time records (Fig. 2.8); however, determination of the shut-in pressures required some subjectivity. Previous analysts of hydrofracture data have used such criteria as the value to which pressure rapidly drops after breakdown has occurred or long-term stable pressure values. Both conditions are affected by instrumentation factors, such as the speed of the chart recorder, as well as by conditions in the rock, such as a connection

of the hydrofracture to another fracture. The approach used in selecting shut-in pressures in this work is based on the pressure-pulse permeability test in a single fracture (Wang et al., 1977). One can consider the post-breakdown pressure behavior as being similar to a pulse test where the fracture aperture is large at pressures greater than the in situ stress and smaller where pressures are less. The pressure-time record should then behave as a two-stage pulse test. The shut-in pressure could then be taken as a sharp break in the semi-logarithmic plot of pressure versus time; an example of such a plot is shown in Fig. 2.11. Shut-in pressures obtained by this technique were in excellent agreement with the pressures required to open the fracture by slow pumping.

2.4.5 Tensile Strength

Tensile strength is a major source of controversy in hydrofracture analysis. Tensile strengths generally have been obtained for cores from small-scale hydraulic fracture experiments (Haimson, 1978). The holes are typically 10 mm or less. It is well-known that tensile strength is size-dependent, but it has not been clear how to extrapolate the small-core data to the expected tensile strength of rock from the 76 mm holes used in field experiments.

Laboratory tensile strength tests were run on 44 samples of core taken from stress measurement zones in SBH-4. Roughly half were from 7 mm (1/4 inch) holes, the other half from 15 mm (1/2 inch) holes. Strength values were influenced by both hole diameter and the presence of healed fractures. Of the healed joints, only epidote or calcite fractures had

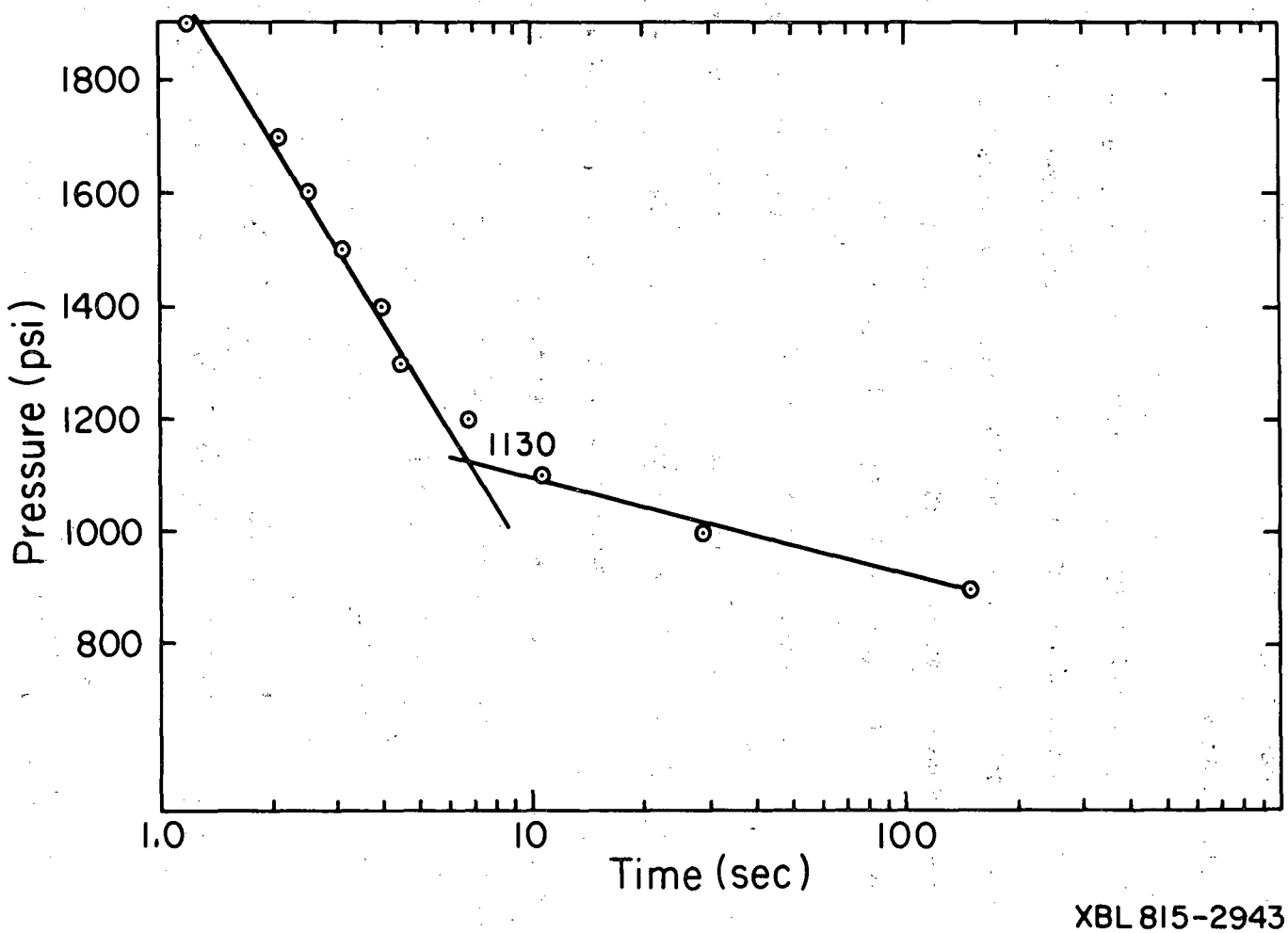

Fig. 2.11 Semi-logarithmic plot of post-breakdown pressure versus time (Test 11, 328.6 m).

any effect; chlorite- or quartz-healed fractures showed no reduction in strength in the intact samples. Table 2.3 summarizes the tensile test results. Figure 2.12 shows examples of failure on both an intact rock and a healed joint.

Acoustic emissions were monitored for each test to determine the onset of failure. Zoback et al. (1977) had found pre-breakdown acoustic behavior, which suggested to them that failure preceded loss of fluid pressure. However, we found little or no acoustic activity before breakdown. Figure 2.13 shows a typical record.

The laboratory tests reaffirmed findings by other investigators that hydrofracture tensile strength is dependent on size. Since the laboratory values are for hole diameters smaller than the 76 mm diameter used in the field, it is necessary to extrapolate these results to the larger diameter. We used two approaches to do this. The first was the deterministic fracture mechanics approach to tensile failure of Paris and Sih (1965). The second was a statistical fracture mechanics approach developed by Ratigan (1981), based on the methods of Weibull.

2.4.6 Deterministic Fracture Mechanics Approach to Tensile Strength

For a sample under no radial load, Abou-Sayed's breakdown equation (1978, Eq. (17)) reduces to:

$$P_b = \frac{K_{1c}}{F(L\sqrt{r})\sqrt{\pi L}} \qquad (2.3)$$

where K_{1c} = critical stress intensity

L = crack length

Table 2.3. Hydrofracture tensile strength data.

	Hole Diameter			
	1/4-inch holes (7 mm)		1/2-inch holes (13 mm)	
	No.	MPa	No.	MPa
Intact rock	12	15.8±1.5	6	12.2±0.6
Chlorite-quartz jointed	5	17.4±0.9	12	13.2±1.7
Epidote-calcite jointed	5	13.0±1.2	4	10.8±0.4

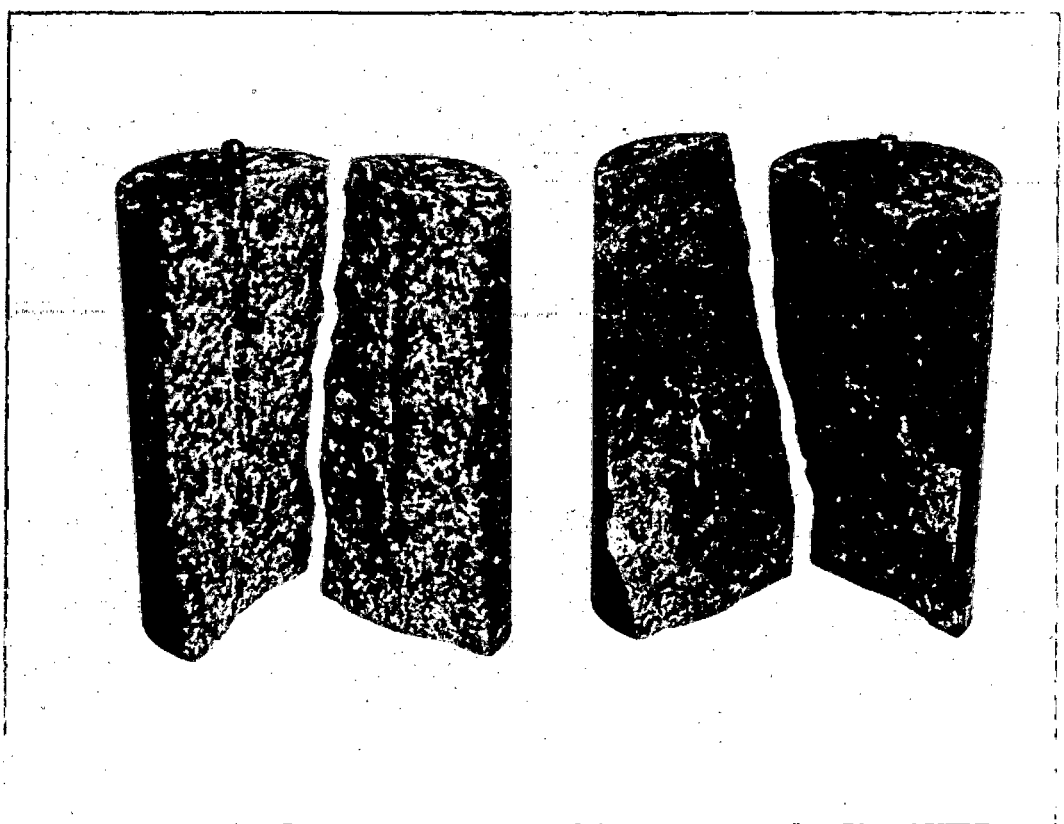

Fig. 2.12 Hydrofracture tensile-strength test specimens: Left, intact rock; right, epidote-coated, jointed specimen.

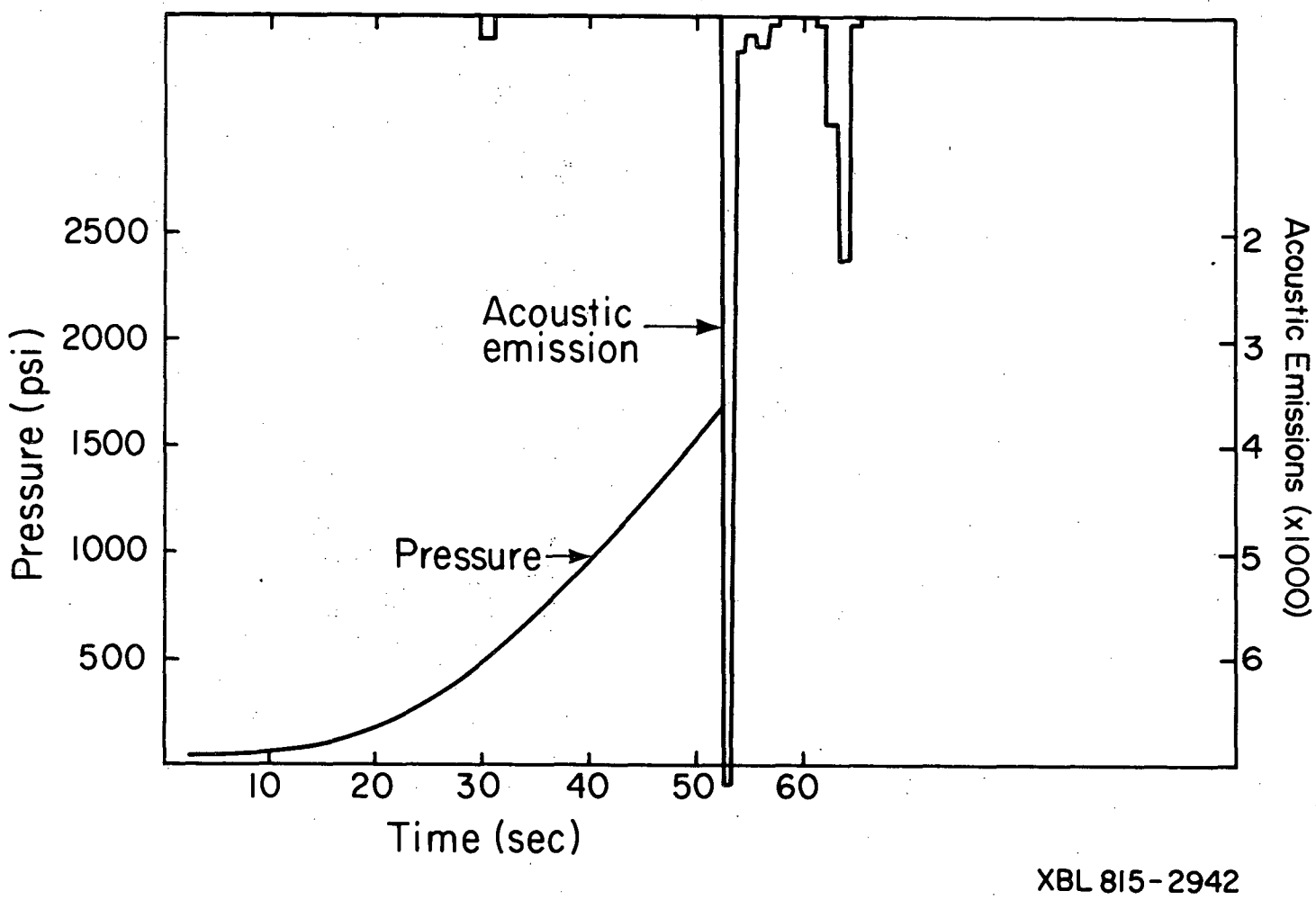

Fig. 2.13 Typical acoustic-emission and pressure-time record for hydro-fracture tensile-strength test.

r = hole radius

$F(L/r)$ = stress intensity coefficient (from Paris and Sih, 1965, Table 7).

Grain sizes of the Stripa granite are 1 to 5 mm (Olkiewicz et al., 1979). Assuming that failure will occur on the larger grain boundary cracks, we can use an L of 5.5 mm (0.25 inch). The ratio of the tensile strengths for two borehole diameters can readily be obtained from Eq. (2.3) as

$$\frac{P_b \text{ at } r_1}{P_b \text{ at } r_2} = \frac{F(L/r_2)}{F(L/r_1)} \tag{2.4}$$

For a crack size of 6 mm, we can use Eq. (2.4) and Table 7 of Paris and Sih to predict size effects in 13 mm and 76 mm holes for a single crack under uniaxial load. Given a tensile strength of 16 MPa for the 6 mm hole, we get the following tensile strengths for the other hole sizes:

Hole Size	L/r	F(L/r)	T(MPa)
3"	0.08	2.84	8 MPa
1/2"	0.5	1.73	13 MPa
1/4"	1	1.37	16 MPa

The calculated strengths for the larger laboratory test holes agree well with the observed strengths. The strengths of 3-inch holes are then calculated as 54% of the 0.25-inch holes; Rummel and Jung (1975) observed that the ratio in their tests in limestone was about 45%. Whereas the failure should be expected to occur on the largest flaws available rather than on the average-sized flaw, one might expect tensile strengths in the larger holes to be smaller than those calculated above. Given the

existing uncertainties in tensile strength, there may be no substitute for tensile tests on large cores. The possibility of using core from the large-scale heater holes at Stripa for such tests is currently being investigated.

2.4.7 Statistical Fracture Mechanics Approach to Tensile Strength

Ratigan (1981) has developed an approach to evaluating the hydrofracture tensile strength of rock based on Weibull's weakest link model (Weibull, 1939). For details of its application to the Stripa granite, see Ratigan (1981); a brief summary is presented below.

Ratigan's modification to Weibull's three-parameter model is based on the strain energy release rate rather than on tensile stress. The model gives the apparent tensile strength, T_a, as

$$T_a = G_u^{1/2} + \int_{G_u^{1/2}}^{\infty} e^{-B} \, dT_a$$

where G_u is the threshold strain energy release rate and B is the risk of rupture, a term dependent on three laboratory testing parameters and the volume or area over which the stresses are applied. The parameters were determined from a series of over 350 indirect tensile strength tests and are:

$G_u = 110 \text{ MPa}^2$

G_o (sealing factor) $= 0.159 \times 10^{-4} \text{ MPa}^2 - \text{m}^{2/\alpha}$

α (modified Weibull modulus) $= 0.525$

As the volume or surface area under load increases, the number of flaws and the risk of encountering a large flow increases. Thus, for tests that affect large surface areas, the risk of rupture becomes very high. Ratigan showed that for the field tests at Stripa the surface area was sufficient to effectively reduce the exponential term in the apparent tensile strength equation to a negligible quantity. The apparent tensile strength used for the analysis of the Stripa stress measurement data was thus the square root of G_u, or 10.5 MPa.

2.5 Discussion of Overcoring and Hydraulic Fracturing Results

Many kinds of statistical treatments are possible and an exhaustive treatment of the statistics of field rock mechanics data is beyond the scope of this report. Here, we will analyze the principal stress data from overcoring only in a descriptive way. Statistical analysis and comparison of the results for overcoring and hydraulic fracturing are made on the basis of the magnitudes and orientations of the vertical and horizontal components of the principal stresses. These components are referred to as secondary stresses. A major reason for using only the secondary stresses is that hydraulic fracturing is not a true three-dimensional technique, and there is general agreement only on the ability of hydrofracturing to measure stresses normal to the borehole, which in this case is vertical. The secondary stresses measured by the two techniques will be compared using linear regression. Confidence intervals will be computed for the magnitudes of the secondary stresses at a depth of 320 m, close to the depth of the underground test facility (348 m) in the Stripa mine.

No attempt is made to separate the effect of instrumental variability from that of natural variability in the in situ stress field. Such an analysis is not straightforward since the true magnitude of the in situ stress field at the Stripa mine is not known. Furthermore, little is currently known from field measurements about the natural variability of in situ stress fields in either magnitude or orientation. Numerical models using uniform far-field stresses and randomly varied material properties (LaPointe, 1981) have shown that the variability of the rock mass modulus can have a great effect on the in situ stress field at specific locations within the rock. Thus a high degree of natural variability in the stresses should not be surprising.

How many stress measurements should be made is an important question both for the comparison of the two techniques and for the execution of a site exploration program. The answer is necessarily arbitrary, because it depends on the degree of uncertainty acceptable to the designer and operator of a facililty. For this study, $\pm$ 10% is used as the confidence interval for predictions of mean stress magnitude, and $\pm$ 10° is used for orientation of the maximum horizontal principal stress.

2.6 Results of Stress Measurements

2.6.1 Principal Stress Data from Overcoring

The results of the overcoring measurements are given in Table 2.1. The orientations of the principal stresses are shown in stereographic projections in Fig. 2.14. The principal stress data show a large degree of scatter in their magnitudes. For example, measurements performed in consecutive one-meter intervals of the hole may differ by 100% or more in

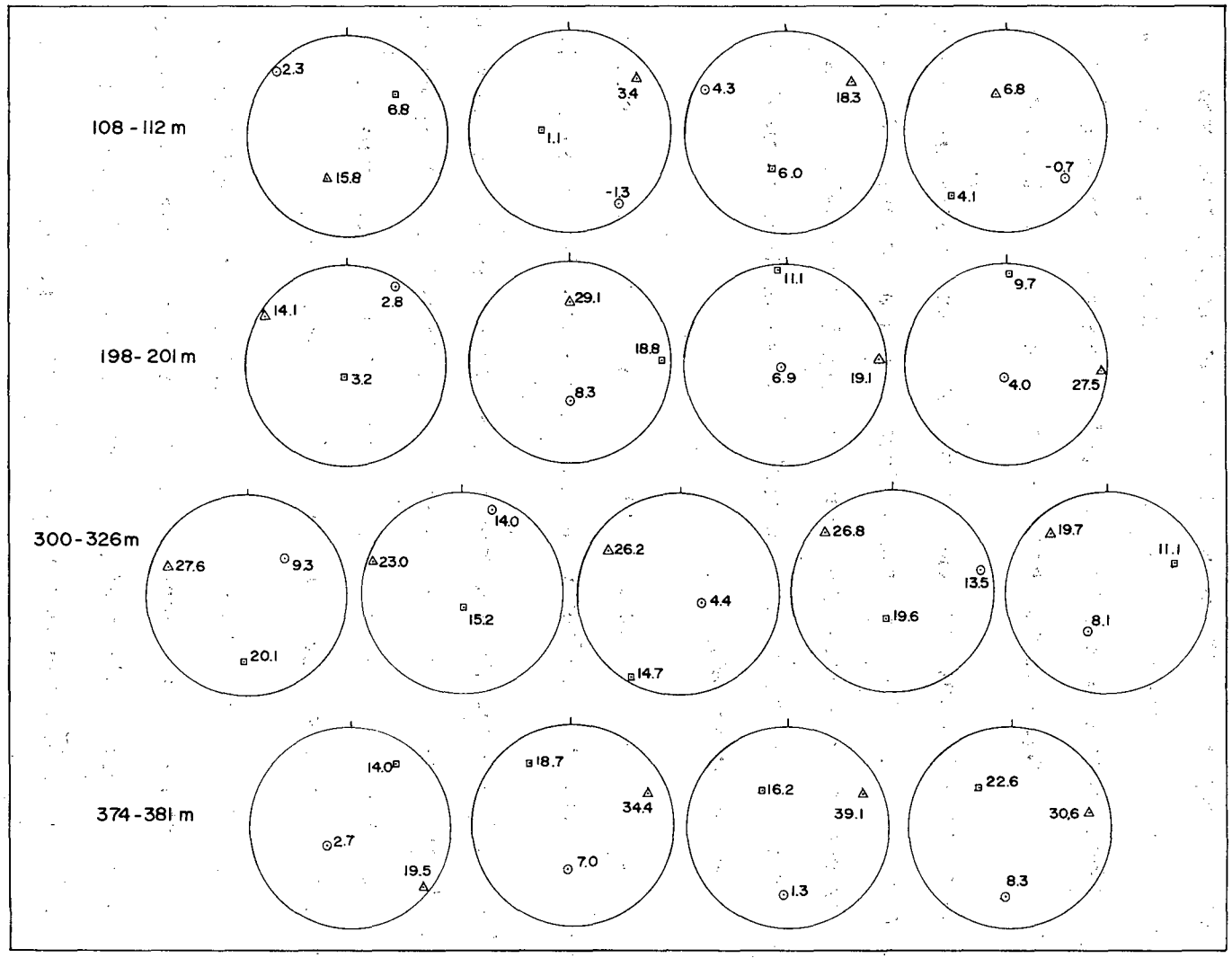

Fig. 2.14 Lower hemisphere equal-area projections of overcoring stress data in MPa. Projections are grouped by depth. σ_1 - triangles, σ_2 - squares, σ_3 - circles.

XBL 814-8968

their magnitudes. The source of this data scatter is not clear; it may reflect either the natural variability of the stress field on the small scale of the overcoring strain gauges or errors by the instrument itself. Calibration of the strain-gauged cores in the laboratory, however, would seem to limit instrument variability, unless there are time-dependent aspects to the gauge cements that are not allowed for in the data reductions.

The orientation data for the 100 m depth measurements show a consistent NW-SE orientation for the minimum principal stress. Two of the four measurements even show the minimum stress to be tensile. The orientations of the other two principal stresses at that depth do not show any preferred orientation.

At the 200 m depth, the principal stresses are close to horizontal and vertical with the maximum principal stress oriented in an E-W direction.

The 300-326 m depth measurements consistently show that the maximum principal stress is close to horizontal and oriented in a NW-SE direction. The other principal stresses do not appear to have consistent orientations, nor are they generally vertical or horizontal.

At the 380 m depth, the maximum principal stress is still horizontal, but with an E-NE orientation. The other principal stresses are skewed with respect to the horizontal and vertical, the minimum principal stresses possibly being oriented toward the mine openings.

2.6.2 Vertical Stress Data from Overcoring

The mean values of the vertical stresses at the depths of the overcoring measurements have been calculated and are generally greater

than the calculated stress based on the weight of the overburden. For the depths of 110, 200, and 300 m, the measured vertical stress varied from 1.5 to 2.3 times the overburden weight. At 380 m, the mean vertical stress is in close correspondence with the overburden weight.

The amplification of the vertical stress over lithostatic values is consistent with calculations of the effect of the mine openings on the stresses at SBH-4 performed by Chan et al. (1981). Unlike the horizontal stress data, the vertical stress has an insignificant correlation coefficient with respect to depth such that calculations based on linear regression have no statistical validity. This lack of correlation may further reflect the influence of the mine on the stresses.

2.6.3 Orientation of the Maximum Horizontal Stress from Overcoring and Hydrofracturing

The orientation data have been analyzed to compare hydrofracturing and overcoring, using only the secondary principal stresses. The data are assumed to follow a half-circular normal distribution, since they start repeating with a 180-degree period. For statistical analysis, the data are converted to a circular distribution by doubling each value. This allows the circular normal distribution (also known as the Von Mises distribution) and its associated significance tests to be used.

The mean orientation is determined by vector summation, using procedures described by Pincus (1953) and Mardia (1972). The mean orientation, d, is given by:

$$d = 1/2 \tan^{-1}\left(\sum_{i=1}^{n} \sin 2\theta_i / \sum_{i=1}^{n} \cos 2\theta_i \right)$$

The normalized vector length, R, provides an estimate of the dispersion of the sample and is given by

$$R = (1/n)\left[\left(\sum_{i=1}^{n} \sin 2\theta_i^2 \right) + \left(\sum_{i=1}^{n} \cos 2\theta_i^2 \right)^{1/2}\right]$$

where n is the number of readings.

Mardia (1972) provides charts for determining 95% confidence levels for the mean direction of circular normal distributions when the sample size and the normalized vector length are given.

The orientations and magnitudes of the secondary principal stresses as determined by overcoring are shown in Fig. 2.15. The hydrofracture orientations are shown in stereographic projections in Fig. 2.16. To compare the data, both the overcoring and hydrofracturing data for the direction of the maximum horizontal stresses are plotted as a function of depth in Fig. 2.17.

For the hydrofracturing data, the orientation of the maximum secondary principal stress is:

$d = N\ 73^\circ\ W \pm 20^\circ$ (n=8).

$R(2\theta) = 0.69$

For the overcoring data, the values are:

$d = N\ 71^\circ\ W \pm 23^\circ$ (N=11).

$R(2\theta) = 0.56$

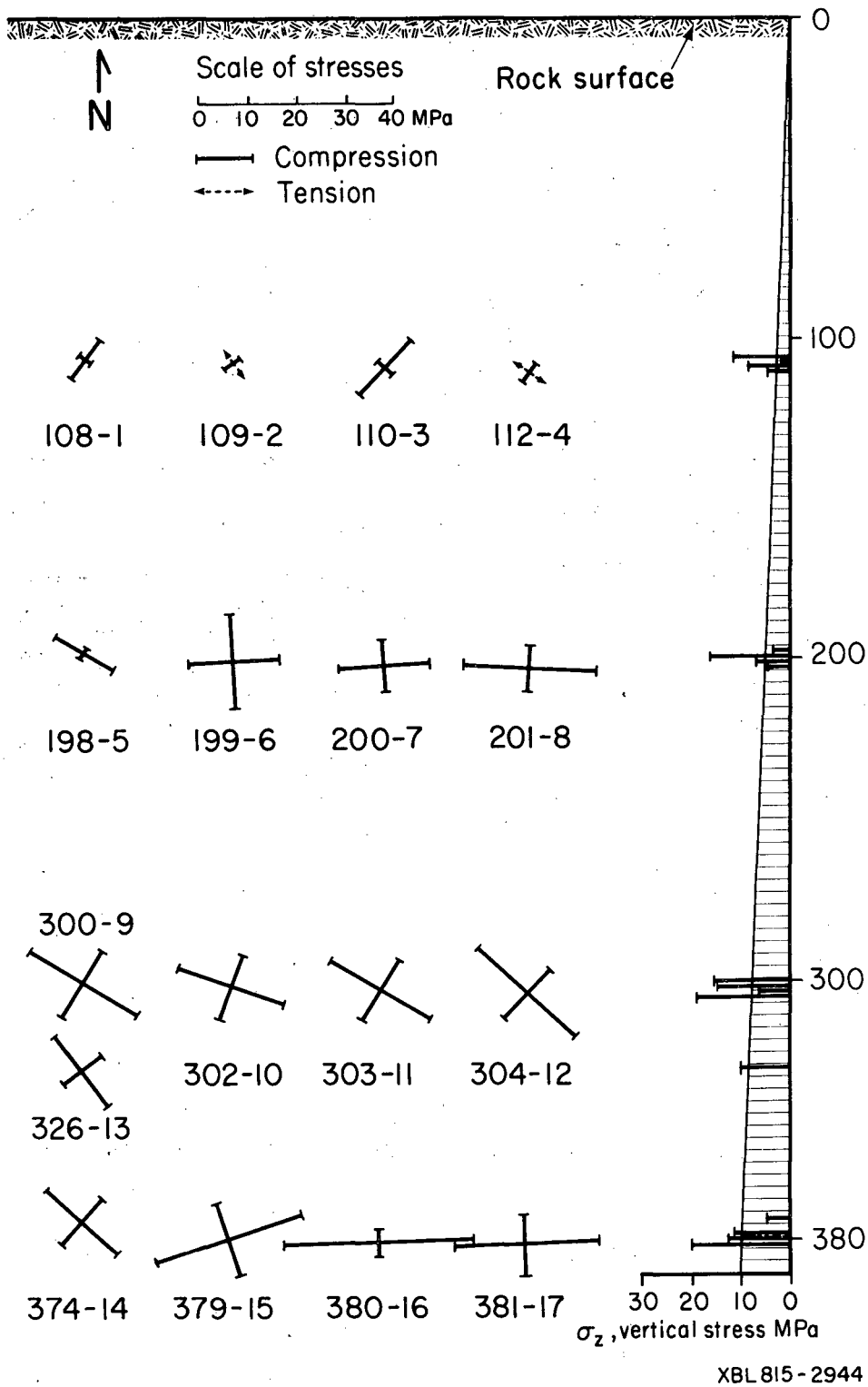

Fig. 2.15 SBH-4: Secondary principal stresses σ_a and σ_b in the horizontal plane and the vertical stress σ_z in relation to depth from Leeman cell overcoring.

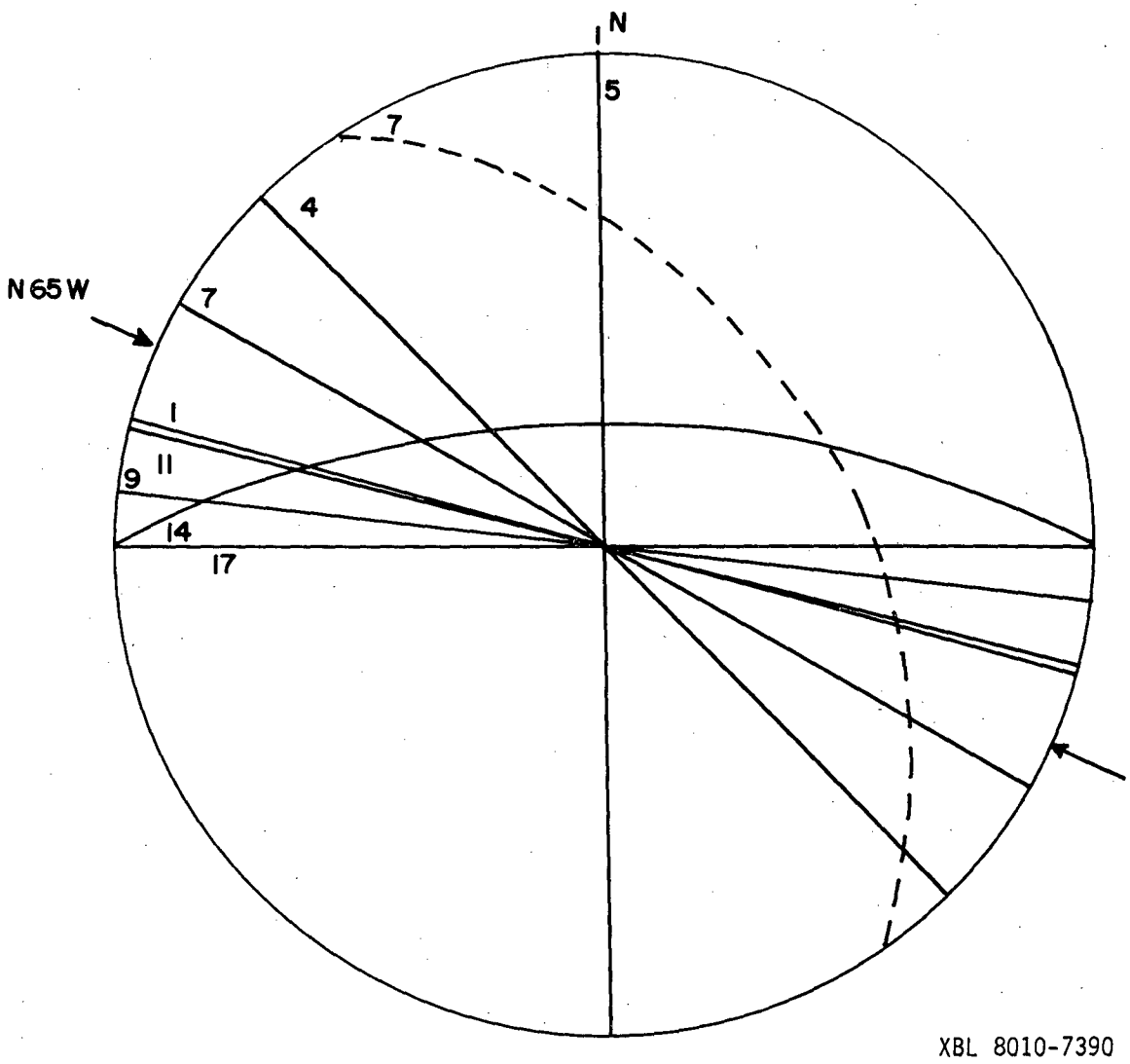

Fig. 2.16 Stereographic lower hemisphere projection of hydrofracture planes. Numbers refer to tests (see Table 2.2).

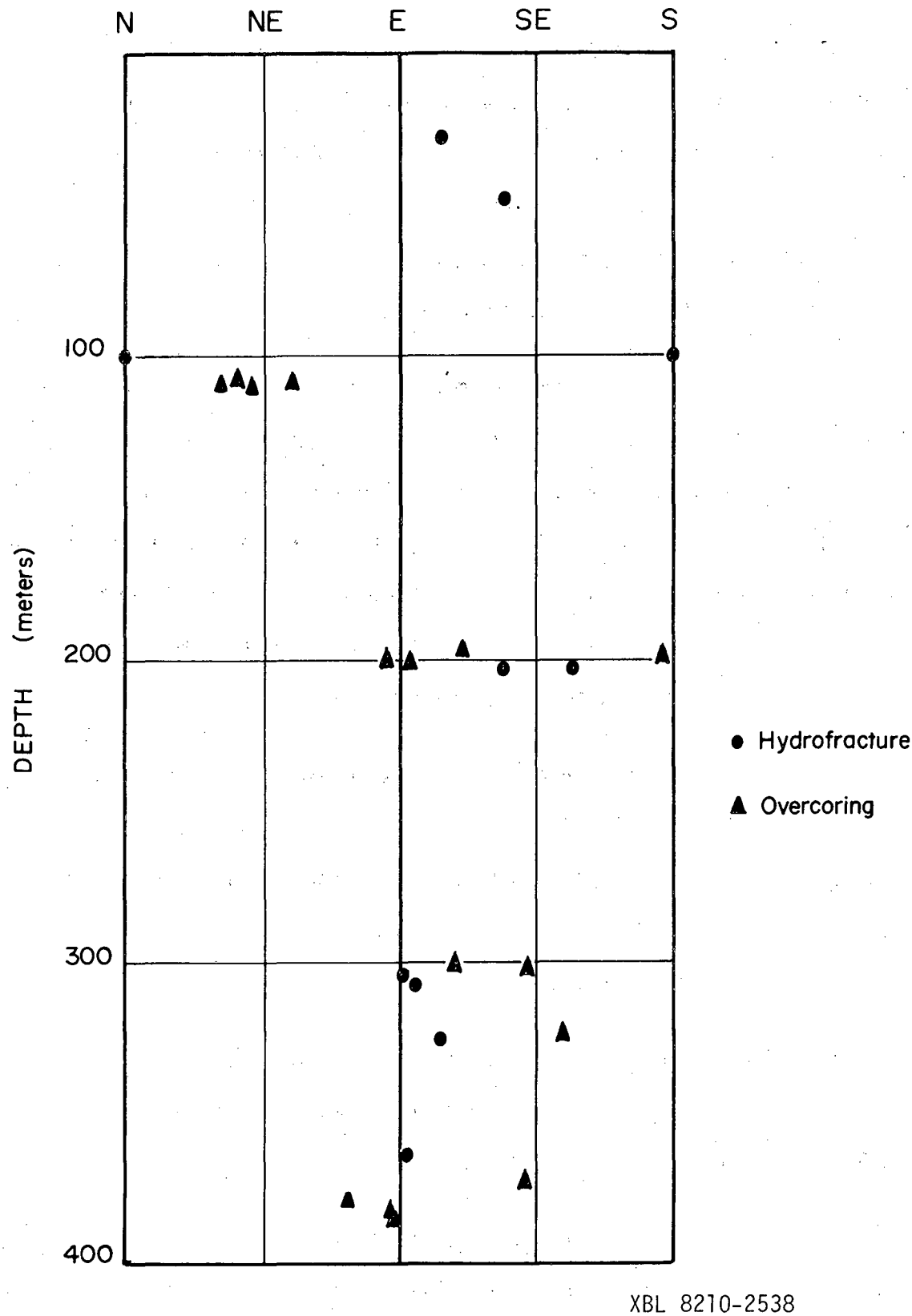

Fig. 2.17 Orientations of the maximum-versus-minimum horizontal stresses vs. depth.

The hydrofracture value is based on all measurements, as is the overcoring value, except for those measurements made around the depth of 100 m, which had a strong northeast direction. Confidence limits are for the 95% level. It is significant that on the basis of the relatively small number of samples, the confidence intervals are well within a 45° band of the mean directions for both overcoring and hydrofracturing.

Analysis of the confidence intervals for the orientations provides a useful means of determining the sufficiency of the amount of data. If we assume that additional hydrofracture orientations were obtained and that the data had the same degree of dispersion, i.e., the same vector length, about 30 measurements would have been required for a $\pm 10°$ confidence interval for the mean. For overcoring 40 to 50 measurements would have been required to meet the same confidence interval.

Since only a limited number of test zones were amenable to either overcoring or hydraulic fracturing, it seems doubtful that a sufficient number of measurements could have been made by either technique to meet the suggested confidence interval for the orientation. Furthermore, the cost would have been prohibitive.

By increasing the number of measurements taken by each technique to 20, the confidence limits could have been reduced to $\pm$ 15°, a more practically attainable goal.

2.6.4 Analysis of the Magnitudes of the Secondary Principal Stresses

The in situ stress values most important for the analysis of the heater test data are the horizontal stresses at the depth of the test

facility. Since the in situ stresses have an approximately linear relationship with depth, the most straightforward way to obtain the needed stress values is by interpolation based on a linear regression. The statistics of the regression lines have been calculated using methods presented in Crow et al. (1960). Since the northeast trend to the maximum horizontal stress suggests that the mine might be having an influence on the stress values, regression analyses were performed both on the data from 200 m depth and on all of the data. Exclusion of the shallow data did not affect the stress values interpolated to the depth of the test facility for either the overcoring or the hydrofracturing techniques; however, the confidence intervals were improved for the analyses performed on the entire data sets.

The horizontal stress data and regression lines are shown in Fig. 2.18 for the overcoring data and in Fig. 2.19 for the hydrofracturing data. The statistics for the regressions are given in Table 2.4. Three measures of reliability are given: the confidence interval for the ordinate to the regression line, the confidence interval for the slope of the regression line, and the standard error of estimate. Each is discussed below.

2.6.5 Confidence Limits of Interpolated Stress Values

The confidence interval for the ordinate of the regression line is a measure of the reliability of an estimate of the mean stress value at any particular depth. The 90% confidence bands for the stress values are shown on either side of the regression line in Figs. 2.18 and 2.19. At the depth of the Stripa test facility, the regression values are:

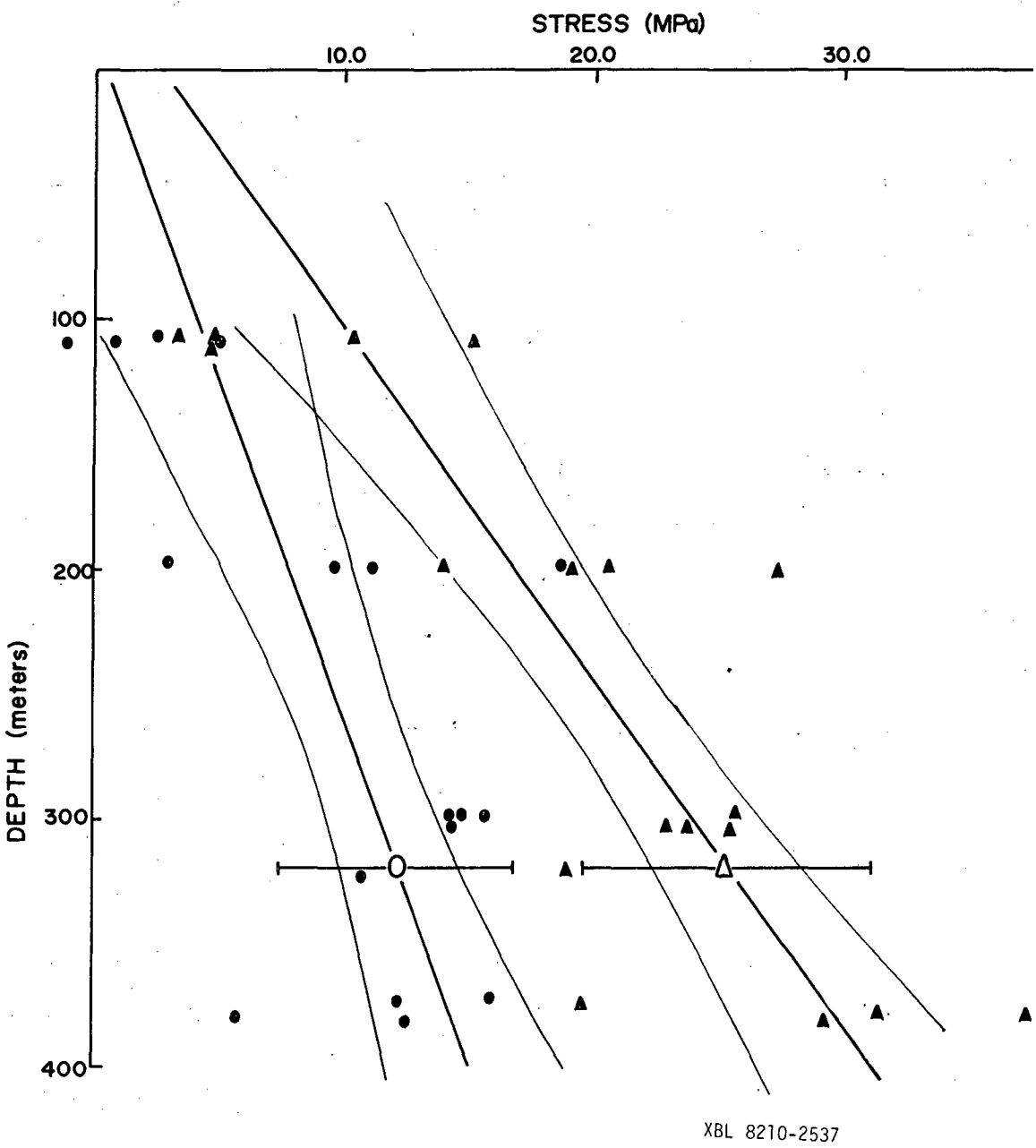

Fig. 2.18 Magnitude of maximum and minimum horizontal stress vs. depth determined by overcoring. Solid circles show minimum horizontal stress values, solid triangles show maximum horizontal stress values. Open symbols are the interpolated stresses at the depth of the test facility and are given with bars showing ± one standard error of estimate. Curved lines are the 90% confidence limits for the position of the regressive line.

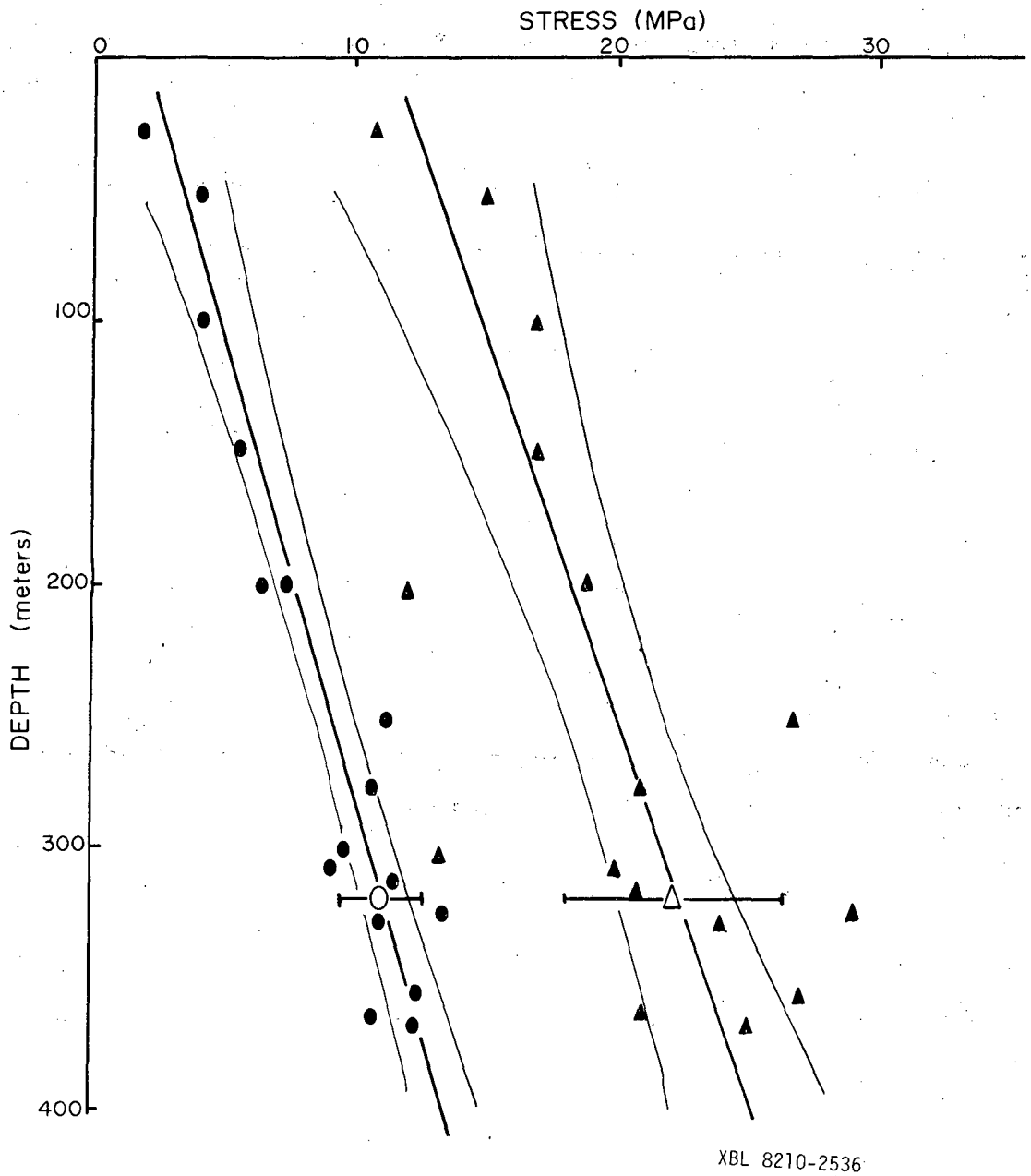

Fig. 2.19 Magnitude of maximum and minimum horizontal stresses vs. depth determined by hydrofracturing. See Fig. 2.18 for explanation of symbols.

Table 2.4. Regression data for horizontal stress data vs. depth.

		Slope b (MPa/m)	Intercept a (MPa)	Correlation coefficient r	Standard error of Estimate $S_{y|x}$ (MPa)
Hydrofracturing (n=16)					
	σ_{Hmax}	0.034±.016	11.3	0.70	4.1
	σ_{Hmin}	0.023±.005	2.1	0.91	1.5
Overcoring (n=17)					
	σ_{Hmax}	0.072±.026	2.3	0.81	4.8
	σ_{Hmin}	0.037±.021	0.3	0.64	5.5
	σ_v [a]	-	-	0.40	-

[a]Correlation coefficient fails significance test.

	σ_{HMax}	σ_{HMin}
Hydrofracturing	22.1 ± 2.1	11.1 ± 0.8
Overcoring	25.4 ± 2.9	12.1 ± 2.4

The stress values used in design of a repository will most likely be the mean values predicted for a given depth; thus these confidence limits are probably the most important for design purposes. The confidence limits are within 10% for the hydrofracturing data, 12% for the overcoring maximum stress, and 20% for the overcoring minimum stress.

The confidence limits are curved rather than straight lines, and the tightest confidence limits occur for the middle depths. This suggests that a higher degree of confidence can be obtained by making measurements over an equal range above and below the depth of interest. If cost is not a consideration, the stresses should be measured to twice the depth of interest to ensure the best reliability in the stress estimate. Although we cannot say that performing measurements to 640 m in SBH-4 would have increased confidence in the data sufficiently to justify the added expense, it is clear that measurements must be made at least to the depth of the proposed underground structure, and preferably somewhat deeper.

2.6.6 Standard Error of Estimate

The confidence intervals discussed in the previous section pertain only to the confidence in the position of the regression line and do not reflect either the uncertainty of an individual measurement or the scatter of the data about the regression line. The standard error of estimate, $S_{y|x}$, provides a measure of the dispersion of the data and is

analagous to a standard deviation. The $\pm S_{y|x}$ limits for the interpolated stresses at the test facility depth are shown in Figs. 2.18 and 2.19 for both measurement techniques. The standard errors given in Table 2.4 reflect the large amount of scatter in the data. The errors are smaller for hydrofracturing than for overcoring, particularly for the minimum-stress hydrofracturing measurements.

The error in the maximum stress for hydrofracturing is higher than that of the corresponding minimum value because of the use of three times the minimum stress in the calculation of the maximum stress. Whatever variability occurs in the shut-in pressure data is thus amplified in the calculation of the maximum stress.

In the overcoring data, the minimum stress has a larger standard error than the maximum stress. This may reflect the fact that the greatest principal stress values were consistently close to horizontal, while the other two principal stresses varied considerably in orientation. This variability may have affected the calculated values of the secondary stresses.

The large values for the standard error of estimate show clearly that a stress measurement program consisting of only a few measurements may not be capable of providing reliable in situ stress data for repository design.

2.6.7 Confidence Intervals for the Regression Slope

The 90% confidence intervals for the slopes of the regression lines are given in Table 2.4. The slopes are not known with a very high degree

of confidence, as all of the limits, except for that of the hydrofracturing σ_{HMin} data, are greater than ±35%. Attempts to estimate the stress values at depths greater than 380 m by extrapolation are clearly subject to error.

2.7 Conclusions

2.7.1 Agreement of Hydrofracturing and Overcoring Results

In comparing the two methods of measurement, it must be remembered that the true state of stress is not known, and that there is no independent basis for determining whether either is correct. If the methods compare favorably, one only has more certainty that they are providing reliable data.

The overcoring and hydraulic fracturing methods have been compared mainly with respect to the orientation of the secondary principal stresses and the magnitude of the horizontal stress at the depth of the test facility.

The orientation of the maximum horizontal stress fortuitously agrees within a degree for the two techniques. The confidence levels are both about ±20°; thus one can conclude that the correspondence between overcoring and hydraulic fracturing is quite good.

The horizontal stress magnitudes also agree closely when the hydraulic fracturing data are interpreted using first breakdown methods. The hydraulic fracturing has somewhat better confidence intervals than the overcoring, particularly for the horizontal minimum stress, but both methods provide estimates for the stress values at the depth of the test facility within ±20% or better.

2.7.2 Influence of the Mine on Stress State

The rotation of the least principal stress from the vertical toward the mine openings may indicate the influence of the mine. Vertical stress values from overcoring are consistent with two-dimensional numerical calculations (Chan et al., 1981) that show the vertical stress exceeding lithostatic values at about 200 m depth.

2.7.3 Analysis of Hydrofracturing Data

The appropriate tensile strength for calculating the maximum horizontal stress can be obtained from laboratory tests, using a statistical fracture mechanics approach to account for the effect of the borehole size. The tensile strength approach may be more reliable than second-breakdown methods, particularly when the horizontal stress ratio is greater than 2.

3. STRESS DETERMINATIONS WITH THE LuH GAUGE
(B. Leijon and W. Hustrulid)

3.1 Description of Technique

The Leeman triaxial strain cell (Leeman, 1971) was developed in 1965 to provide the complete state of stress in a rock mass from measurements in a single hole. Leeman's cell contained three 3-component strain gauge rosettes cemented to the wall of an EX pilot borehole Each gauge rosette was placed to provide axial, tangential, and oblique strains at a point. The changes in the strain gauge readings after overcoring are used to calculate the stress from the formulas of Leeman (1971).

The values for Young's modulus and Poisson's ratio required in the calculations could be obtained from laboratory tests conducted on pieces of core or by inserting the core containing the strain cell in a biaxial chamber. By monitoring the strain changes as a function of applied pressure, one can obtain the required elastic constants as well as a check on the gauges.

The University of Luleå (LuH) gauge is a modified version of the original Leeman cell. Improvements have been made in the-hole cleaning technique, the installation tool, and the readout equipment. Also, four-component strain gauges are substituted for three-component gauges. This last modification provides greater redundancy in the strain data (only six independent strain readings being required for solution), allowing a more reliable measurement of the stress field. A schematic diagram of the LuH gauge is shown in Fig. 3.1; a complete description is given in Stillborg and Leijon (in press).

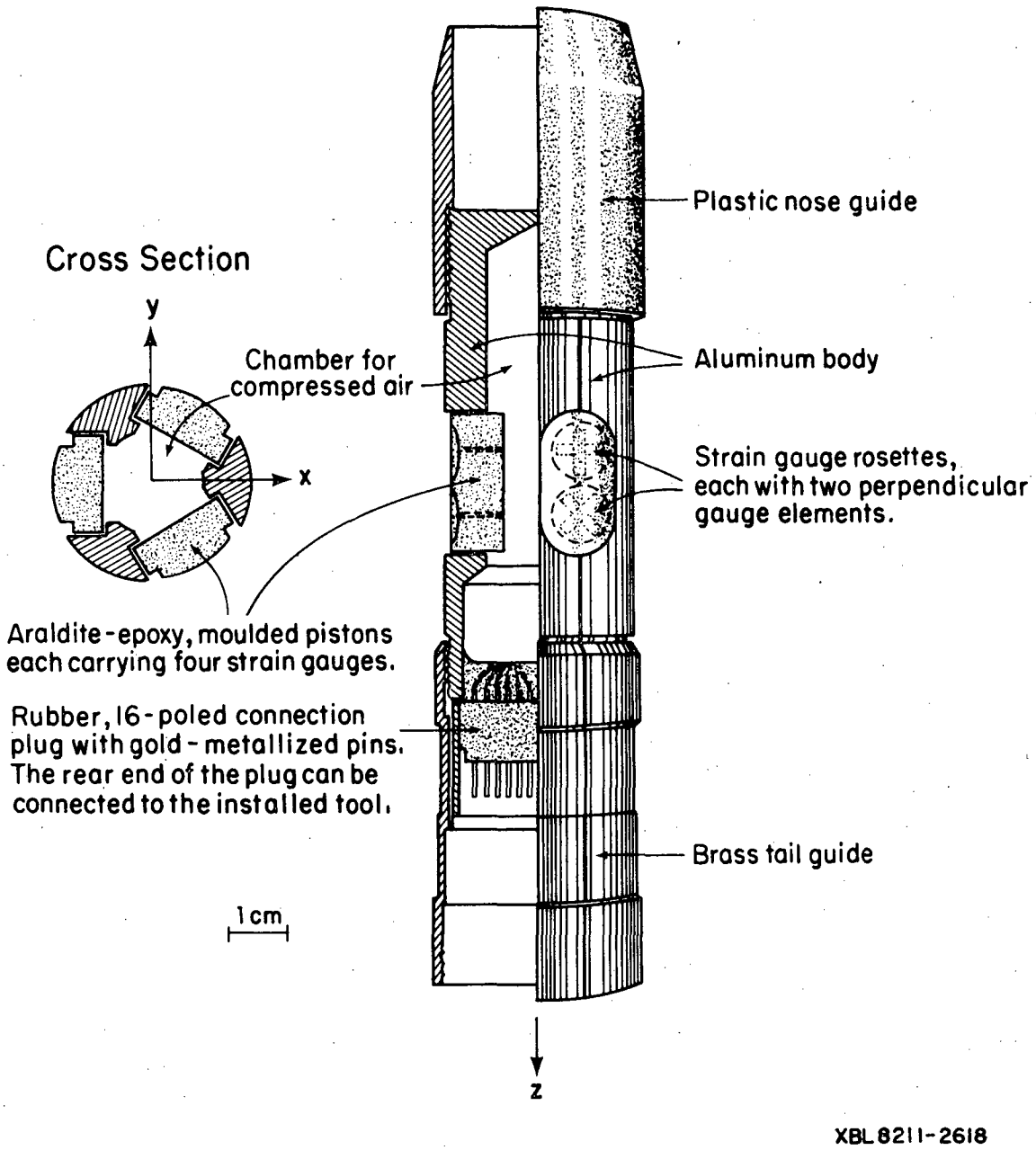

Fig. 3.1 Diagram of LuH stress measurement gauge.

The position of the rosettes within the hole and of the gauges in each rosette are shown in Fig. 3.2, with the angular values tabulated in Table 3.1.

The LuH gauge is normally overcored with an 82 mm (3.2 inch) diameter bit, but, in these measurements, the overcoring bit had a 142 mm diameter because USBM gauge measurements were run in the same hole. An advantage of the larger bit is a lower risk of breaking the core during overcoring.

3.2 Installation Procedure

After drilling the 38 mm diameter pilot hole, the hole is cleaned twice with acetone and dry air, using a compressed-air-driven injector designed at Lulea. The strain cell body contains three oval pistons whose surfaces are matched to the curvature of the borehole wall, to which have been cemented the three strain rosettes. After the gauges are carefully cleaned with acetone, a rapid-setting cement (Schnellklepstoff X-60, manufactured by Hottinger) is applied. With special installing tools, the cell is inserted into the hole to the proper depth. A mercury switch assures proper orientation in the hole. When lowering is completed, compressed air forces the pistons and gauges against the wall of the borehole. The pressure is maintained until the cement has cured (approximately 45 minutes). At this point, the initial strain cell readings are taken. The installing tool is then disconnected from the strain cell and removed. Since there is no cable in the hole, a plug can be inserted in the collar to prevent the entry of drilling water.

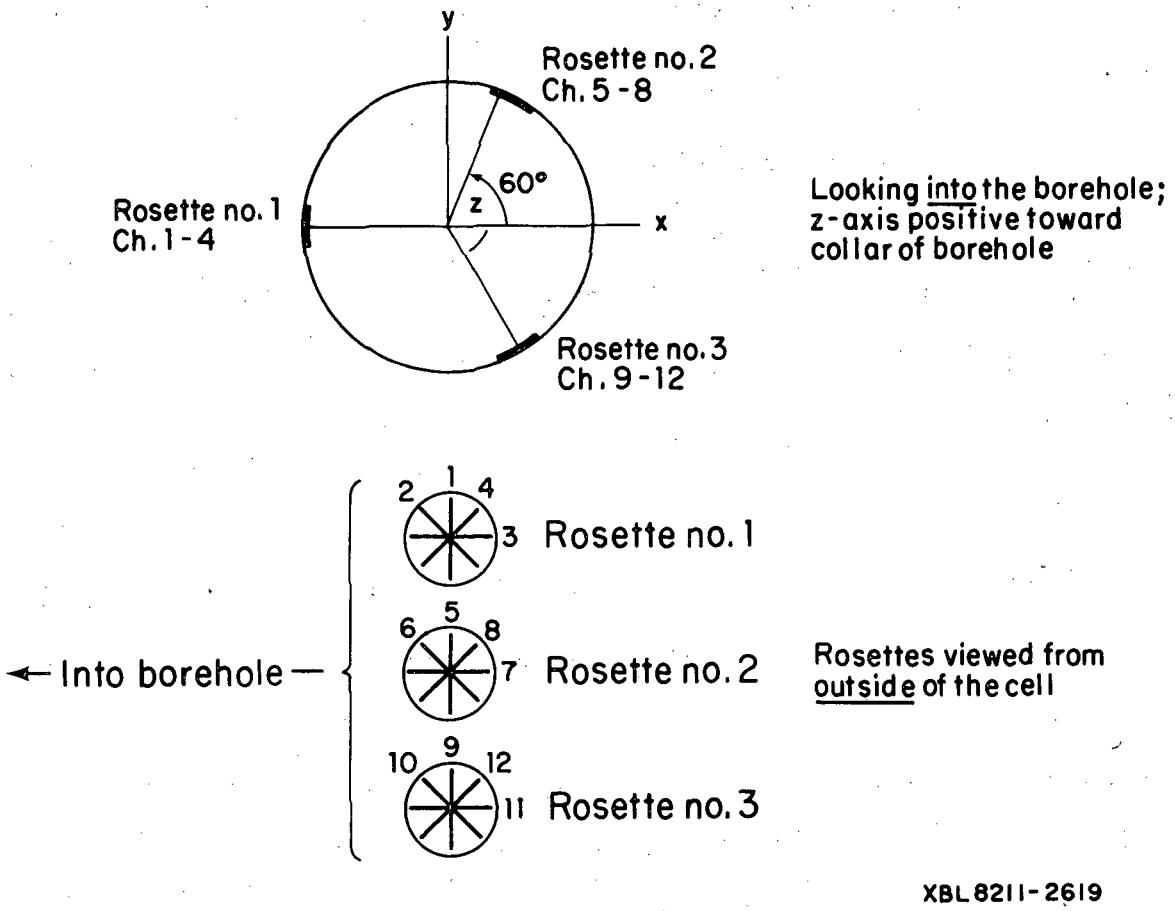

Fig. 3.2 Positions of the strain rosettes in the LuH cell and of the individual gauges within each rosette.

Table 3.1. Angular orientation of the strain gauges within the LuH gauge.

Gauge	Θ (degrees)	β (degrees)
1	270	90
2	270	45
3	270	0
4	270	135
5	30	90
6	30	45
7	30	0
8	30	135
9	150	90
10	150	45
11	150	0
12	150	135

Angle Θ is the rosette position measured clockwise with respect to the vertical.

Angle β is the gauge orientation measured clockwise with respect to the hole axis.

Overcoring now commences. When the proper depth is reached (approximately 20 cm past the gauges), the drill is stopped. The core is broken off and removed and the installing tool is reconnected to the strain cell for final reading of the strains, using a data logger. The data logger is designed especially for the LuH gauge and provides output readings in strain units on an LED display or on paper tape. The readout cable is attached to the strain indicator in a quarter bridge, three-wire circuit. The electrical stability of each channel is noted. The mercury switch is again attached to the cell, and core's true orientation is determined.

3.3 Field Results

The hole depths at which LuH gauges were installed are shown in Table 3.2 and Fig. 3.3.

Because of the LuH cell's short length and the absence of a cable, both a USBM gauge and an LuH gauge could be installed in the pilot hole during an overcoring run. This was done during LuH tests 4 and 7. Table 3.3 provides a summary of installation and overcoring comments.

3.4 Biaxial Testing of the Overcores.

To convert the strain changes obtained during overcoring into stress magnitudes and directions, one needs to know appropriate values of Young's modulus and Poisson's ratio. The cores from tests 2, 6, and 8 were suitable for tests to derive these values. These cores were placed in the biaxial chamber, and the applied pressure was increased from 0 up to 21 MPa in increments of 2.1 MPa. The strain readings were recorded by

Table 3.2. Hole depths for the LuH gauge tests.

LuH Test	Hole Depth (β)
1	2.5
2	5.09
3	7.02
4	7.62 *
5	8.11
6	9.23
7	9.81*
8	11.16

*Done in conjunction with the USBM. tests.

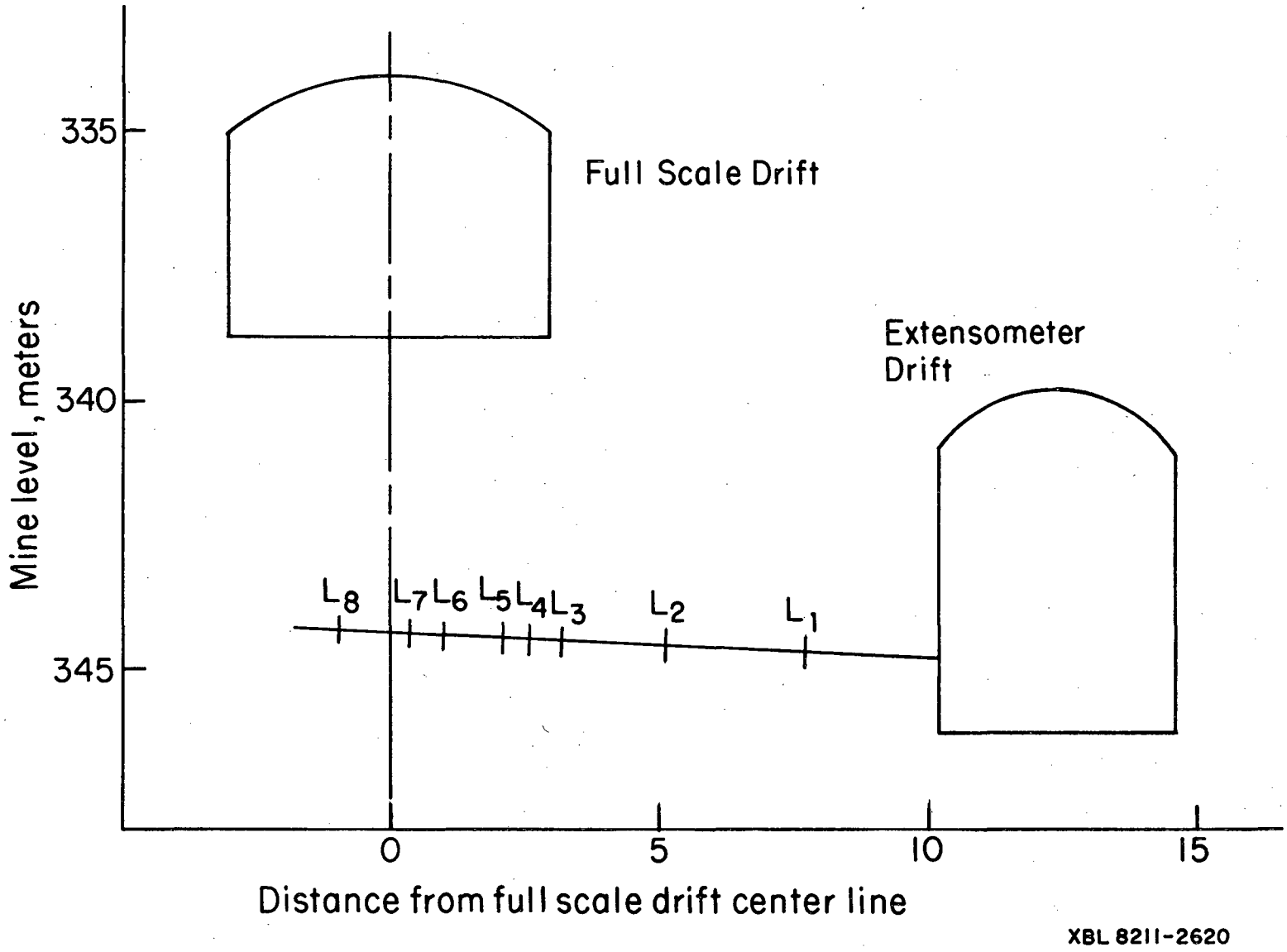

Fig. 3.3 Locations of LuH (modified Leeman) tests.

Table 3.3 Summary of the LuH gauge installation and overcoring.

Overcore	Depth (m)	Comments
LuH 1	2.50	The end of the 142 mm hole was at a depth of 2.18 m. The gauge was installed at 2.50 m and the cement allowed to dry overnight. Overcoring was successfully completed to a depth of 2.79 m. When the gauge and core were removed, a natural joint was found at the gauge position. The 6" core was broken approximately 7 cm from the gauge position and no biaxial testing was possible.
LuH 2	5.09	The end of the 142 mm hole was at a depth of 4.83 m. The gauge was installed at a depth of 5.09 m. Cementing and overcoring were done within 2 hours. The core broke along a joint (depth 5.31 m); however, the results appear good.
LuH 3	7.02	It was initially planned to install this gauge at a depth of 6.48 m. However, the pilot and overcore holes were not sufficiently concentric, so the position was moved to 7.02 m. The initial face of the 142 mm diameter hole was 6.28 m. The cement was allowed to dry overnight. Overcoring to a depth of 7.12 m was successful. The 6" core was broken 9 cm behind and 5 cm ahead of gauge position, so no biaxial testing was possible.
LuH 4	7.68	This gauge was overcored at the same time as USBM gauge 7, and because of the cable no plugging of the 38 mm hole was possible. Therefore, the cell was water filled. Channels 6, 8, and 9 were unstable (+ 15με) after overcoring. The 6" core was broken 5 cm from the gauge position, so biaxial testing was possible.

Table 3.3 Summary of the LuH gauge installation and overcoring (continued)

Overcore	Depth (m)	Comments
LuH 5	8.11	The initial 142 mm hole face was at 7.90 m. The gauge was installed at a depth of 8.11 m Overcoring was to a depth of 8.30 m. However, the core broke along a natural joint during removal at about 8.14 m. The remaining core had to be removed in a second step. Channel 3 unstable when compressed air was switched off and on (≃ 100 με). Everything else was satisfactory.
LuH 6	9.23	The initial 142 mm hole face was at 8.89 m. The gauge was installed at 9.23 m and allowed to set over the next 48 hours. Overcoring continued to a depth of 9.38 m.
LuH 7	9.81	Installation was satisfactory. The gauge was overcored together with USBM gauge 9 and hence the 38 mm hole could not be plugged. The gauge filled with water. The 6" core broke off along a joint very close to the gauge position (front edge of rosette 1). The readings were, however, stable.
LuH 8	11.16	The initial large hole face was at a depth of 10.94 m. Gauge was installed at 11.16 m and overcored to a depth of 11.29 m 1 1/2 hours.

the data logger at each pressure, and the results are presented in Tables 3.4-3.6.

The isotropy of the rock can be checked by comparing the following gauge pairs: 2 and 4, 6 and 8, and 10 and 12. The closeness of the results show that the assumption of isotropy is valid.

The pressure-strain curves are quite linear and, for gauge 1 of overcore 2, the strain returns to zero after completing the loading-unloading cycle. The average ratio of the unloading and loading moduli is 1.03. The same ratio was found in a test of an LuH gauge in an aluminum cylinder. This similarity suggests that the remaining strains are attributable to plastic effects in the cement. It would therefore appear that the Stripa granite satisfies very well the assumptions of being linear, elastic, and isotropic.

The elastic modulus can be obtained from the pressure-strain relationships of the following strain gauges:

gauge 1 in rosette 1

gauge 5 in rosette 2

gauge 9 in rosette 3

through the equation

$$E = \frac{2}{1-(D_i/D_o)^2}(P/\varepsilon)$$
$$= 2.157\ (P/\varepsilon)$$

where

E = Young's modulus

P = biaxial pressure

Table 3.4. Biaxial testing results for LuH overcore #2 (strain-gauge outputs are in microstrains).

Pressure (MPa)	Gauge Number 1	2	3	4	5	6	7	8	9	10	11	12
0	0	0	0	0	0	0	0	0	0	0	0	0
2.1	-101	- 26	13	- 34	-79	- 30	23	- 33	- 79	- 24	24	-.29
4.1	-208	- 52	24	- 70	-158	- 61	46	- 65	-157	- 48	47	- 61
6.2	-309	- 78	35	-104	-236	- 92	66	- 98	-234	- 71	69	- 94
8.3	-406	-104	57	-136	-315	-123	87	-129	-309	- 95	90	-126
10.3	-494	-129	59	-167	-390	-152	108	-160	-384	-118	111	-157
12.4	-578	-154	72	-197	-464	-183	128	-190	-457	-140	132	-187
14.5	-659	-177	85	-225	-536	-211	148	-218	-576	-162	152	-216
16.6	-734	-200	98	-253	-606	-240	167	-246	-594	-184	172	-245
18.6	-808	-223	111	-280	-676	-267	186	-273	-661	-205	192	-273
20.7	-880	-244	124	-305	-743	-293	204	-298	-727	-225	211	-300
0	-132	- 11	- 19	- 25	9	5	3	6	6	10	4	1

Table 3.5. Biaxial testing results for LuH overcore #6 (strain-gauge outputs are in microstrains).

	Gauge Number											
Pressure (MPa)	1	2	3	4	5	6	7	8	9	10	11	12
0	0	0	0	0	0	0	0	0	0	0	0	0
2.1	- 76	- 26	24	- 28	-77	- 34	26	- 24	- 71	- 21	24	+.26
4.1	-157	- 55	46	- 61	-157	- 73	51	- 48	-142	- 42	45	- 54
6.2	-239	- 84	68	- 93	239	-114	75	- 75	-216	- 63	67	- 83
8.3	-323	-113	90	-127	-322	-155	100	-102	-290	- 85	88	-113
10.3	-400	-141	113	-160	-404	-195	124	-127	-365	-107	110	-143
12.4	-480	-168	134	-101	-483	-234	149	-153	-438	-129	130	-173
14.5	-556	-193	156	-223	-558	-270	172	-178	-511	-150	151	-202
16.6	-634	-221	178	-255	-634	-306	195	-202	-583	-172	171	-230
18.6	-703	-243	198	-283	-703	-336	218	-224	-651	-193	191	-257
20.7	-772	-266	219	-311	-769	-366	240	-246	-718	-214	210	-282
0	- 45	- 20	9	- 25	-6	-4	3	0	-2	5	5	1

Table 3.6. Biaxial testing results for LuH overcore #8 (strain-gauge outputs are in microstrains).

Pressure (MPa)	Gauge Number 1	2	3	4	5	6	7	8	9	10	11	12
0	0	0	0	0	0	0	0	0	0	0	0	0
2.1	- 82	- 29	21	- 34	-103	- 49	28	- 29	- 79	- 31	23	- 28
4.1	-160	- 55	47	- 64	-207	-102	54	- 56	-156	- 61	46	- 55
6.2	-239	- 84	170	- 95	-308	-154	78	- 82	-236	- 92	70	- 84
8.3	-319	-113	92	-127	-401	-203	101	-108	-312	-122	94	-113
10.3	-395	-141	115	-158	-491	-249	123	-132	-391	-152	117	-142
12.4	-472	-170	137	-188	-577	-292	145	-155	-466	-180	140	-171
14.5	-545	-197	158	-217	-658	-332	165	-178	-539	-208	162	-198
16.6	-616	-224	179	-246	-735	-370	184	-198	-609	-236	184	-224
18.6	-686	-250	199	-275	-811	-406	204	-218	-678	-262	204	-249
20.7	-755	-275	219	-302	-884	-441	223	-237	-745	-289	224	-273
0	- 13	-7	-6	-8	- 13	10	-4	-4	-7	-6	-2	-7

ϵ = strain

D_i = inner core diameter = 38.2 mm

D_o = outer core diameter = 141.5 mm

Values for Poisson's ratio (ν_i) can be determined from the strain outputs of the axial and circumferential strain gauges.

Rosette 1: $\nu_1 = -(\epsilon_3/\epsilon_1)$

Rosette 2: $\nu_2 = -(\epsilon_7/\epsilon_5)$

Rosette 3: $\nu_3 = -(\epsilon_{11}/\epsilon_9)$

The values obtained will of course depend on the pressure range considered. Three calculations have been made to illustrate this point:

Calculation 1 - Linear fit over the range 0 to 20.7 MPa

Calculation 2 - Linear fit over the range 6.2-20.7 MPa

Calculation 3 - Secant value using the origin and the strain at 20.7 MPa.

The results are presented in Tables 3.7 through 3.9. As can be seen, the secant fit and linear fit over the entire range are in close agreement, reflecting the linearity of the curves. The linear fit over the higher pressure range gives higher values of the stress as might be expected. For the stress calculations, the results of the linear fit between 0 and 20.7 MPa will be used, since it more clearly fits the requirements of the theoretical equation.

Table 3.7 Young's modulus and Poisson's ratio determinations for LuH overcore 2.

Rosette	Young's modulus (GPa)					
	Calculation 1		Calculation 2		Calculation 3	
	E	ν	E	ν	E	ν
1	50.7	0.139	55.0	0.158	51.9	0.141
2	59.9	0.273	61.9	0.273	60.1	0.275
3	61.3	0.289	63.4	0.289	61.2	0.290
Average	57.3	0.234	60.1	0.240	57.3	0.235

Table 3.8 Young's modulus and Poisson's ratio determinations for LuH overcore 6.

Rosette	Young's modulus GPa					
	Calculation 1		Calculation 2		Calculation 3	
	E	ν	E	ν	E	ν
1	57.2	0.280	58.5	0.283	57.7	0.284
2	57.2	0.308	58.8	0.310	58.1	0.312
3	61.6	0.289	62.0	0.284	62.1	0.292
Average	58.7	0.292	59.7	0.292	59.3	0.296

Table 3.9 Young's modulus and Poisson's ratio determinations for LuH overcore 8.

Rosette	Young's modulus GPa					
	Calculation 1		Calculation 2		Calculation 3	
	E	ν	E	ν	E	ν
1	59.0	0.291	60.6	0.289	59.1	0.290
2	50.6	0.250	54.3	0.251	50.5	0.252
3	59.6	0.302	61.2	0.302	59.9	0.301
Average	56.3	0.281	58.8	0.281	56.5	0.281

The modulus values obtained with the LuH gauge agree very well with those determined from the USBM gauge (Chapter 4).

3.5 In Situ Stress Results

The strains resulting from overcoring ($\Delta\varepsilon$), obtained for each channels in each overcoring run, are given in Table 3.10.

A computer program developed by R. G. Friday of CSIRO for use with the CSIRO cell has calculated the stress magnitudes and directions from the strain changes. For overcores 2, 6, and 8, the average elastic properties obtained from biaxial testing were used. For the remaining overcores, the values $E = 55.4$ GPa and $\nu = 0.277$ were assumed.

Only six of the 12 gauge readings are required to calculate the in situ stress. Friday's program calculates the stress using a multiple least squares fit to the possible solutions. Since individual gauges may be untrustworthy because of rock conditions or the cement bond, the data reduction program repeats the calculation several times, each time discarding the gauge with the worst fit to the solution. The results of computer runs 1 (all strain values included) and 5 (the four strain values with the highest deviations removed) are given in Tables 3.11 and 3.12 respectively. As can be seen, the difference is small. The principal stress directions for run 5 are given in Fig. 3.4. Principal stress magnitudes are plotted against the hole depth in Fig. 3.5.

It would appear that

- The direction of σ_1 is very consistent.
- The magnitude of σ_1 appears to decrease as the full-scale drift is approached (overcores 5 and 6). The stress continues to decrease as the hole passes under the drift.

Table 3.10. Strain changes recorded during overcoring of LuH gauges.

Over-core No.	Depth	Strain by gauge number (microstrains)											
		1	2	3	4	5	6	7	8	9	10	11	12
1	2.50	-141	184	2	-277	694	213	-74	460	707	360	-61	354
2	5.09	- 53	153	46	-127	435	32	23	448	567	337	36	270
3	7.02	- 54	72	7	-131	512	138	33	515	488	364	4	148
4	7.62	- 68	75	-13	-177	589	32	-87	367	405	348	17	241
5	8.11	-144	46	106	- 67	745	147	-31	593	825	590	29	254
6	9.23	-296	- 5	58	-246	720	264	32	562	945	566	68	439
7	9.81	-116	40	60	25	641	250	14	515	633	382	77	309
8	11.16	-183	34	85	-126	828	360	31	519	564	403	67	256

Table 3.11. LuH principal stress results from run 1.

Over-core No.	σ_1(MPa)			σ_2(MPa)			σ_3(MPa)		
	Mag.	Dip	Bearing	Mag.	Dip	Bear.	Mag.	Dip	Bear.
1	21.36	0.5	68.0	9.07	46.5	158.5	-0.58	-43.5	157.6
2	16.88	1.1	81.1	9.15	42.4	172.1	1.51	-47.5	169.8
3	17.16	6.4	82.7	6.54	36.7	177.5	2.79	-52.5	164.3
4	15.61	6.1	76.3	5.59	49.4	173.5	0.65	-39.9	161.2
5	25.05	0.1	260.4	8.94	26.1	170.3	5.11	-63.9	170.7
6	28.38	3.0	252.0	12.75	18.9	161.0	2.25	-70.9	170.6
7	20.28	2.3	74.8	10.21	11.5	165.3	5.28	-78.3	153.7
8	22.90	7.9	72.3	10.93	9.4	163.6	3.78	-77.7	123.1

Table 3.12. LuH principal stress results from run 5.

Over-core No.	σ_1(MPa)			σ_2(MPa)			σ_3(MPa)		
	Mag.	Dip	Bearing	Mag.	Dip	Bear.	Mag.	Dip	Bear.
1	20.94	0.1	67.4	7.01	51.7	157.6	-0.53	-38.2	157.4
2	16.90	2.2	81.8	9.66	41.6	173.8	0.93	-48.3	169.3
3	16.31	5.3	81.8	5.94	45.9	177.3	1.89	-43.6	166.7
4	14.99	9.0	66.4	6.17	42.8	164.8	0.80	-45.8	147.0
5	25.08	0.5	259.0	8.39	14.2	168.9	5.15	-75.8	170.9
6	28.25	3.1	253.2	12.71	19.6	162.1	2.18	-70.1	171.9
7	19.81	1.7	72.4	9.90	17.5	162.9	4.15	-72.4	156.9
8	23.59	8.9	78.0	11.87	10.3	169.7	3.68	-76.3	128.2

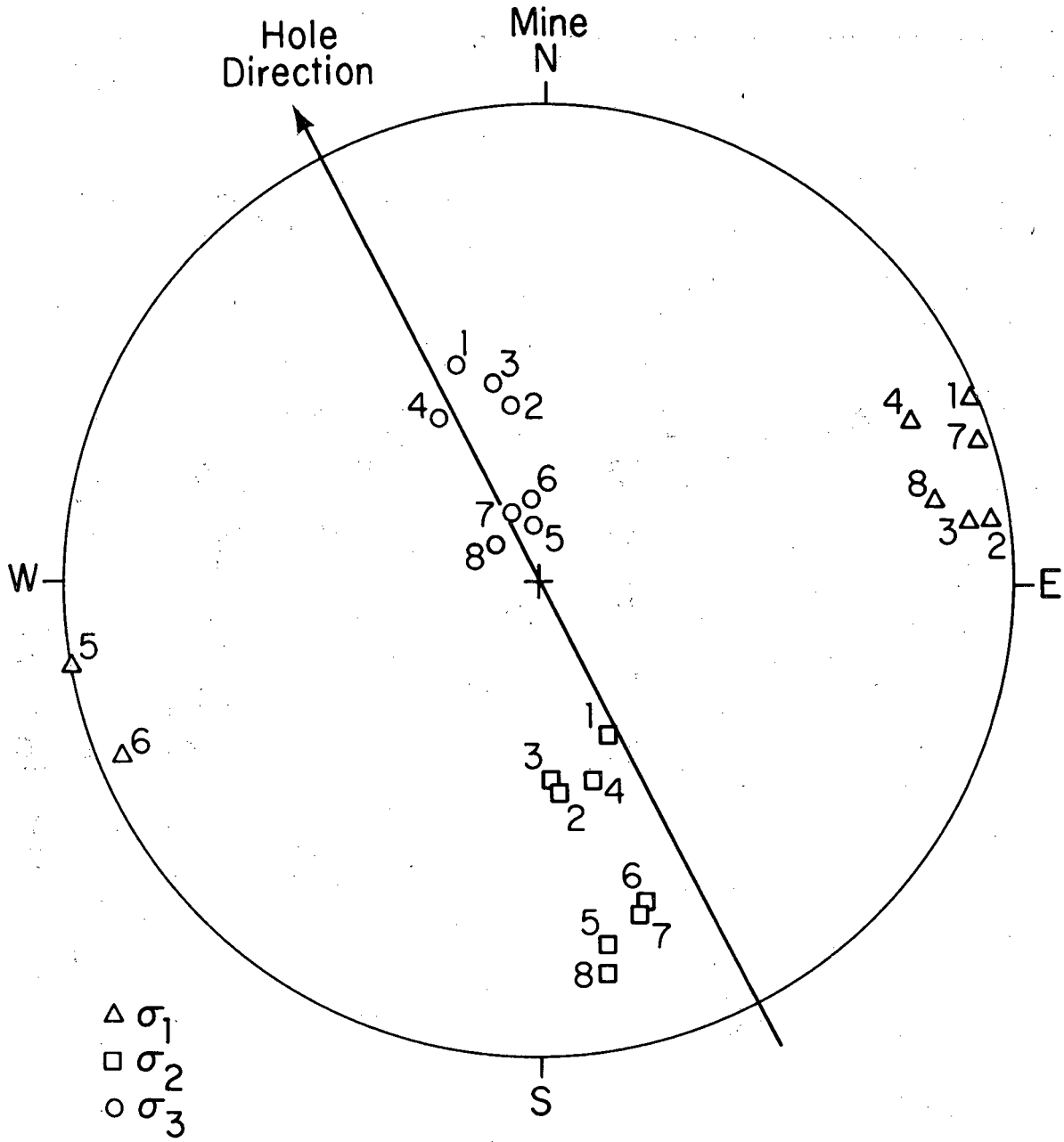

Fig. 3.4 Principal stress directions for the LuH gauge overcoring data.

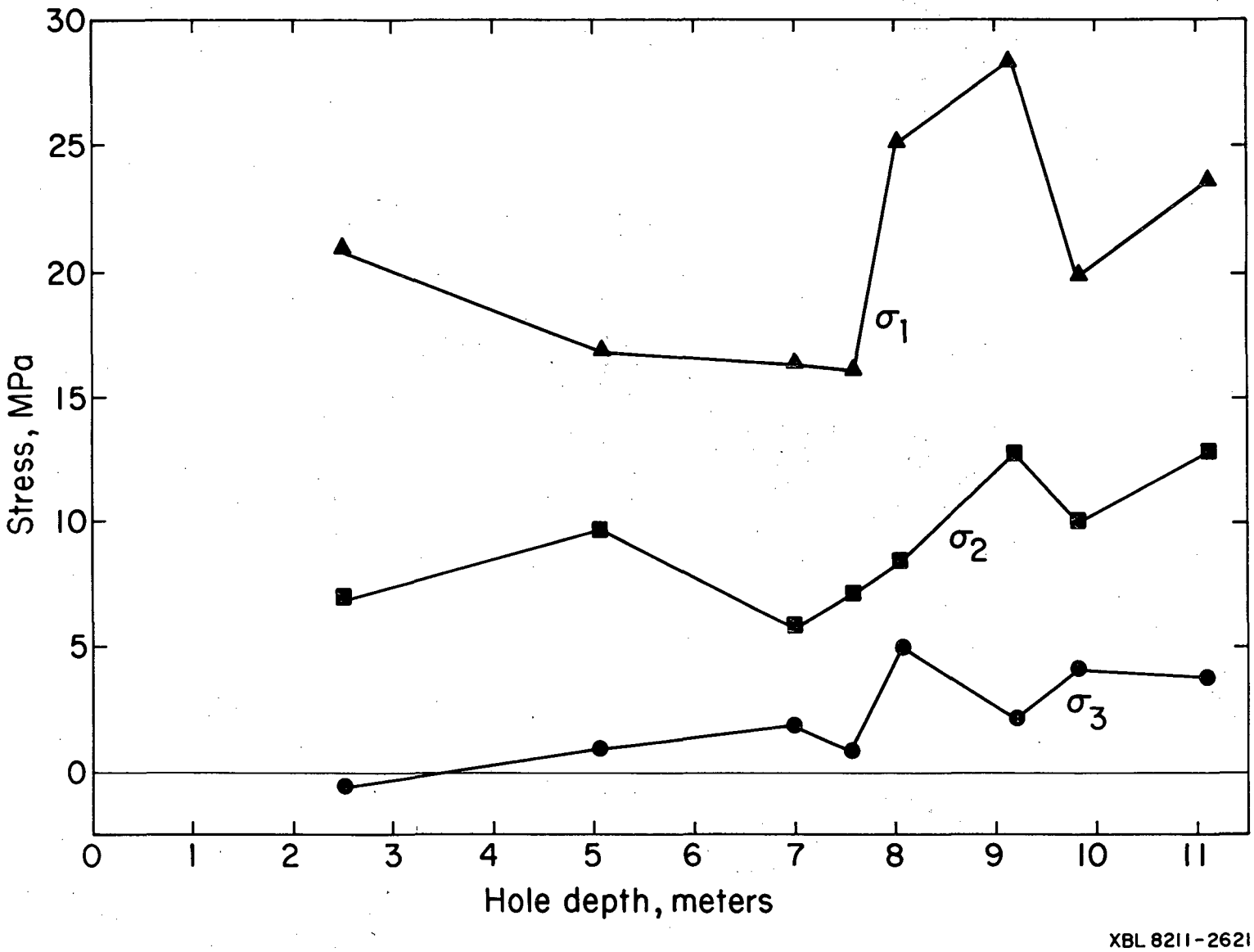

Fig. 3.5 Magnitudes of principal stresses in BSP-3.

- The magnitude of σ_2 is very consistent.

- In relation to magnitude, σ_3 varies more than σ_1 and σ_2. This may be due to the presence of joints along the borehole.

- The directions of σ_2 and σ_3 appear to rotate from measuring points 1 to 8 by about 45°.

Another way of presenting this data is to calculate the principal stresses and directions in the plane perpendicular to the borehole. In this way, the values will be directly comparable to those obtained with the USBM borehole deformation gauge. The LuH gauge results are given in Table 3.13 and plotted against hole depth in Fig. 3.6.

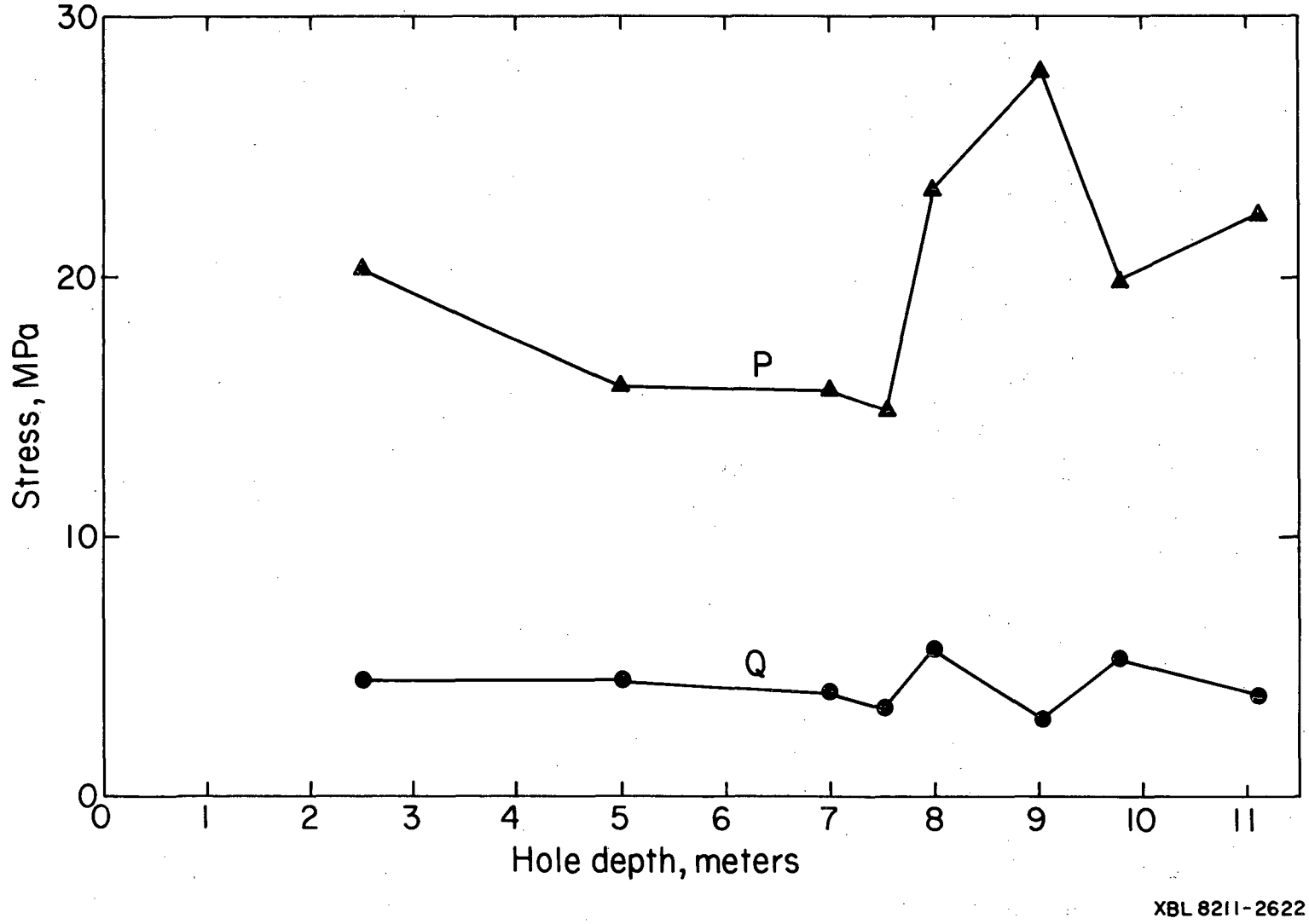

Fig. 3.6 Magnitudes of secondary principal stresses in BSP-3.

Table 3.13. Secondary principal stresses in plane normal to the borehole, LuH gauge.

Overcore No.	P°(MPa)	Q(MPa)	ϕ
1	21.36	4.47	5.43
2	15.89	4.51	5.88
3	15.73	4.07	-2.66
4	14.88	3.38	-2.54
5	23.47	5.69	2.45
6	27.94	3.00	4.52
7	19.80	5.41	-1.03
8	22.51	3.92	-6.94

4.0 STRESS DETERMINATIONS WITH THE USBM BOREHOLE DEFORMATION GAUGE (W. Hustrulid and B. Leijon)

4.1 Description of Technique

The U.S. Bureau of Mines (USBM) borehole deformation gauge was developed in the early 1960s for stress measurement. It has been extensively used in the United States since then, and procedures for its use have been standardized by Hooker and Bickel (1972). In this gauge, cantilevers measure the diameter change of the pilot hole during overcoring. Unlike the other strain cells described in this report, the USBM gauge does not require bonding of strain gauges to the rock, thus eliminating the tricky and time-consuming work of downhole cementing. As the gauge measures deformation only in the plane normal to the hole, measurements in more than one hole are required to obtain the complete state of stress. USBM gauge measurements were performed at Stripa only in BSP-3, and the results are thus restricted to the components of the principal stress in the plane normal to the hole. These components are referred to as P and Q, the maximum and minimum secondary principal stresses.

The basic sensing elements consist of three pairs of strain-gauged cantilevers (U_1, U_2, U_3) deflected by tungsten carbide-tipped pistons that contact the hole wall (see Fig. 4.1.) Each of the pistons can be removed from the cell body and lengthened or shortened by adding or removing shim washers. In this way, the "preset" or deflection of the cantilevers can be adjusted so that they will follow motion both toward and away from the hole center. The maximum deflection of one cantilever pair is about 0.71 mm (or 0.36 mm per cantilever) and

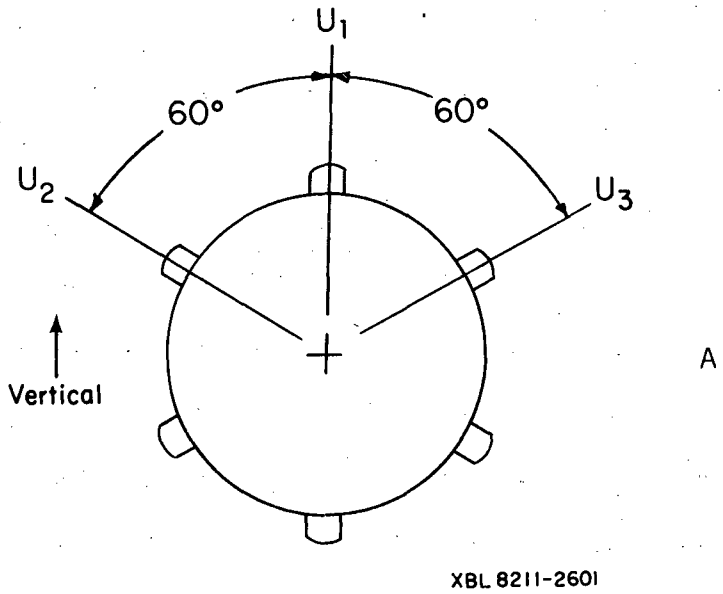

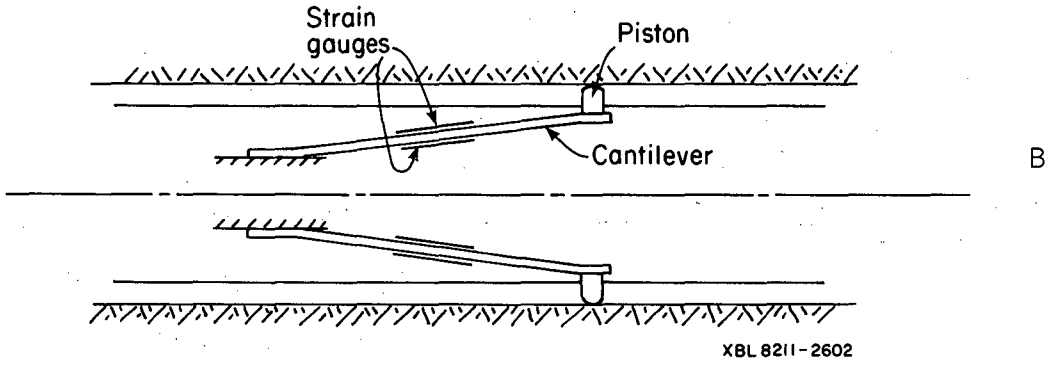

Fig. 4.1 (a) Orientation of the USBM borehole deformation gauge as installed in BSP-3. (b) Diagrammatic view of the USBM gauge in the hole.

the preset should take this into account. The exact shape of the hole at the test location is of course unknown and a couple of trials (changing washers) may be required to obtain the proper interference. The abrasiveness of the rock produces wear on the buttons as they are pushed into the hole, thereby reducing the initial interference.

The strain gauges on each pair of cantilevers are wired to form a complete bridge circuit. Careful gauge matching and application compensates for temperature effects. Hence, one only needs to supply a bridge voltage and read the bridge output.

Standard procedures for stress measurement with USBM gauges call for readings during overcoring, using either a single strain indicator with a switching and balancing box (Budd Type 350, for example) or three separate strain indicators. The internal power supply for the indicator is 1.5 V. The strain indicator system has the following advantages:

- o It is inexpensive, portable, and rugged (suitable for mine use).
- o It provides a good visual indication of strain changes.
- o Its output is in strain units.

A major disadvantage is that an observer must continually follow the strain changes with the dial and must write down the readings. Readings cannot be taken more frequently than about one per minute, and there is a possibility of error in recording the numbers.

In the present USBM and CSIRO experiments, the bridge used a 6-volt HLAB model 6244A power supply. The bridge output was recorded on paper tape by a

Fluke model 2240B data logger. Using a data logger has these following advantages:

- o The data collection rate is limited only by the scan rate (one scan per 3 seconds).
- o Data are printed on paper tapes.
- o Time and other data are given.
- o The printer output provides a visual indication of changes.

The disadvantages are that it relatively expensive, and is less portable and less rugged than the strain indicator system.

In the present application, however, no portability was required, and an environmental case protected the data logger and power supply. This system's overall advantages far outweigh those of a strain indicator system.

The equations for translating the measured hole deformations into the desired values of principal stress and principal stress directions require that the material be isotropic and linearly elastic. Furthermore, the standard solutions assume plane stress behavior; i.e., the axial stress in the section of rock being overcored is zero. The basic equation:

$$U = \frac{d}{E} [(P+Q) + (P-Q) \cos 2\theta] \qquad (4.1)$$

yields the deformation of a circular hole in a thin plate produced by the principal secondary stresses P and Q acting normal to the axis of the hole, where:

U = diametral hole deformation (outward = +)

d = hole diameter

E = Young's modulus

P = maximum secondary principal stress (+ = tension)

Q = minimum secondary principal stress (+ = tension)

Θ = angle between the direction of U and P.

The three diametral measurements are made at 60° intervals, and one can solve for P, Q, and Θ.

The appropriate equations become (Obert and Duvall, 1967):

$$P = \frac{E}{6d}\left\{(U_1 + U_2 + U_3) + \frac{\sqrt{2}}{2}\left[(U_1-U_2)^2 + (U_2-U_3^2) + (U_3-U_1^2\right]^{1/2}\right\} \quad (4.2)$$

$$Q = \frac{E}{6d}\left\{(U_1+U_2+U_3) - \frac{\sqrt{2}}{2}\left[(U_1-U_2)^2 + (U_2-U_3)^2 + (U_3-U_1)^2\right]^{1/2}\right\} \quad (4.3)$$

$$\Theta_p = \frac{1}{2}\tan^{-1}\frac{3(U_2-U_3)}{2U_1-U_2-U_3} \quad (4.4)$$

where U is positive for an increasing diameter and Θ_p is measured from U_1 to P (counterclockwise is positive).

Note that the inverse tangent operator in Eq. (4.4) yields two possible angles. Selecting of the correct angle requires analyzing the relative magnitudes of the displacements, U_i, according to Table 4.1.

Table 4.1. Table for determining correct quadrant of Θ_p.

Case	Constraints		Θ_p
I	$U_2 > U_3$	$U_2+U_3 < 2U_1$	$0° \leq \Theta_p \leq 45°$
II	$U_2 > U_3$	$U_2+U_3 > 2U_1$	$45° \leq \Theta_p \leq 90°$
III	$U_2 < U_3$	$U_2+U_3 > 2U_1$	$90° \leq \Theta_p \leq 135°$
IV	$U_2 < U_3$	$U_2+U_3 < 2U_1$	$135° \leq \Theta_p \leq 180°$

At Stripa, all USBM gauges were installed so that the U_1 position was vertical. The direction of Θ_p is therefore determined with respect to the vertical.

4.2 Calibration

Each USBM gauge was calibrated before use, several times during actual testing, and after completion of the program. The calibration schedule is shown in Table 4.2.

The calibration procedure is as follows. The USBM gauge is inserted into a calibration fixture equipped with a micrometer. A cable was attached to the input terminals of the Fluke data logger, and the power supply was adjusted to provide 6 volts. The gauge was oriented to align one set of buttons with the micrometer plungers. Initial contact of the plungers and buttons was made, and a slight preload (cantilever displacement) was applied.

The initial reading was taken with the data logger. Each micrometer was then extended by 0.05 mm and a scan made. This was repeated until each cantilever had been deflected by about 0.65 mm. Readings were done in the same way during unloading.

Linear curves were fitted to the loading and unloading portions of each calibration. As each gauge was calibrated four times, eight values for the slope of the voltage/displacement curve were obtained for each set of cantilevers. There was little variation in the slope values between calibrations, and it was decided that average values of the slopes of each

Table 4.2. Calibration schedule for the USBM gauges.

Gauge 1 (Serial No. 414)		
Calibration	Date	Comment
1	June 16, 1981	Prior to overcore 1
2	June 17, 1981	After overcore 2
3	June 22, 1981	Prior to biaxial testing
4	June 25, 1981	After biaxial testing

cantilever set would be used for calculating the stresses. These calibration values are given with their standard deviations in Table 4.3. The complete calibration data are available in Hustrulid et al. (1982).

4.3 Installation Procedure

The installing tool attaches to two pins at the back of the gauge. During installation, the tool and the gauge are oriented so that, when the desired depth is reached, a slight clockwise rotation is needed to bring the U_1 position vertical (Fig. 4.2). The orientation is controlled by a spirit level held on the handle of the tool. The torsion of the installing rods results in some uncertainty over the true orientation of the gauge. Although the accuracy is felt to be fairly good (<5°), much of this uncertainty by including a mercury switch in the installing tool similar to that of the LuH gauge (Chapter 3).

Once the gauge has been emplaced, the installing tool is disengaged by turning counterclockwise and pulling backward. Once detached, the rods are removed from the hole. The transmission cable is strung through the drill rods and the water swivel and connected to the data logger. Initially, we attempted to remove only the water swivel and install the USBM gauge through the drill string (which thus not be removed from the hole each time). This would have saved time and allowed the drill string to center the gauge in the hole. Unfortunately, a small lip between the drill string and the 150 mm overcoring barrel caused the installing tools to hang up. Hence, the drill

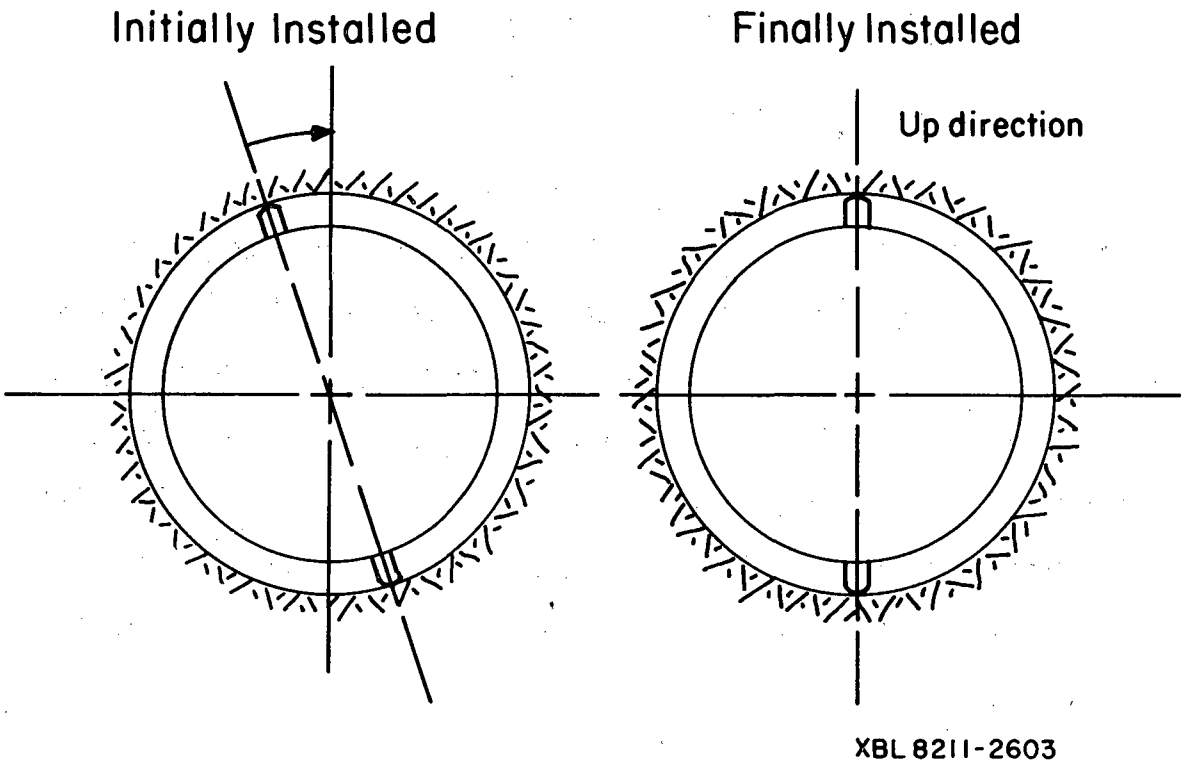

Fig. 4.2 Diagram of installation procedure for the USBM gauge.

Table 4.3. Calibration values used for reducing the USBM borehole deformation gauge data.

Gauge	Channel	Slope (v/mm)	
		Mean	S.D.
1	U_1	0.0244	0.0004
	U_2	0.0244	0.0004
	U_3	0.0224	0.0004
2	U_1	0.0240	0.0001
	U_2	0.0240	0.0001
	U_3	0.0241	0.0001

string was removed each time, and installation was through the empty 150 mm diameter hole with the EX hole at the end. A wooden sled rode along the bottom of the hole. Its width aligned the gauge with the EX hole. A second set of installing rods pushed the sled down the hole while maintaining orientation control of the gauge. With a little practice, this system worked very well. Once the gauge was installed, the sled was pulled by a cable from the hole.

During installation, the USBM gauge was connected to the data logger so that the readings revealed whether the preload on the cantilevers was satisfactory. Sometimes an initially undesirable gauge placement could be improved by moving the gauge inward or outward from the initial position, the readings changing because of varying hole diameters. If the gauge readings were still not satisfactory, the gauge was removed from the hole, the washers on the pistons adjusted, and the process repeated. If the readings were satisfactory, then the cable was detached from the data logger, inserted through the drill string and water swivel, and reattached to the data logger.

The gauge was positioned in the hole so that the plane of the buttons was about 20 cm away from the initiation of overcoring. In general, overcoring would continue about 20 cm past the button plane. The U.S. Bureau of Mines has shown that these distances are needed to avoid end effects.

4.4 Overcoring

A scale was formed by marking 1 cm increments on strips of masking tape

attached to a section of the drill string near the machine. The progress of the marks with respect to a fixed reference point was noted, and the data logger scan was initiated as each mark passed the reference. The data logger recorded the time, bridge voltage, and output from the three bridge channels.

Before to beginning an overcoring run, the drill water was turned on for 5 to 10 minutes, and readings were made to check for bridge drift due to temperature effects. No temperature effects were observed. The same procedure was followed at the end of a test.

During the overcoring, five people were normally involved: the driller, the driller's helper, the cable holder, the data logger attendant, and drill advance observer. The functions of the driller, advance observer, and data logger attendant are obvious, but it is perhaps worthwhile to discuss the functions of the driller's helper and the cable holder. Because of the high rotational speed used in the overcoring, high vibration could arise in the drill string even with the stabilizing effect of the core barrel at the front and the use of stabilizers along the string. These stabilizers acted like lumped masses that produced high vibrations in the drill string near the collar. This could be overcome somewhat by controlling drill rotation and thrust, but the most effective technique was to stabilize the string at the collar through wooden wedges. The driller's helper maintained the integrity of this "wooden stabilizer" during overcoring. The high rotation rate also required a cable holder to maintain a uniform tension on the cable

coming through the swivel. If the cable somehow became slack, it could be damaged by rotating with the drill string. Another danger was that the core would break along a joint and turn along with the core barrel. This did occur from time to time, but with fast response by all involved no damage occurred.

The only serious mishap during overcoring was the failure of a drill rod. The broken rod sliced through the cable of USBM gauge 1, thus requiring completion of the program with gauge 2.

After overcoring was completed, the cable was disconnected from the data logger and run through the drill string as it was from the hole. Sometimes the gauge was removed from the core with the installing tool before the core was broken off; at other times, it remained in the hole. When a core was removed, care was taken to maintain its hole orientation. This allowed a check on the orientation of gauges left in the hole.

The locations of the USBM borehole deformation gauge measurements are shown in Fig. 4.3. Some pertinent observations made before, during, and after overcoring for all 9 overcores are summarized in Table 4.4.

4.5 Biaxial Chamber Tests

4.5.1 Theory

An appropriate value of the elastic modulus is required in determining stresses from changes in deformation. The technique employed in these tests

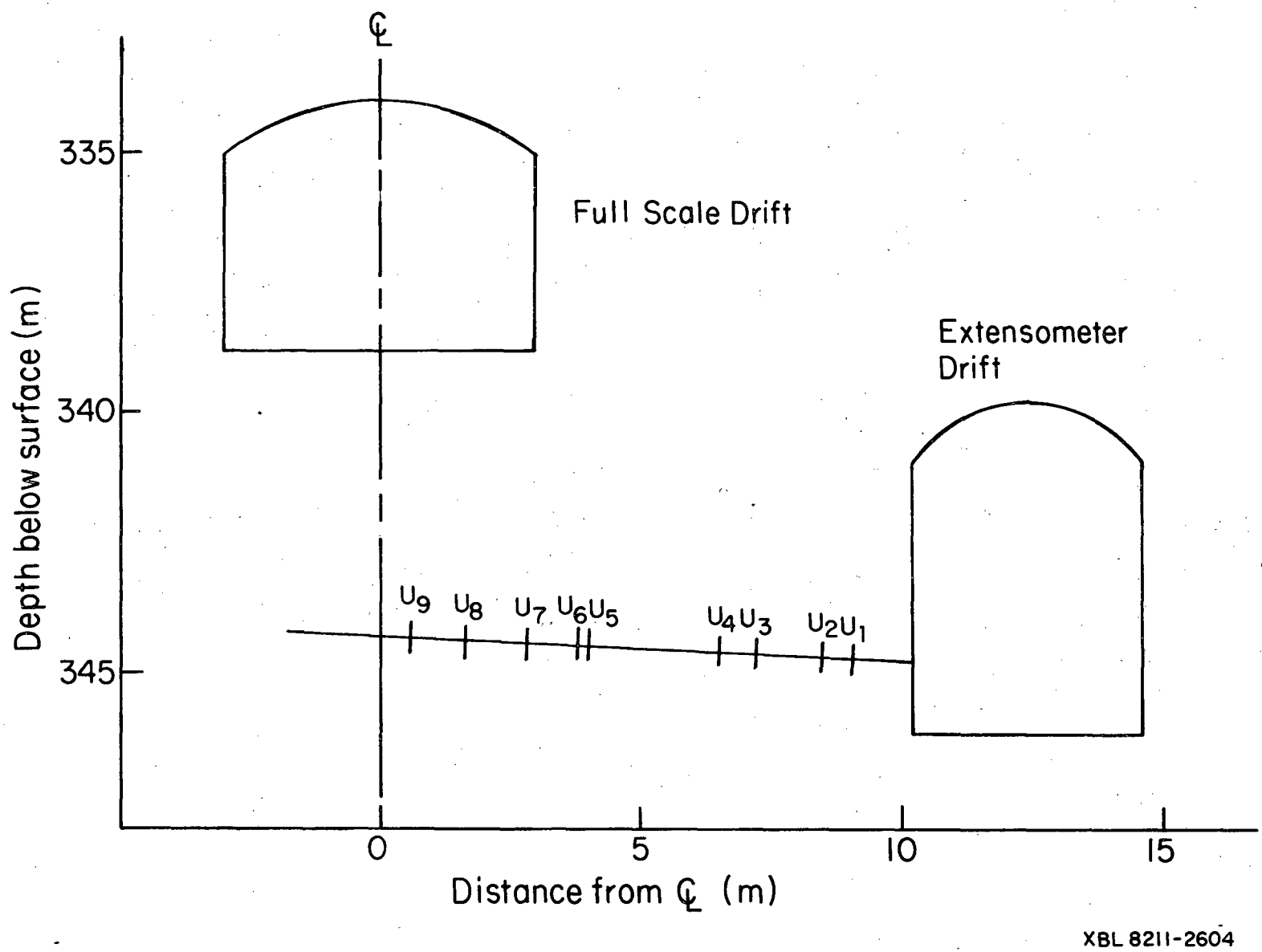

Fig. 4.3 Location of USBM gauge measurements in BSP-3.

Table 4.4. Comments on USBM overcoring.

Overcore	Depth (m)	Comments
1	1.15	Gauge installed with buttons at 1.15 m. The end of the large hole was at 0.90 m and overcoring continued until 1.35 m. Overcoring successful.
2	1.75	Gauge installed with buttons at 1.75 m. The end of the large hole was at 1.58 m and final depth was 1.95 m. Overcoring successful.
3	3.00	The end of the large hole was initially at 2.79 m. Trouble was experienced in installing the gauge but installation finally succeeded at about 3.0 m. Overcoring continued to 3.20 m. Upon removing the core, it was found that the buttons were within 3 cm of a joint. Stress relief occurred.
4	3.75	The end of the large hole was at 3.20 m. A drill pipe was selected so that about 75 cm of overcoring could be accomplished. Gauge was installed at 3.75 m. Initial overcoring was rough due to a high drill stem vibration. This was overcome by stabilizing the string at hole collar using wood pieces. Overcored to a depth of 3.90 m. Overcoring successful.
5	6.23	The end of the large hole was initially at 6.05 m where it had broken along a joint. The gauge was installed at 6.23 m and no problems were experienced. Overcoring continued to a depth of 6.23 m. The plan was then to reinstall the USBM gauge at 6.43 m. On reconnecting the installing tool to the back of the gauge, it was found that the U_1 axis was oriented about 45° clockwise from the vertical. (It had been improperly in stalled). The overcoring was successful and this angle correction should be applied to the final results.

Table 4.4. Comments on USBM overcoring.(continued)

Overcore	Depth (m)	Comments
6	6.43	The gauge was moved ahead in the hole to 6.43 m. Overcoring continued to a depth of 6.60 m. The overcoring was successful.
7	7.44	LuH gauge 4 was installed at a depth of 7.62 m. USBM gauge 7 was then installed at 7.44 m to compare readings. The initial end of the large hole was at 7.12 m. Overcoring proceeded to a depth of 7.55 m, at which point the large core broke along a joint. The core and gauge were rotating in the hole but the drill was stopped before serious damage occurred. The cable was quite twisted but intact. After the gauge and core had been recovered from the hole, it appeared as if the gauge had not rotated with respect to the core. This was checked with the LuH gauge and found to be correct. Overcoring was good. Due to the high rpm and water pressure it was necessary to hold tightly on the cable. Prior to strain relief slipping of the gauge in the hole was observed and the tension was reduced.
8	8.60	Initial hole bottom was at 8.30 m. The gauge was installed at 8.60 m and overcoring was initiated. Initially the drillers were using a high rpm and, due to its twisting from the previous test, the cable was being pulled into the swivel. This required a higher tension on the cable moving the gauge. The drill was stopped and the problem corrected. Overcoring continued at a lower rpm. The overcoring was successful, and, upon retrieving the core and gauge from the hole (together), it was found that the U_1 axis was rotated 8° clockwise from the vertical. This correction should be made.

was to apply a uniform pressure upon the core with a biaxial chamber and to monitor the borehole deformation with the USBM gauge. The core and the gauge are oriented as closely as possible to their in situ condition.

The appropriate formula (plane stress conditions) is:

$$U = \frac{4r_i r_o^2}{r_o^2 - r_i^2} \left(\frac{P}{E}\right) \tag{4.5}$$

where:

U = diametral deformation

r_i = inner radius of core

r_o = outer radius of core

E = Young's modulus

P = applied pressure on outer radius.

The modulus can be written as:

$$E = \frac{4r_i r_o^2}{r_o^2 - r_i^2} \left(\frac{P}{U}\right) \tag{4.6}$$

or

$$E = \frac{2D_i}{\{1 - (D_i/D_o)^2\}} \left(\frac{P}{U}\right) \tag{4.7}$$

where:

D_i = inner diameter

D_o = outer diameter

The most appropriate E for the overcoring data is the average of the values obtained during the unloading of the core from the approximate in situ condition of stress to zero stress, as this is the unloading condition for the in situ stress measurement. The usual practice, however, is to use the loading modulus (some investigators use a tangent modulus, others a secant modulus). In this application the average modulus, including the point at zero stress, was used.

4.5.2. Results from the Biaxial Tests

Unfortunately, because of the presence of joints, it was not possible to test all of the USBM overcore segments in the biaxial chamber, and even for some cores that could be loaded, the USBM gauge had to be translated from its actual in situ position.

Table 4.5 lists the locations in the core where biaxial tests were performed and the corresponding numbers and depths of the stress measurements. Most biaxial tests used USBM gauge 2, as gauge 1 was damaged during stress measurement 8.

Details of the biaxial testing are described in Hustrulid et al. (1982), and only a summary is presented here. Biaxial tests were conducted in 2.1 MPa pressure increments from 0 to 21 MPa and back to 0. The modulus values were calculated from the average of the slopes of the loading and unloading curves. The ratio of two slopes was 1.06; hence the error in selecting one curve over the other is considered small.

Table 4.5. Locations of biaxial tests.

Biaxial Test	USBM Gauge	Position in Core (m)	Corresponding Stress Measurement no. with Depth (m)
1	1	0.6	--
2	1	1.10	1 (1.15)
3	1	1.75	2 (1.75)
4	2	1.12	1 (1.15)
5	2	1.71	2 (1.75)
6	2	3.50	3 (3.00) 4 (3.70)
7	2	6.23	5 (6.48)
8	2	6.43	6 (6.48)
9	2	7.36	7 (7.44)
10	2	8.60	8 (8.60)
11	2	9.66	9 (9.67)

The anisotropy ratio (defined as the ratio of the moduli calculated from the cantilever pairs with greatest and least displacements) ranged between 1.08 and 1.23. This observation, along with the linearity of the pressure-displacement curves, suggests that the assumptions of linear elasticity and isotropy are generally valid for the stress calculations.

The moduli values used in calculating the stresses are given in Table 4.6. Table 4.5 shows which biaxial test was used for each stress measurement. The modulus value for stress measurement 1 is the average of biaxial tests 2 and 4; the modulus value for stress measurement 2 is the average of biaxial tests 3 and 5.

4.6 In Situ Stress Results

Stress measurements using the USBM gauge yielded two types of results: the performance of the gauge and the results of stress calculations.

The USBM gauge performed very well, as all attempted measurements were successful. The outputs of the strain-gauge bridges were stable and showed negligible drift with time. An example of this stability is shown in Fig. 4.4. The deformation of the borehole was readily obtained from plots of bridge output versus drilling penetration. Deformations along the axes; U_1, U_2 and U_3 (Table 4.7) were calculated using the drilling data of Table 4.4 and the bridge outputs of Table 4.7 and are listed in Table 4.8. The sign convention for deformations is that increases in diameter are positive.

Table 4.9 gives the in situ stress values calculated from the displacements of Table 4.8 and the moduli of Table 4.6. The results of Table 4.9

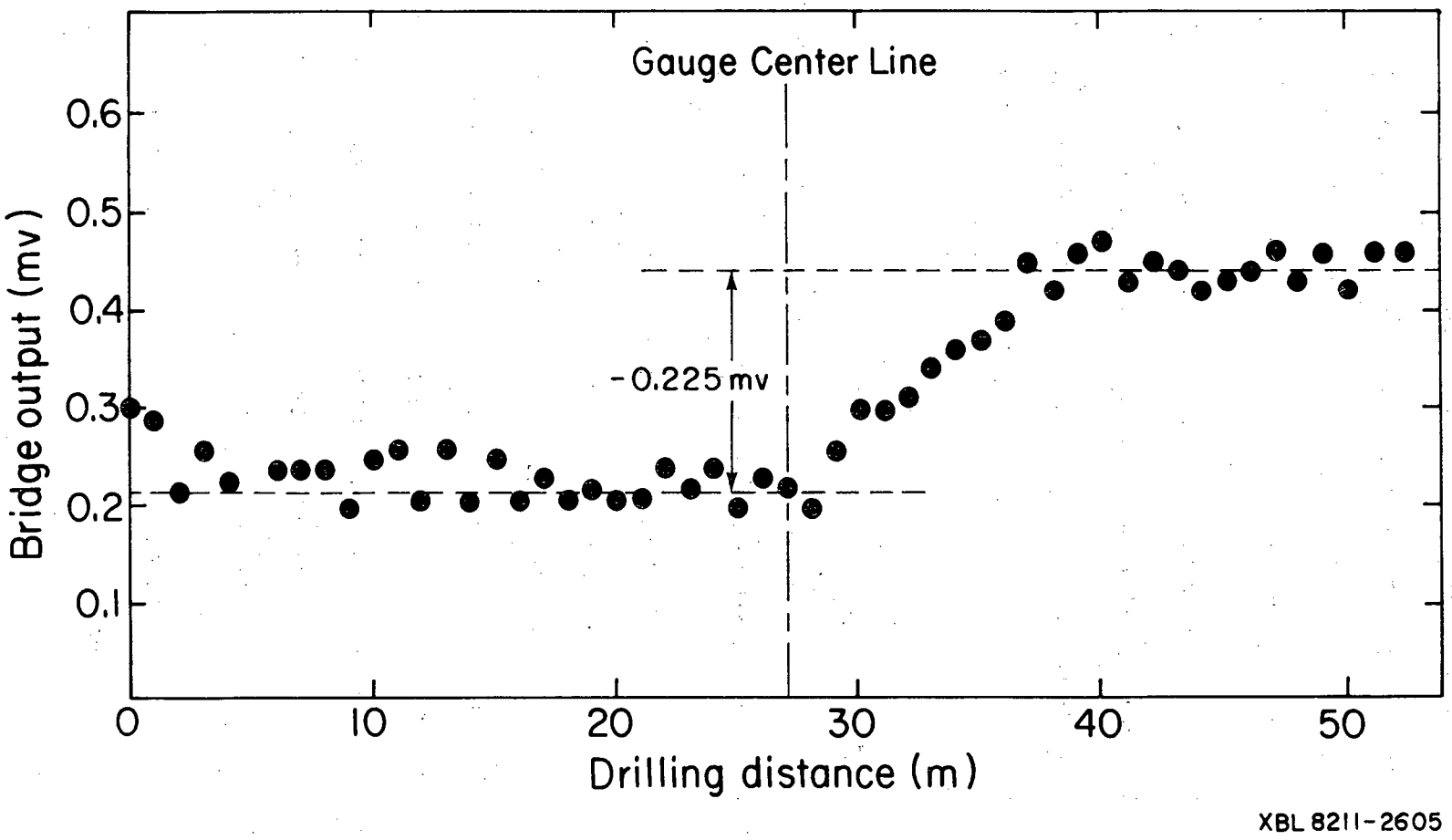

Fig. 4.4 Bridge output vs. drilling distance for USBM measurement 9; depth = 9.67 m

Table 4.6 Elastic moduli values for reducing overcoring data.

Stress Measurement	Depth (m)	Young's Modulus (MPa)
1	1.15	52.6
2	1.75	59.7
3	3.00	50.8
4	3.70	50.8
5	6.23	52.2
6	6.48	57.9
7	7.44	50.6
8	8.60	54.1
9	9.67	58.6

Table 4.7. Summary of the U.S.B.M. gauge output voltage changes (10^{-3} V) obtained during overcoring.

Position	Gauge	Depth (m)	U_1 (mV)	U_2 (mV)	U_3 (mV)
1	1	1.15	0.05	0.495	0.43
2	1	1.75	0.025	0.705	0.58
3	1	3.00	-0.15	0.66	0.645
4	1	3.70	0.025	0.69	0.65
5	1	6.23	0.365	-0.020	0.735
6	1	6.48	-0.065	0.39	0.575
7	1	7.44	-0.08	0.655	0.515
8	1	8.60	-0.14	0.59	0.63
9	1	9.67	-0.225	0.675	0.665

Positive values indicate that the hole increased in diameter.

Table 4.8. Summary of the borehole stress deformation.

Stress Measurement	USBM Gauge	Depth (m)	U_1 (mm)	U_2 (mm)	U_3 (mm)
1	1	1.15	2.05	20.5	19.23
2	1	1.75	1.02	29.2	25.95
3	1	3.00	-6.15	27.4	28.86
4	1	3.70	1.02	28.6	29.08
5	1	6.23	14.96	-.83	32.89
6	1	6.48	-2.66	16.2	25.73
7	1	7.44	-3.28	27.2	23.04
8	1	8.60	-5.74	24.5	28.12
9	1	9.67	-9.38	28.3	27.50

Table 4.9. Principal stresses and directions as determined from the USBM borehole deformation gauge overcoring.

Depth (m)	Principal Stresses (MPa) P	Q	Θ_p(degrees)	ϕ
1.15	13.7	5.5	86.7	-3.3
1.75	21.6	7.7	84.6	-5.4
3.00	18.7	3.5	91.7	1.7
3.70	19.2	6.8	90.6	0.6
6.23	17.3	2.5	135.5[a]	0.5
6.48	16.2	3.6	105.5	10.5
7.44	16.9	4.1	83.7	-6.3
8.60	20.1	3.7	93.72[b]	-4.3
9.67	21.5	2.3	89.1	-0.9

[a] This gauge was indvertently installed with the U_1 axis rotated approximately 45° clockwise from the vertical. The corrected value is 90.5°.

[b] This gauge was installed with the U_1 axis rotated approximately 8° clockwise from the vertical. The corrected value is 85.7.

are plotted against hole depth in Fig. 4.5. Some general characteristics of the results follow. First, orientation of the maximum stress is consistently close to horizontal, as shown by the ϕ angle values. The largest deviation from the horizontal is 10°, and most values are less than 5°.

The maximum stress rises sharply in the first 2 m of the hole, which may reflect a stress concentration around the extensometer drift; it then declines to a minimum value at 6.5 m, approximately at the edge of the full-scale drift. The stress value then rises, possibly because of stress concentrations around the full-scale drift.

Minimum stress shows a gradual decline with hole depth. As this stress is generally vertical, the decline may reflect the stress relief of the full-scale drift.

Comparison of the USBM gauge results with those of other measurements are presented in Chapter 10.

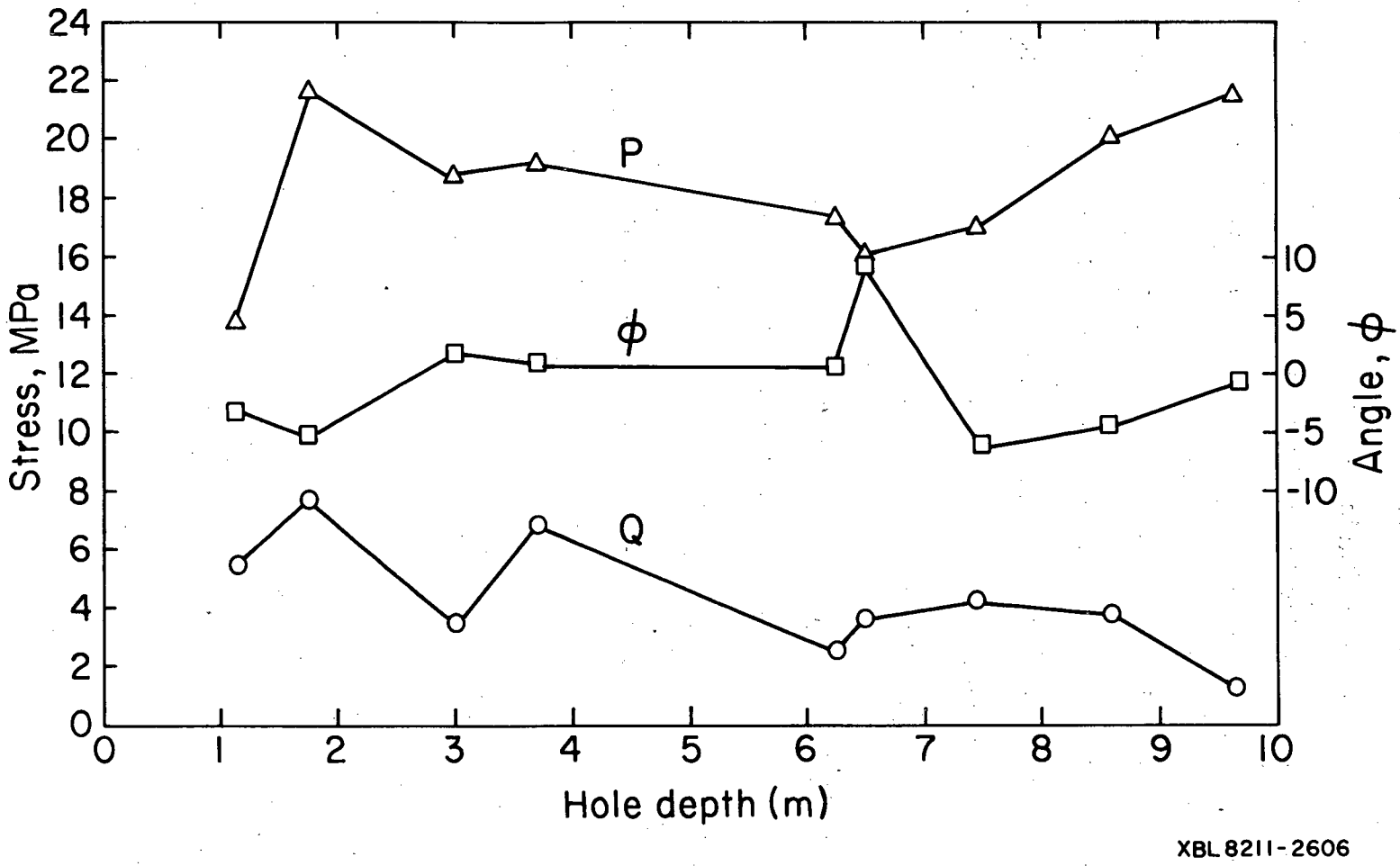

Fig. 4.5 Secondary principal stresses from USBM gauge stress measurements, BSP-3.

5. STRESS DETERMINATIONS IN BSP-1 WITH THE SWEDISH STATE POWER BOARD DEEP-HOLE LEEMAN CELL

(K. Ingevald and L. Strindell)

5.1 Introduction

Six stress measurements using the Swedish State Power Board's deep hole Leeman triaxial cell were performed in BSP-1 between the depths of 1.30 and 9.97 meters. The Power Board Deep Hole cell uses three strain-gauge rosettes. Each rosette contains three gauges with different orientations: axial, tangential, and oblique. Figure 5.1 shows the location of the hole and the measurement points. Originally, the six measurements were to be one meter apart, but closely spaced fractures near the top of the borehole forced us to use slightly longer intervals. The purpose was to compare the BSP-1 Leeman cell results with both hydraulic fracturing and other, more conventional overcoring methods. As this cell is emplaced by a wire line, it was not feasible to perform the measurements in a nonvertical hole such as BSP-2 or 3. While this prevented performing all the overcoring methods in the same hole, it was still possible to compare the BSP-3 and BSP-1 overcoring data because these measurements were performed in the same vicinity under the full-scale drift. All but one of the six Leeman cell measurements were successful; at point 4, the compass failed and the cell could not be oriented. Stress values have been calculated for point 4, but only the vertical stress is properly oriented.

5.2 Field and Laboratory Procedures

The procedures used in the Power Board overcoring measurements are the same as those followed for the deep surface hole, SBH-4, described in Chapter 2. The elastic properties of the rock were determined for each overcored sample by applying both biaxial and uniaxial loads. Biaxial

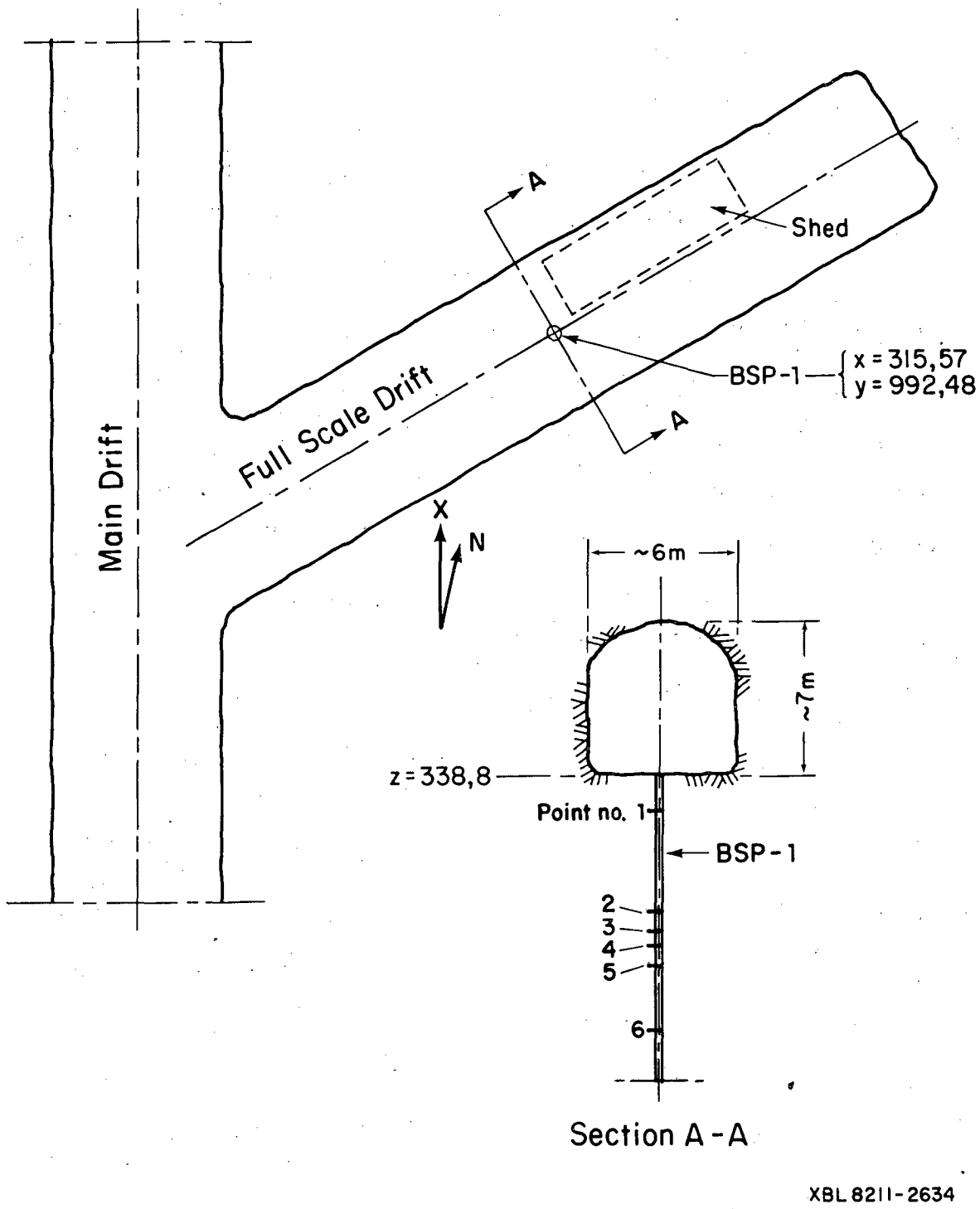

Fig. 5.1 BSP-1: Location of the borehole and power board stress measurement points.

loading was performed in a cell similar to that used for the other overcoring tests. The biaxial pressure ranged from 0 to 6 MPa. The uniaxial loads varied from 0 to 40 kN, or, in units of stress, from 0 to 11.4 MPa. A typical set of calibration curves is shown in Fig. 5.2. The elastic constants determined from laboratory testing are given in Table 5.1. The Young's modulus varied between 50 and 65 GPa, and Poisson's ratio values varied between 0.13 and 0.16. In addition to providing the elastic data for the stress calculations, the laboratory testing was a valuable means of determining the quality of the rosette cementing to the borehole wall.

5.3 Calculation of Stress

As in all Leeman cell measurements, the stresses are calculated on the basis of the strains resulting from the overcoring. Because the cable is detached from the cell during drilling, strain readings are taken only before drilling and after the core is removed; thus no determination of drift similar to that made for the CSIRO and USBM gauges can be made. The strain changes observed for each gauge are given in Table 5.2.

Stress calculations used the same formulae of Leeman (1971) as the LuH and CSIRO measurements. The Young's modulus values came from the laboratory tests on the cores, and the Poisson's ratio was taken as 0.15. The calculations also used a least-squares regression of the strain-gauge data similar to that of used for other overcoring methods. The principal stresses and their orientations are given in Table 5.3 and shown in stereographic projection in Fig. 5.3. The secondary principal stresses, which are the vertical

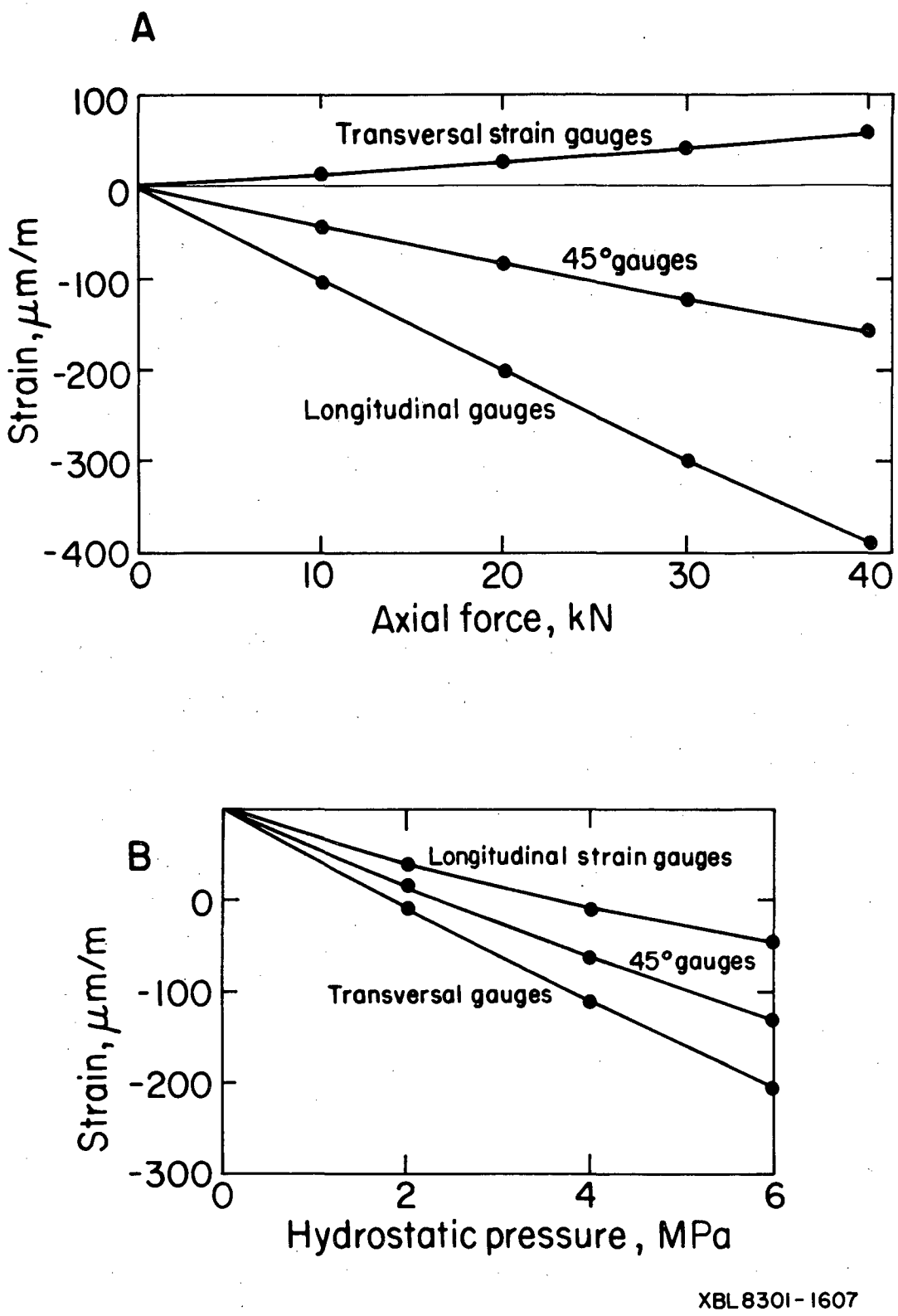

Fig. 5.2 Axial (top) and biaxial (bottom) calibration curves for Power Board overcore 1.

Table 5.1 Depth and bearing of triaxial cell and summary of biaxial test results.

Point	Depth (m)	Compass Bearing (degrees)	Young's Modulus GPa	Poisson's Ratio
1	1.30	333	56.0	0.15
2	5.30	135	64.0	0.15
3	6.05	214	60.0	0.15
4	6.60	a	60.0	0.15
5	7.45	78	56.0	0.15
6	9.97	36	56.0	0.15

[a]Compass damaged

Table 5.2 Summary of strain changes after overcoring (in microstrains).

	Rosette 1			Rosette 2			Rosette 3		
Point	ε_a	ε_θ	ε_{45}	ε_a	ε_θ	ε_{45}	ε_a	ε_θ	ε_{45}
1	57	691	425	154	88	35	36	141	188
2	46	1014	357	60	570	428	61	-288	-73
3	131	24	151	133	336	211	196	1172	854
4	93	915	666	85	736	114	133	-276	34
5	1	-39	100	40	791	389	38	426	83
6	100	430	559	135	54	-9	41	805	266

ε_a - axial strain; ε_θ - tangential strain; ε_{45} - oblique strain

Table 5.3 Principal stress data, BSP-1, overcoring (in MPa).

	σ_1	Plunge ϕ	Trend θ	σ_2	Plunge ϕ	Trend θ	σ_3	Plunge ϕ	Trend θ
1	15.5	5.5	62.8	9.2	61.7	163.2	2.4	27.6	329.9
2	29.4	13.0	64.6	7.6	74.5	211.4	4.2	8.2	332.7
3	28.9	11.4	55.9	14.4	76.1	217.1	5.9	7.8	147.7
4	29.8	a	a	10.2	a	a	1.6	a	a
5	19.3	4.2	66.2	8.7	46.3	160.6	1.0	43.4	332.2
6	22.5	25.6	89.2	10.9	37.4	200.6	2.7	41.8	333.8

[a]Compass damaged

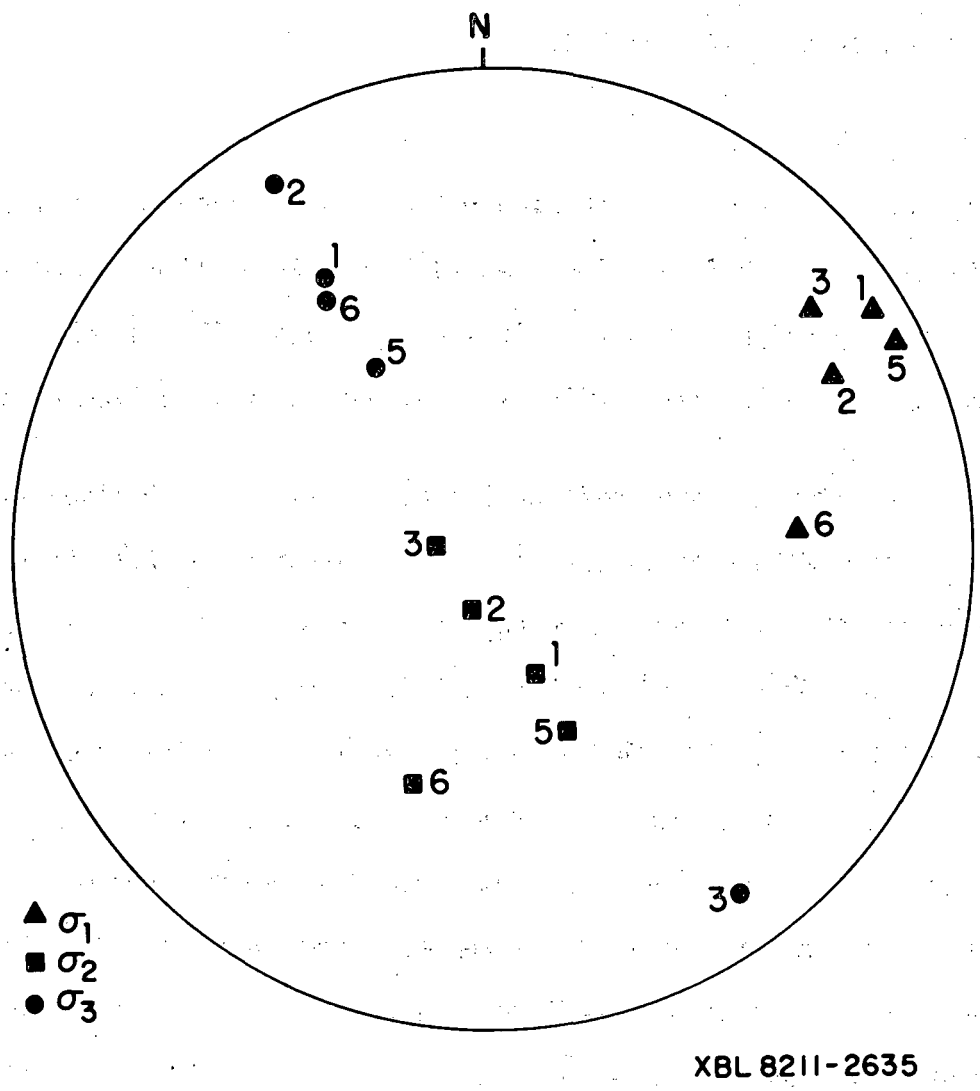

Fig. 5.3 Lower hemisphere stereographic projection of the principal stress directions determined by overcoring in the vertical borehole, BSP-1. Identification numbers are given for each test.

stress and the maximum and minimum horizontal stresses, are given in Table 5.4 and shown in Fig. 5.4.

5.4 Discussion

The maximum principal stress was found to be oriented parallel to the axis of the full-scale drift and inclined less than 25.6° from the horizontal. As the maximum principal stress, σ, is nearly horizontal, its values and orientations are close to those calculated for the maximum horizontal stress, P.

The intermediate and least principal stresses are inclined with respect to the horizontal and vertical. The intermediate principal stresses are oriented off the vertical an average of about 60°. The minimum principal stresses are within 30° of the horizontal. There is little discernible trend to the changes in orientation of the minor principal stresses with depth. Surprisingly, the least stress is the closer of the two to being horizontal, contrary to what one would expect from the proximity of the the full-scale drift. This stress relationship is reflected in the consistently higher value of the vertical stresses relative to the minimum horizontal stresses. The vertical stresses are also in excess of the lithostatic stress calculated from the weight of the overburden (8.4 MPa based on a 24.9 kPa/m stress gradient). Conversely, the minimum horizontal stress values seem to be low, particularly the four shallowest values, which would be within the zone of tangential stress concentration due to the full-scale drift. If the far-field minimum horizontal stress were equal to the lithostatic pressure, then this stress concentration would be twice the value of the lithostatic stress at the floor of the drift (or 16.8 MPa) and would

Table 5.4. Secondary principal stresses, BSP-1, overcoring (in MPa).

	$\sigma_{H_{Max}}$	$\sigma_{H_{Min}}$	σ_v	Bearing of σ_{HMax}
1	15.5	3.9	7.8	61.5
2	28.3	4.2	8.6	64.3
3	28.3	6.0	14.8	56.4
4	27.1	3.4	11.1	a
5	19.2	4.6	5.1	65.1
6	19.7	6.9	9.4	81.1

[a]Compass damaged

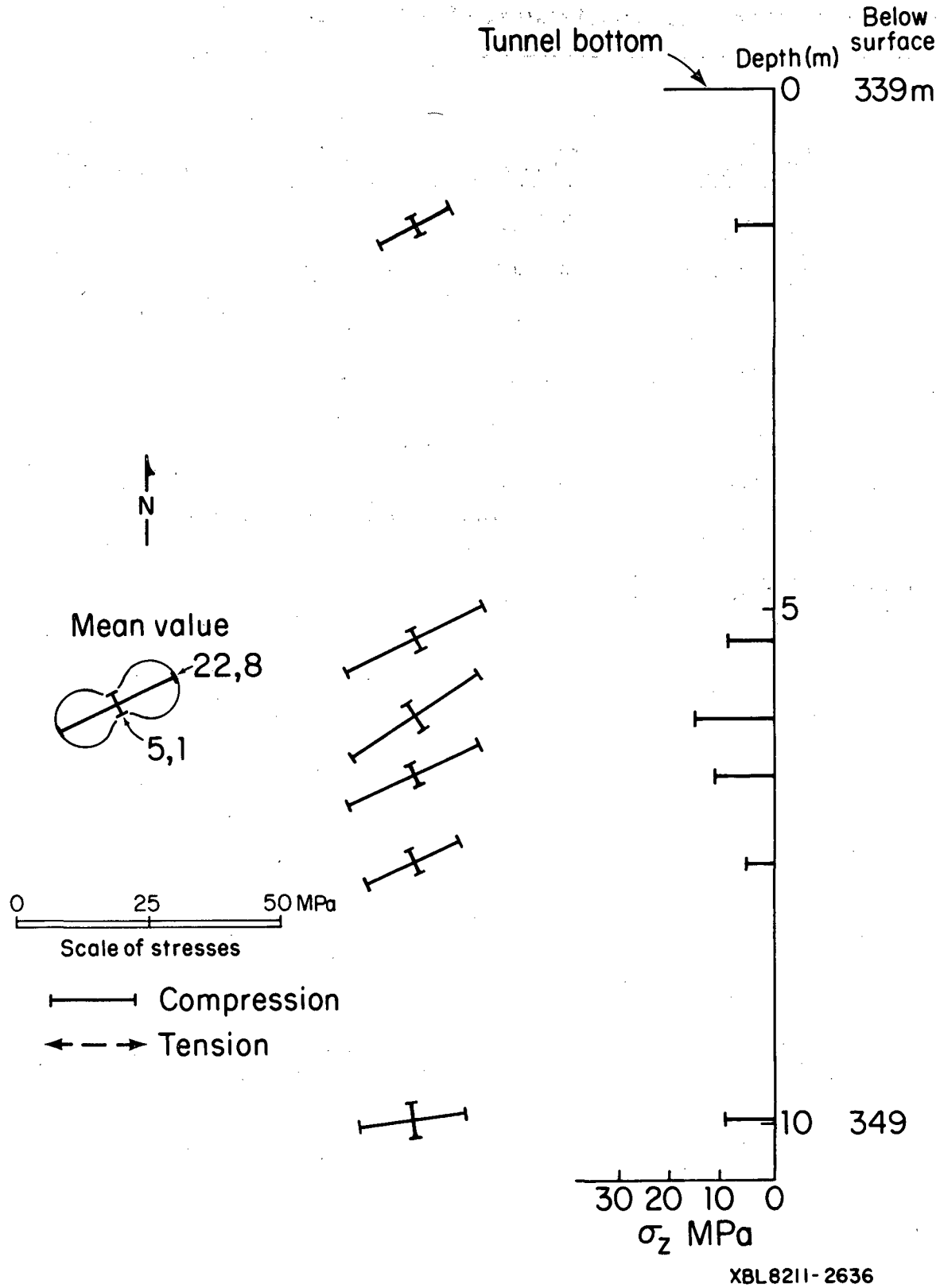

Fig. 5.4 Secondary stresses measured in BSP-1 using Power Board overcoring.

fall rapidly to 9.9 MPa at a depth of 6.0 meters. The values for the minimum horizontal stress within 6.6 m of the drift vary from 3.4 to 6.0 MPa suggesting either that the far-field horizontal minimum stress is much less than lithostatic or that the stresses have been partially relieved, possibly by fracturing.

Although the calculations of the maximum principal and horizontal stresses for the Power Board overcoring and the other overcoring measurements are similar, the orientation of the other stresses are not consistent, as the BSP-3 result with the LuH cell showed minimum stresses closer to the vertical. Further discussion of the Power Board results compared with those of the other methods is contained in Chapter 10.

6. CSIRO STRAIN CELL MEASUREMENTS
(W. Hustrulid and B. Leijon)

6.1 Introduction

In 1972, the Australian Council of Scientific and Industrial Research Organizations (CSIRO) began to develop a strain cell that would provide the complete state of stress from measurements performed in a single borehole. It was to be of the same basic design as the CSIR (Leeman) triaxial strain cell in that it employed three 3-element strain-gauge rosettes, but with modifications so that (1) full protection would be given to the electric circuitry and (2) strain observations could be made during overcoring.

The final result was the CSIRO hollow inclusion (H.I) gauge (Fig. 6.1). It is constructed as follows: the strain-gauge rosettes are glued to a thin-walled (35 mm O.D., 32 mm I.D.) epoxy pipe with an epoxy cement. After the leads have been attached, a thin coating of Araldite D is applied to protect the gauges. The final cell diameter is 36 mm.

The strain cell is glued to the wall of the nominal 38 mm diameter borehole with a special Araldite-based cement. The strain gauges are thus separated from the wall of the borehole by an epoxy-filled gap 1.5 mm in thickness. Worotnicki and Walton (1976) have shown that this epoxy gap does not affect the measured value of the axial strain but that the circumferential and off-axial strains are slightly higher than if the strain gauges had been glued directly to the rock surface. As a result, four correction factors (K_1 through K_4) must be used to convert the measured strains into their equivalent values at the borehole wall. Once these strains have been determined, the equations developed by Leeman (1971) for interpreting triaxial cell

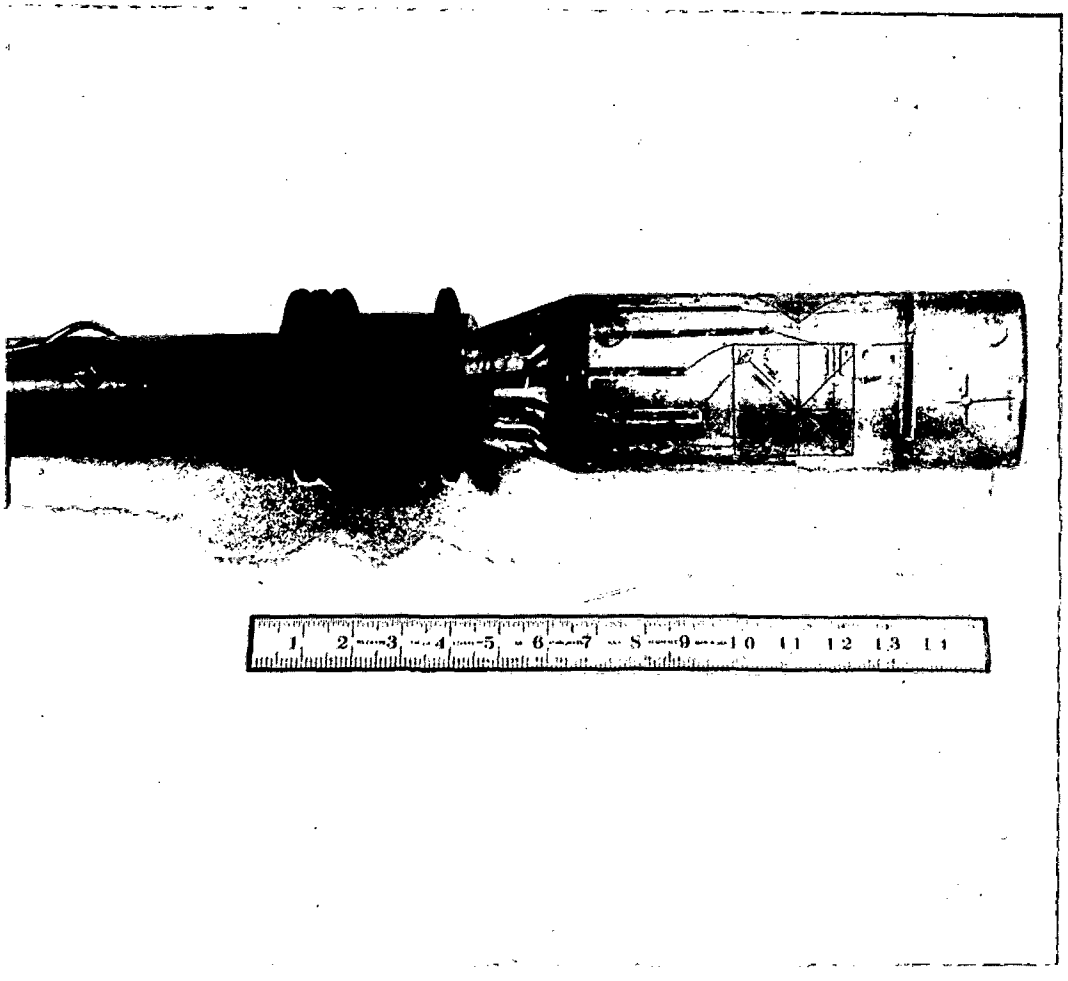

Fig. 6.1 Photograph of CSIRO gauge for use in horizontal holes.

triaxial cell strain results can be applied. Table 6.1 shows that the values of the K factors depend on the ratio of the elastic moduli of the rock and strain cell (E_r:E_{pl}), and on the radius (r_{sg}) to the strain gauge position.

The elastic properties for the epoxy pipe and the cement, E_{pl} and ν_{pl}, are assumed to be the same and equal to:

E_{pl} = Young's modulus = 2.8 to 3.5 GPa.

ν_{pl} = Poisson's ratio = 0.35 to 0.40.

Since the rock has an elastic modulus (E_r) of about 55 GPa, and r_{sg} - 17.5 mm, the correction factors become:

K_1 = 1.12 K_3 = 1.08

K_2 = 1.13 K_4 = 0.91

To specify the location and orientation of the gauge in the hole, two angles (α and β) are required where

α = angle of the rosette in the hole, measured clockwise from north or up, looking down the hole.

β = angle of gauge in the rosette, measured clockwise from down hole axis.

For the Stripa measurements, rosette B was installed on the bottom side of the horizontal hole as shown in Fig. 6.2; the α and β angles are given in Table 6.2. The rock should be isotropic and linearly elastic.

Table 6.1. Variation in K factors for modifying the CSIRO strain readings with rock-cell modulus ratio and strain gauge radius (r_{sg}).

E_r E_{pl}	r_{sg} (mm)	K_1	K_2	K_3	K_4
20	17.0	1.18	1.20	1.11	0.88
20	17.5	1.12	1.13	1.08	0.91
20	18.0	1.07	1.07	1.05	0.95
10	17.5	1.10	1.08	1.08	
5	17.5	1.08	1.02	1.08	
3	17.5	1.04	1.00		

Table 6.2. Location and orientation of the strain gauges in the CSIRO cell.

Rosette	Gauge	α(deg)	β(deg)
A	1	322.9	0
	2	300.0	90
	3	300.0	45
B	4	163.6	45
	5	163.6	135
	6	180.0	90
C	7	82.9	0
	8	60.0	90
	9	60.0	45

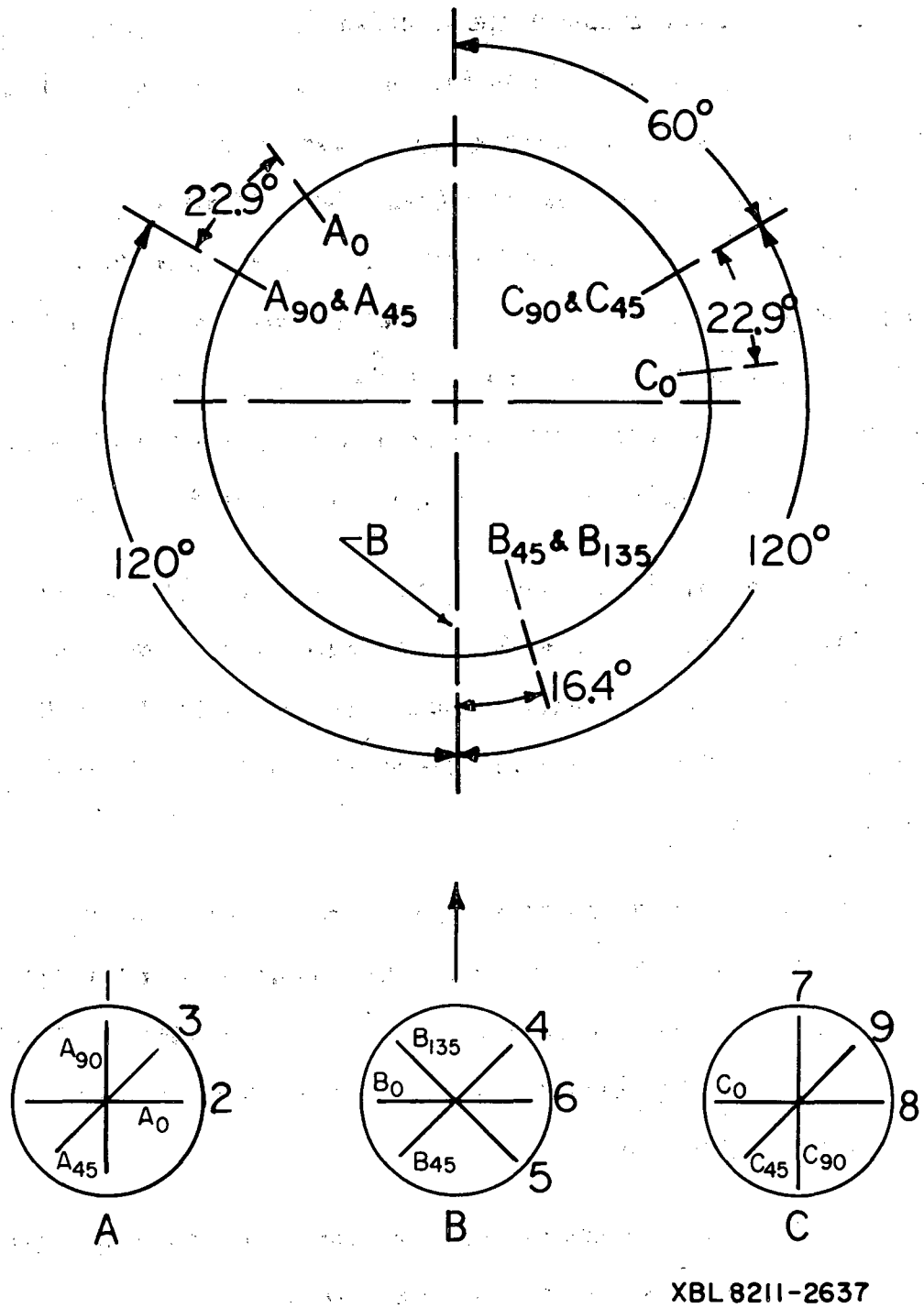

Fig. 6.2 Location and orientation of the strain gauges in the CSIRO cell.

A diagram of the gauge is shown in Fig. 6.3. The recommended field procedure is summarized in Fig. 6.4. Some major points regarding installation, data collection, and data analysis taken from the instruction manual (CSIRO, no date) are summarized as follows. The pilot (38 mm) hole in which the gauge is to be installed is drilled approximately 60 cm deeper than the large-diameter hole. At least 18 cm of full-diameter core bounding the CSIRO gauge must be recovered for representative results. The epoxy grout requires a minimum of 12 hours and preferably 16 hours to cure and must be blended differently for different rock temperatures (see Table 6.3).

The readout cable is attached to a strain indicator in quarter-bridge configuration. Once the initial set of readings are taken, the drilling water is turned on. Readings are taken at 5-minute intervals until consecutive readings are repeatable to within 5 microstrains (this normally takes 10 minutes).

Overcoring begins once the base readings are established. Drilling should proceed at about 2 cm per minute, without pausing for strain readings. Overcoring should continue well past the gauge positions (30 cm is a reasonable limit). Final readings are taken 5 and 10 minutes after drillng ceases with drilling water turned off.

A "typical" overcoring result reproduced from the CSIRO manual is shown in Fig. 6.5. The strain change for each channel is taken as the microstrain change in output between readings taken 10 cm before and 15 cm after the gauge position.

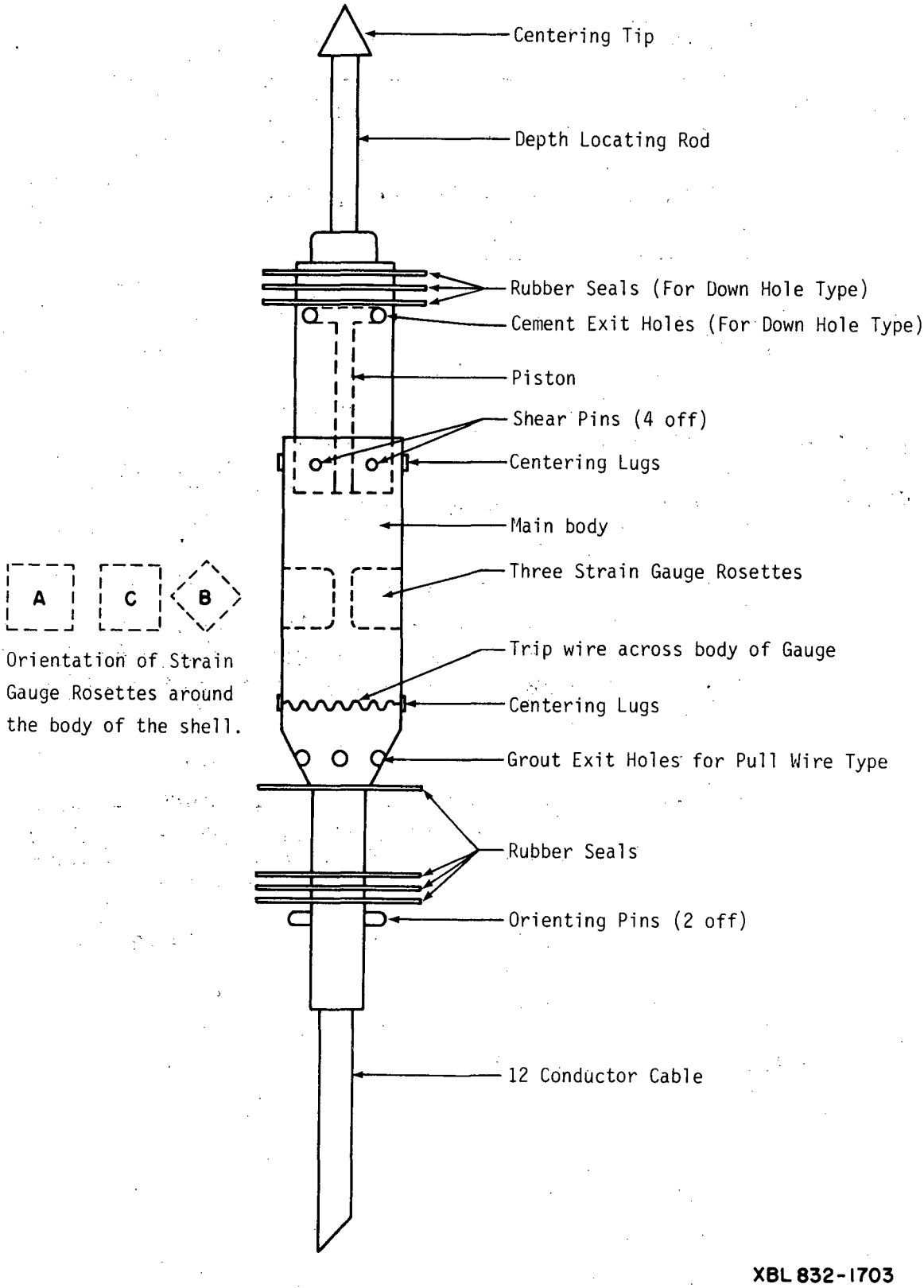

Fig. 6.3 Schematic layout of CSIRO cell.

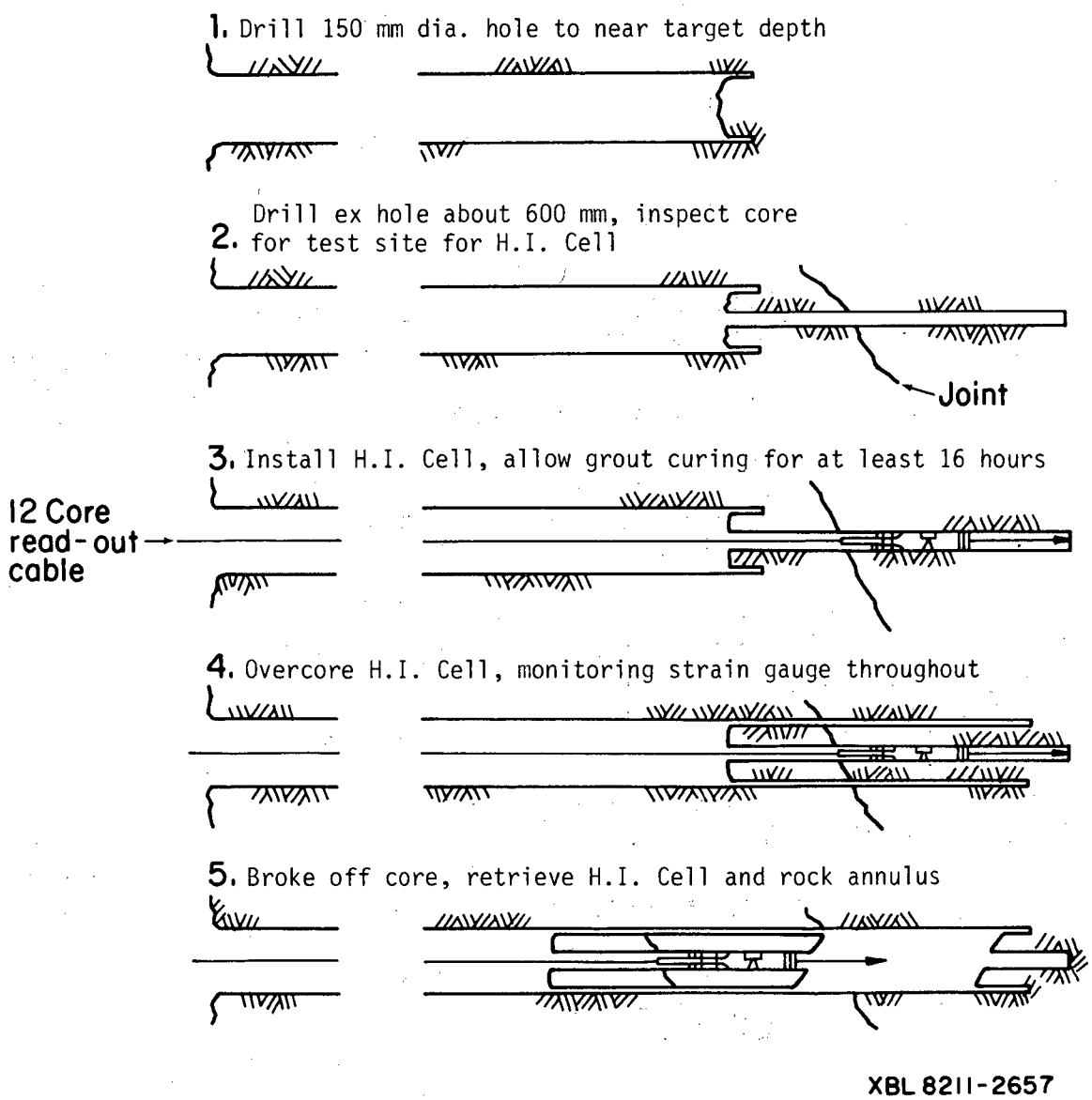

Fig. 6.4 Field procedure for stress measurement with CSIRO cell.

Table 6.3. Epoxy grout mixtures for various rock tempertures.

Rock Temperature C°	F°	Araldite Resin (g) LC 230	"D"	Araldite Hardener (g) LC 230	Hardener (g) HY 956
10-15	50- 59	100	100	120	20
15-20	59- 68	100	100	90	18
20-40	68-104	100	95	60	17

Note: These components are unavailable in the U.S; Araldite 1255 can be substituted for LC230 and Araldite 502 for "D".

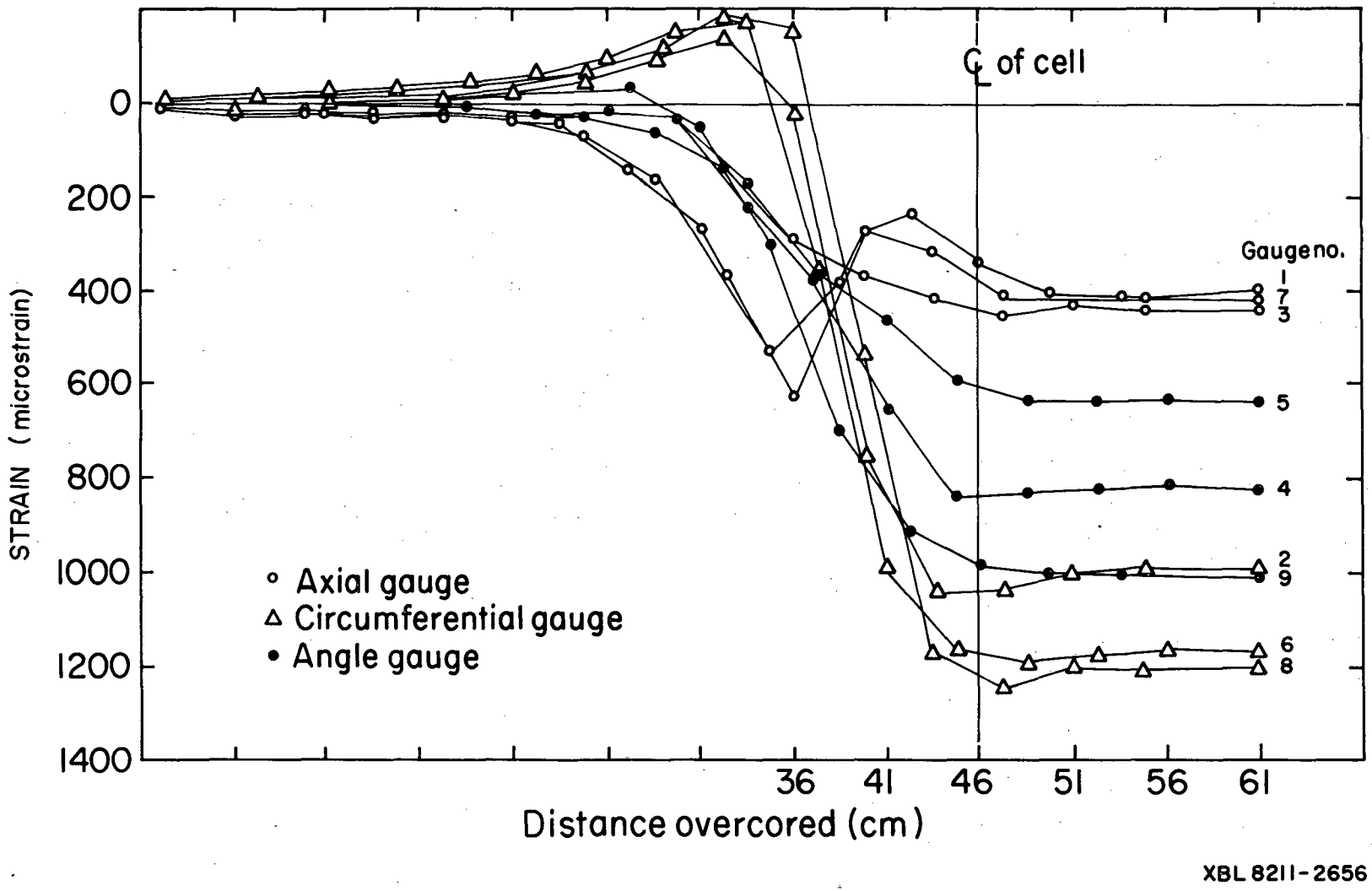

Fig. 6.5 Ideal changes in strain-gauge readings during overcoring of CSIRO gauge (from CSIRO manual, no date).

Like the LuH cell, a minimum of six strains is required for the measurement, and elastic constants are obtained by biaxial testing of the core with the cell intact.

6.2 Field Overcoring Results

6.2.1 General Comments

The recommended procedures for installing the CSIRO gauges as outlined in the CSIRO instruction manual were followed for the BSP-3 measurements. For the strain readout, a bridge completion circuit (Fig. 6.6), an HLAB power supply, and a Fluke data logger were used in place of a strain indicator system. As a result, each of the nine strain channels plus the bridge voltage were read and recorded on paper tape for every 1 cm of drill advance. This was a very convenient method for obtaining the data. The location of the CSIRO tests is shown in Fig. 6.7. Specific remarks on each test can be found in Table 6.4.

It is suspected that the cement used for overcoring tests 1 and 2 (10-15°C temperature range, as shown in Table 6.3) did not properly set even though the time allowed should have been adequate and the proportions of the components followed CSIRO procedures. The estimated rock temperature of 10-12° was possibly too cold. No strain relief was observed with overcoring test 2, and the results have not been analyzed or included. Because of these difficulties, the cement was replaced by a low-temperature type supplied by the Swedish Mining Research Foundation. The cement consisted of the following mixture:

Araldite	BY154	50 g
Hardener	MY2992	15 g
Silica flour	KB or $KIN8_0$	70 g

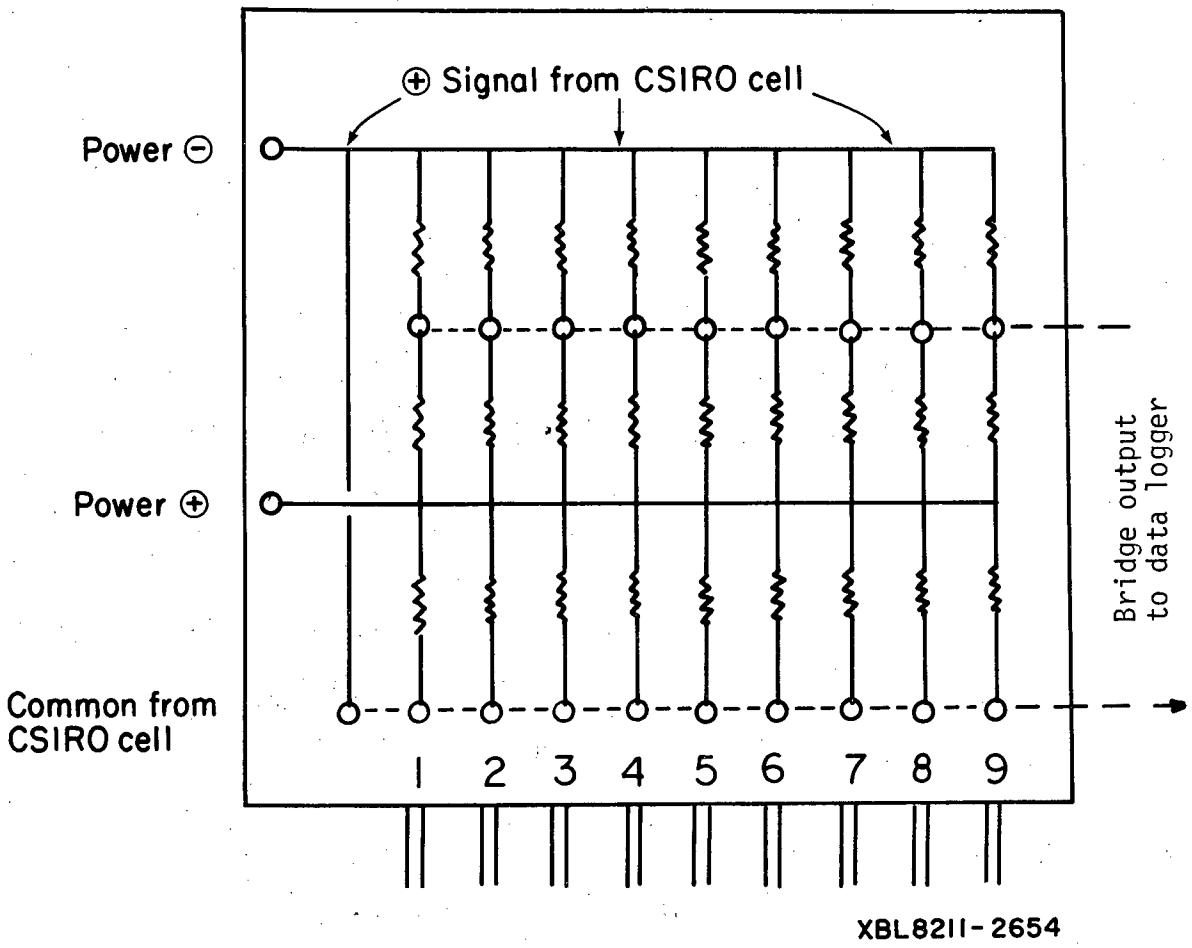

Fig. 6.6 Bridge completion circuit used with the CSIRO gauges.

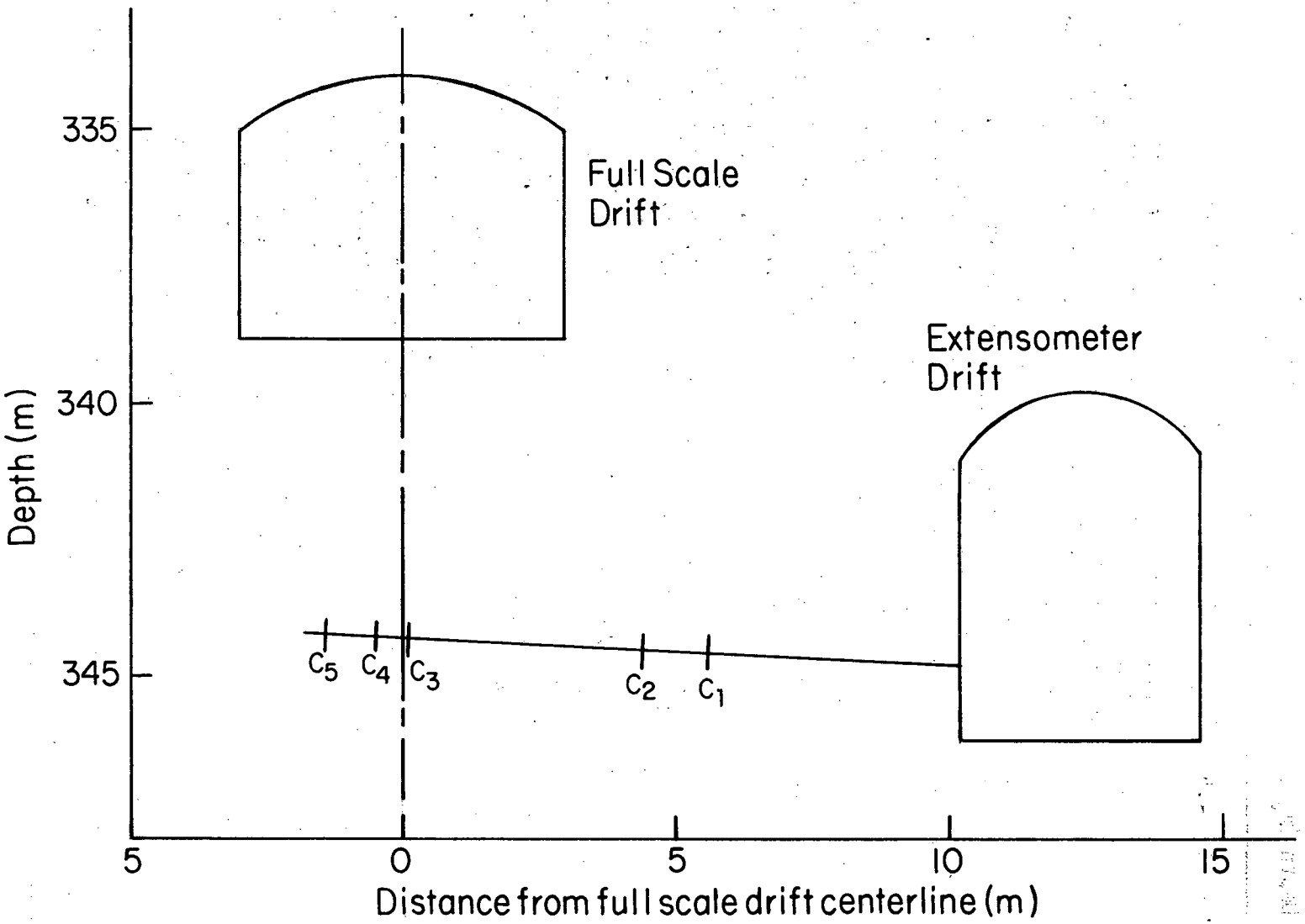

Fig. 6.7 Location of CSIRO measurements in BSP-3.

Table 6.4. Comments on the CSIRO overcoring.

Overcore	Depth (m)	Comments
CSIRO 1	4.62	The end of the large hole was at 4.39 m. CSIRO Gauge 1 (Serial No. 136201) was installed at a depth of 4.62 m at 7:00 p.m. The 38 mm hole was cleaned first with the LuH device and then with degreaser-impregnated gauze wrapped around the installing tool. The four-component (pre-measured) Araldite cement supplied with the gauges was used. The "B" rosette was oriented in the down position in the hole with the orientation controlled using the mercury switch. At 6:20 the following morning, the cement remaining in the mixing dish was solid but not hard or brittle. The mine air and rock temperature was about 10-11°C and possibly this was the reason. The gauge was connected to the data logger via the bridge. The power supply was set at 6.00. With the water turned on, the gauge readings appeared to drift. After about 20 minutes drift was still present; however, the rate was fairly low and constant. Overcoring went smoothly with readings being taken every 1 cm of advance. Strain relief occurred as the bit passed at a depth of 4.83 m. The water was allowed to continue running for 20 minutes with readings being taken. The drift was very large. An examination of the core and gauge revealed that much of the cement appeared to move backward rather than foward over the gauges. It was not possible to ascertain which gauges were good.
CSIRO 2	5.83	The face of the large hole was at 5.68 m. CSIRO 2 (serial no. 1362801) was installed at a depth of 5.83 m using the four component cement. The gauge was installed later in the afternoon. At 6:40 the following morning, the cement in the mixing dish was solid although the surface was a little tacky. The water was turned on, readings were taken for approximately 20 minutes. Drift occurred as in CSIRO 1. Overcoring commenced and was completed successfully. Drift continued after the drill was stopped while leaving the water running. The core broke along a natural joint (depth about 6.0 m).

Table 6.4. (Cont'd)

Overcore	Depth	Comments
CSIRO 3	10.12	The CSIRO #3 (serial number 1362101) was installed at a depth of 10.12 m using the special cold temperature cement supplied by the Swedish Mining Research Foundation (SMRF). Gauge installation was completed at 7:15 p.m. and the cement allowed to dry overnight. Upon returning to the mine at 6:20 a.m., the cement remaining in the mixing dish was hard and brittle. The gauge was connected to the data logger, and overcoring to a depth of 10.44 m was completed at 8:00 a.m. to study any drift. The core was then removed from the hole.
CSIRO 4	10.44	With the end of the large hole at 10.44 m, the pilot hole was extended to a depth of 11.90 m. CSIRO gauge 4 (1363101) was installed at a depth of 10.74 m at 12 noon, using the same cement as CSIRO #3. The next morning the cement was hard. At 7:20 a.m. the gauge was connected to the data logger and the water turned on. Overcoring was completed at 8:00 a.m. and the core was removed at 8:40 a.m. The end of the large hole was at 10.96 m. During this test as in the others, changes in the initial zero readings were observed without any drilling taking place but with the water turned on. This may be due to changes in the drill water temperature. Initially water is taken from a 55 gallon drum which is then replenished from the mine supply.
CSIRO 5	11.61	The bottom of the large hole was at 11.29 m and gauge was installed at 11.61 m in the afternoon using the SMRP cement. The following morning the leftover cement was observed to be quite hard. The gauge was connected to the data logger and overcoring was completed by 8:50 a.m. The hole bottom was at 11.9 m. Changes in the bridge output suggested that strain relief had been accomplished.

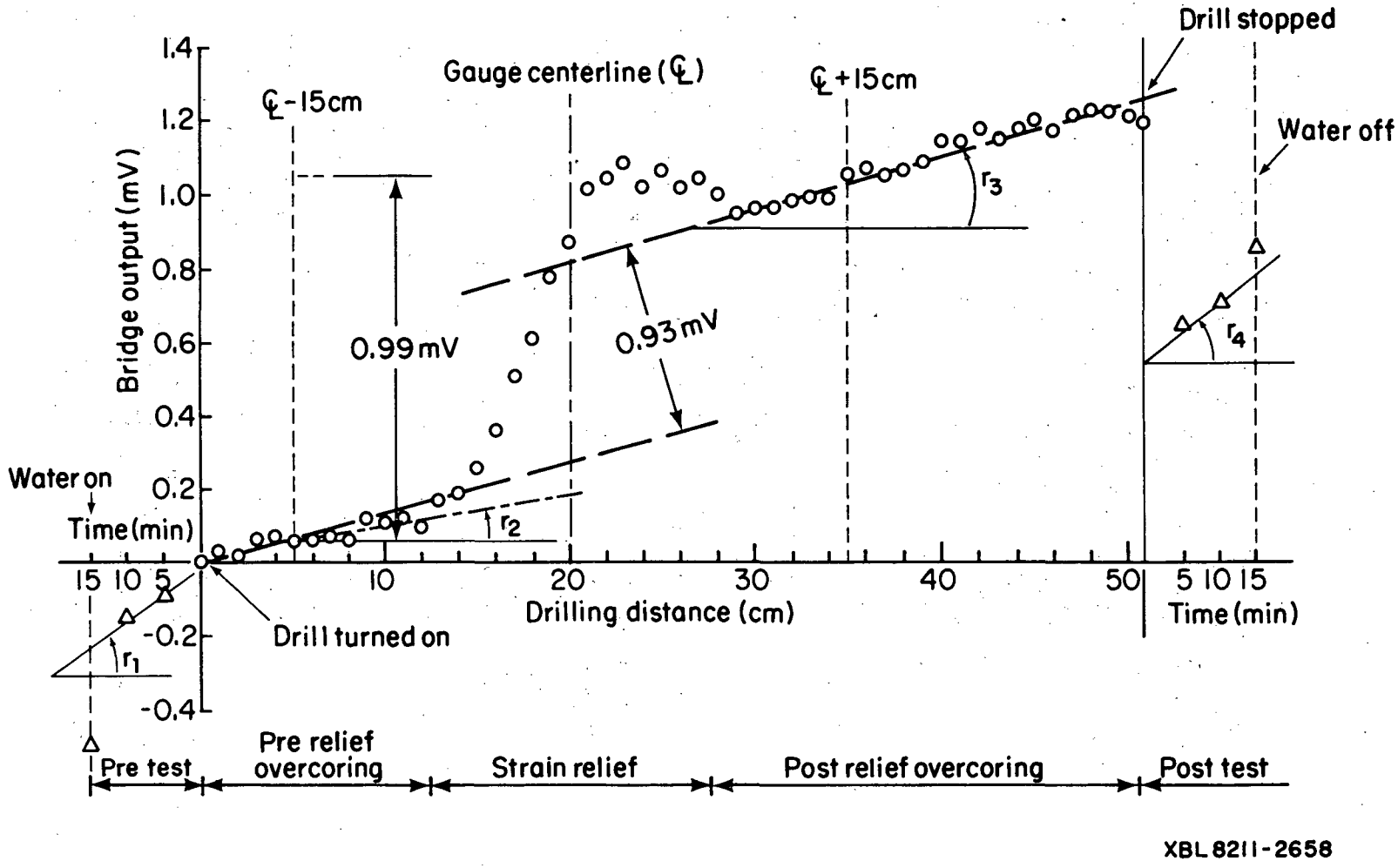

Fig. 6.8 Typical bridge output (strain) as a function of drilling distance (from CSIRO test 3).

This cement has been found satisfactory for temperatures down to 3°C. No hardening problems were encountered during the remaining measurements.

6.2.2 Analysis of the Strain Relief Records

A typical output voltage (strain)-time curve for overcores 3, 4, and 5 is shown in Fig. 6.8. The curve can be broken down into five sections: pre-test; pre-relief overcoring; strain relief; post-relief overcoring; and post test.

During pretest, the drilling water has been turned on, but drilling has not commenced. As Fig. 6.8 shows, there is a large change (112 με apparent compression) during the first 5 minutes; then the bridge output changes at a steady rate (r_1) with time. For the case shown:

$$r_1 = 0.016 \text{ mV/min} = 5.1 \text{ με/min}^*$$

This is much higher than the suggested acceptable drift rate of 1 με/ min in the instruction manual.

Pre-relief overcoring begins when the drilling starts and continues to a point about 8-10 cm in front of the gauge. The curve in Fig. 6.8 departs from the "typical" curves in Fig. 6.5 in that the bridge output continues to change, suggesting apparent tension with both time and drilling distance. Because the drilling proceeded at a constant rate, the rate of drift can be expressed in terms of either time or distance. The rate of drift for section 2 (r_2) is:

$$r_2 = 0.0087 \text{ mV/cm} = 2.8 \text{ με/cm}.$$

*The conversion from millivolts to με is 1 mV = 319 με.

Strain relief occurs within ± 10 cm of the gauge's center line. The curve shows a compressive strain as the bit approaches the gauge, tensile relief during its passage past the gauge position, and then a compressive rebound. This is very similar to the "typical" curve shape of Fig. 6.5 as well as that observed during the overcoring of the USBM borehole deformation gauges.

During post-relief overcoring, output voltage, in theory, should not change with time. Instead, Fig. 6.8 shows the output changing at a constant rate (r_3) with overcoring distance:

$$r_3 = 0.0145 \text{ mV/cm} = 4.5 \ \mu\varepsilon/\text{cm}.$$

Finally, in post-test, the drill is stopped, but the water is allowed to run. During the first 5 minutes there is a considerable change (175 $\mu\varepsilon$), which is an apparent compression. Then the drift with time continues, but in a tensile direction:

$$r_4 = 0.020 \text{ mV/min} = 6.4 \ \mu\varepsilon/\text{min}.$$

Two approaches were used to determine the strain relief. The first was to locate the positions 15 cm on each side of the gauge center line. The strains at each point were read from the paper tape record and the difference was obtained by subtraction. For the curve shown in Fig. 6.8:

$$\Delta\varepsilon = 0.99 \text{ mV} = 316 \ \mu\varepsilon.$$

For CSIRO 1, each curve was examined, the more-or-less flat portions prior to and after strain relief were selected by eye, and $\Delta\varepsilon$ was calculated.

The second approach was to include the effect of the apparent drift. The drift rate, both before overcoring (r_1) and during it (either r_2 or r_3, whichever period was longer) was calculated. The results are presented in Table 6.5. The calculations used the average drill rates, which are also given.

From the tables and the overcoring records, it is found that:

- The initial drift when turning on the water is typical for temperature effects on ill-balanced bridge circuits.
- With the exception of overcore 1, the direction of the drift changes from apparent compression to apparent tension as drilling begins.
- The drift rates during overcoring are very similar for overcorings 3, 4, and 5. They are also much higher than before overcoring (on a average, by a factor of 6).
- For overcorings 3-5, all gauges behave similarly until drilling is completed. The post-overcoring drift varies considerably, as some gauges appear to stabilize, while others continue to drift.
- Overcoring 1 (standard cement) is different from the others (SMRF cement) in that drift rates during overcoring are negative (apparent compression) and much lower.

Clearly, the strain records demand further explanation with respect to the complicated drift behavior found.

Table 6.5 Drift rates prior to and during overcoring[a].

Gauge No.	Drift Rate (με/min)							
	OC 1		OC 3		OC 4		OC 5	
	Prior	During	Prior	During	Prior	During	Prior	During
1	7.3	-1.0	5.4	5.7	6.1	5.9	5.7	5.9
2	8.0	-2.0	5.1	4.5	6.4	5.0	5.1	5.5
3	8.6	-2.1	3.2	4.8	6.4	4.8	4.5	5.9
4	8.9	-2.2	3.8	4.3	6.1	4.5	3.8	4.8
5	7.0	-1.8	4.8	4.4	6.1	4.6	4.8	5.1
6	7.0	-2.4	5.7	4.5	6.1	3.6	6.1	3.4
7	8.0	-2.0	5.1	6.2	5.7	6.0	4.8	5.7
8	8.9	-2.3	3.8	4.6	6.4	4.7	4.8	5.7
9	8.9	-1.7	4.5	6.3	6.1	5.1	4.5	6.6
Avg	8.0	-1.9	4.5		6.1	4.9	4.9	5.5

[a]No strain relief was observed for OC 2; hence, results are not included. Average drill rates were: OC 1, 5.53 cm/min; OC 3, 5.05 cm/min; OC 4, 6.77 cm/min; and OC 5, 6.33 cm/min.

One explanation is in the bridge circuit developed for the data logger. Unlike conventional strain indicators, the data-logger circuit is not compensated for changes in cable resistance with temperature. Thus, the drift observed in CSIRO 3, 4, and 5 may reflect changes in cable temperature caused by circulating drill water.

Strain values commonly peak as the drill passes the gauge center line because of the stress concentration around the bit kerf, but the magnitude of the peak in Fig. 6.9 is much greater than would be expected from this effect. An alternative explanation is that large borehole deformations broke the cement bond between the cell and the rock.

The consequences of ignoring or accepting the peak value are considerable. The gauge 6 strains, if the peak is ignored, are 258 με without drift or 26 με with drift. If we use the peak value, these strains are 1034 με without drift and 1008 με with drift.

It is useful to summarize the problems of interpreting the CSIRO data given so far. The basic analytical method described in the CSIRO manual calls for taking the difference between the bridge outputs 15 cm before and after the gauge center line. We question this approach for our data because of the large drift rate. To solve this problem, we draw parallel straight lines through the pre-relief and post-relief drift curves. If these lines have a slope angle, Θ, and if the y-axis separation of the lines is "x," then the bridge voltage change for strain calculations will be $x/\cos\Theta$. On one test, CSIRO 5, there is a large peak at strain relief. We feel this peak may reflect decoupling of the gauge; thus strain relief should be based on the peak-value. The peak-value strain relief may be calculated either with or without the effect of drift.

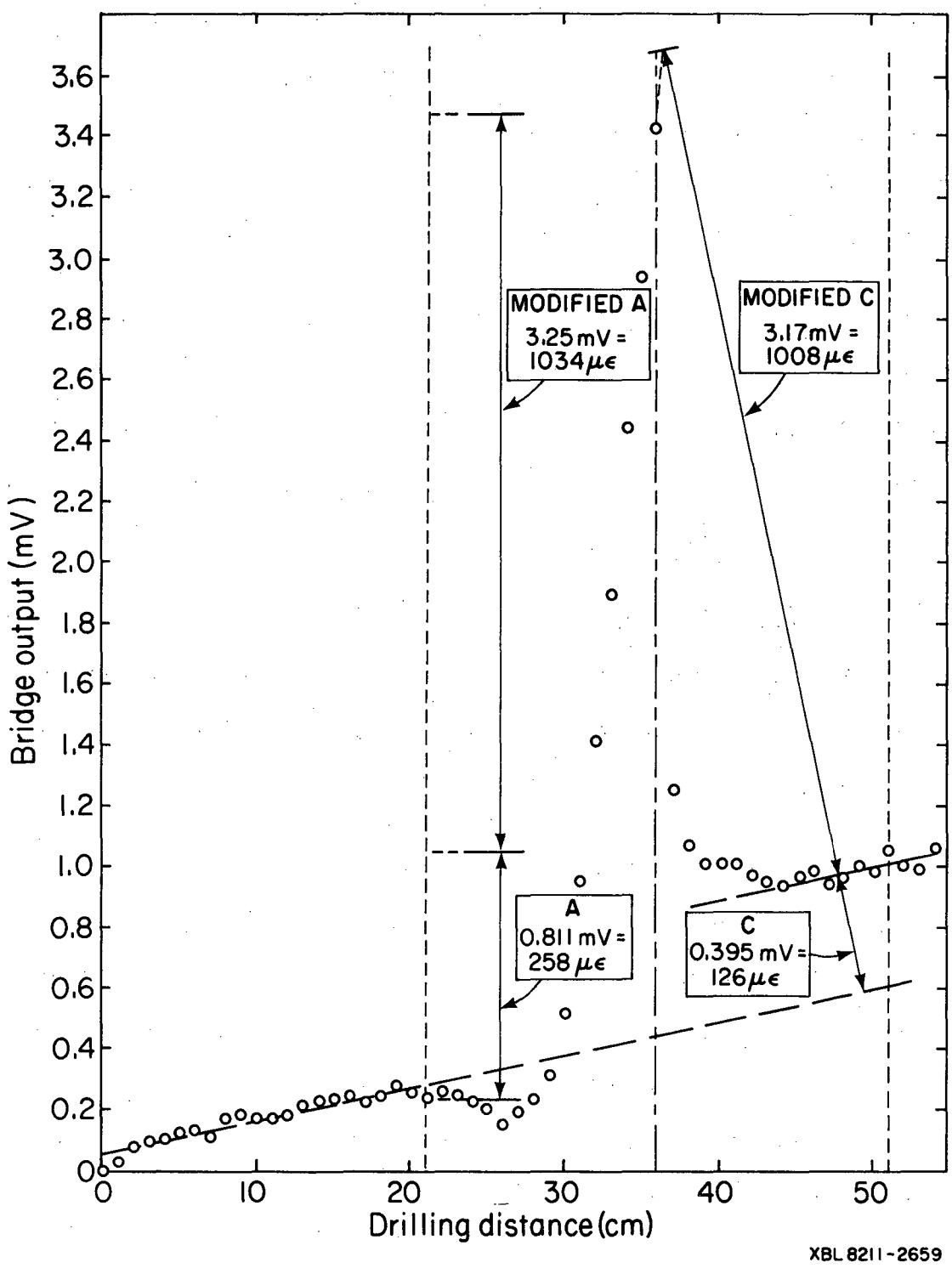

Fig. 6.9 Bridge output as a function of drilling distance for CSIRO 5, gauge 6. "A" and "C" indicate alternate interpretations of strain change due to overcoring.

The application of these methods to calculating stresses is discussed further in Section 6.4.

6.3 Biaxial Testing Results

The cores obtained during the overcoring process were inserted into the biaxial chamber, and strains were recorded for 2.1 MPa pressure increments from 0 to 21 MPa and back to 0.

If the rock is elastic, isotropic, and homogeneous and if the cementing of each overcore is identical, then the slopes of the curves obtained during biaxial testing from similarly oriented gauges should be identical.

But gauges that should have recorded equal strain often did not give equal results. To improve the quality of the field results, we used a "calibration" technique, in which the rosette providing the most linear data is selected for calculating "calibration factors" relating the biaxial test outputs of the gauges in this rosette with gauges of corresponding orientation. These factors can then be applied to the field overcoring strains. This process is described further in Section 6.4.

Poisson's ratio can be obtained by plotting the output of gauge 1 against that of gauge 2 as well as gauges 7 and 8.

Young's modulus can be determined from examining the applied pressure and the outputs of circumferential gauges 2, 6, and 8, using the formula:

$$E = 5.22 \times 10^{-2} P/V$$

where:

E = Young's modulus (GPa)

P = applied biaxial pressure (MPa)

V = output voltage (mV)

These calculations are based on the following parameters:

bridge voltage	= 6.04
gauge factor	= 2.09
inner diameter	= 38.2 mm
outer core diameter	= 141.5 mm
gap factor	= 1.12

A summary of the results of biaxial testing data is given in Table 6.6. Besides providing needed elastic property data, the biaxial curves (a) give an indication as to the linearity of the gauge-rock intereaction, (b) help to suggest which gauges are most reliable, and (c) allow a "calibration" adjustment to be made.

6.4 Principal Stress Magnitudes and Directions

Section 6.2 described two methods of interpreting the bridge output voltages to obtain strains: (1) the standard CSIRO procedure and (2) a

Table 6.6 Biaxial elastic property determinations using the CSIRO overcores.

Overcore	Strain Gauge Pairs	Load(L) Unload (U)	Poisson's Ratio	Young's Modulus (GPa)	Linear?
1	1-2	L	0.315		Yes
		U	0.320		No
	7-8	L	0.235		Yes
		U	0.231		Yes
	2	L		72.1	Yes
		U		70.3	Yes
	6	L		59.6	Yes
		U		59.0	Yes
	8	L		62.0	Yes
		U		61.5	Yes
3	1-2	L	0.268		Yes
		U	0.296		Yes
	7-8	L	0.265		Range of 8.3 to 3000 psi
		U	0.323		
	2	L		63.9	Yes
		U		67.4	Yes
	6	L		53.5	Yes
		U		56.1	Yes

Table 6.6 (Cont'd)

Overcore	Strain Gauge of Pairs	Load(L) Unload (U)	Poisson's Ratio	Young's Modulus (gpa)	Linear?
	8	L		87.0	No
		U		94.1	No
4	1-2	L	0.322		Yes
		U	0.350		Yes
	7-8	L	0.204		Initial portion nonlinear
			0.228		
	2	L		70.90	Nonlinear as the beginning
				67.1	
	6	L		91.0	Very non-linear at beginning
		U		79.3	
	8	L		54.3	Yes
		U		56.9	Yes
5	1-2	L	0.322		Yes
		U	0.350		Yes
	7-8	L	0.205		Initial portion is non-linear
		U	0.229		
	2	L		75.4	Yes
		U		75.2	Yes

Table 6.6 (Cont'd)

Overcore	Strain Gauge of Pairs	Load(L) Unload (U)	Poisson's Ratio	Young's Modulus (GPa)	Linear?
	6	L		99.9	Initial portion is non-linear
		U		73.9	
	8	L		72.6	Initial portion is very nonlinear
		U		75.0	

modified procedure that allows for drift. Section 6.3 described two methods of applying the biaxial chamber modulus test data: (1) using all gauge data and (2) weighting the gauge outputs in favor of those that appear to be working properly.

Thus, there are four combinations of analyses that can be done:

A = strain changes obtained using the measured strains at points $\geq$ 15 cm from the gauge center line.

B = strain changes obtained by applying calibration factors to the "A" strains.

C = observed strain changes when bridge drift is included.

D = strain changes obtained by applying calibration factors to the "C" strains.

The basic data for calculating principal stress magnitudes and directions for CSIRO overcores 1, 3, 4, and 5 are given in Tables 6.7 through 6.10. In addition, a separate analysis of CSIRO 5 has been made in which values for the "corrected" curves (gauges 6, 8, and 9) have been substituted for those in Table 6-10. These substitutions appear in Table 6.11.

As indicated earlier, only six values of strain change are needed to solve for the magnitudes and directions to the principal stresses. To assist in identifying the gauge readings that might be the best, a qualitative summary of the biaxial and field results has been constructed (Table 6.12). In the calculation of the stresses, the quality of the gauge readings is evaluated by a computer program (described in Chapter 5) that compares the predicted strains according to a least squares fit of all the data with the actual values and rejects the one showing the largest deviation. This is successively repeated until the minimum number of six values remain.

Table 6.7. Strain changes during the overcoring of CSIRO 1 as a function of selection procedure and data interpretation.

	Strain Changes During Overcoring (με)			
Gauge	A	B	C	D
1	57	56	49	48
2	93	104	160	179
3	108	119	137	151
4	57	71	93	116
5	54	42	96	75
6	89	82	160	156
7	73	74	67	68
8	112	108	172	166
9	83	72	105	91

A = center line ± 15 cm
B = calibration factor applied to A
C = bridge drift included
D = calibration factor applied to C

Calibration Factor	Young's Modulus (GPa)	Poisson's Ratio
No	64.0	0.275
Yes	64.0	0.275

Table 6.8. Strain changes during the overcoring of CSIRO 3 as a function of selection procedure and data interpretation.

	Strain Changes During Overcoring (με)			
Gauge	A	B	C	D
1	223	223	51	51
2	316	344	169	184
3	236	246	70	73
4	842	868	689	710
5	526	486	399	369
6	1285	1168	1155	1050
7	255	190	71	53
8	380	559	216	318
9	309	621	102	205

A = center line ± 15 cm

B = calibration factor applied to A

C = bridge drift included

D = calibration factor applied to C

Calibration Factor	Young's Modulus (GPa)	Poisson's Ratio
No	60.4	.288
Yes	58.7	.266

Table 6.9. Strain changes during the overcoring of CSIRO 4 as a function of selection procedure and data interpretation.

	Strain Changes During Overcoring (με)			
Gauge	A	B	C	D
1	182	170	45	42
2	166	183	19	21
3	- 77	- 77	- 186	- 186
4	520	832	383	617
5	242	332	97	133
6	584	749	456	585
7	166	175	18	19
8	249	229	114	105
9	255	255	120	120

A = center line ± 15 cm

B = calibration factor applied to A

C = bridge drift included

D = calibration factor applied to C

Calibration Factor	Young's Modulus GPa	Poisson's Ratio
No	65.7	0.265
Yes	62.3	0.265

Table 6.10. Strain changes during the overcoring of CSIRO 5 as a function of selection procedure and data interpretation.

	Strain Changes During Overing (με)			
Gauge	A	B	C	D
1	198	198	20	20
2	278	280	113	114
3	265	262	105	104
4	616	456	458	339
5	651	602	455	421
6	258	256	126	125
7	450	332	291	215
8	57	57	-102	-102
9	217	235	37	40

A = center line ± 15 cm

B = calibration factor applied to A

C = bridge drift included

D = calibration factor applied to C

Calibration Factor	Young's Modulus GPa	Poisson's Ratio
No	74.4	0.277
Yes	74.4	0.277

Table 6.11. "Corrected" strain changes for CSIRO 5

Gauge	Strain changes During Overcoring (με)			
	A	B	C	D
6	1034	1026	1009	1001
8	494	494	408	408
9	303	328	109	118

The principal stress magnitudes and directions have been calculated for each of the four cases (A, B, C, D) for overcores 1, 3, 4 and 5. The "starred" values for overcore 5 are those calculated using the corrected strains of Table 6.11. The results are shown in Tables 6.13 through 6.16 and in Figures 6.10 through 6.14. As can be seen, the choice of technique has a great effect on the results. In evaluating them it is most helpful to keep in mind those obtained with the LuH and USBM techniques.

For case A the magnitudes and directions of the principal stresses vary widely even over the short distances between CSIRO tests 3, 4, and 5. The addition of calibration factors (case B) improves the consistency of results over the depth range of 10.12 to 11.61 m, but those for CSIRO 1 are still much lower than the others. This might be thought due to the effect of depth, but no such effort has appeared with the other techniques. Rather, cement 1 probably did not allow the full transmittal of strains to the gauge. The inclusion of drift (case C), yields directions for overcores 3 and 4 that are similar to those determined by the LuH gauges, but the direction of CSIRO 5 is still very different. The magnitudes found from CSIRO 3 are also very close to the LuH results. The magnitudes suggested by CSIRO 4 are approximately one-half of those for CSIRO 3 even though the tests are only separated by 30 cm of hole length. Again, poor cementing may have been the reason. The use of the calibration factors (case D) seems to improve the agreement of CSIRO 3 with the LuH results.

As indicated eariler, a "shift" apparently occurred in the readings for gauges 6, 8, and 9 of CSIRO 5. Results using "corrected" readings and moduli

Table 6.12. Evaluation of strain-gauge data for stress determinations from field and laboratory records (X = yes, N = no).

Gauge	overcore 1		overcore 3		overcore 4		overcore 5	
	field	lab	field	lab	field	lab	field	lab
1	X	X	X	X	X	X	X	X
2	X	X	X	X	X	?	X	X
3	X	X	X	X	X	?	X	X
4	X	X	X	X	X	N	X	N
5	X	X	X	X	X	N	X	X
6	X	X	X?	X	X	N	X	?
7	X	X	X	X?	X	X	X?	X
8	X	X	X	N	X	X	X	?
9	X	X	X	N	X	X	X	N?

Table 6.13. Principal stress magnitudes and directions for the CSIRO overcores: Case A.

Over-core No.	Depth (m)	σ_1 (MPa)			σ_2 (MPa)			σ_3 (MPa)		
		Mag.	Dip	Bear.	Mag.	Dip	Bear.	Mag.	Dip	Bear.
1	4.62	6.71	-11.2	338.6	3.74	-58.5	229.7	3.23	29.0	254.9
3	10.12	31.12	0.2	88.7	23.86	6.7	358.7	11.26	83.3	180.6
4	10.44	19.95	- 9.7	115.3	13.36	-23.4	209.5	5.38	64.5	184.3
5	11.61	42.57	- 0.2	322.2	13.20	-37.2	52.3	8.78	52.8	52.0

Table 6.14. Principal stress magnitudes and directions for the CSIRO overcores: Case B.

Overcore No.	Depth (m)	σ_1(MPa)			σ_2(MPa)			σ_3 (MPa)		
		Mag.	Dip	Bear.	Mag.	Dip	Bear.	Mag.	Dip	Bear.
1	4.62	7.03	-14.3	333.7	3.72	74.5	358.5	3.34	6.3	245.3
3	10.12	27.49	4.3	69.2	26.41	24.9	337.2	10.32	-64.6	348.3
4	10.44	26.64	-10.1	110.2	12.86	-32.1	206.6	3.25	55.9	184.9
5	11.61	33.02	- 1.3	146.2	12.82	-33.4	55.3	7.96	56.6	58.3

Table 6.15. Principal stress magnitudes and directions for the CSIRO overcores: Case C.

Overcore No.	Depth (m)	σ_1(MPa)			σ_2(MPa)			σ_3(MPa)		
		Mag.	Dip	Bear.	Mag.	Dip	Bear.	Mag.	Dip	Bear.
1	4.62	7.42	-17.6	342.0	5.68	-34.8	239.3	5.25	-49.8	94.1
3	10.12	25.24	1.3	75.6	11.84	6.0	345.4	5.78	-83.8	357.5
4	10.44	11.14	0.7	82.2	6.40	30.0	351.8	0.59	-60.0	353.5
5	11.61	26.87	- 0.2	137.7	6.00	-35.4	47.5	1.68	54.6	48.0

Table 6.16. Principal stress magnitudes and directions for the CSIRO overcores: Case D.

Overcore No.	Depth (m)	σ_1(MPa)			σ_2(MPa)			σ_3(MPa)		
		Mag.	Dip	Bear.	Mag.	Dip	Bear.	Mag.	Dip	Bear.
1	4.62	7.89	-21.6	330.0	5.70	-49.3	87.5	5.37	32.5	45.4
3	10.12	22.60	3.4	72.2	11.37	21.8	340.8	6.38	-67.9	350.5
4	10.44	13.14	0.0	80.5	6.69	28.6	350.5	0.32	-61.4	350.5
5	11.61	20.02	- 1.3	139.7	5.80	-31.4	49.0	1.13	58.6	51.8

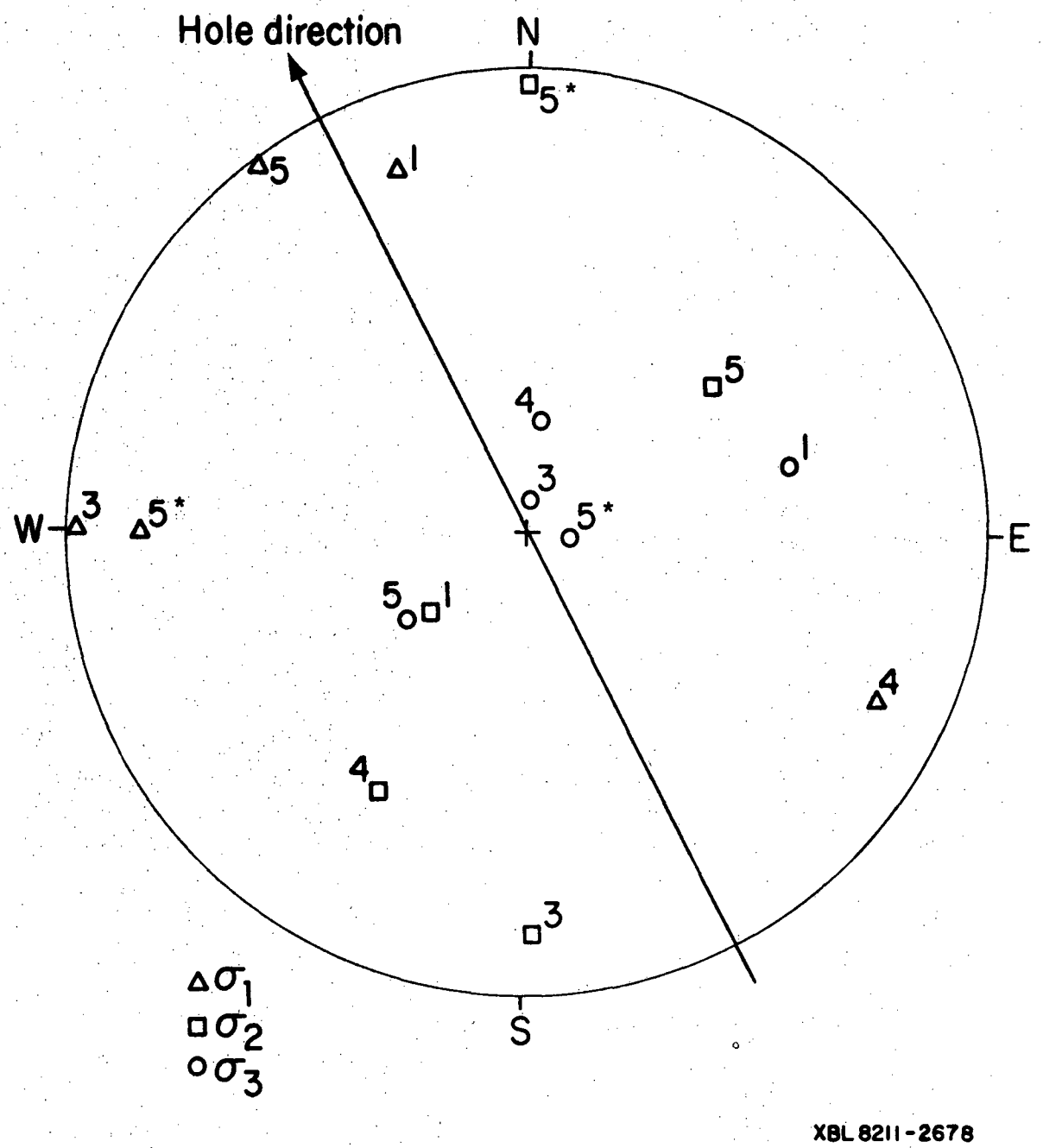

Fig. 6.10 Principal stress directions for case A analysis of CSIRO measurements. Numbers identify tests. Asterisks indicate "corrected" analyses.

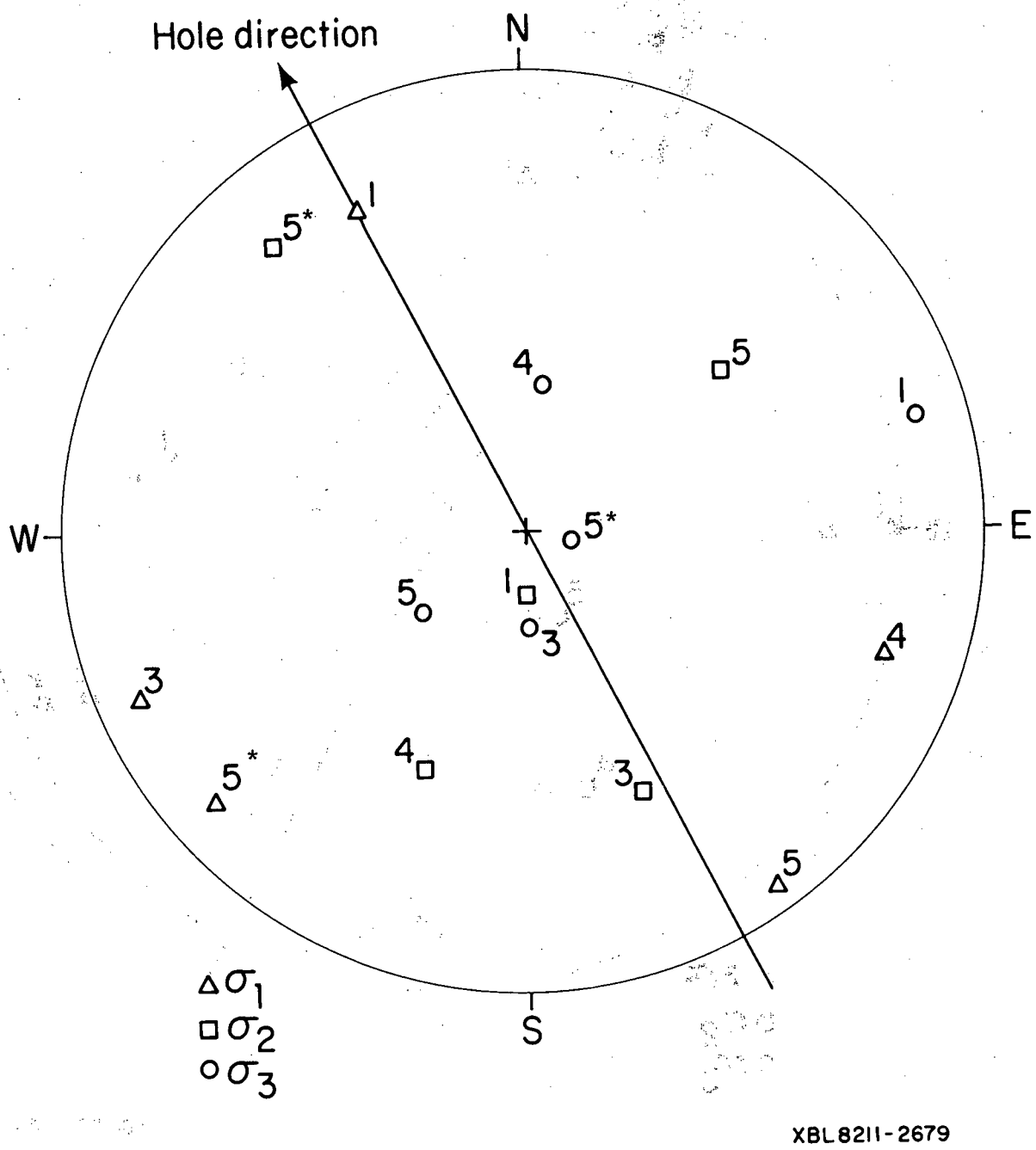

Fig. 6.11 Principal stress directions for Case B analysis of the CSIRO measurements. Numbers identify test. Asterisks indicate "corrected" analyses.

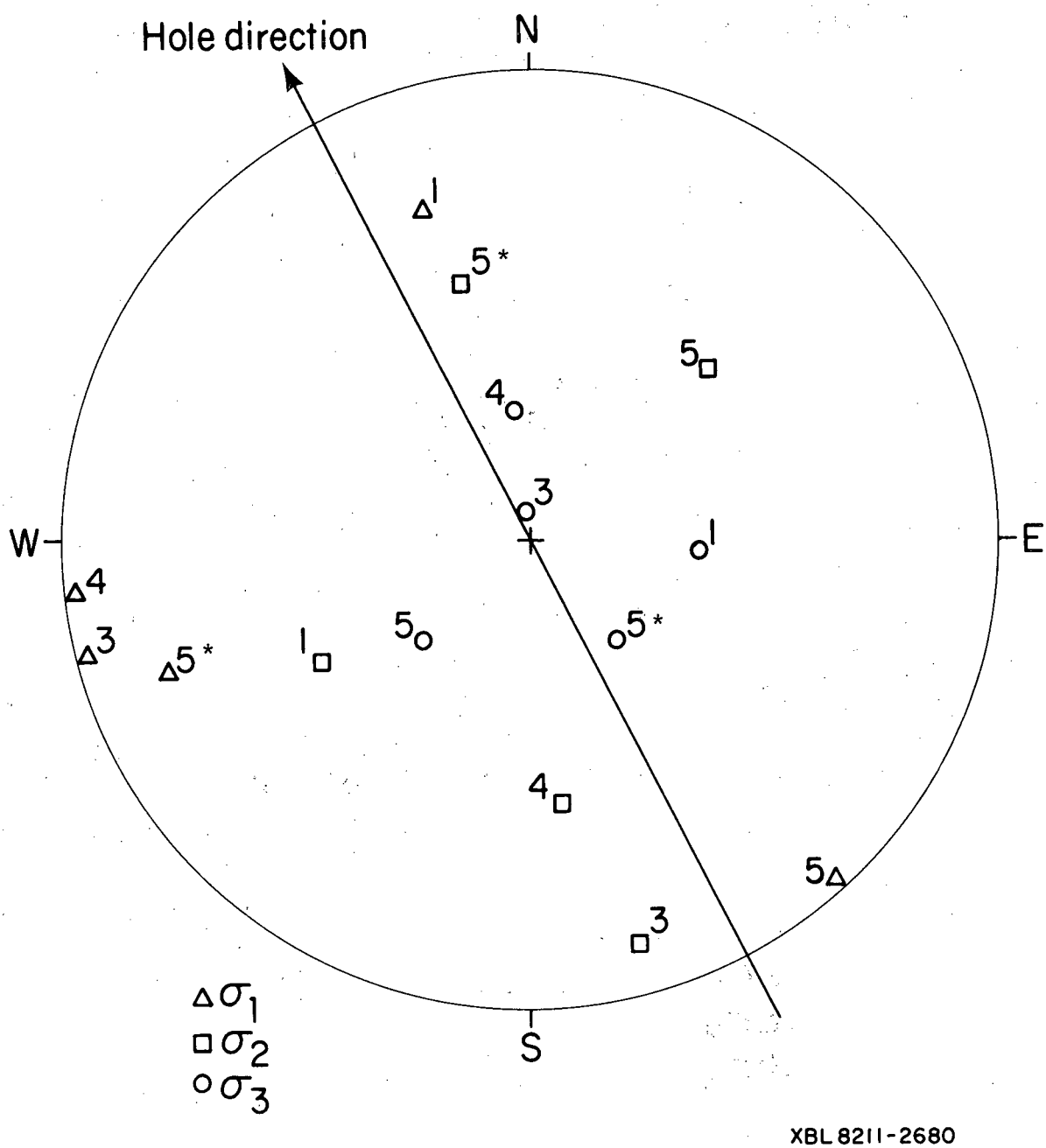

Fig. 6.12 Principal stress directions for Case C analysis of the CSIRO measurements. Numbers identify test. Asterisks indicate "corrected" analyses.

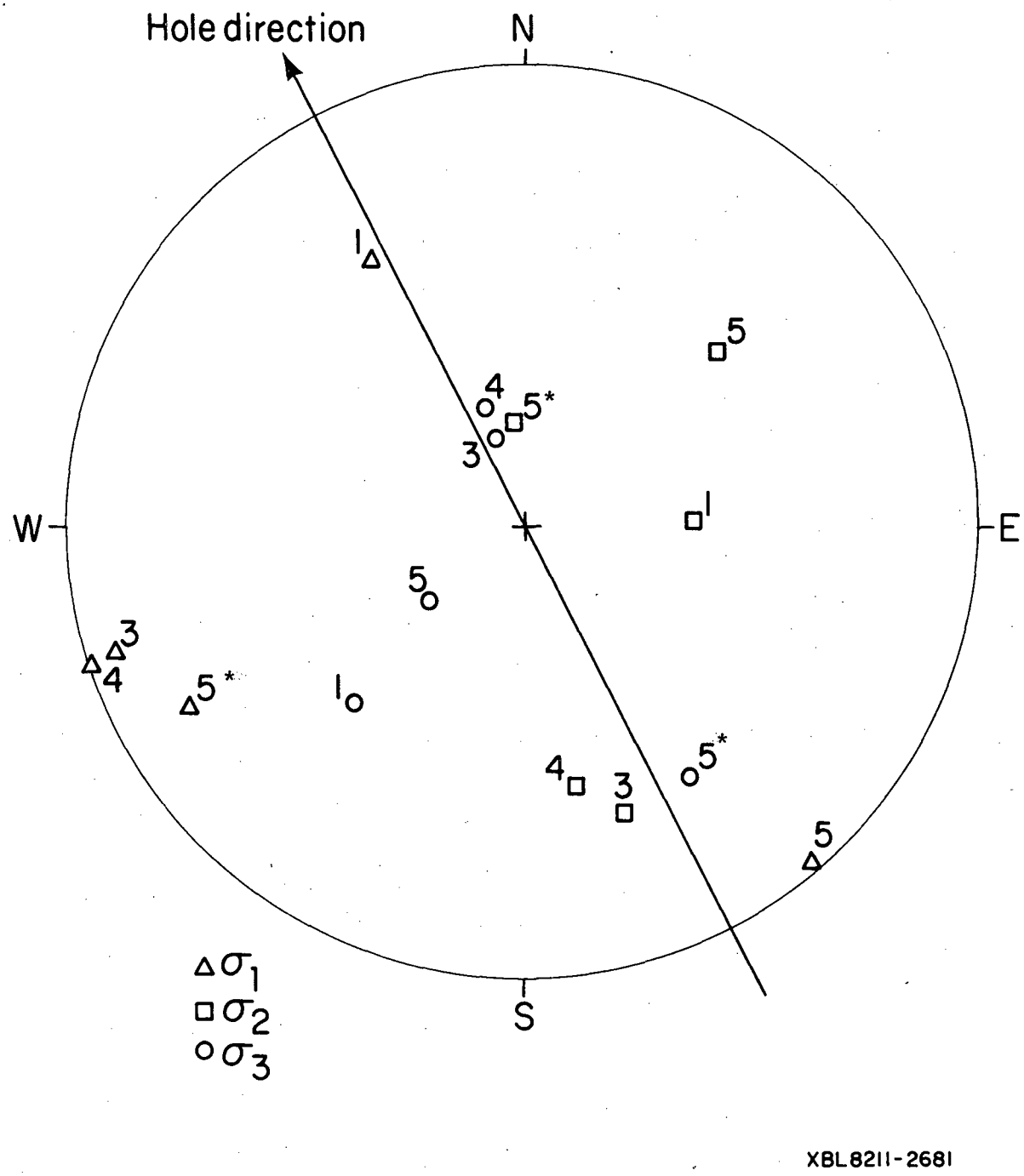

Fig. 6.13 Principal stress directions for Case D analysis of the CSIRO measurements. Numbers identify test. Asterisks indicate "corrected" analyses.

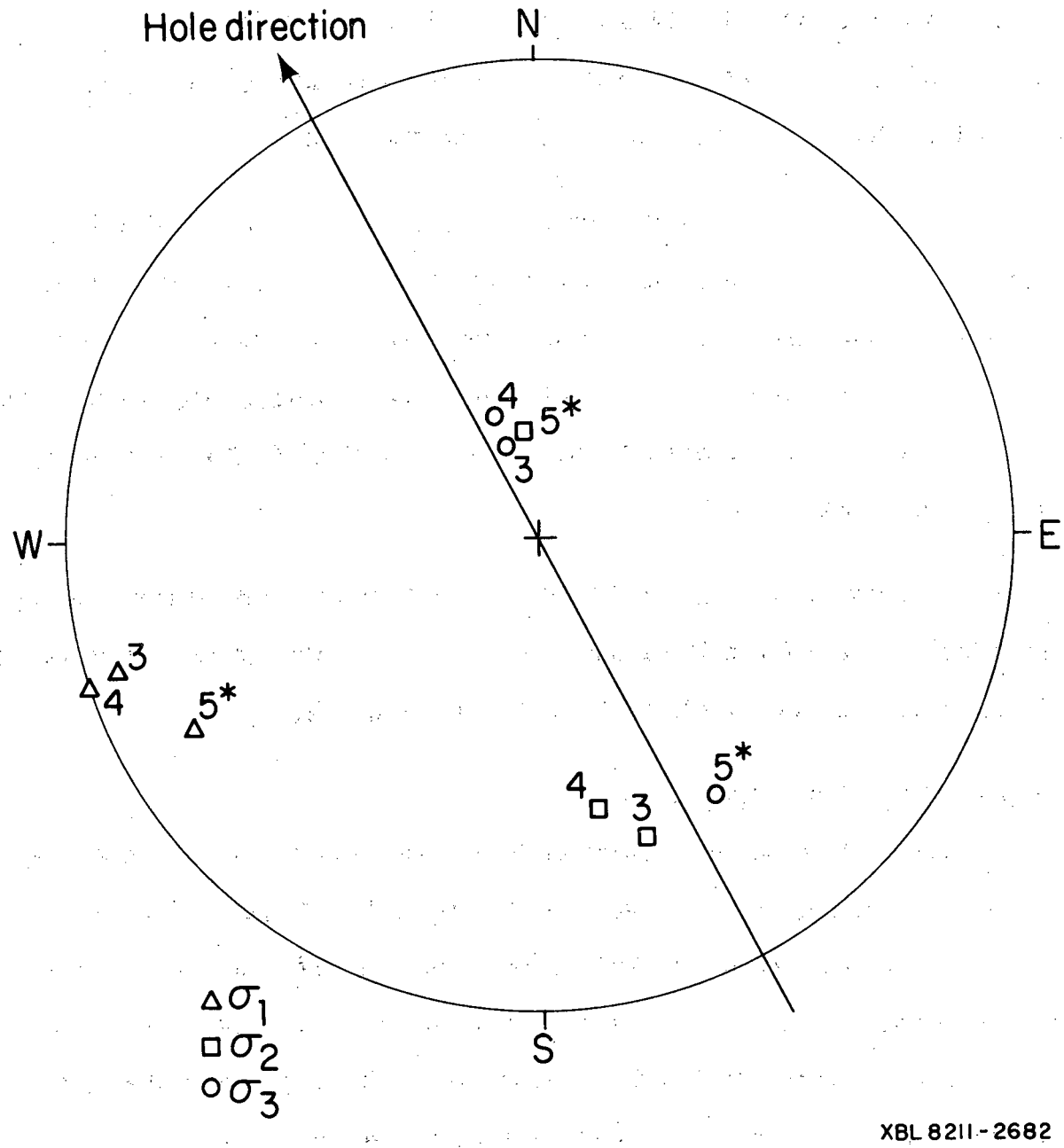

Fig. 6.14 Principal stress directions for the Case D analysis of the CSIRO overcoring data for measurements 3, 4, and "corrected" values of 5. Numbers identify test. Asterisks indicate "corrected" analyses.

of 42.0 GPa and 56.4 GPa are shown in Table 6.17. The apparent modulus from the biaxial tests is 74.4 GPa psi, considerably higher than values observed from other CSIRO tests as well as from the LuH and USBM cores. Hence, an average modulus value of 56.4 GPa is considered more appropriate.

The results for the "corrected" analysis of CSIRO 5 are denoted by the asterisks (*) in the stress direction plots (Figs. 6.10-6.13). As can be seen in Fig. 6.14, the stress directions for overcores 3, 4, and 5 now correspond very well. A comparison of these directions with those obtained using the LuH gauge reveals good agreement. The magnitudes of CSIRO gauges 3 and 5 are also in good agreement.

In order to compare the CSIRO and USBM results, the magnitudes and directions of the principal stresses in the plane of the borehole have been calculated for cases C (Table 6.18) and D (Table 6.19).

6.5 CSIRO Measurement Summary

Compared with other overcoring methods, the CSIRO measurements were more time-consuming, and the strain relief was difficult to interpret. On the first point, the CSIRO cell required at least 17 hours of curing time in the hole, making it difficult to conduct more than one measurement per day. For the cold conditions in the Stripa mine, even this length of time was insufficient for the recommended cement to cure.

Table 6.17. Principal stress magnitudes and directions using "corrected" strain changes for CSIRO 5.

Case	σ_1(MPa)			σ_2(MPa)			σ_3 (MPa)		
	Mag.	Dip	Bear.	Mag.	Dip	Bear.	Mag.	Dip	Bear.
A[a]	32.2	9.5	89.3	28.1	2.1	179.6	15.4	-80.3	101.8
B[a]	31.0	6.3	48.9	23.4	10.2	140.0	14.5	-78.3	107.5
C[a]	27.8	10.4	68.8	12.2	30.7	165.1	7.7	-57.3	142.2
D[a]	21.1	9.4	61.3	9.2	65.2	172.4	3.8	-22.7	147.3
C[b]	21.1	20.4	68.8	9.3	30.7	165.1	5.8	-57.3	142.2
D[a]	20.2	9.4	61.3	7.0	65.2	172.4	2.9	-22.7	147.3

[a]E = 42.0 GPa
[b]E = 56.4 GPa

Table 6.18. Principal stress magnitudes and directions in the plane normal to the borehole: Case C.

Over-core No.	Principal Stress (MPa)		Direction Θp (degrees)
	P	Q	
1	5.67	5.45	37.37
3	24.50	5.85	1.23
4	10.37	2.07	5.98
5	7.25	1.88	-28.94
5[a]	27.6	8.8	9.5
5[b]	20.9	6.7	9.5

[a]E = 74.4 GPa
[b]E = 56.4 GPa

Table 6.19. Principal stress magnitudes and directions in the plane normal to the borehole: Case D.

Over-core No.	Principal Stress (MPa) P	Principal Stress (MPa) Q	Direction Θ_p (degrees)
1	5.9	5.4	17.6
3	22.2	7.2	4.1
4	12.4	2.0	4.0
5	6.5	1.2	-29.1
5[a]	26.7	8.1	9.5
5[b]	20.2	6.2	9.5

[a] E = 74.4 GPa
[b] E = 56.4 GPa

Analysis of the strain relief records was hampered by several factors, such as:

- o large drift rates in the gauge outputs,
- o apparent decoupling of the gauge from the borehole on some measurements, and
- o high apparent modulus values.

The high drift rates were thought at first to reflect the curing of the cement; however, on re-examination of the wiring of the gauges and the data logger, it appeared that the cables were not compensated for resistance changes with temperature. The drift thus may have been caused by the cooling effect of drill water with on cable resistance. This effect would not have arisen with conventional strain indicators. Such strain indicators, however, cannot take readings with sufficient frequency to capture the peaks observed for CSIRO Measurement 5. The data logger system thus remains preferred for its ability to sample all gauge outputs with high frequency.

7. HYDRAULIC FRACTURING STRESS MEASUREMENTS IN BSP-1 AND BSP-2 (T. W. Doe)

7.1 Introduction

The second phase of the Stripa stress measurement program was to measure the in situ stress in the immediate vicinity of the full-scale heater experiment (Fig. 7.1). Two holes for hydraulic fracturing stress measurements were drilled. BSP-1 was vertical and drilled along the center line of the drift to a depth of 25 m. This hole, 76 mm in diameter, was also used for overcoring by the Swedish State Power Board method. BSP-2 was drilled from the extensometer drift under the full-scale drift. The hole had a diameter of 76 mm, was 20 m long, and was used exclusively for hydrofracturing. The hole was drilled 3° downward from the horizontal to assure that it would remain full of water during the hydrofracturing tests.

An acoustic emission experiment was set up by Ernest Majer of LBL to detect the propagation of the hydraulic fractures and to map their location (Chapter 9).

In addition to providing data for comparison with overcoring techniques, the hydraulic fracturing experiments in BSP-1 and BSP-2 were designed to resolve some of the controversies surrounding the interpretation of hydraulic fracturing results. The main question concerns interpretating the records when the borehole is not drilled in the direction of the intermediate principal stress. If a borehole has been drilled in the direction of a principal stress other than the intermediate stress, Zoback and Pollard (1978) have suggested that the fracture will initiate parallel to the borehole (normal to the intermediate stress) and then rotate to be perpendicular to the least principal stress (Fig. 7.2a). The resulting pressure-time record for the fracture should show a decrease in the shut-in pressure with

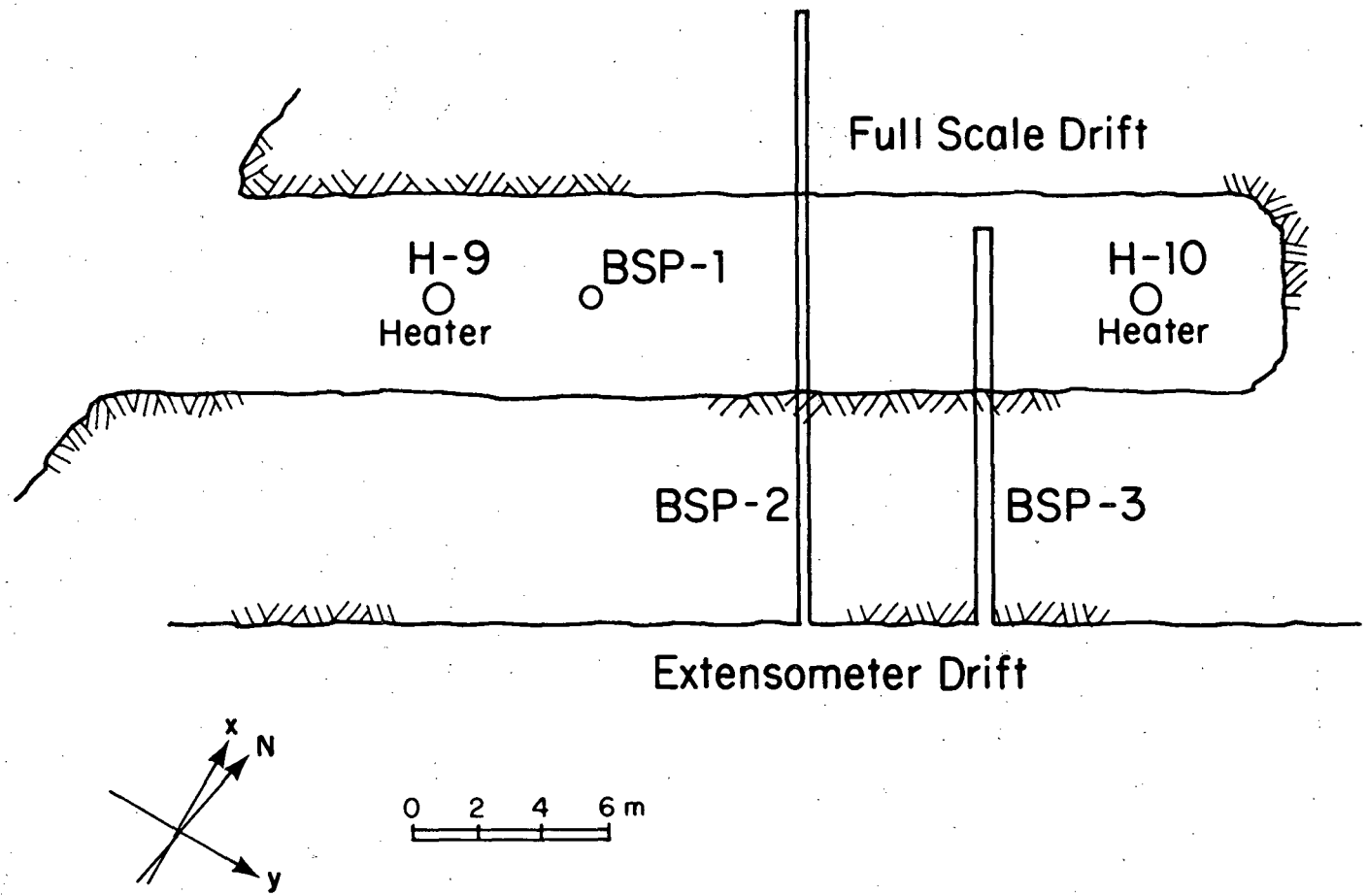

Fig. 7.1 Location of stress measurement holes.

pumping cycle. Shut-in pressures for the early cycles would indicate the intermediate stress, and shut-in pressures for pumping cycles occurring after the fracture has rotated should indicate the least principal stress (Fig. 7.2b). It has been claimed that this method could obtain the complete state of stress from hydraulic fracturing, and it has been applied by Haimson (1978) as well as by Zoback et al. (1980). Unfortunately, these methods have not been applied where overcoring methods have independently given the complete state of stress, nor have methods been available to confirm whether a fracture indeed changed its orientation away from the hole.

The experiments in the full-scale drift area provided an opportunity to test the Zoback-Pollard hypothesis under conditions where all three principal stresses and and their orientations would be known from overcoring and where the true position of the fracture away from the borehole would be known from acoustic emission mapping.

7.2 Locations, Equipment, and Procedures

Nine hydraulic fracturing stress measurements were carried out in BSP-1 over 0.6 m test intervals at depths ranging from 2.3 m to 20.1 m from the full-scale drift. Eight measurements were performed in BSP-2 using the same test interval over distances from the extensometer drift walls of 3.8 m to 16.7 m. The locations of the holes and the measurements are shown in Fig. 7.3.

The equipment and procedures for conducting the tests and evaluating the results were essentially the same as those for the far-field stress measurement work in SBH-4 discussed in Chapter 2. A straddle packer system

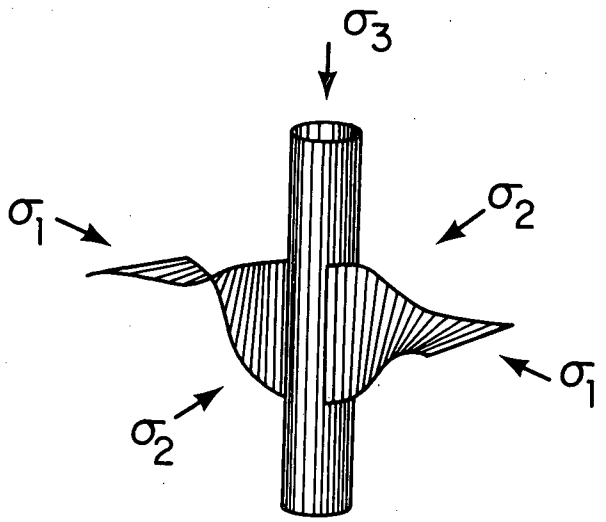

A

XBL 8211-2661

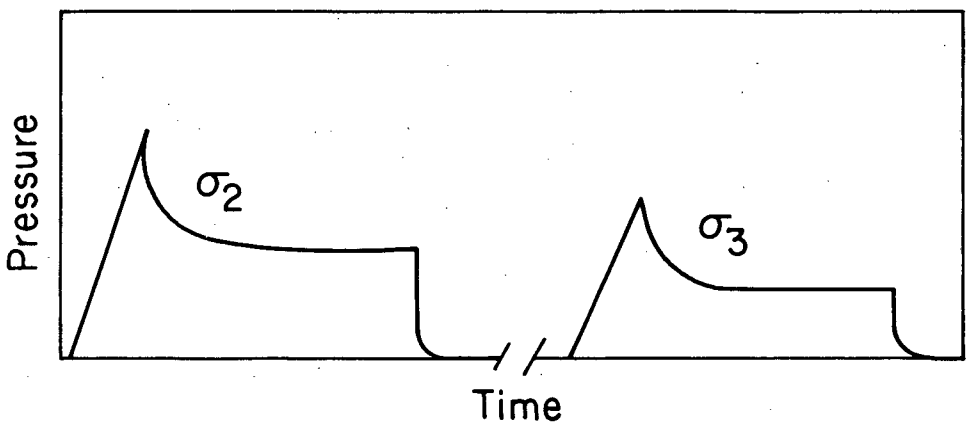

B

XBL 8211-2660

Fig. 7.2 (a) Hypothetical rotation of hydrofracture away from borehole. (b) Hypothetical pressure-time record for test with rotating fractures. Note lower shut in pressure for late cycle.

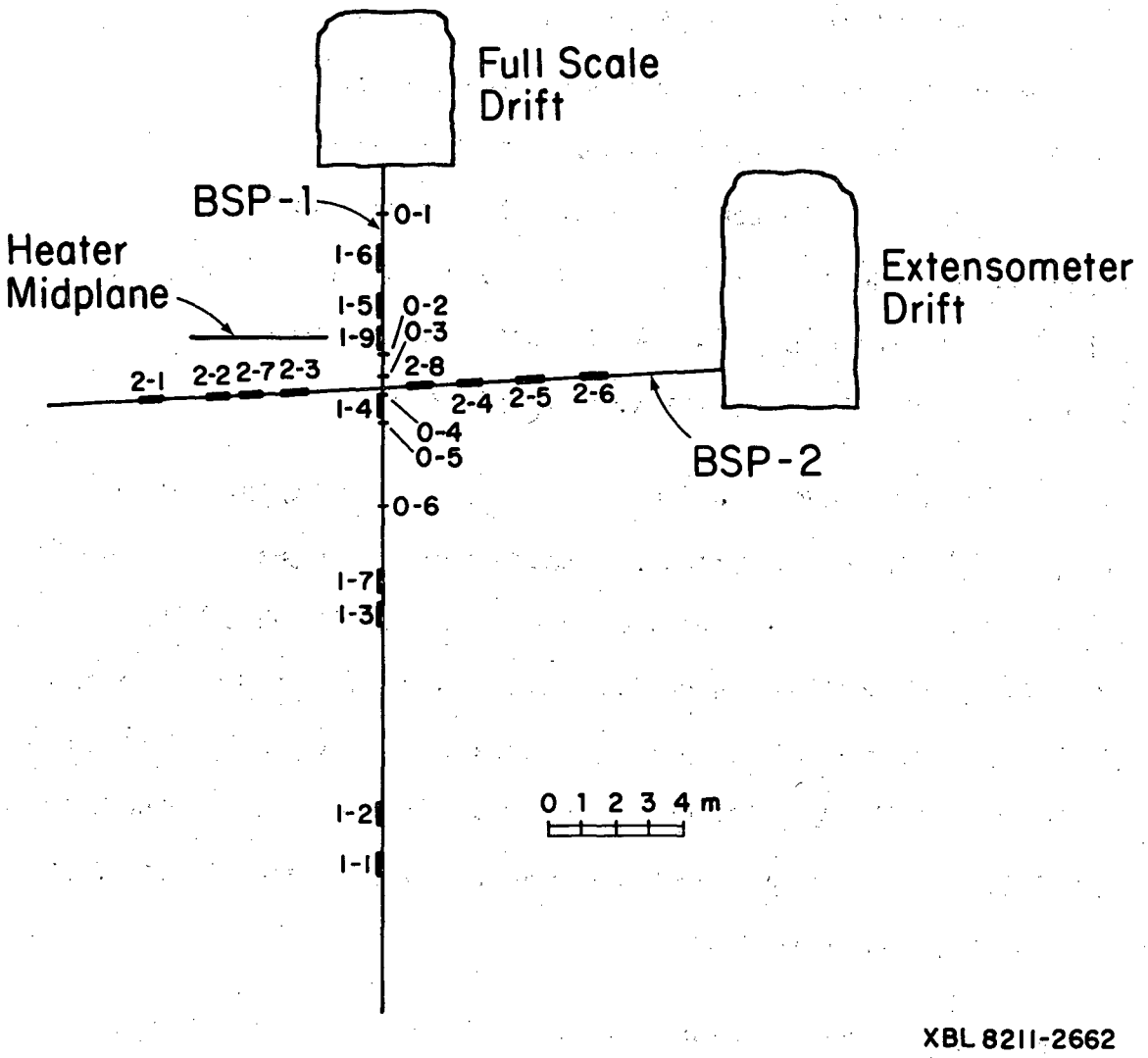

Fig. 7.3 Location of stress measurements in BSP-1 and BSP-2. Power Board overcores denoted with "0".

using two Lynes elements isolated the fracturing zone. The packers were inflated with a small-diameter high-pressure hose. Above the packers was a housing containing pressure transducers for monitoring both the injection pressure and the packer inflation pressure. For the horizontal hole, sets of rollers were made to lift the packers off the borehole wall, thus eliminating unnecessary abrasion to the packer and making the system easier the move in and out of the hole. The roller system (Fig. 7.4) was used on both the straddle packer and impression packer assemblies.

Unlike the measurements in SBH-4, we found that we could set the packers at a low initial pressure and that this pressure would automatically build up along with the injection pressure to maintain the seal. The SBH-4 used carbide grit embedded into the ends of the packers, and we feel that the grit prevented adjustments in the position and shape of the packers that would have allowed them to respond to the injection pressure. The packers in the BSP holes did not have these grit inserts, and the pressure in the packers readily adjusted to the changes in the injection pressure.

A typical pressure-time record is shown in Fig. 7.5. It is similar to the pressure-time curves of the SBH-4 work, except that we added a long, fast pumping cycle to extend the fracture as far as practicable. If the hole were not oriented in the direction of the intermediate principal stress, this extension would ensure that the fracture would be propagated far enough from the borehole to change its orientation. The shut-in pressures before and after the fast pumping cycles were expected to reflect the change in fracture orientation. The rate for the fast pumping cycle was 4.5 liters per minute, the capacity of the air-driven, positive-displacement pump. In contrast to this rate, our first and second breakdowns

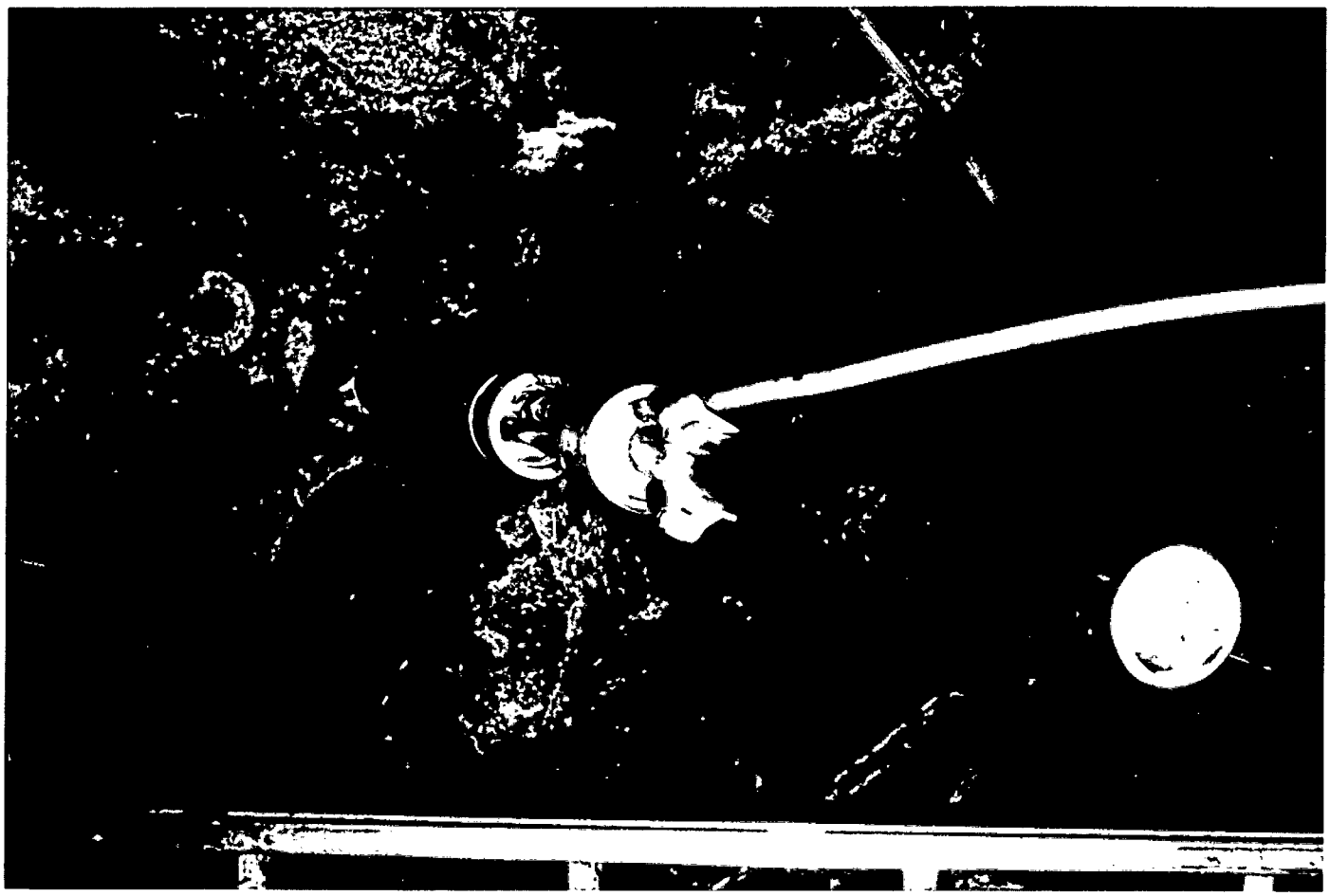

Fig. 7.4 Photograph of roller system used to keep packers from rubbing walls of horizontal borehole.

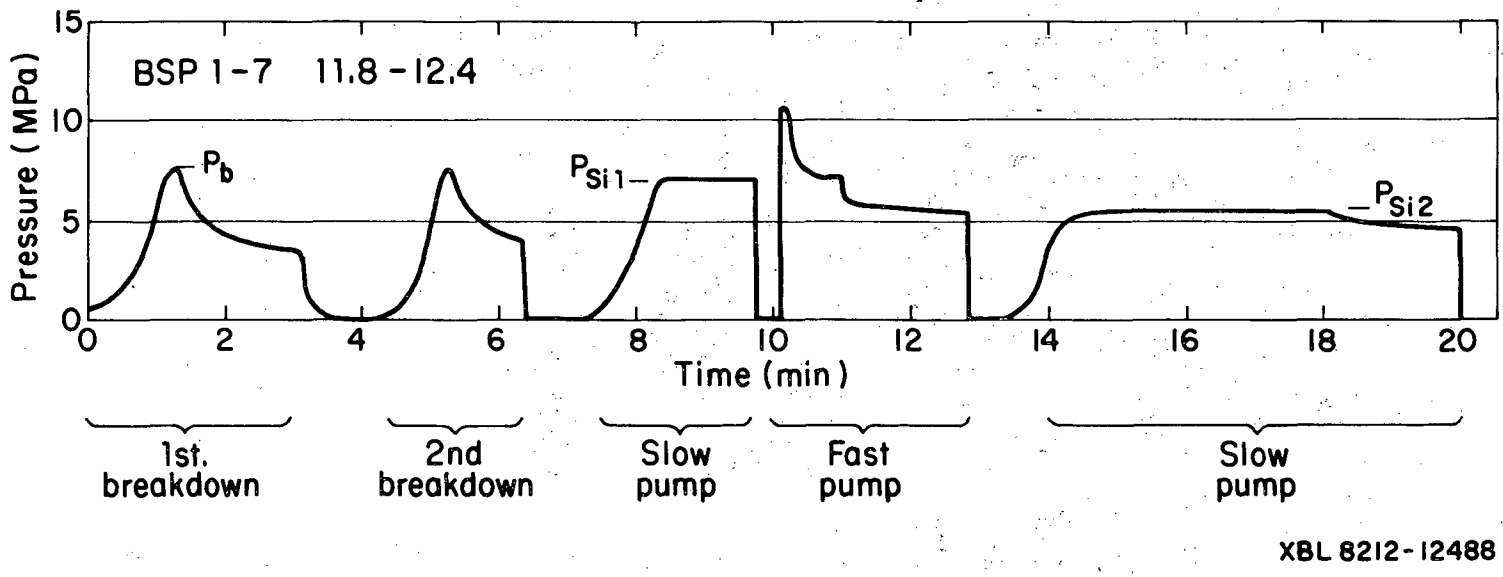

Fig. 7.5 Typical pressure-time record for hydraulic fracturing.

were performed at about 1 liter per minute. The slow pumping cycle for determining the fracture re-opening pressure was run at about 0.25 l/min.

7.3 Stress Magnitude Results

The breakdown and shut-in pressures and the stress results are given in Table 7.1. The stresses were calculated using the formula given in Chapter 2. The minimum stress normal to the hole is based on the first shut-in pressure; the absolute minimum stress is based on the shut-in pressure determined in a slow pumping cycle after the fast cycle. In contrast to SBH-4, the shut-in pressures decreased with additional pumping cycles in most tests; hence a determination of the minumum stress using Zoback's hypothesis was possible. The maximum stresses normal to the borehole were determined from the first breakdown pressure and the tensile strength value obtained by Ratigan (1981), discussed in Chapter 2. The area of the full scale drift was considered to be drained of water, so the pore pressure term was zero.

The magnitudes of the calculated stresses are shown as a function of hole depth in Fig. 7.6. In both BSP-1 and BSP-2, the stress values do not vary greatly along the length of the holes. Confidence intervals for the stress values are mostly within ± 10% of the mean.

The stresses normal to the boreholes calculated for BSP-1 and BSP-2 are surprisingly similar, even though that the holes are nearly perpendicular to one another. This similarity is discussed in Section 7.5.

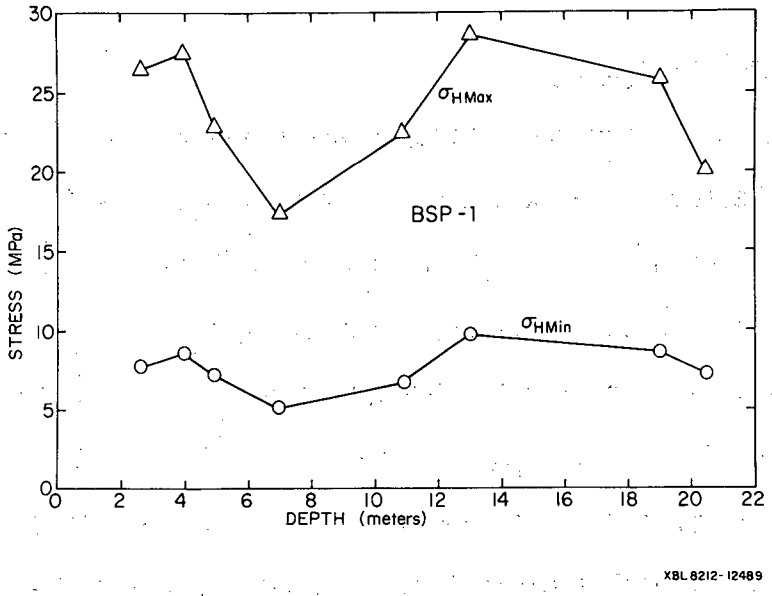

A

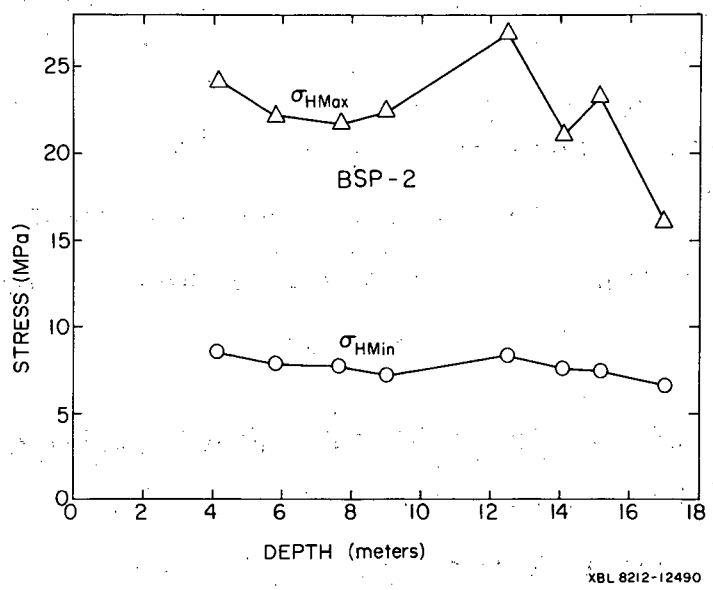

B

Fig. 7.6 Stress vs. depth: (a) BSP-1, (b) BSP-2.

Table 7.1. Hydraulic fracturing data for BSP-1 and BSP-2[a].

Depth (meters)	Test	P_b	P_{sil} (MPa)	P_{i2}	σ_{Hmax}	σ_{Hmin} (MPa)	σ_{min}
BSP-1							
2.3-2.9	1-6	11.7	7.9	4.5	26.6	7.9	4.5
3.7-4.3	1-5	8.6	8.6	5.5	27.6	8.6	5.5
4.6-5.2	1-9	9.3	7.2	5.0	22.8	7.2	5.0
6.6-7-2	1-4	8.6	5.2	4.1	17.2	5.1	4.1
11.8-12.4	1-7	7.6	6.6	-	22.4	6.5	-
12.7-13.3	1-3	10.8	9.7	6.2	28.5	9.7	6.2
18.8-19.4	1-2	9.5	8.6	-	26.8	8.6	-
20.2-20.8	1-1	12.1	7.2	-	20.0	7.2	-
Average[b]					24.0± 2.7	7.6± 1.0	5.1± 0.8
BSP-2							
3.8-4.4	2-6	12.1	8.6	5.2	24.1	8.6	5.2
5.5-6.1	2-5	12.1	7.9	-	22.1	7.9	-
7.3-7.9	2-4	11.9	7.7	4.3	21.7	7.7	4.3
8.7-9.3	2-8	9.3	7.2	6.0	22.3	7.2	6.0
12.5-13.1	2-3	12.1	8.3	6.1	26.9	8.3	6.1
13.8-14.4	2-7	10.7	7.6	6.9	21.0	7.5	6.9
14-9-15.5	2-2	9.7	7.6	5.4	23.4	7.6	5.4
16.7-17-3	2-1	12.1	6.2	-	16.9	6.2	-
Average[b]					23.3± 1.9	7.6± 0.5	5.7± 0.7

[a]Number on shut in pressures refer to initial pumping cycle and final pumping cycle. Hmax and Hmin refer to stresses normal to borehole axis and not necessarily horizontal stresses.

[b]Given with 90% confidence intervals.

7.4 Orientation

The orientations of the hydrofractures at the borehole wall were obtained using Lynes 5.7 cm (2-1/4 inch) impression packers. Since the holes were short, we felt a compass was unnecessary and used scribed tubing to orient the packer. Each tube length carried a scribe line machined on each end. The scribes were aligned with one another as the tubes were placed in the hole. For the vertical hole, BSP-1, a line was painted on the floor of the full-scale drift along its axis. A rod about 1 m long was placed in a hole drilled along the scribe in the top coupling of the tubing. Alignment of this rod with the line on the drift floor was used to orient the packer scribe with respect to the drift axis.

We used the same scribed tubes for the horizontal hole, BSP-2. Rather than use a scribe line on the drift walls we inserted a pin with a flat plate attached into the hole at the end of the tubing. A bubble level was placed on the plate and rotated until horizontal. Thus the pin and the packer scribe were vertical for each test (Fig 7.7). The impression packer assembly was equipped with rollers to keep the packer from rubbing the wall of the borehole and damaging the impression. Figure 7.8 shows a typical impression packer as it was removed from BSP-1; the impression has been traced with paint to make it more visible. Figure 7.9 shows the orientation of the hydrofracture planes at the borehole wall for the vertical hole, BSP-1, and Fig. 7.10 the orientations for the horizontal hole, BSP-2.

The fracture orientations in BSP-1 are strongly aligned parallel to the axis of the full-scale and extensometer drifts, and thus agree closely in

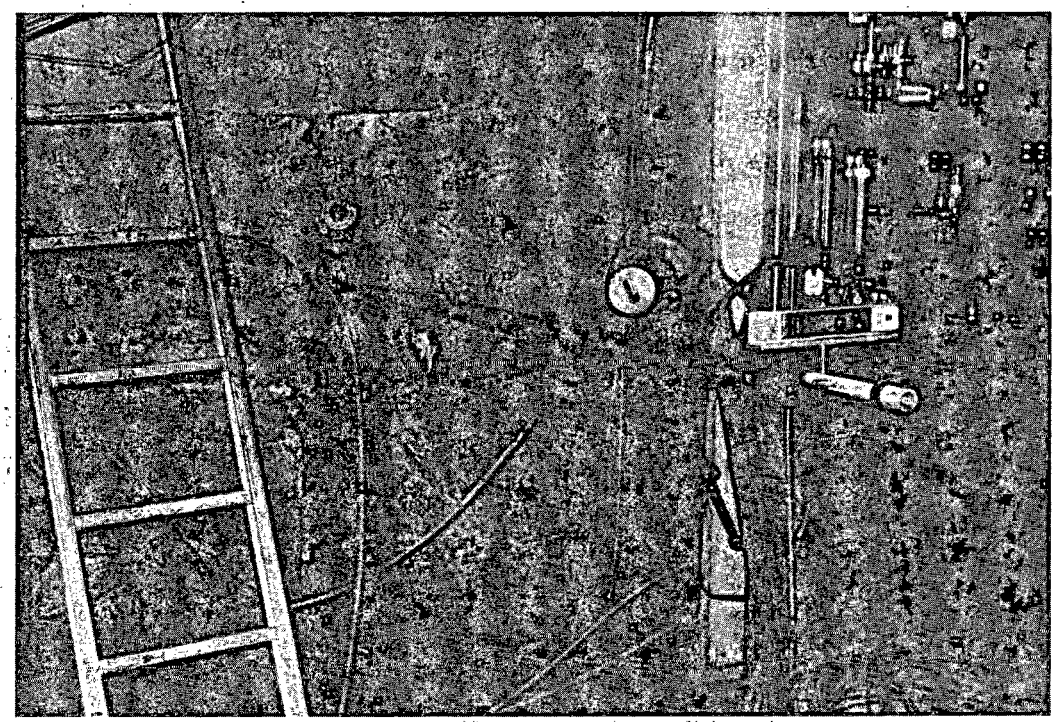

Fig. 7.7 Bubble level system for orienting impression packer in horizontal hole.

Fig. 7.8 Impression packer from BSP-1 showing hydraulic fracture trace; fracture has been highlighted with white paint.

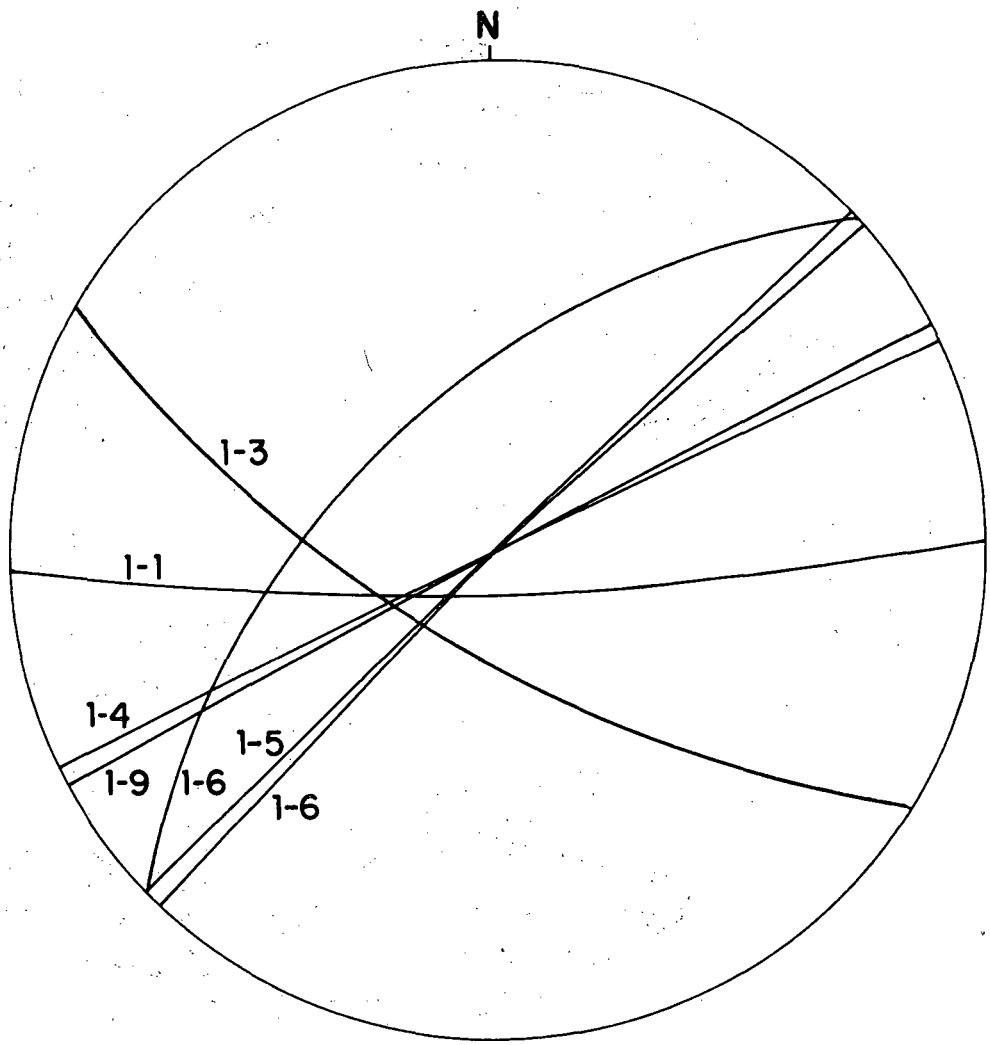

Fig. 7.9 Lower hemisphere stereographic projection of the hydrofracture planes in the vertical borehole, BSP-1. Identification numbers are given for each test.

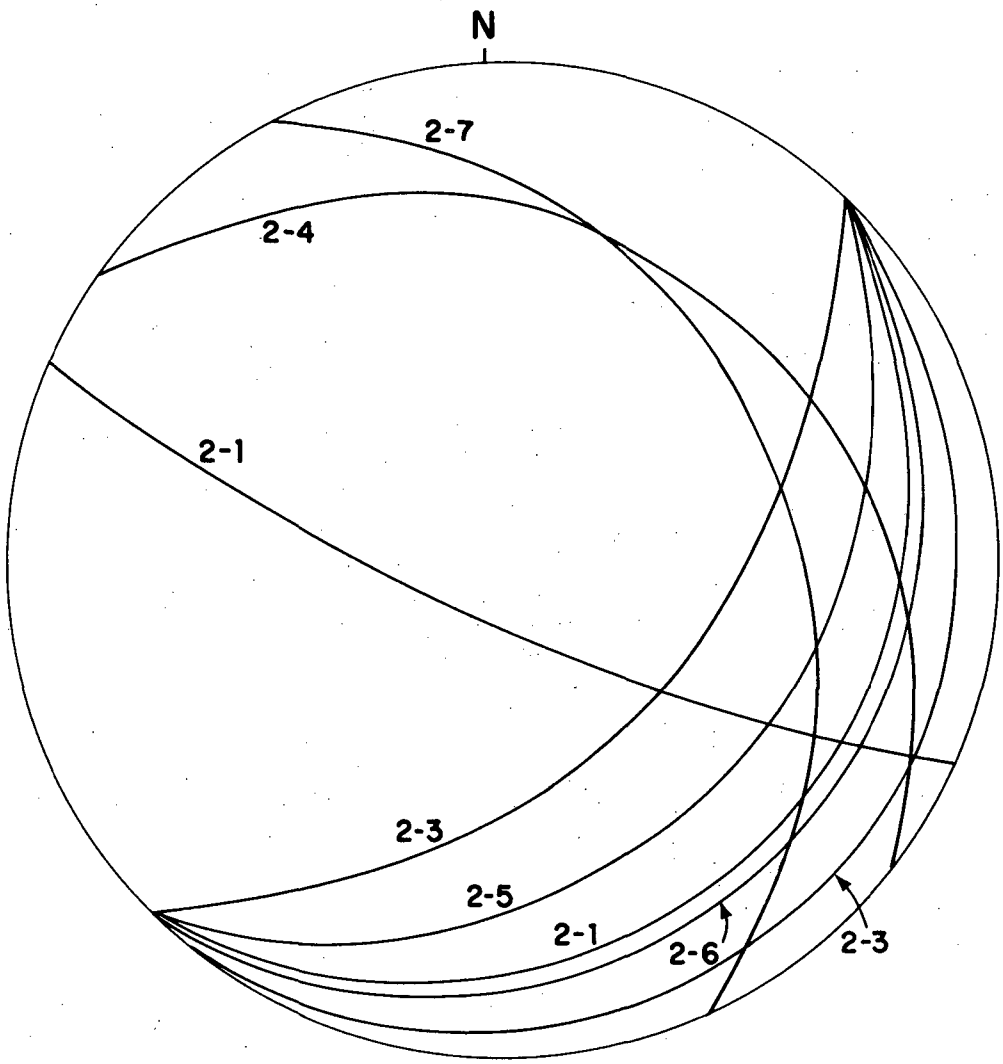

Fig. 7.10 Lower hemisphere stereographic projection of the hydrofracture planes in the sub-horizontal hole BSP-21 Identification numbers. given for each test. Case 1, $_2$ parallel to BSP-1, $_2$ parallel BSP-2; Case 2, $_3$ parallel to BSP-1, $_2$ parallel BSP-2; Case 3, principal stresses parallel to neither hole.

orientation with the maximum principal stress direction determined by the overcoring measurements.

The fractures created from BSP-2 are generally subhorizontal with a shallow dip towards the extensometer drift. A few fracture planes are nearly perpendicular to the minimum principal stress direction as determined by the LuH cell in BSP-3. Since the fractures are nearly horizontal, they are following the plane that contains the directions of the borehole axis and the maximum principal stress as determined by the overcoring measurements and the hydraulic fracturing in BSP-1.

The results of the impression packer surveys in BSP-1 and BSP-2 suggest that the borehole axis strongly affects the orientation of the fracture, as most fractures are coaxial with boreholes. The measurements are consistent between BSP-1 and BSP-2 in that both planes contain the direction of maximum principal stress, which overcoring measurements indicate is roughly parallel to the axis of the full-scale drift. Clearly, however, it is not possible for both the BSP-1 and the BSP-2 fractures to be perpendicular to the minimum stress, particularly in the area beneath the full-scale drift.

7.5 Discussion of Results

The overcoring results indicate strongly that the maximum principal stress is aligned with the axis of the full-scale drift and is nearly horizontal. The orientations of the hydraulic fractures support this conclusion, as the planes of the hydrofractures of both BSP-1 and BSP-2 contain the maximum stress direction. One can therefore conclude that the plane containing the two boreholes is normal to the maximum stress and contains the directions of the intermediate and least principal stresses.

Having determined that the maximum principal stress is normal to the plane containing BSP-1 and BSP-2, let us consider how the intermediate and least principal stresses lie within that plane. There are three possible stress configurations (Fig. 7.11).

The first possibility is that the intermediate and least principal stresses are equal. If this were the case, the first shut-in pressures measured in BSP-2 and BSP-3 should be equal, but there should not be a second shut-in pressure for either hole. As there are clear second shut-in pressures observed in both holes, we can dismiss the hypothesis that the lesser principal stresses are equal.

The second possibility (Fig. 7.11, Cases 1 and 2) is that the intermediate and least stresses are unequal in magnitude and parallel to the two holes. This stress condition should give first shut-in pressures that are unequal, and the larger shut-in pressure should be recorded in the hole drilled parallel to the least stress and normal to the intermediate stress. This hole should also show a second shut-in pressure equal to the first shut-in pressure measured in the hole drilled normal to the least principal stress. This hypothesis can also be dismissed as inconsistent with the field data, as both BSP-1 and BSP-2 have clear second shut-in pressures and the first shut-in pressures in the two wells are equal.

The third possibility is that neither hole is parallel to a principal stress (Fig. 7.11, Case 3). In this case, two shut-in pressures should be measured in both holes. The first would reflect the stress normal to the fracture and the second would reflect the minimum principal stress. This hypothesis is consistent

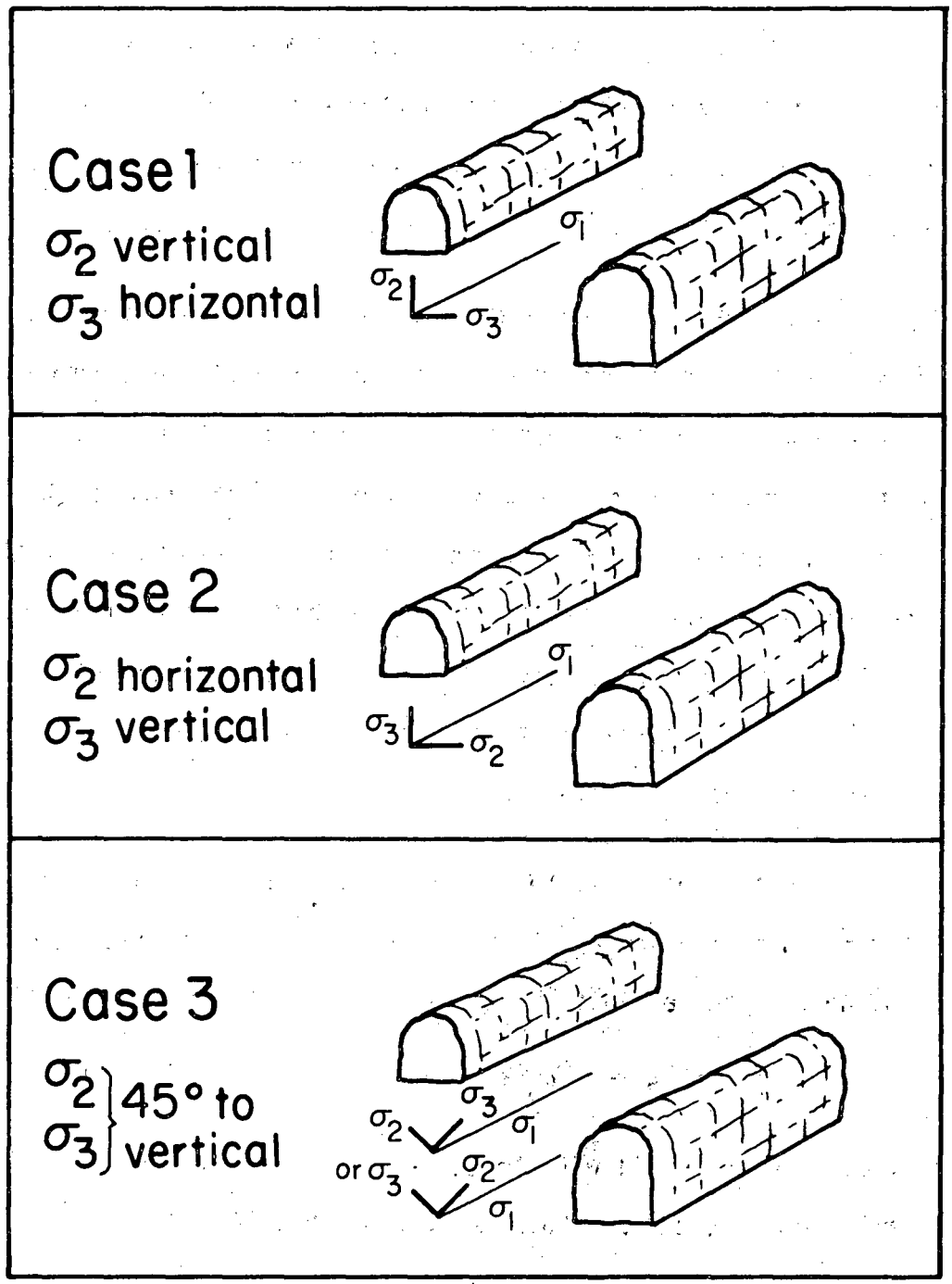

Fig. 7.11 Possible stress conditions between full scale and extensometer drifts. Case 1, $_2$ parallel to BSP-1, $_2$ parallel BSP-2; Case 2, $_3$ parallel to BSP-1, $_2$ parallel BSP-2; Case 3, principal stresses parallel to neither hole.

with the field data, which did exhibit two shut-in pressure values for each hole. Furthermore, if the intermediate and least principal stress directions are oriented 45° from the borehole directions, the first and second shut-in pressure values measured in BSP-1 should be the same as those measured in BSP-2. Such correspondence between the two holes was indeed observed.

The hypothesis that the intermediate and least principal stresses are oriented at 45° to the directions of BSP-1 and BSP-2 can be checked by calculating the values of the intermediate and least principal stresses and comparing the results with the stresses measured by overcoring. The least principal stress can be taken as the second shut-in pressure, and the intermediate principal stress can be calculated as follows. The stress, σ, normal to the hydraulic fractures generated in the two boreholes is equal to the first shut-in pressure and can be related to the intermediate and least principal stresses by

$$\sigma = \sigma_2 \sin^2 \theta + \sigma_3 \cos^2 \theta$$

where σ_2 and σ_3 are the intermediate and least stresses and θ is the angle between the direction of σ and σ_2. The average first shut-in pressure, σ, is 7.6 MPa, and the average second shut-in pressure is 5.4 MPa. For $\theta = 45°$,

$$\sigma_2 = \frac{\sigma}{\sin^2\theta} - \sigma_3 = \frac{7.6}{0.5} - 5.4 = 9.8 \text{ MPa}$$

This value of σ_2 compares well with those obtained with the LuH gauge in BSP-3 (9.2 MPa) and by the Power Board (10.0 MPa) in BSP-1.

Thus the pressure records and the fracture orientations support this interpretation of the stress field: the maximum stress is normal to the plane of the boreholes, and the intermediate and least stresses are oriented about 45° from the boreholes.

This interpretation only shows that the intermediate and least stresses are at 45° relative to the boreholes; it does not indicate which stress has which of the two possible orientations. The orientations of the minor stress could have been determined from acoustic mapping of the orientation of the fracture, but the acoustic work (Chapter 9) was unable to locate the events with sufficient accuracy.

8.0 STRESS DETERMINATION IN THE LULEÅ DRIFT
(B. Lejon and H. Carlsson)

8.1 Introduction

Stress measurements were conducted in the Luleå drift as part of a pilot heater test program conducted by the University of Luleå. Although the results have been previously reported (Carlsson, 1978), they are included here for two reasons: (1) the data are valuable for comparison with the stress results from the full-scale drift area; and (2) a minor error was discovered in the computer program used to reduce the previously reported results. The error affected only the orientation data. The mean orientation of the stress data remain unchanged, but the latest calculations have reduced the data scatter.

The Leeman cells used in the measurements were manufactured in South Africa. The design is a predecessor of the LuH gauge described in Chapter 4. The Leeman cells differ from the LuH gauge in the following ways:

- Use of 3-component strain gauges
- Overcore diameter of 32 mm
- Less effective methods of hole cleaning.

8.2 Description of Tests

Carlsson (1978) performed a series of 19 stress measurements in a 20 m long hole (location, Fig. 8.1). This subhorizontal hole had an approximate bearing of N64°S. In his calculations, geographic north rather than mine north was chosen as the reference. Geographic north is about 10° east of mine north, a difference that must be taken into account when comparing results. In

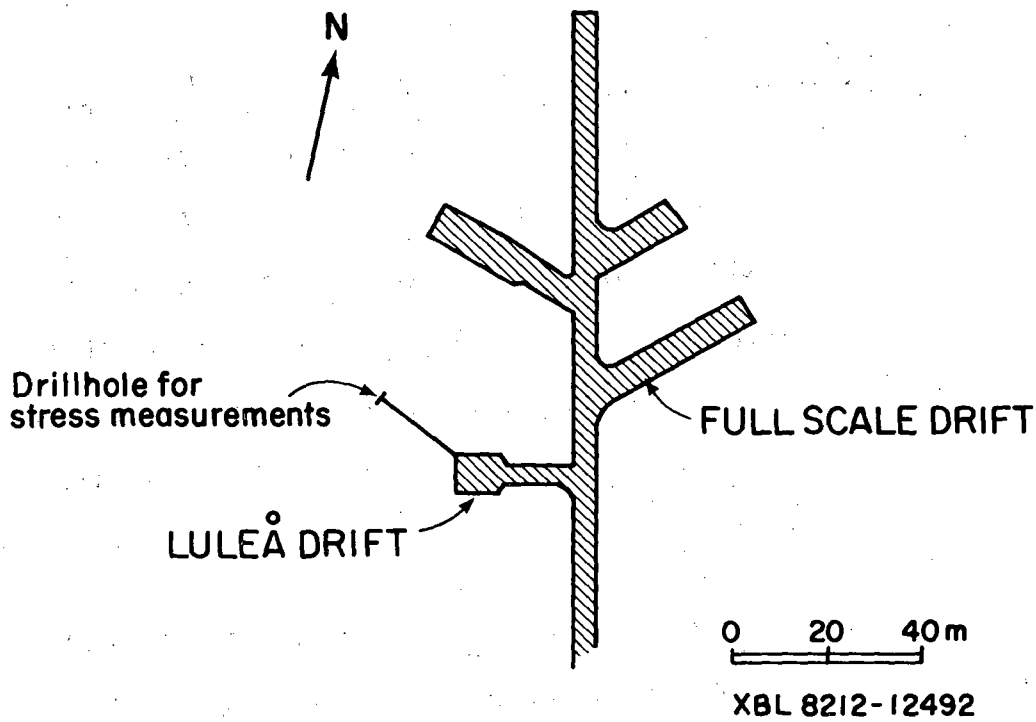

Fig. 8.1 Location of Luleå drift stress measurements (348 m level).

the analysis of Carlsson's results, the elastic properties were derived from axial compression tests (Table 8.1).

The borehole was collared in a diabase dike that ended after 0.87 m. To check the influence of the dike on the stresses in the granite, the first measuring location was placed at a depth of 1.55 mm in the borehole. Unfortunately, the diabase again occurred at 2.05 m. At 2.87 m the diabase ended, and the granite persisted throughout the remainder of the borehole. Close to the dike, the granite was highly fractured, which made it impossible to perform any measurements. As a result, the second strain measurement was at 4.41 m. The last strain measurement was at of 19.63 m.

8.3 Stress Results

Table 8.2 gives the calculated principal stresses for each location. Figure 8.2 plots the principal stresses as a function of borehole depth, and the orientation of the principal stresses is shown in Fig. 8.3.

The mean values for the magnitudes and directions of the principal stresses over the length of 6.03-16.53 m, initially reported by Carlsson in 1978, are given with the corrected values in Table 8.3.

The biaxial horizontal components, σ_A and σ_B, of the principal stresses have also been computed. These are called "secondary horizontal principal stresses" and are listed in Table 8.2. The mean value for σ_A is 15.58 MPa; and for σ_B, 8.68 MPa.

The azimuth of the maximum principal stress in the Luleå hole is close

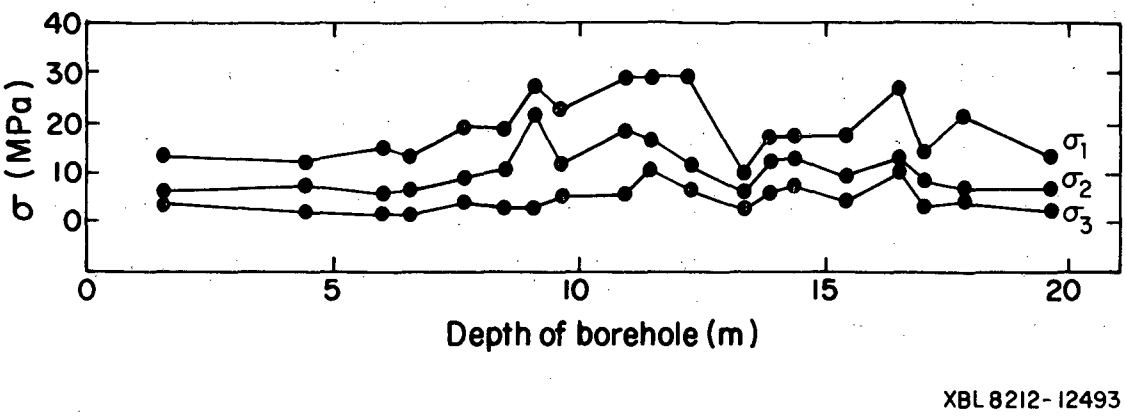

Fig. 8.2 Variations of principal stress magnitudes with depth, Luleå hole.

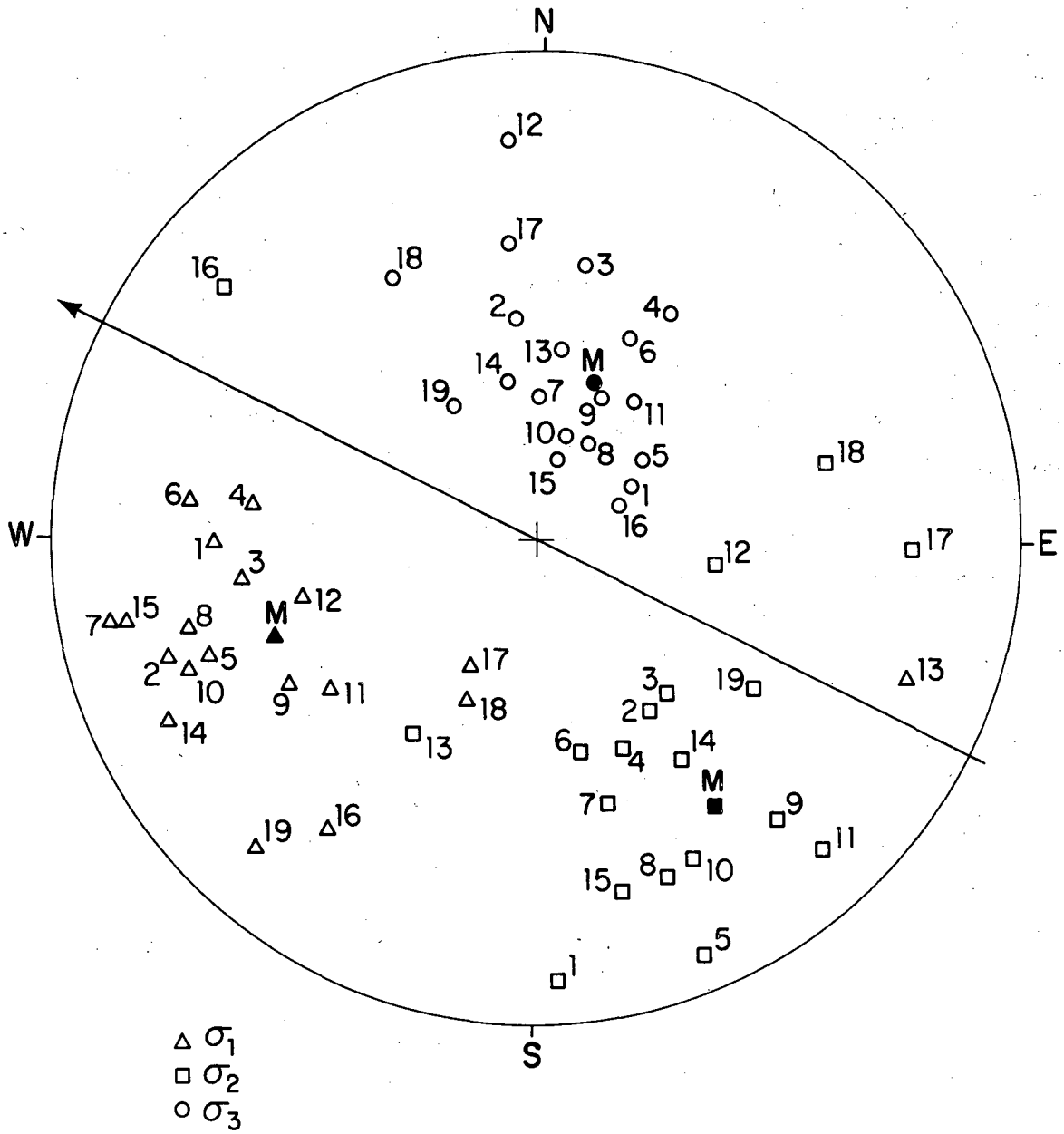

XBL 8212-12494

Fig. 8.3 Lower hemisphere stereographic projection of principal stress data from Luleå drift. Numbers of test given beside points. Mean orientations shown by "M" and solid symbols.

Table 8.1. Mechanical properties of the Stripa granite cores. (core diameter = 72 mm, length = 180 mm).

Depth (m)	Young's Modulus (GPa)	Poisson's Ratio υ	Failure Stress (MPa)
6.03	59.97	0.19	151.39
7.68	56.46	0.17	140.40
8.53	59.94	0.19	152.50
10.10	61.68	0.22	141.40
11.44	59.06	0.19	154.70
Avg.	59.42	0.19	148.01

Table 8.2. Calculated principal stresses (after Carlsson, 1978).

Depth (m)	Principal Stresses (MPa)		Vertical Stress (MPa)		Secondary Horizontal Principal Stresses (MPa)	
	σ_1	σ_2	σ_1	σ_v	σ_A	σ_b
1.55	13.46	6.08	3.92	11.58	6.16	5.70
4.41	12.28	7.98	2.26	6.02	11.06	5.44
6.03	15.00	5.50	1.80	4.86	13.37	4.04
6.53	13.86	5.26	1.88	6.94	10.24	3.81
7.68	19.36	8.44	4.04	11.56	11.88	8.40
8.53	18.58	10.84	3.16	12.22	14.40	5.96
9.08	27.28	21.38	3.48	17.20	23.66	11.29
9.60	23.06	12.26	5.18	14.04	15.02	11.45
10.93	28.96	18.30	6.10	10.62	24.63	18.10
11.44	29.80	16.88	10.40	18.26	22.19	16.26
12.22	29.52	11.74	6.88	10.68	25.69	11.76
13.31	9.78	6.44	3.28	4.82	9.87	4.80
13.87	16.96	12.30	5.62	14.62	14.65	5.63
14.37	17.36	13.14	7.26	10.48	15.75	11.51
15.43	16.60	9.42	4.42	11.74	10.62	8.08
16.54	27.50	12.68	10.30	11.56	26.70	12.21
17.02	14.18	8.70	3.30	5.98	11.85	8.34
17.83	21.58	6.48	4.08	11.62	14.68	5.86
19.63	13.94	6.98	2.78	3.70	13.64	6.36

Table 8.3. Mean stresses in Luleå drift (Carlsson, 1978, and corrected).

	Principal Stresses	Magnitude (MPa)	Bearing	Dip
Carlsson, 1978	σ_1	20.0	S68°W	31°
	σ_2	11.4	S32°E	13°
	σ_3	5.4	N29°E	56°
Corrected	σ_1	20.0	S69°W	24°
	σ_2	11.4	S34°E	23°
	σ_3	5.4	N20°E	53°

to that found in the full-scale drift area, but the direction of the stress is rotated from the vertical. Likewise, the other principal stresses are skewed with respect to horizontal and vertical. Unlike the LuH gauge results in the full-scale area, the orientations do not smoothly change with depth. This irregularity suggests that the variation in orientation reflects instrumentation variability or small-scale rock heterogeneity rather than larger features such as underground openings.

9.0 LOCATION OF HYDRAULIC FRACTURES BY ACOUSTIC EMISSION (E. Majer)

9.1 Introduction

Determining principal stress directions in a rock mass by hydraulic fracturing requires accurate location and orientation of the generated fracture. The usual practice employs post-fracturing downhole measurements with impression packers or borehole televiewing equipment. However, such methods do not define the fracture away from the borehole. Inhomogeneities in the stress field and/or rock mass may produce a different fracture pattern from the often-assumed symmetric double-winged vertical crack. As a first step in testing this assumption, an experiment was set up to monitor the acoustic emission (AE) associated with hydrofracturing. The experiment sought to determine (1) the existence of detectable acoustic emissions associated with hydraulic fracturing; (2) if these emission existed, their magnitude and occurrence relative to pressurization, breakdown, and fracture propagation; (3) the character of the AE activity (were discrete events or near-continuous swarms?) (4) given discrete events, whether the signal-to-noise ratio was sufficient to determine the event's orientation, magnitude, and source characteristics; and (5) given an affirmative answere to question (4) the number of AE sensors needed to apply practically these techniques in a hydrofracturing exercise.

9.2 Procedure and Results

A 12-element vertical array of piezoelectric transducers was deployed in a three-dimensional configuration around one vertical and one vertical and one horizontal hydrofracture hole (Fig. 9.1). The specifications of the AE sensors and amplifiers are given in Table 9.1. These instruments are identical in gain and frequency to those monitoring AE activity in the Climax Stock

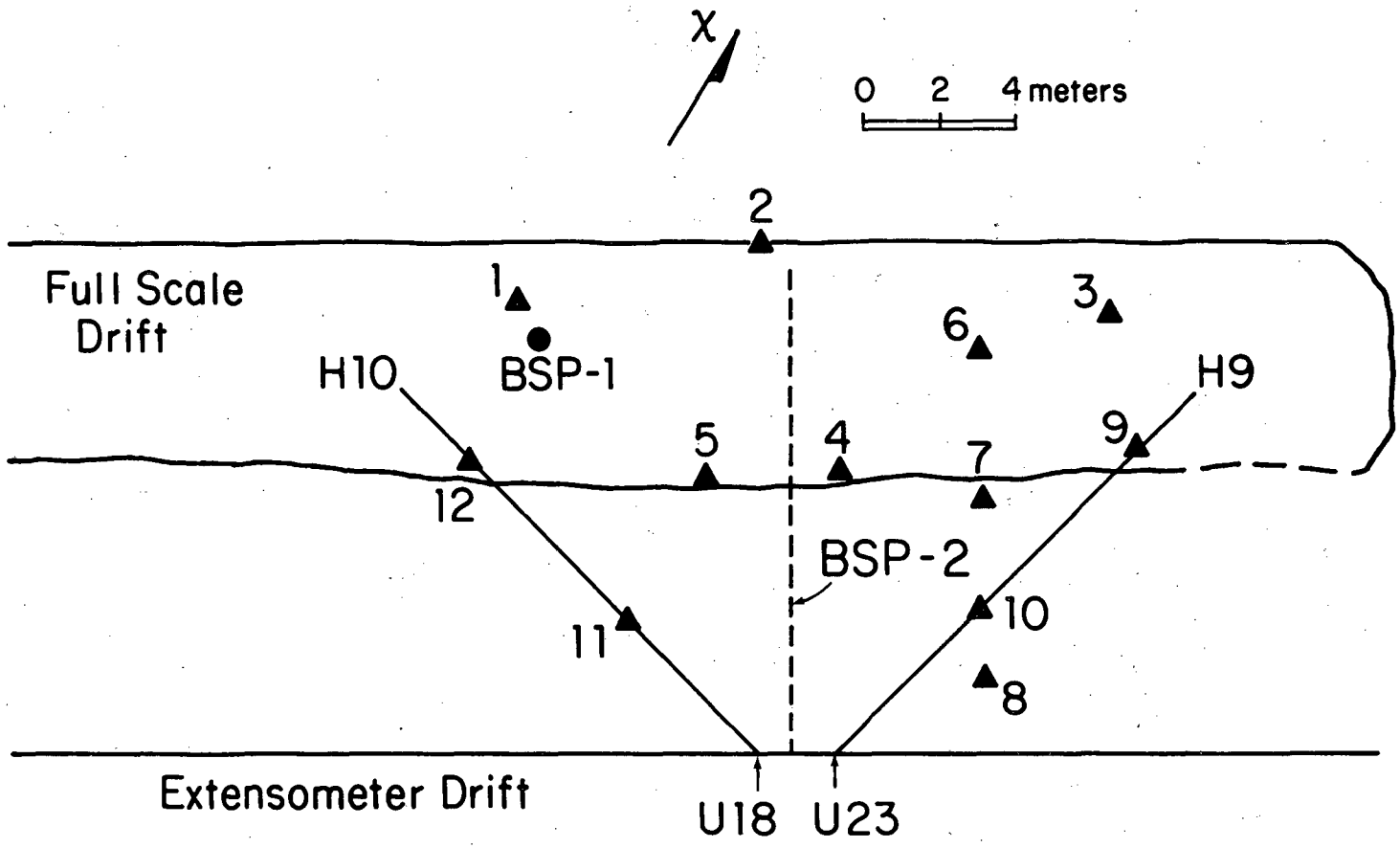

Fig. 9.1 Plan view of experimental area showing stress measurement holes and associated sensor locations. Stations 1 and 3 are emplaced from the Extensometer drift 5 m below the floor of the full-scale drift.

Table 9.1. Specifications of acoustic monitoring instruments.

Columbia 5002 Transducer	
Sensitivity	13 pcoul/g
Frequency Response	2 Hz to 10 kHz, ± 5%
Resonant Frequency	50 kHz
Capacitance	850 pF
Outpt Resistance	2×10^{10} ohms
Columbia 9021 Charge Amplifier	
Source Impedance	Capacitive device, 500 pF max
Charge Gain	100 mV/pcoul (40dB)
Output Impedance	125 ohms
Frequency Response	1 kHz to 10 kHz, ± 5%

1 pole rc filter at 10 kHz

g = acceleration of gravity

repository, an experiment also in granite using similar array dimensions (Majer et al. 1981). The coordinates of the stations and of the vertical hydrofracture in BSP-1are listed in Table 9.2. Experience at the Climax Stock site with this equipment (Columbia 5002 transducer and 9021 charge amplifier) has shown that serious noise problems can be introduced by ground loops (the transducers being underground, multiple grounds in the system can occur). To avoid this problem, the transducers were mounted on non-conducting material (epoxy discs) before mounting on the rock. The sensors were mounted in several ways. The "surface" stations (i.e., nos. 2, 4, and 5) were attached to the rock by epoxy cement. Stations 1 and 3 in the vertical borehole were secured with a plaster compound (Hydrocol). The remaining stations in the horizontal hole were clamped tightly to the rock by using a spring arrangement (Fig. 9.2). Because of time constraints (five 7-hour days for setup, experiment, and removal), not all of the sensors could be attached with epoxy cement for the best coupling. Consequently, the best data (and, in most cases, the only usable data) were obtained from the surface stations.

Data were recorded on a Honeywell 5600 C 14-channel tape recorder with frequency response of 300 to 20,000 Hz. Care was taken to properly adjust and balance all tape recorder channels, yielding a 54 dB dynamic range and using one channel as compensation. Unfortunately, this primary recorder developed a malfunction after arriving at the Stripa mine, and another tape recorder with only 40 dB dynamic range (also 5600 C) had to be substituted; this resulted in a substantial degradation of the data quality. Time was recorded simultaneously on the tape and on the pressure logs, allowing correlation between AE activity and various states of the hydrofracture process.

Table 9.2. Stripa station coordinates (in meters).

Station	X	Y	Z
1	315.823	990.576	345.889
2	320.634	996.587	338.761
3	323.050	1003.999	345.876
4	316.649	1000.704	338.783
5	314.752	997.642	338.758
6	320.800	1000.750	344.300
7	317.950	1000.150	344.500
8	313.500	1006.550	344.700
9	320.250	1006.350	342.350
10	314.850	1004.850	342.350
11	310.110	996.850	342.350
12	311.500	991.150	342.350
BSP-1	315.570	992.48	343.80-344.30

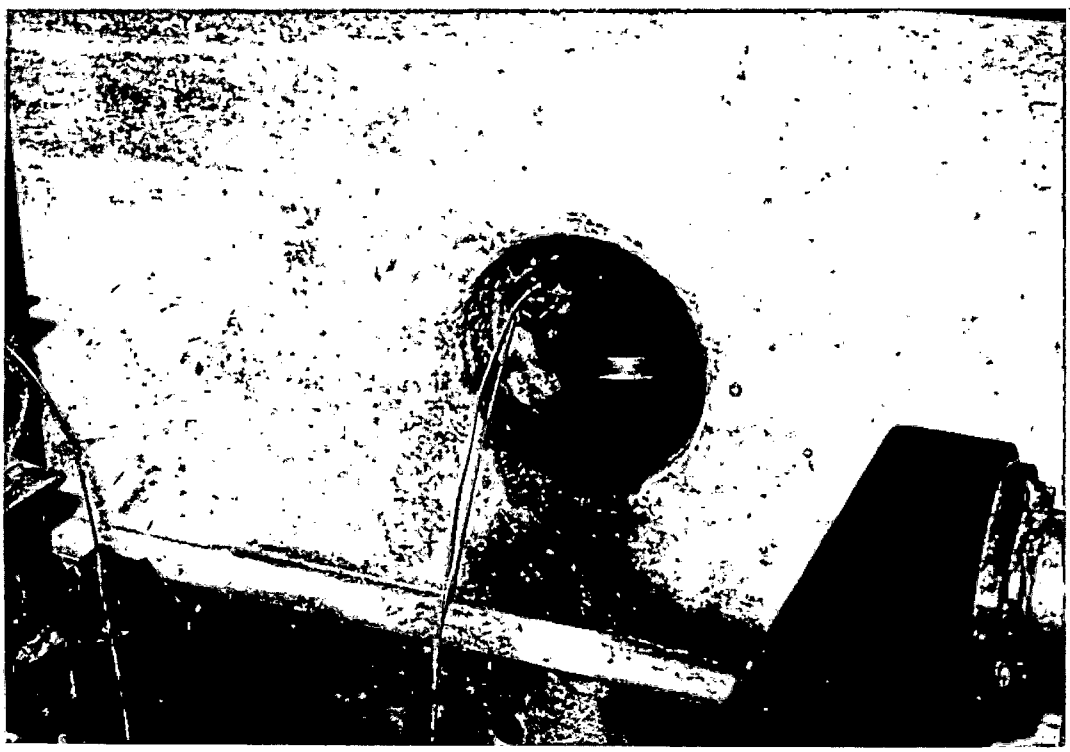

Fig. 9.2 Spring-loaded acoustic sensor for use in boreholes.

Figure 9.3 shows one of the larger events recorded from the vertical hydrofracture hole. Although the signal-to-noise ratio is barely adequate, several significant points can be noted: (1) discrete events occur during the hydrofracture process; (2) all events recorded are similar, i.e., impulsively beginning P and S waves (S-P times give reasonable source distances); and (3) time separations between events are enough for us to analyze each one for location, size, and source type. If not for the problems with the substitute tape recorder, it appears that the data quality would have been sufficient to adequately define the fracture characteristics. The poor data quality was due not to noise generated by the hydrofracture process, but to the recording instrument.

Figure 9.4 gives the rate of AE activity versus pumping rate through breakdown. Note that no AE activity was detected during the initial breakdown. The only significant activity occurred when fast pumping (4.5 liters/minute) was under way. From Fig. 9.4 it also appears that AE activity (or rock fracture) occurred several minutes after pressurization. The threshold of AE detection was approximately 10^{-2} g (g = acceleration of gravity) at 10 kHz. Most of the events shown predominate at frequencies near 10 kHz. If these events follow the scaling theories of conventional earthquake source mechanics, the size of the fracture should be several centimeters in length. Futherfore, if AE activity indicates fracture growth, then hydrofracturing produces a series of discrete fractures that combine to create a larger fracture. Thus, even on a scale of centimeters, the local fracturing process is a response to the overall applied stress field.

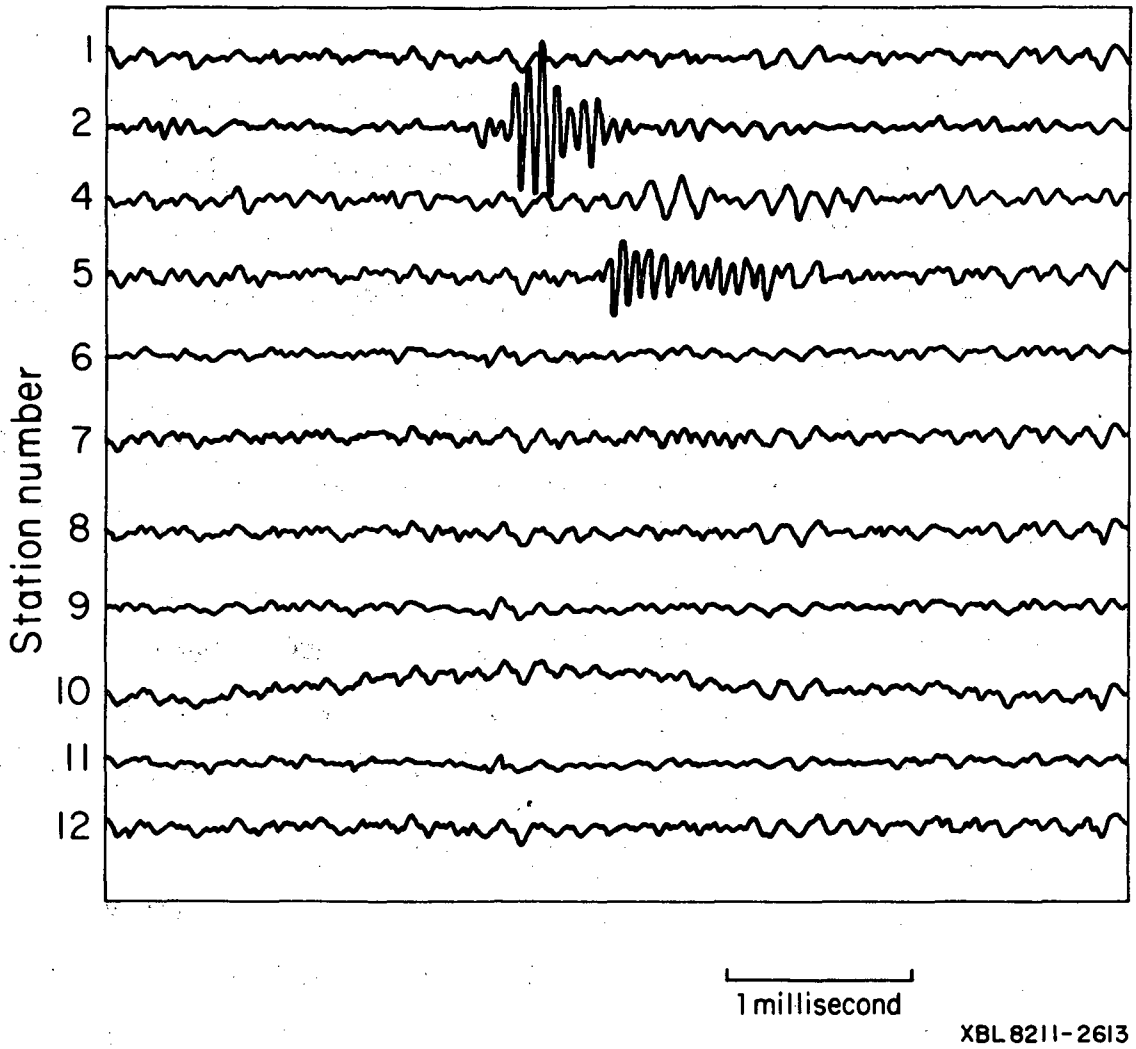

Fig. 9.3 Seismic record of acoustic event recorded from BSP-1.

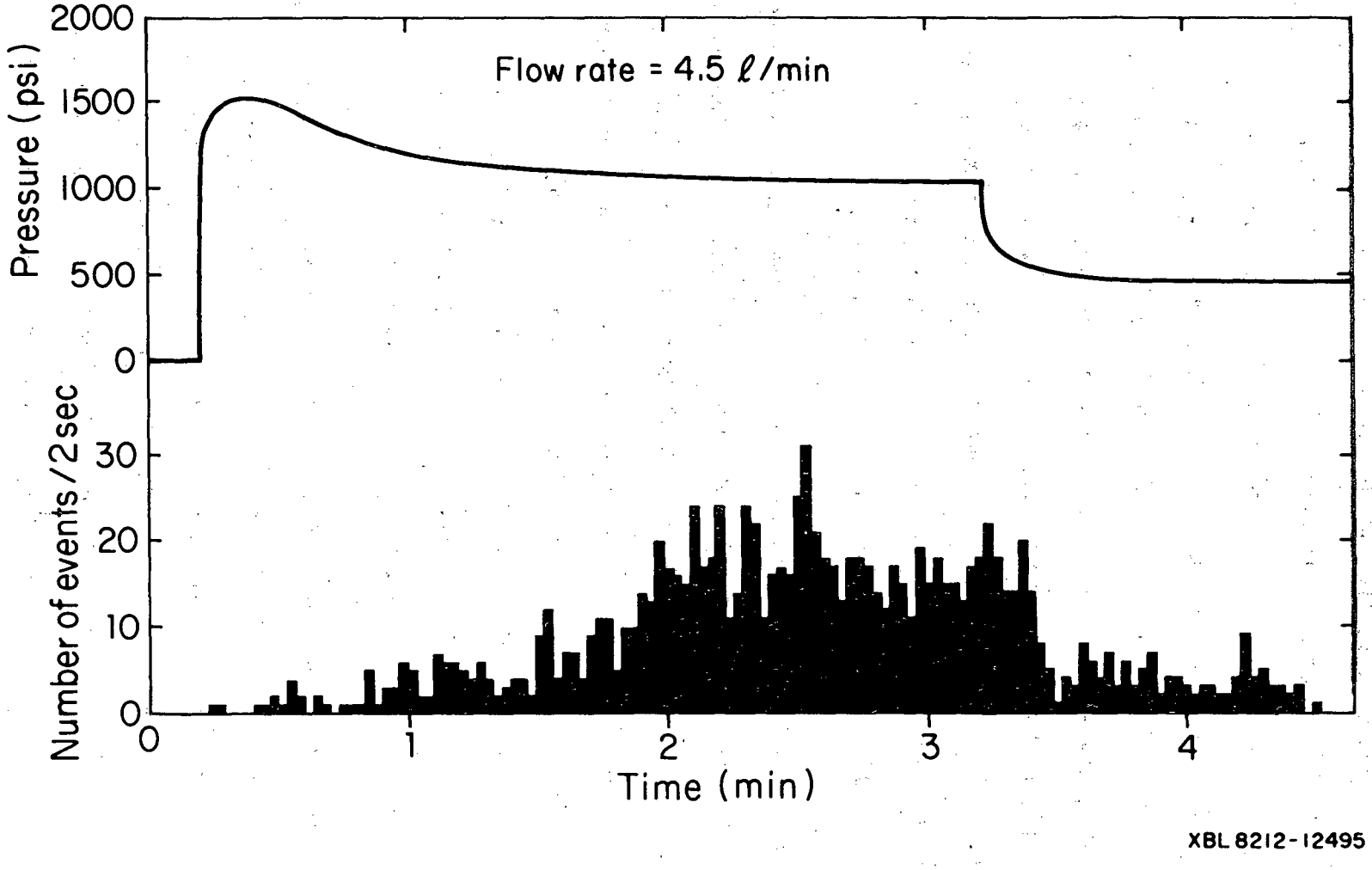

Fig. 9.4 Acoustic events per 2-second interval versus pumping pressure for fast pumping into BSP-1 (100 psi = 6.9 MPa).

The recorded events typically had shear-wave amplitudes that were large compared to those of the compressional wave (Fig. 9.2). The large shear-wave amplitude suggests that the source of the activity is shear failure rather than purely tensile failure, which occurs in principal stress planes and would therefore have no shear displacement. Pearson (1981) also concluded that the events most likely to be detected during hydrofracture operation are shear failures induced by increased pore pressure. These shear events are not on the same plane as the tensional failures induced by high fluid pressures but are closely associated with the main fracture. Therefore, by locating the shear events, the growth of the hydrofracture can be traced.

Another indication that the events detected are shear failures from increased pore pressures is the time lag between pressurization and the initiation of the events. Several minutes elapsed between "breakdown" and the beginning of the acoustic emissions. This indicates that a threshold of pressure must be reached in the formation before shear failure is initiated. This lag time is undoubtedly a function of fluid volume, permeability, and the stress field. A careful study of the lag time and the rate of AE activity may yield important information on these critical parameters.

Unfortunately, accurate source locations and fault-plane solutions could not be obtained for most events. Several larger events that occurred during fast pumping were analyzed for locations, as shown in Fig. 9.5. The locations indicate that the fracturing process is not symmetrical. This asymmetry was determined from the S-P times and the first station of arrival. Symmetry is usually assumed in the hydrofracturing process, but these results, although somewhat inconclusive

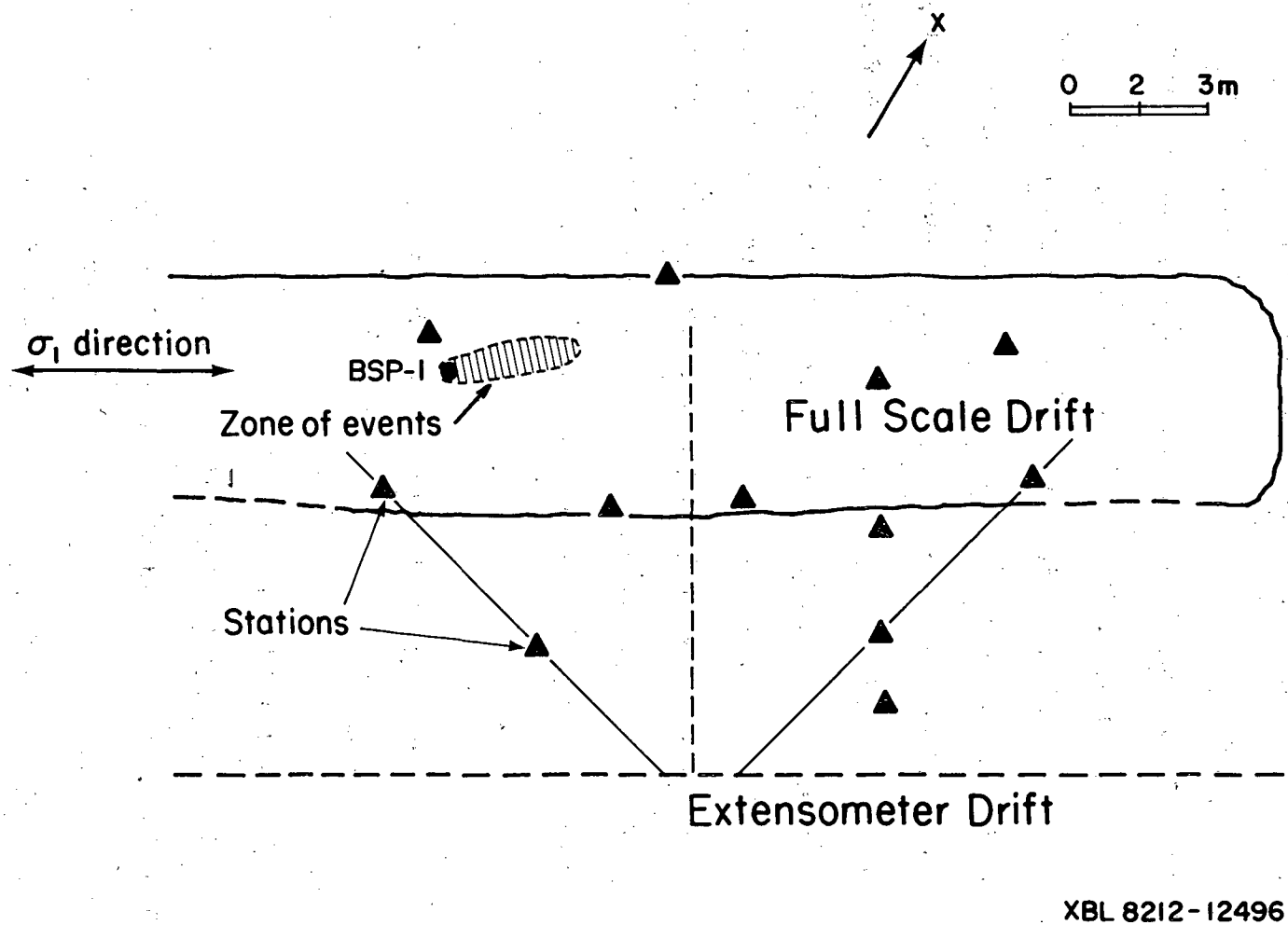

Fig. 9.5 Approximate location of acoustic events during hydrofracturing of BSP-1.

because of poor data, seem to contradict the symmetry hypothesis. However, as noted earlier, the wave forms suggest that the events located were the shear failure events associated with the build-up of pore pressure, rather than the tensile events associated with the initial breakdown. What we may be observing is asymmetry in the rock properties, i.e., permeability, rather than asymmetry in the initial breakdown fracture. Almost all events occurred in the northeast side of the hydrofracture hole. That is, station 2 was always the location of the first arrival (station 1 failed). Although the events appear to line up in a NE-trending plane, the location data are not of sufficient quality to prove that the fracture propagated in this direction. Impression packer work indicated a double-wing fracture propagation, almost on the axis of the drift. There were not enough good data to detect any change in first-motion patterns with time, which would have indicated a fracture "turn-over." The fault plane solution would also help resolve the question whether shear failure or tensional failure was detected. Although there was a definite amplitude distribution, the poor dynamic range prevented calculation of a meaningful b-value.

9.3 Summary and Conclusions

Detailed mapping of the fracture process was not achieved in this experiment, but several results are noteworthy.

(1) If the lack of AE activity during breakdown is characteristic, the initial breakdown represents (a) one large crack with frequency content much less than 1 kHz, (b) a slow (aseismic) process of crack growth, or (c) a radiation of energy too high in frequency to detect with our 20 kHz bandwidth tape recorder, i.e., the signal from the crack tip in a tensional failure is on the order of 100 kHz.

(2) On the basis of both the strong S-wave generation relative to P-wave amplitude and the time history of AE response, it appears that the observable AE activity is due to shear failure from resulting from pore pressures generated by the fluid injection.

(3) The AE activity slowly builds during fast pumping after pressurization pumping to a more or less constant level. This lag time may be a function of permeability, in that all the permeable cracks may have to be pressurized before significant fracture activity occurs. Other evidence for this may be in the faster decay of activity after pumping is stopped but as shut-in pressure is held. It is not clear how to scale the time constant with the size of the fracture produced.

(4) The determination of hydrofracture growth and location details by seismological methods appears quite feasible. If not for the time and equipment constraints on this project, the data quality would probably have allowed the location and characteristics of individual fractures to be calculated.

(5) The few source locations determined are consistent with data from the impression packers, but with the major fracture propagating in an asymmetrical fashion mainly in the NE direction from the hole.

It is hoped that an experiment similar to the one described here can be carried out again. However, several modifications to the procedure should be

made. The data should be recorded digitally with at least 12 bits of resolution. Also, the lower band edge should be reduced to 100 Hz. If the initial breakdown is generating lower frequency signals (100 - 500 Hz), they should be detected with conventional high frequency geophones. It is important, though, to retain the high frequency content of the signal (10 to 20 kHz) in order to completely characterize the fracturing process. Retaining high frequencies, however, limits the distance at which detectors can be placed from the hydrofracture hole. A new instrument may be needed.

Ideally, one would like to monitor the hydrofracturing process from the same hole as the fracture. This experiment indicates that the noise problems associated with acoustically monitoring the hydrofracture from the same hole are not insurmountable. It appears quite possible to develop a sonde that that would collect wide-band, three-component data beneath the hydrofracture zone. Each component would be a small array of sensors tuned to detect signals from the rock formation and ignore unwanted signals from the hole (i.e., noise from pumping, tube waves, etc.).

If successful on a small scale, this technology might be expanded for use with massive hydrofracturing in commercial applications. Determining the hydrofracture path seems to be of critical importance, not only for understanding stress measurements but for determining the success of well stimulation operations. With the recent advance of in-field seismic processing and high-speed, low-power-consumption computers, now is the time to bring all the techniques of fracture characterization in earthquake seismology to bear upon the problem of hydrofracture monitoring.

10.0 SUMMARY, CONCLUSIONS, AND RECOMMENDATIONS
(T. W. Doe)

10.1 Introduction

This chapter summarizes and draws conclusions from the stress measurement data discussed in the preceding chapters. The conclusions can be related to the following key questions:

- How do the overcoring and hydraulic fracturing data compare in SBH-4 in the underground area, and what is the state of stress at the depth of the test facility (348 m)?
- On the basis of these results, what recommendations can be made concerning the design of stress measurement programs and the procedures to be used at waste repository sites?

10.2 Comparison of the Far-Field Hydrofracturing and Overcoring Results

Two bases for comparing the results of the overcoring and hydraulic fracturing have been used in this report: the orientation of the maximum horizontal stress, and the magnitudes of the maximum and minimum horizontal stresses at a depth of 320 m in the SBH-4, the depth of the test facility. The horizontal stresses are used for comparison because the hydrofracture test measures mainly the stress components normal to the borehole. The stress magnitude at the test facility depth has been determined by interpolation of a linear regression of stress versus depth.

The data for the orientation of the maximum horizontal stress versus depth are shown in Fig. 10.1. The mean orientations of the maximum horizontal stress directions are N83°W for both techniques. The 95% confidence

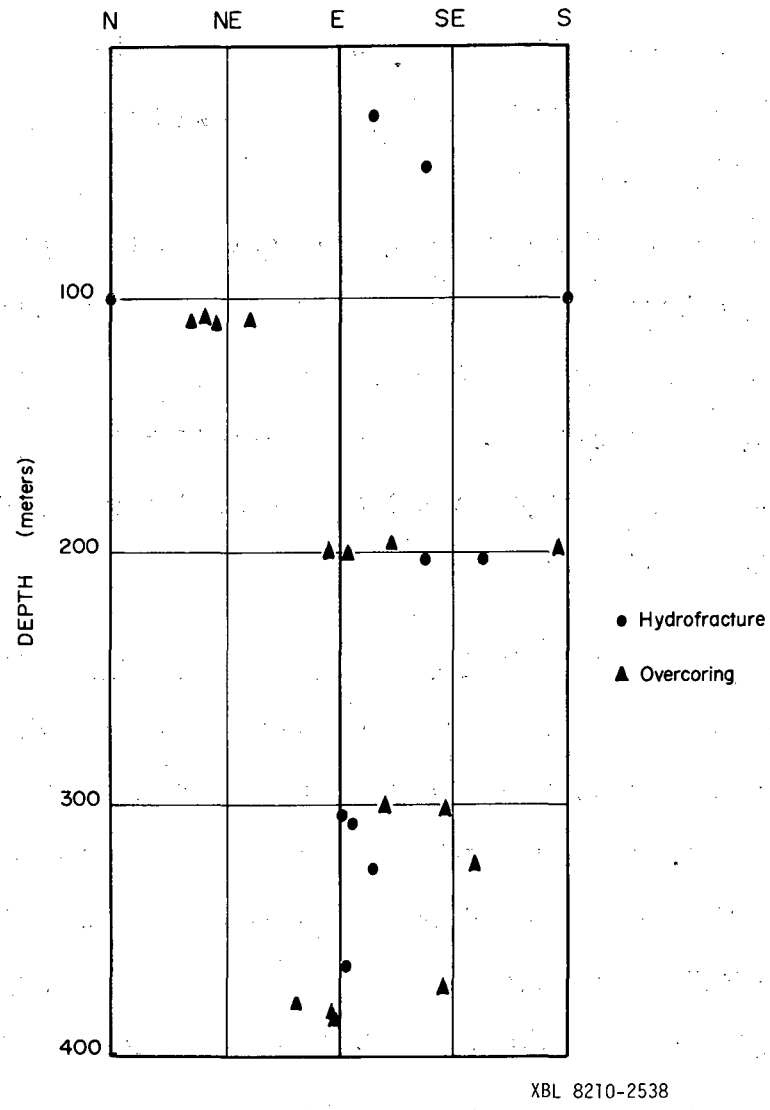

Fig. 10.1 Orientations of maximum horizontal stress versus depth as determined by hydraulic fracturing and overcoring in SBH-4.

levels for the means are both about ± 20°; thus one can conclude that the correspondence between the overcoring and hydraulic fracturing is quite good. The confidence intervals could have been improved to about ± 15° had more than 20 measurements been made. Further improvement in the statistics with larger numbers of measurements is probably not practical because of cost and the lack of suitable test zones.

The magnitudes of the horizontal stresses for the overcoring and the hydrofracturing agree closely (Figs. 10.2 and 10.3). The hydraulic fracturing has somewhat better confidence intervals than the overcoring, particularly for the horizontal minimum stress, but both methods provide estimates for the mean stress values at the depth of the test facility within ± 20% or better. At this depth, the regression values are:

	σ_{HMax} (MPa)	σ_{HMin} (MPa)
Hydrofracturing (first breakdown method)	22.1 ± 2.1	11.1 ± 0.8
Hydrofracturing (second breakdown method)	16.3 ± 2.2	11.1 ± 0.8
Overcoring	25.4 ± 2.9	12.1 ± 2.4

The standard errors of estimate for all the measurements and the confidence intervals for the regression slopes are as high as ± 50% for the magnitude data.

The large standard errors of estimate and the large confidence intervals for the slopes of the regression lines show that reliable predictions of the in situ stresses at depth cannot be made either on the basis of a few measurements or by extrapolating the results of a set of measurements taken at shallow depth.

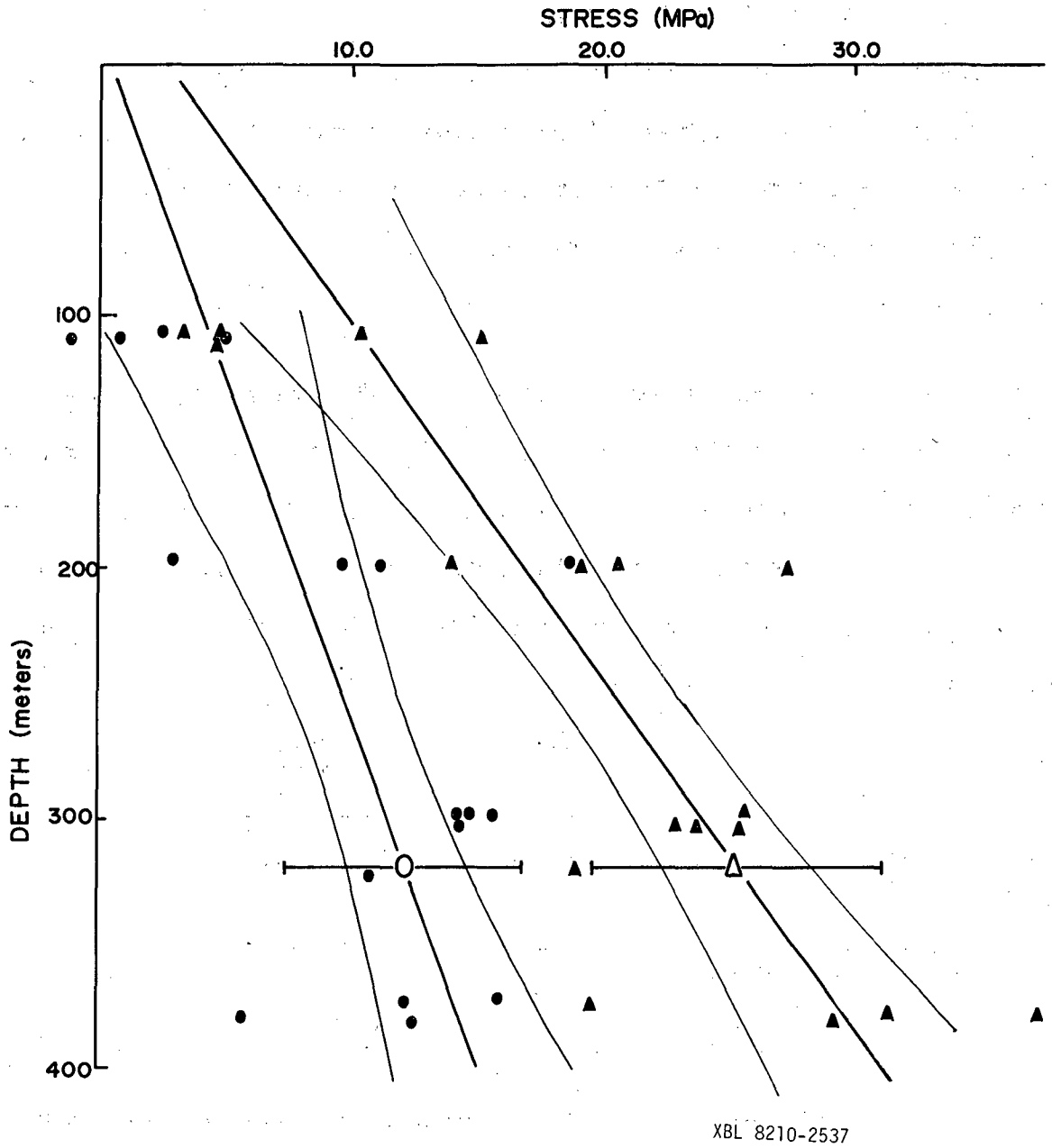

Fig. 10.2 Magnitudes of horizontal stresses determined by hydraulic fracturing in SBH-4. Curved lines are the 90% confidence intervals for the ordinate to the regression line. Large, open data points are the values of stress at the depth of the test facility as predicted by the regression. Error bars on either side of the open points are equal to the standard error of estimate.

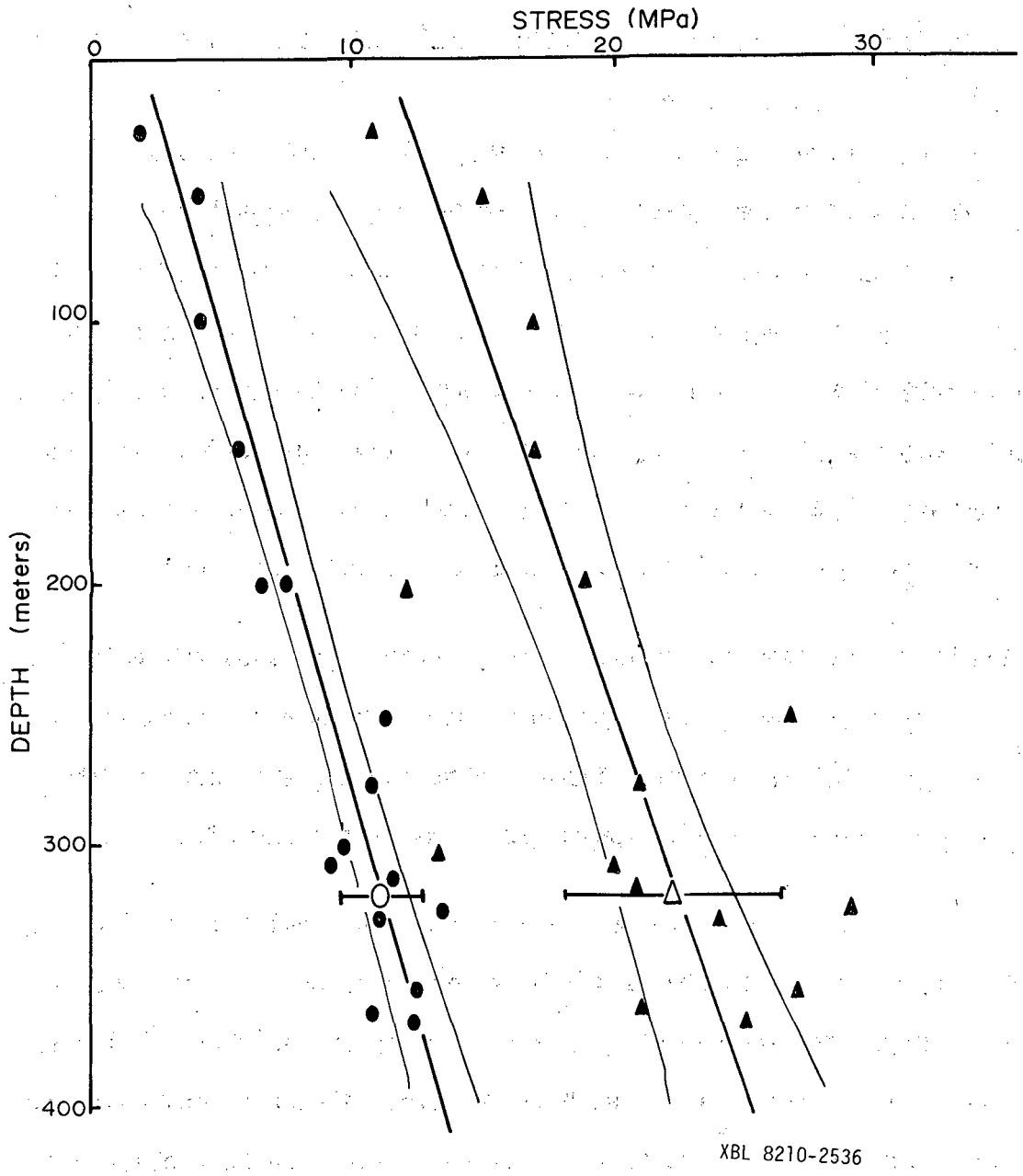

Fig. 10.3 Magnitudes of horizontal stress determined by overcoring in SBH-4. Triangles are maximum horizontal stress, circles are minimum horizontal stress. See Fig. 10.2 for explanation.

10.3 Comparison of Near Field Overcoring and Hydraulic Fracturing Results

10.3.1 Measurements in BSP-1

The stress measurements in BSP-1 by hydraulic fracturing and overcoring in BSP-1 agree well with one another, particularly in the magnitude and orientation of the maximum stress. Figure 10.4 shows the orientations of the principal stresses obtained by overcoring and the orientation of the hydraulic fracture impressions at the borehole wall. The hydraulic fractures are mostly vertical and striking parallel to the maximum principal stress direction obtained by the overcoring. The data agree strongly that the maximum principal stress direction is oriented parallel to the axis of the full-scale drift.

For the overcoring, the intermediate principal stresses are oriented off the vertical an average of about 60°. The minimum principal stresses are within about 30° of the horizontal. There is little discernible trend to the changes in orientation of the minor principal stresses with depth.

The magnitudes of the stresses calculated by hydraulic fracturing and overcoring do not vary systematically along the borehole. This was expected from the calculations of Chan et al. (1981), which showed that the stress in the full-scale drift did not strongly affect stress orientations along BSP-1, and that the stress concentration due to the drift decreased rapidly within the first few meters of the hole (Fig. 10.5).

The magnitude of the maximum principal stress agrees well between the overcoring (24.0 MPa average) and the hydraulic fracturing (24.2 MPa); however, the hydraulic fracturing results are more consistent, having 90% confidence intervals of ± 2.7 MPa against ± 5.0 MPa for the overcoring.

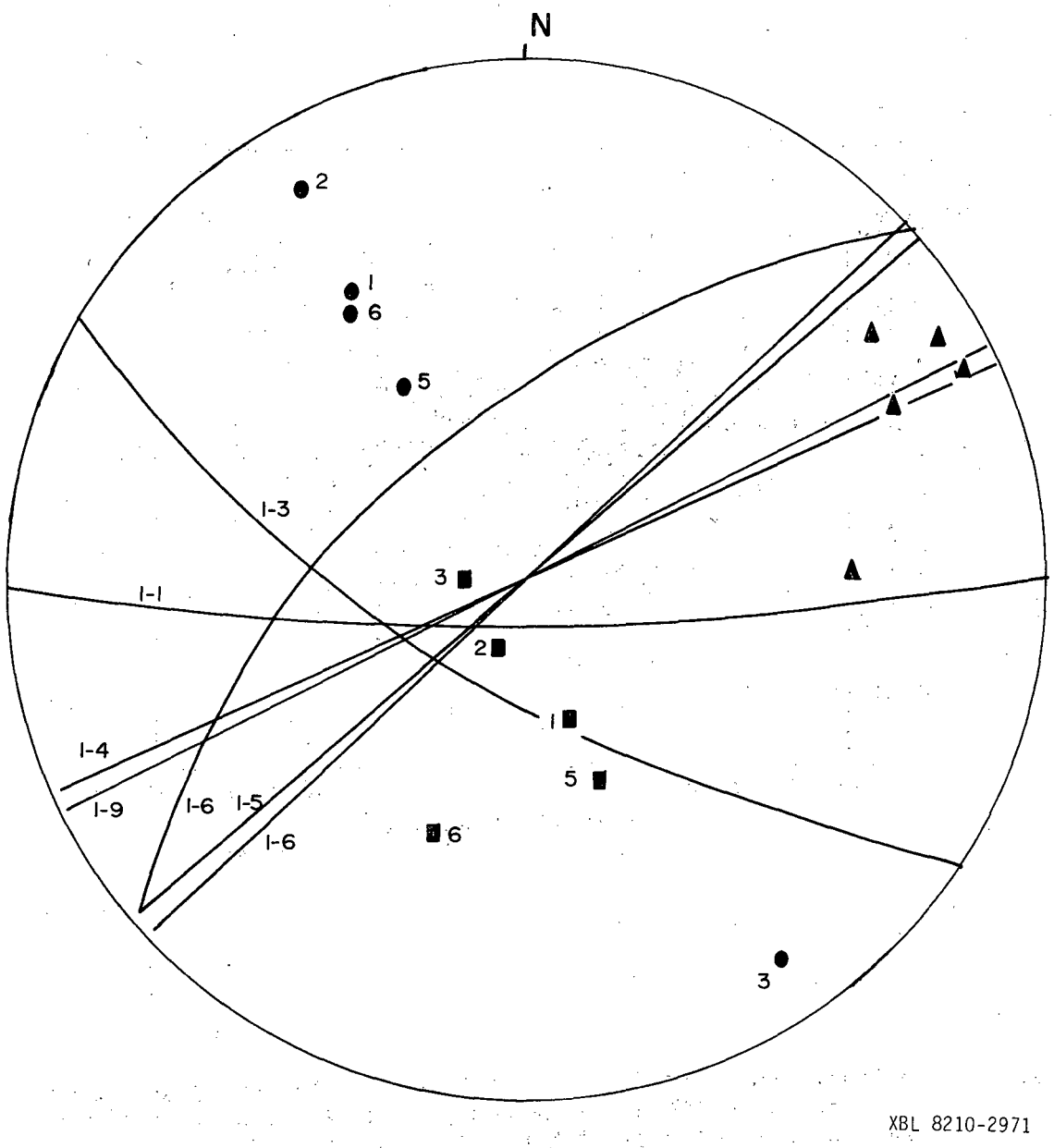

Fig. 10.4 Lower hemisphere stereographic projection of the hydrofracture planes and the principal stress directions determined by overcoring in the vertical borehole, BSP-1. Identification numbers are given for each test; σ_1 - triangle, σ_2 - square, σ_3 - circle.

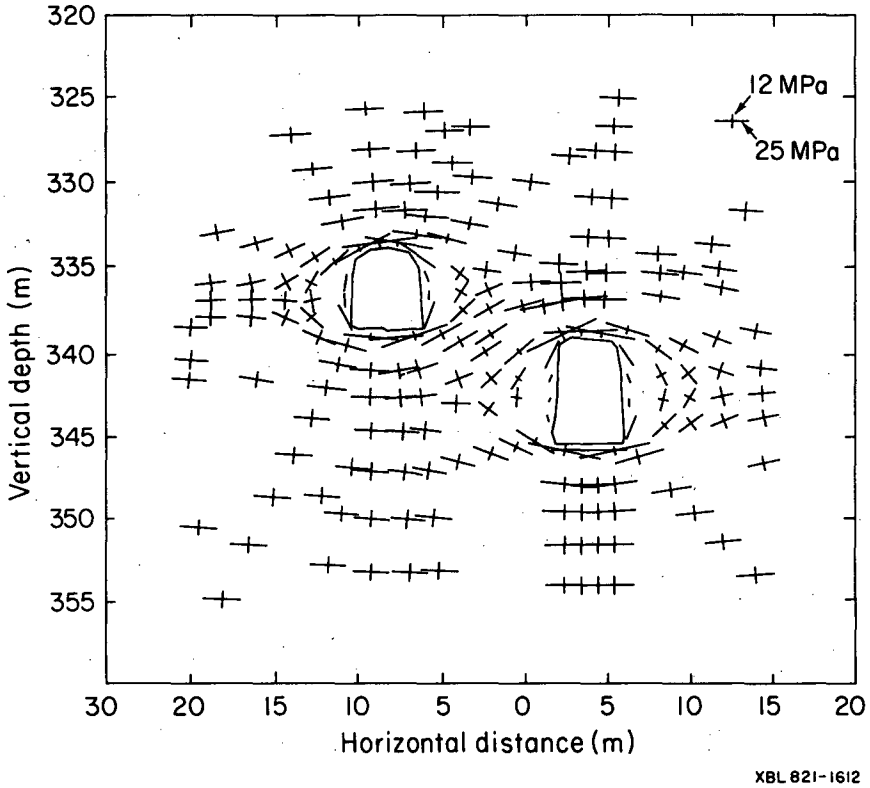

Fig. 10.5 Stress distributions around the full-scale and extensometer drifts, as predicted by boundary element calculation based on the far-field stress results (Chan and Saari, 1981).

The minimum horizontal stress determined from the early time shut-in pressure and the minimum stress determined from the late time shut-in pressure do not correspond well with the values determined by overcoring. The average value of the minimum secondary stress determined by overcoring is 4.8 + 1.1 MPa compared to 7.6 + 1.0 MPa for the hydraulic fracturing. The minimum stress determined by hydraulic fracturing was 5.1 + 0.8 MPa compared with 3.4 + 1.3 MPa for overcoring.

The lack of correspondence of the lesser stress magnitudes between the overcoring and hydraulic fracturing would not greatly affect calculations of stress ratios, nor would it strongly influence design strategies were Stripa an actual repository. But, if we assume the overcoring data are correct, an the analysis based on hydraulic fracturing records in a case where the lesser stresses are not coaxially oriented with the borehole may give stress values that are too high.

10.3.2 Measurements in BSP-2 and BSP-3

BSP-2 and BSP-3 were horizontal holes drilled under the full-scale drift from the extensometer drift. BSP-2 was used for hydraulic fracturing and BSP-3 for overcoring using the USBM, LuH triaxial cell, and CSIRO triaxial cell. Numerical models of the full-scale drift area prepared by Chan et al. (1981) based on the SBH-4 measurements showed that a rotation of the principal stresses should be found along the horizontal holes (Fig. 10.5). This rotation is related to the presence of the experimental drifts. In the first few meters of the holes, the calculated minimum stress is directed towards the free surface of the extensometer drift wall. As the hole passes under the full-scale drift, the influence of the drift floor becomes more pronounced and the minimum stress rotates to become vertical.

Table 10.1 Average values of principal and secondary stresses at Stripa. Values given with 90% confidence interval.

	Principal Stresses (MPa)			Secondary Stresses[a] (MPa)		
	σ_1	σ_2	σ_3	σ_{Max}	σ_{Min}	σ_{Ax}
SBH-4[b] Hydrofrac	-	-	-	22.1±2.1	11.1±0.8	-
SBH-4[b] Power Board	-	-	-	25.4±2.9	12.1±2.4	-
BSP-1 Hydrofrac	-	-	-	24.0±2.9	7.6±1.0	5.1±0.8
BSP-1 Power Board	24.2±5.0	10.0±1.9	1.9±1.6	23.0±4.5	4.8±1.1	9.5±0.8
BSP-2 Hydrofrac	-	-	-	22.3±1.9	7.8±0.5	5.7±0.7
BSP-3 LuH	20.8±3.1	9.2±1.1	1.9±1.6	20.2±3.2	4.3±0.7	-
BSP-3 CSIRO	18.7±5.5	8.0±3.4	2.6±1.2	18.3±6.0	5.1±3.2	-
BSP-3 USBM	-	-	-	18.3±1.7	4.4±1.2	-
Lulea Drift Leeman Cell	19.5±2.9	8.0±3.2	4.8±1.2	15.6±2.8	8.7±1.9	10.4±1.9
V1-150m Power Board	27.9±5.0	19.1±5.3	11.4±1.0	26.0±5.1	18.3±5.9	13.4±1.4
V1-300m Power Board	22.7±6.3	13.0±4.0	9.2±2.4	19.7±7.1	11.7±3.3	13.6±1.4

[a] Max and Min are the stresses normal to the borehole, Ax is the stress along the borehole axis. Ax is vertical except for BSP-2, BSP-3, and Lulea Drift.

[b] Interpolated values at depth of test facility (338 m level).

The average values of the principal stresses are given in Table 10.1, and the orientations are shown in Fig. 10.6. The magnitudes of the principal stresses vary along the length of the hole, but not to the extent predicted by the modeling. The maximum principal stress is consistently parallel to the axis of the drifts and coincides closely with the direction measured by the Power Board. The intermediate and minor principal stresses are nearly 45° off the vertical and horizontal directions near the collar of the hole. As the hole approaches the full-scale drift, the intermediate stress rotates toward the horizontal, and the least stress rotates toward the vertical. This rotation is consistent with the predictions of the boundary element model shown in Fig. 10.5.

The mean orientations of the principal stresses agree well with those measured by the Power Board in BSP-1; however, one would expect that the Luleå measurements closest to the end of the hole--which is near the center line of the full-scale drift--would be those most closely coinciding with the Power Board results. Instead, they, show the greatest divergence.

The USBM borehole deformation gauge was used in the same hole as the LuH cell and CSIRO cell measurements. Unlike the triaxial strain cells, the USBM gauge measures only the stress components normal to the hole axis. This disadvantage is balanced against the greater rapidity and reliability of the USBM gauge. Strain-cell measurements and deformation-gauge measurements complement one another when used in the same hole. The strain cells provide the three-dimensional information, and the deformation gauge provides the larger number of measurements necessary for confidence in the stress determination for a site.

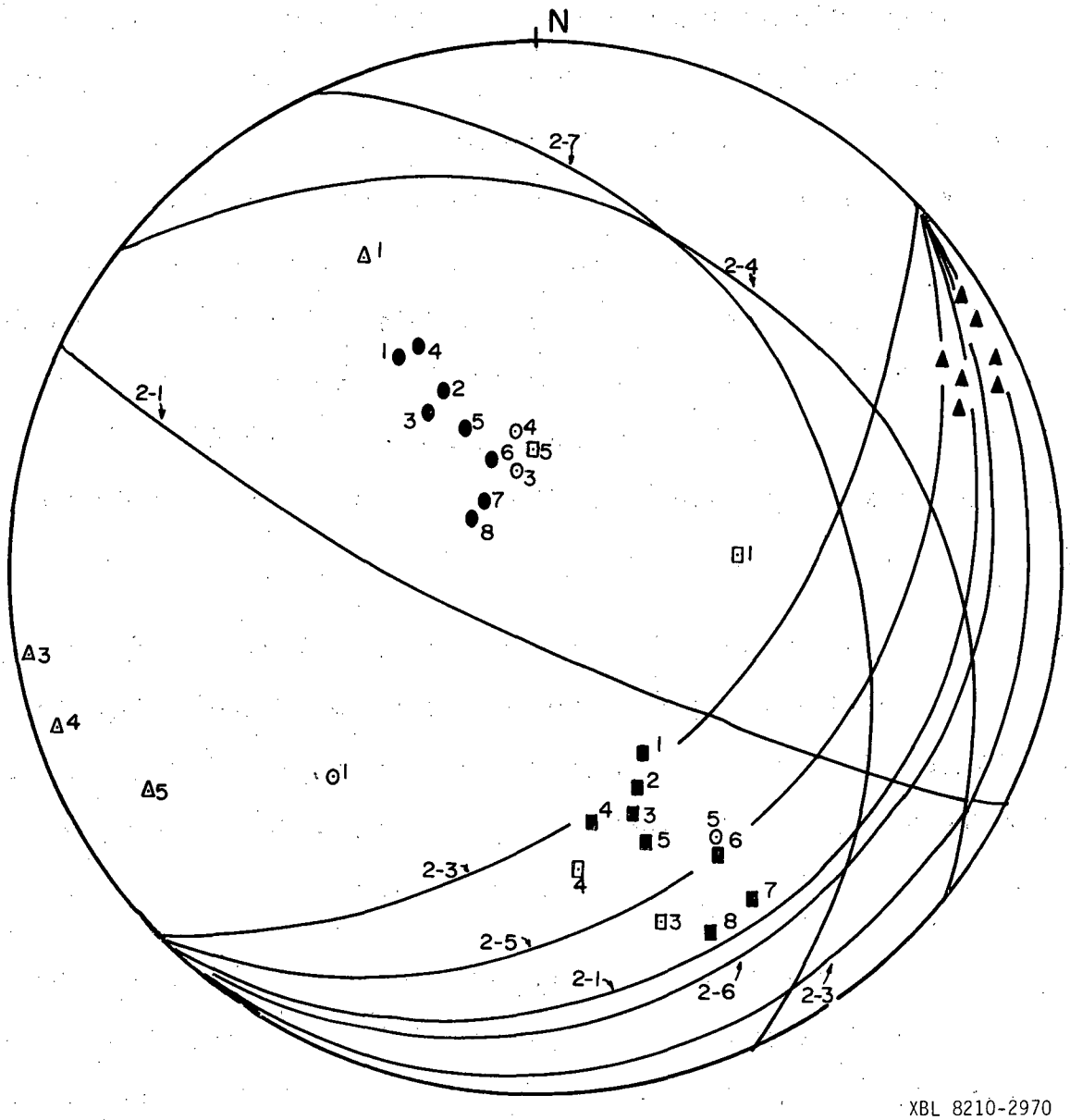

Fig. 10.6 Lower hemisphere stereographic projection of the hydrofracture planes and the principal stress directions determined by the LuH cell (solid symbols) and CSIRO (open symbols) overcoring in the sub-horizontal holes, BSP-2 and 3. Identification numbers given for each test; triangle - σ_1, square - σ_2, circle - σ_3.

The results of the USBM measurements are plotted along with the secondary stress data for the LuH cell measurements in Fig. 10.7. The agreement is excellent for both magnitude and orientation. The mean secondary stresses with 90% confidence levels for the means are:

	σ_{Hmax} (MPa)	σ_{Hmin} (MPa)
LuH	20.0 ± 3.3	4.5 ± 0.8
USBM gauge	17.5 ± 3.3	4.5 ± 0.8

The maximum secondary stress, which is very close to being the maximum principal stress, is horizontal for both techniques.

The CSIRO cell has several practical advantages over the Leeman cell, including the protection of the electronic circuitry from drilling fluids and the capability of monitoring the strain gauge outputs during overcoring. Its disadvantage is that the cements require 17 hours or more to cure to an acceptable hardness.

Five CSIRO measurements were made in BSP-3. Even though curing times exceeded 17 hours, the first two measurements did not appear to be adequately bonded to the pilot borehole walls. Even after switching to a faster curing cement for the final three measurements, the gauge values showed an average drift rate of about 5 microstrains per minute before and after the overcoring. The orientation and magnitude data are calculated using strain data from which the linear drift has been subtracted. The data, shown in Fig. 10.6, are consistent with the LuH results in both orientation and magnitude.

The hydraulic fracturing stress measurements in BSP-2 yielded results comparable to those obtained by overcoring in BSP-3. The fractures were subhorizontal and generally coaxial with the borehole. There was a slight dip

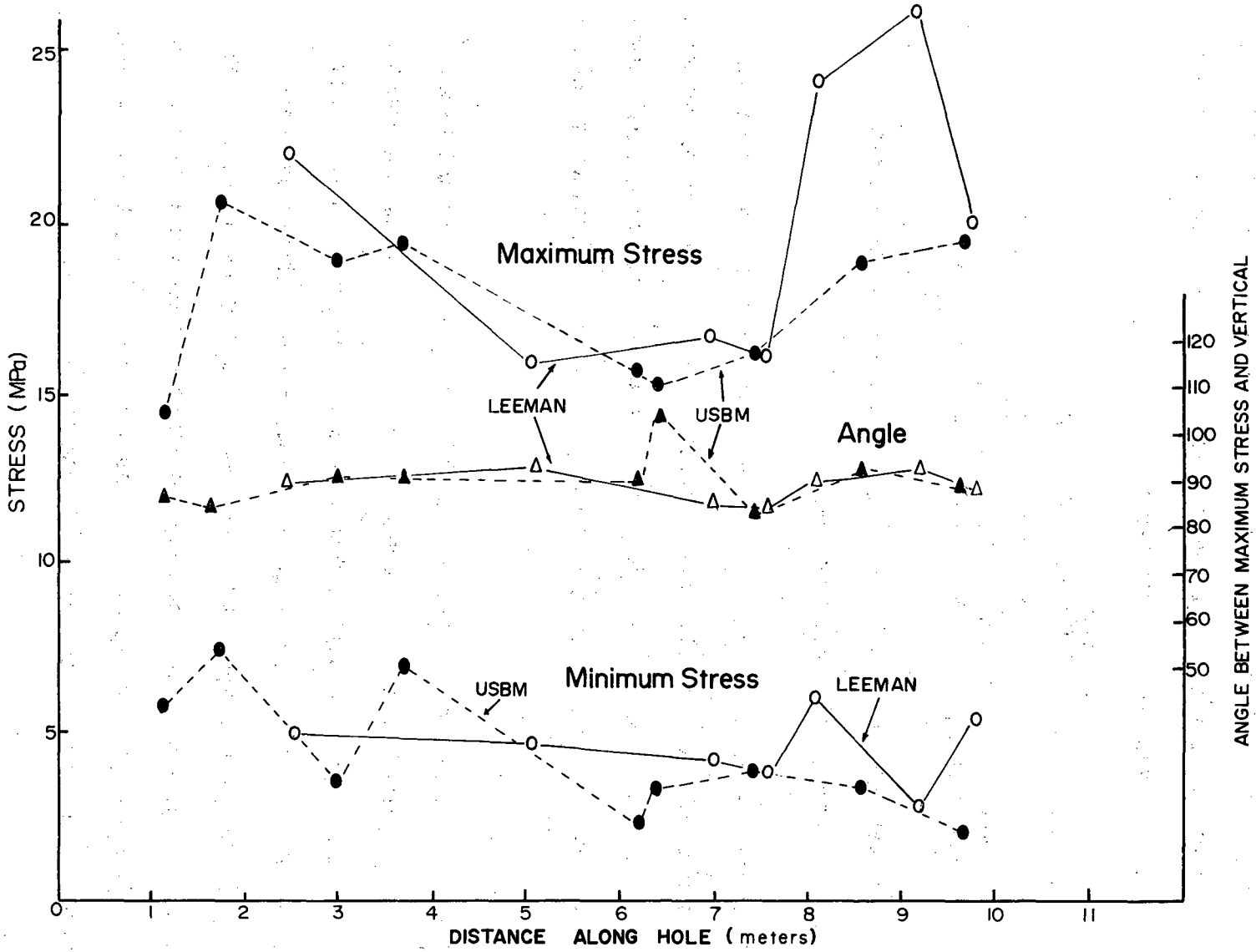

XBL 8210-2969

Fig. 10.7 Maximum and minimum stresses normal to the direction of BSP-3 measured by LuH triaxial cell (Leeman) and USBM deformation gauge overcoring. Right-hand scale gives the values for the plot of the angle between the maximum stress direction and the vertical.

toward the extensometer drift such that some of the fractures were approximately normal to the minimum stress directions determined with the LuH cell (Fig. 10.6). The maximum horizontal stress values of the hydraulic fracturing average 24.0 ± 2.7 MPa versus 20.8 ± 3.1 MPa for the LuH cell in BSP-3.

In summary, the agreement between the results of the overcoring and the hydraulic fracturing for the near-field measurements is best in the magnitude and orientation of the maximum principal stress. All the techniques are in agreement that the direction of the maximum stress is horizontal and parallel to the axis of the full-scale and extensometer drifts. The magnitudes for the stresses cover a range within about ± 20% of 22 MPa.

The values for the magnitudes of the intermediate and least stresses are in general agreement; however, two inconsistencies exist in the results. The first is the difference in minor stress orientations between the BSP-1 Power Board results and the BSP-3 LuH results. The magnitudes and mean orientations are in general agreement, but the Power Board's least stress is oriented more towards the extensometer drift, and the LuH least stress is oriented more towards the full-scale drift. The second inconsistency is in the shut-in pressure values for the orthogonal holes, BSP-1 and BSP-2. The pressure-time records for hydrofractures in both holes show two shut-in pressures, and these pressures have the same values in each hole. As discussed in Chapter 7, the only resolution to this paradox is that the principal stresses are oriented at 45° to the two holes. Fortuitously, this interpretation is consistent with both the orientation and the magnitude data from the overcoring.

10.4 Comparison of All Stripa Stress Measurements

Stress measurements have now been performed in four areas of the Stripa mine, the full-scale/extensometer drift area, the Luleå drift (Carlsson, 1978), the far-field area north of the mine (SBH-4), and in the deep borehole, V1, drilled 505 m downward from the 360 m level of the mine (Strindell and Andersson, 1981). The average directions and magnitudes of the stresses determined in each of these areas are shown in Fig. 10.8. The most striking feature of the data is the difference in maximum stress orientations between the underground stress measurements and SBH-4. Although there is considerable scatter in the magnitude data of V1 and of the Luleå drift, the orientation of the maximum stress is consistently in a NE-SW direction. On the other hand, the SBH-4 measurements indicate that the maximum stress is oriented WNW-ESE, a 45° to 60° difference from the underground measurements.

The agreement between different stress measurements in the orientations of the maximum stresses suggests strongly that the rotation of the stresses is real and not an artifact of the measurements.

The most apparent source of this rotation is perturbation from the mine itself. The strike of the orebody and the associated stopes is perpendicular to the direction of the stresses measured in SBH-4. In the vicinity of the openings, the minimum stress should be normal to their walls. The resulting streses concentration might cause the maximum stress to be parallel to the trend of the workings. By this line of reasoning, the stress measurements performed near the mine workings should show the influence of these stress perturbations.

This explanation is not entirely satisfactory, as stress concentrations around openings generally die out within a few tunnel radii. The only way

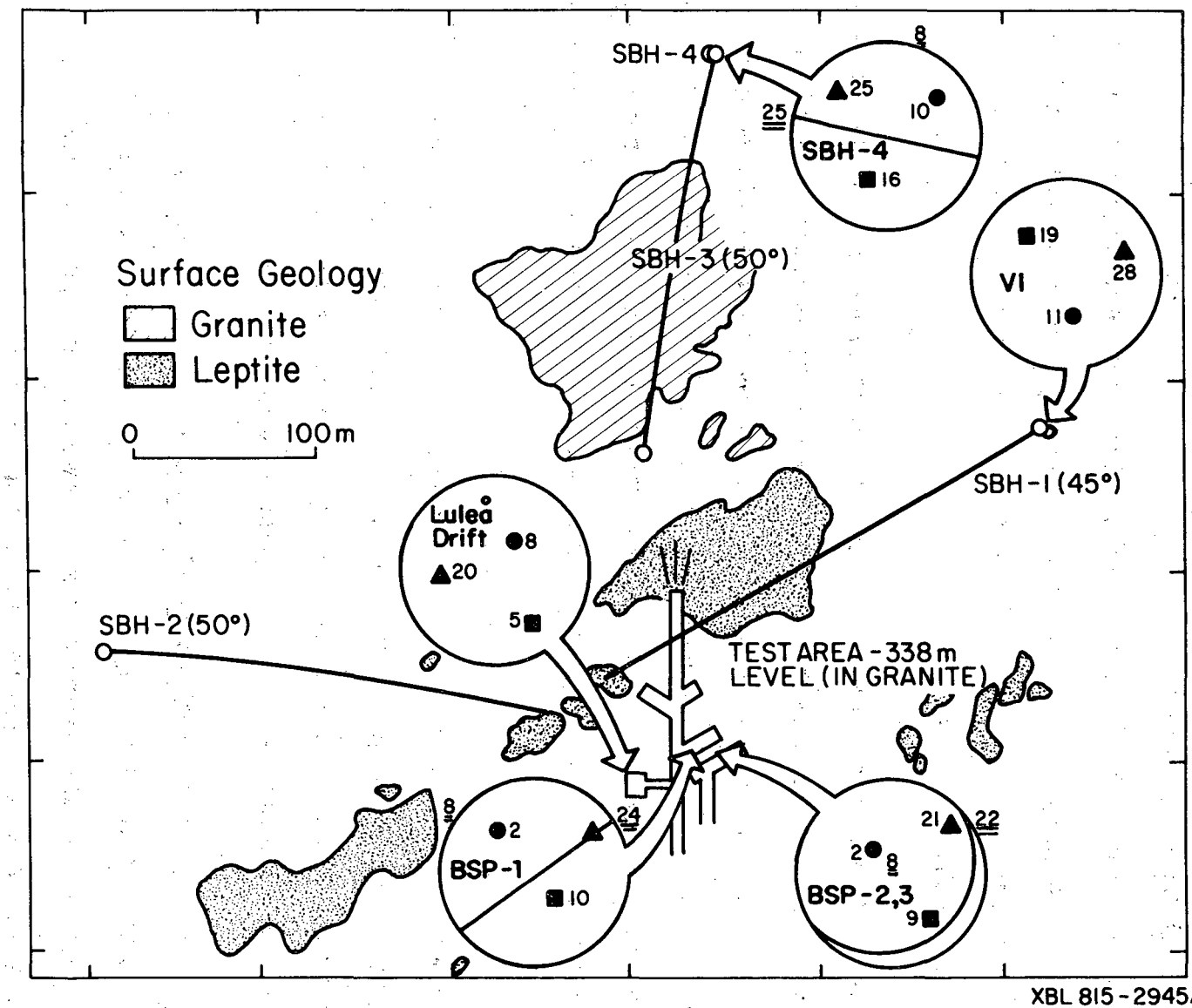

Fig. 10.8 Stereographic projections showing average magnitudes and orientations of principal stresses (overcoring) and secondary stresses (hydraulic fracturing). Hydraulic fracture stresses are double underlined. 1 - triangle, 2 - square, 3 - circle. Hydraulic fracture orientations shown as planes.

that the mine's influence can be demonstrated is to prepare a three-dimensional model of the mine workings; because of their geometric complexity, this would be a very major undertaking. Chan et al. (1981) made a simplified two-dimensional model of the mine. Their plane-strain model calculated the stress concentrations as if the entire orebody had been removed as a single slab. These calculations showed that the mine would have a relatively small influence on the stresses at SBH-4, except at shallow depths.

Another possible explanation for the stress rotation between the test and far-field area is that the changes reflect variability in the geology and in the elastic properties of the rocks. An argument against this hypothesis is that, in areas of the United States such as the upper Midwest, the maximum stress direction is very consistent over areas of hundreds of square kilometers. Nonetheless, this geologic hypothesis cannot be confirmed or rejected without appropriate numerical calculations.

Stress variability due to local geology would have important implications for repository site characterization. Stress measurements made in a single exploration hole might not be representative of the areas where the excavation would take place, so that several holes might have to be tested.

10.5 Recommendations for Stress Measurement Programs in Hard Rock Sites

On the basis of the work on stress measurement that has been completed at Stripa, we conclude that the design of stress measurement programs for nuclear waste repository sites should answer three basic questions:

- At what stage should stress measurements be done?
- What methods should be used?
- How many measurements should be performed?

Our recommendations regarding the answers to these questions are given below.

10.5.1 Timing of Stress Measurement in Exploration Programs and Selection of Methods

Stress measurements should be performed before the construction of underground workings begins. The stress data should be used to determine whether the stress conditions are unfavorable for the stability of openings and to determine what measures should be taken to assure proper working conditions.

In the past, the design stages of many underground projects used assumptions of stress magnitudes that were based on gravity loading alone. For examples, Heim's rule states that stresses should be hydrostatic and equal to the stress generated by the weight of the overburden. This assumption is based on the premise that creep will bring all the stresses into equilibruim. Another gravity-based prediction states that only the vertical stress should be equal to the overburden pressure and that the horizontal stress should be due only to Poisson's effect. For a Poisson's ratio of 0.25, the horizontal stress would be one-third of the vertical stress.

Predictions of the stress state based on gravity would be in error if applied at Stripa. The maximum horizontal stress is at least a factor of 2 greater than the theoretical gravity-induced value. This condition is similar to that observed in stress measurements in the Canadian Shield rocks of the United States (Haimson, 1978). Repository design should therefore be based on actual stress measurements rather than on assumptions of the stress state based on theory.

Stress measurements should be performed as part of the early borehole exploration of a candidate site. Hydraulic fracturing should be comple-

mented by overcoring measurements from the surface. In general, hydraulic fracturing is capable of providing sufficient data on the stress ratios and orientations. But, in cases where the stress ratios are large or the principal stresses are not parallel with the borehole, the interpretation of the hydraulic fracturing records may be in error.

The goal of the stress measurement program should be to obtain the value of the stresses at the depth of the repository. These values can be obtained either by (1) performing a number of measurements at the depth of interest, or (2) interpolating the value from linear regression over a range of depths. In either case the number of measurements will be about the same. As there may not be enough suitable test zones in the depth range of interest, one may need to use the linear regression approach. It is difficult to specify a number of tests required to obtain a particular confidence interval, because the quality of the estimate will depend on how the data are distributed with respect to depth. A program where the stresses are measured from the surface to a depth twice as great as the horizon of interest will provide data with the highest degree of confidence for designing the underground facility, but if that is not practical, tests should be made at least as deep as the target depth.

The first stress measurements--from boreholes drilled from the surface--can be used to qualify a candidate site and to design the initial shaft and underground test facilities. Once the shaft is completed, these surface-hole measurements should be confirmed underground using reliable overcoring methods such as the USBM gauge or the Leeman triaxial cell. These may be

complemented by hydraulic fracturing. Hydraulic fracturing will be especially useful if an acoustic experiment is performed to map the propagation of the hydraulic fracture. Past experience has shown that overcoring results can be highly variable. Causes of this variability may be due to the short lengths over which strains are measured and to local heterogeneities. Hydraulic fracturing, on the other hand, provides a larger scale of measurement. An acoustic determination of the orientation of the hydraulic fracture should be a reliable indicator of the plane of the maximum and intermediate principal stresses and thus provide a valuable confirmation of the overcoring results.

The Stripa experiments showed that principal stress directions can vary considerably over hundreds of meters (the distance between SBH-4 and the full-scale drift). It is therefore important that stress measurements continue to be carried out as new areas of the rock mass are opened during the development of a repository, particularly if major variations in rock material properties or lithology are discovered at the site.

10.5.2 Required Numbers of Measurements

In situ stress data--both orientation and magnitude--are notorious for having considerable scatter. Repository designs will most likely use the mean values of the stress determinations. Given the scatter in the stress measurements, it is important to have enough measurements performed so that the confidence intervals for the means will be narrowly defined. No guidelines for confidence intervals in stress data currently exist, however. We suggest that the magnitudes be known within ± 10% of the mean and that the orientation of the maximum horzontal

stress be known within ± 15°.

These confidence limits are based on the following considerations. A complete stress analysis of a repository site cannot be made at present, but for purposes of considering the required reliability of the data, one can consider a simple case such as the stresses around a single tunnel. In general, it is preferable to avoid having large differential stresses in the plane normal to the tunnel axis. If a granite site had a ratio of the maximum horizontal to vertical stress greater than 2.1:1, portions of the sidewall might be in a state of tension (Hoek and Brown, 1980). If the rock is unjointed, tensile failure might occur, or, if the rock is jointed, the joints may open to provide leakage paths for the waste. The in situ stress ratio in the plane normal to the tunnel axis can be minimized by orienting the tunnel in the direction of the maximum horizontal stress. If one were to make an adjustment of the alignment of the tunnels to avoid unfavorable sidewall stress, it would be very important to know the mean direction of the maximum horizontal stress with a high degree of confidence, perhaps about ± 15°. Data with confidence limits approaching 45° would be virtually useless as the limits would include both the most favorable and least favorable tunnel directions.

If the confidence intervals for the stress magnitudes are large, the stress ratios cannot be very accurately defined. For example, if the mean maximum and minimum horizontal stresses at the depth of interest were 20 and 10 MPa with a confidence interval of ± 5 MPa, the stress ratio could be anything from 1 (hydrostatic) to 5. Conservatively designing around the higher ratio might entail considerable additional expense in the excavation and operation of the repository. By designing the stress measurement program so as to obtain data with tighter confidence limits, the stress ratios would be restricted to a smaller range,

thus allowing use of a simpler, less costly repository design. There are therefore important economic reasons for having tight confidence intervals for the stress magnitudes, particularly since the ratios of the maximum horizontal stress to the minimum horizontal stress and the vertical stress are commonly in the vicinity of 2:1.

Using the standard error of estimate values for the SBH-4 measurement and the standard deviation values for the underground measurements, we have constructed graphs showing the variation in confidence interval with the number of measurements (Fig. 10.9). For the stress magnitudes, 20 measurements should be sufficient to define the mean values within 10% of the maximum stress value. Since the improvement in the confidence interval is not great with additional data points, performing many more tests does not appear justified. Fifteen measurements are sufficient to define the maximum stress orientation within 20°, and again there is little improvement that can be attained with additional data points.

In general, the underground test data were more consistent than the data from SBH-4. The recommended confidence intervals should be attainable with ten measurements by each technique for sites where the data are as variable as that of the full-scale drift area.

10.6 Recommendations for Stress Measurement Procedures

10.6.1 Overcoring Measurements

The use of a data logger to directly record the output voltages of the strain gauges was found to have advantages over the conventional strain indicator system. The relative ease of reading all the strain data channels made it easier to record the strain changes as a function of drill penetration

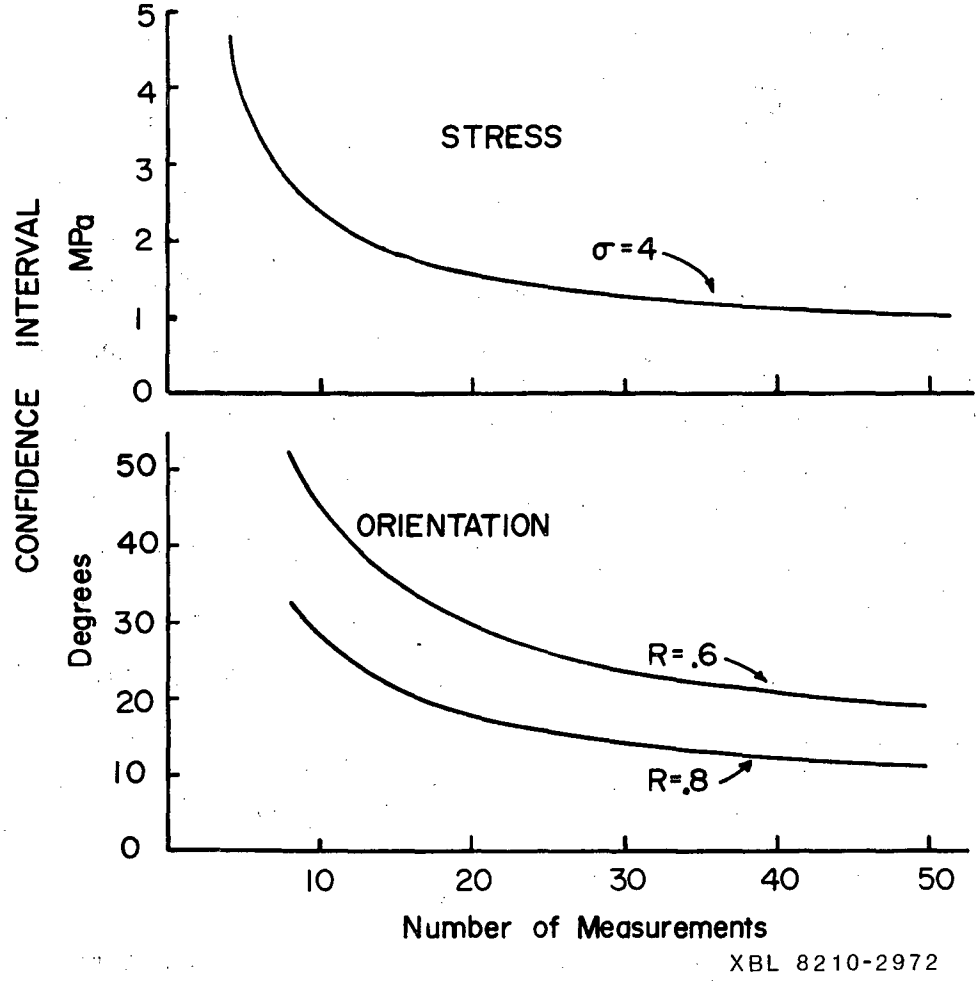

Fig. 10.9 Reduction in confidence interval for stress magnitude and orientation with number of measurements for standard deviation of 4 MPa and vector lengths of 0.6 and 0.8.

during the overcoring. The data logger's printer was very useful for providing a permanent record of the strains.

The USBM gauge and the LuH cell could be used very easily in the same pilot borehole, thus allowing two overcoring measurements to be performed simultaneously.

10.6.2 Hydraulic Fracturing

The calculation of the stresses using the first breakdown pressure and the tensile strength was found to be in better agreement with the overcoring than the calculation using the second breakdown pressure. The first breakdown method has been out of favor for several years due to problems in finding an appropriate tensile strength value. Ratigan (1981) has developed statistical fracture mechanics methods for determining values of tensile strength, and these have been applied in the Stripa work.

The shut-in pressures were determined by low flow-rate pressure build-up and semi-logarithmic plots of post-breakdown pressure versus time. The agreement of the two methods was very good.

Because of equipment problems, the acoustic emission mapping was not successful in accurately locating the hydraulic fractures. However, the experiment successfully showed that fracture propagation occurred in discrete, recognizable events that can be analyzed for location. The results were therefore encouraging and the method should be applied where possible in the future.

ACKNOWLEDGMENTS

M. Holmberg and A. Tarikka of the Swedish Mining Research Foundation helped with the overcoring measurements underground. Hans Carlsson of KBS, a division of the Swedish Nuclear Fuel Supply Co., and Per-Axel Halen were invaluable in setting up the details of the work in Sweden. Bezalel Haimson assisted with the field work and reviewed the interpretations of the SBH-4 tests; Milton Moebus deserves credit for the successful performance of the hydraulic fracturing equipment in the field. Joe Ratigan provided the analysis of the laboratory tensile strength values. N. G. W. Cook provided many helpful comments on this report. Laurel Egenberger coordinated the preparation of the manuscript. The program was managed at LBL by W. Thur and W. Stromdahl. Michael Lemcoe of Battelle Memorial Institute provided useful oversight from the Office of Nuclear Waste Isolation.

This work was supported by the Assistant Secretary of Nuclear Energy, Office of Waste Isolation of the U.S. Department of Energy under contract number DE-AC03-76SF0098. Funding for the project was administered by the Office of Nuclear Waste Isolation at the Battelle Memorial Institute.

REFERENCES

Abou-Sayed, A., C. Brechtel, and R. Clifton, 1978. "In-situ Stress Determination by Hydrofracturing: A Fracture Mechanics Approach," J. Geophys. Res., v. 83, pp. 2851-2862.

Bredehoeft, J., R. Wolff, W. Keys, and E. Sutter, 1976. "Hydraulic Fracturing Determine Regional Stress Field, Piceance Basin, Colorado", Geol. Soc. Amer. Bull., v. 87, pp. 250-258.

Carlsson, H., 1978. Stress Measurements in Stripa Granite, Lawrence Berkeley Laboratory Report LBL-7078, SAC-04.

Chan, T., V. Guvanasen, and N. Littlestone, 1981. Numerical Modeling to Assess Possible Influence of the Mine Openings at Stripa on Far Field in-situ Stress Measurements, Lawrence Berkeley Laboratory Report 12469, SAC-33.

Crow, E.L., F. Davis, and M. Maxfield, 1960. Statistics Manual, Dover, New York, 288 p.

C.S.I.R.O. (no date). Field Manual for C.S.I.R.O Hollow inclusion Gauge, Council of Scientific and Industrial Research Organizations (Australia), 23 p.

Haimson, B., 1968. Hydraulic Fracturing in Porous and Non-Porous Rock and Its Potential for Determining Stresses at Great Depth, Ph.D. Thesis, University of Minnesota, 233 p.

Haimson, B., 1978. The Hydraulic Fracturing Stress Measuring Method and Recent Results, Int. Jour. Rock Mech. Min. Sci., v. 15, pp. 167-178.

Haimson, B.C., 1981. Confirmation of Hydrofracturing Through Comparisons with Other Results, in Proceedings 22nd U.S. Rock Mechanics Symposium. Massachusetts Institute of Technology, pp. 379-385.

Haimson, B., and C. Fairhurst, 1970. "In-situ Stress Determination at Great Depth by Hydraulic Fracturing," in Rock Mechanics--Theory and Practice; Proceedings 11th Symposium on Rock Mechanics, pp. 559-584.

Hiltscher, J., F. Martna, and L. Strindell, 1979. "The Measurement of Triaxial Stresses in Deep Boreholes in the Design and Construction of Underground Openings," Proceedings 4th Congress of the International Society for Rock Mechanics, v. 1, pp. 227-234.

Hoek, E. and E. Brown, 1980. Underground Excavations in Rock, Institution of Mining and Metalurgy, London, 527 p.

Hooker, V. and D. Bickel, 1972. Overcoring Equipment and Techniques Used in Rock Stress Determination, U. S. Bureau of Mines Information Circular 8618, 32 p.

Hustrulid, W., B. Leijon, A. Tarikka, and M. Holmberg, 1982. In situ Stress and Modulus Determinations at the Stripa Mine, Sweden, contract report to Lawrence Berkeley Laboratory.

La Pointe, P. 1981. "Improved Numerical Modeling of Rock Masses Through Geostatistical Characterization," Proceedings 22d U.S. Symposium on Rock Mechanics, Massachusetts Institute of Technology, pp. 386-397.

Majer, E., T. McEvilly, and M. King, 1981. "Monitoring an Underground Repository with Modern Seismological Methods," Int. J. Rock Mechanics Min. Sci., v. 18, pp. 517-527.

Majer, E. and T. McEVilly, 1982. "Stripa Acoustic Emission Experiment," in Proceedings of Workshop XVII, Workshop on Hydraulic Fracturing Stress Measurements, U.S. Geological Survey Open File Report 82-1075, pp. 569-581.

Mardia, K.V., 1972. Statistics of Orientation Data, Academic Press, London, 357 p.

Olkiewicz, A., J. Gale, R. Thorpe, and B. Paulsson, 1979. Geology and Fracture System at Stripa, Lawrence Berkeley Laboratory Report LBL-8907, SAC-21, 163 p.

Paris, P. and G. Sih, 1965. "Stress Analysis of Cracks," in Fracture Toughness and its Testing, American Society for Testing and Materials Special Publication 381, p. 30-83.

Pearson, C., 1981. "The Relationship Between Microseismicity and High Pore Pressure During Hydraulic Stimulation Experiments in Low Permeability Granitic Roads," J. Geophys. Res., v. 86, pp. 7855-7865.

Pincus, H.J., 1953. "Analysis of Aggregates of Orientation Data," Journal of Geology, v. 61, pp. 482-509.

Ratigan, J., 1981. A Statistical Fracture Mechanics Approach to the Strength of Brittle Rock, Ph.D. dissertation, University of California, Berkeley.

Rummel, F., and R. Jung, 1975. "Hydraulic Fracturing Stress Measurements near the Hohenzollern Graben Structure, Southwestern Germany," Pure Appl. Geophysics, v. 131, pp. 321-330.

Stilborg, B., and B. Leijon, 1982. A Comparative Study of Rock Stress Measurements at the Luossavoria Mine; SB8276, Swedish Mining Research Foundation.

Strindell, L. and M. Anderson, 1981. Measurement of Triaxial Rock Stresses in Borehole V1, Swedish Nuclear Fuel Supply Co. (KBS div.) Internal Report 81-05, part 2, 11 p.

Wang, J., T. Tsang, T. Narasimhan, and P. Witherspoon, 1977. "Transient Flow in Tight Fractures, Proc. 1st Invitational Well Test Symposium, Lawrence Berkeley Laboratory.

Weibull, W., 1939. A Statistical Theory for the Strength of Materials, Ingeniorsvetenskap Akadamiens Handlingar, No. 153, 45 p.

Worotnicki, G. and R. Walton, 1976. "Triaxial Hollow Inclusion Gauges for Measurements of Triaxial Rock Stresses," in Proceedings I.S.R.M. Symposium on Investigation of Stress in Rock, Institution of Engineers, Australia National Conference Publication No. 76/4, pp. 1-8.

Zoback, M. and D. Pollard, 1978. "Hydraulic Fracture Propagation and the Interpretation of in situ Stress Measurements, in Proceedings 19th U.S. Rock Mechanics Symposium, University of Nevada, Reno, pp. 14-22.

Zoback, M., F. Rummel, R. Jung, C. Rayleigh, 1977. Laboratory Hydraulic Fracturing Experiments in Intact and Pre-Fractured rock; Int. Jour. Rock Mech. Min. Sci., v. 14, pp. 49-58.

Zoback, M., H. Tsukahara, and S. Hickman, 1980. Stress Measurements at Depth along the San Andreas Fault: Implications of the Magnitude of Shear Stress at Depth, J. Geophys. Res., v. 85, pp. 6157-6173.

This report is part of a cooperative Swedish-American project supported by the U.S. Department of Energy and/or the Swedish Nuclear Fuel Supply Company. Any conclusions or opinions expressed in this report represent solely those of the author(s) and not necessarily those of The Regents of the University of California, the Lawrence Berkeley Laboratory, the Department of Energy, or the Swedish Nuclear Fuel Supply Company.

TECHNICAL INFORMATION DEPARTMENT
LAWRENCE BERKELEY LABORATORY
UNIVERSITY OF CALIFORNIA
BERKELEY, CALIFORNIA 94720